THE UNIVERSITY
of EDINBURGH

Fluctuation and Dissipation Dynamics in the Early Universe

Joël Mabillard

Doctor of Philosophy
The University of Edinburgh
May 2019

Abstract

The aim of this thesis is to study the effects of fluctuation and dissipation dynamics in Early Universe cosmology. The formal description of the Early Universe relies on cosmological fields that, in general, are not completely isolated from and, therefore, interact with their environment. These interactions might lead to two non-negligible effects. Fluctuations, acting as stochastic forces, tend to perturb the motion of the field. In addition, some fraction of the energy is transferred from the field to other degrees of freedom, corresponding to dissipation. We are interested in three situations where fluctuation and dissipation dynamics plays a significant role for cosmology.

After a brief review of the prevailing model of cosmology, the Standard Big Bang Model, we study the formation of embedded defects. This particular realization of topological defects is not stable by construction. While considering one of the simplest examples, the pion string, we show that the interactions with a thermal and dense medium might, in some circumstances, provide a stabilization mechanism.

We then turn our interest to the warm realization of inflation. Ideas borrowed from the renormalization group are applied to warm inflation in order to define universality classes among the different models of inflation. Beyond the identification of universality, this approach is well-suited for an analytical treatment of warm inflation and helps in the characterization of the possible smooth transition to the radiation-dominated regime.

Finally, we extend the Kramers problem to quantum field theory. In the presence of fluctuation and dissipation dynamics, there is a non-vanishing probability for a field initially located at a minimum of its potential to escape from the well. We define and derive the escape rate for a scalar field, due to thermal fluctuations, and discuss the applications for cosmology.

Lay Summary

Fluctuation and dissipation dynamics is a common phenomenon in physics. One of the simplest illustrations appears in Brownian motion, which describes, for example, the random motion of a particle suspended in a liquid or a gas. The interactions between the particle and its surrounding, the fluid, generate two competing effects. Fluctuations, acting as random forces, perturb the motion of the particle. In addition, a damping leads to the dissipation of a fraction of the particle energy. Such phenomena are ubiquitous in physics. Problems described by Brownian motion, or related fluctuation and dissipation dynamics, appear in subject areas ranging from condensed matter to astrophysics.

In the present work, we are interested in the consequences of fluctuation and dissipation dynamics in Early Universe cosmology. The formal description of the Early Universe is based on cosmological fields. In general, a field is not entirely isolated from and, therefore, interacts with its environment, which can lead to fluctuation and dissipation dynamics. Despite its prevalence in the subject of cosmology, the influence of this dynamics has not been extensively studied so far. We are particularly interested in three situations where fluctuation and dissipation dynamics plays a significant role : phase transition and formation of topological defects, warm inflation, and in the escape problem.

Declaration

I declare that this thesis was composed by myself, that the work contained herein is my own except where explicitly stated otherwise in the text, and that this work has not been submitted for any other degree or professional qualification except as specified.

Parts of this work have been published in [1, 2].

(*Joël Mabillard, May 2019*)

Acknowledgements

First of all, I would like to express my deep gratitude to my supervisor, Prof. Arjun Berera. The uninterrupted care, guidance and encouragements given throughout my Phd have been extremely helpful, precious and appreciated. I also thank Prof. Rudnei Ramos for his constant help and for making the visit to the UERJ possible. I am specially grateful to Dr. Mauro Pieroni, for being such a great collaborator and friend. I wish to thank also the people I had the chance to work with, in particular, Angelo, Bruno and Francesco.

To the members of the PPT at the University of Edinburgh I would like to say thanks, I have much appreciated being a member of the group. To James, Julia and Saad, who have been great officemates. To Alex, Andreas, Andries, José and Vincenzo, for the interesting discussions, especially at the coffee breaks. I am specially grateful to Christian and Gianluca, who made the time spent in Edinburgh the most enjoyable. I would like to thank the other people I have met in Edinburgh and that I forget to cite here.

Je souhaite remercier ma famille et en particulier mes parents, Joseph et Marie-Thérèse, qui ont toujours été d'un soutien inconditionnel, notamment pendant mes études. Ce sont eux qui m'ont transmis cette curiosité pour le monde qui nous entoure, et qui, de fil en aiguille, m'a conduit vers la physique. Je remercie aussi Loïc, Mélanie, Jicky et Claude pour leur soutient constant.

Je remercie tout particulièrement Aurelia, qui a toujours été présente pour moi. Ses encouragements, son soutien et son aide, en particulier dans les moments plus difficiles, ont été extrêmement précieux. J'ai beaucoup de chance de t'avoir dans ma vie.

Finally, I have a special thought for Prof. Pierre Binétruy, who unfortunately left us too soon. Pierre was not only one of the greatest physicists I have ever met, he was also a very kind person. Pierre was my Master thesis supervisor, and I am specially thankful to him for encouraging me to pursue my studies with a Phd.

Contents

List of Figures

List of Tables

Chapter 1

Introduction

Over the last decades, the observational developments brought cosmology to the level of an experimentally testable science. The experimental results together with the theoretical framework of the Standard Big Bang Model (SBBM), developed since the formulation of general relativity (GR), gave birth to the current model for our Universe, the ΛCDM. This parametrization corresponds to a flat universe in which the energy is dominated by a cosmological constant Λ and where matter is principally in the form of cold dark matter (CDM). The successes of this relatively simple model, the main assumptions being isotropy and homogeneity of space on large scales, are remarkable. The model predicts the abundance of most of the light elements, such as hydrogen or helium, the formation of the cosmic microwave background (CMB) and its blackbody spectrum, the large-scale structure of the distribution of the galaxies and the current acceleration of the expansion. Moreover, these predictions concern different stages in the Universe's history and, therefore, increase the confidence on the model. The inclusion of an early phase of accelerated expansion, the period of inflation, allows explaining further the anisotropies observed in the temperature of the photons in the CMB and the origin of the flatness of the space. The theory of inflation also provides a mechanism for the formation of structures. The ΛCDM including a period of inflation is therefore a very strong cosmological model.

The Standard Big Bang Model is mostly based on two ingredients, on one side general relativity and, on the other, the Standard Model (SM) of particle physics. The SM describes the elementary particles and the fundamental interactions between them. The theoretical formulation of the SM has been achieved by

the mid-seventies and its experimental tests continue until today, in particular, with the Large Hadron Collider (LHC). The list of the experimental successes of the SM is long, to cite a few, the discovery of the quarks or the existence of the neutral-current interaction. One prediction, today experimentally confirmed, has a particular importance for cosmology, the existence of the Higgs boson. The Higgs field has been introduced to generate the masses of the bosons using the Higgs mechanism. The particle has been searched for by experimentalists for years until finally observed at the LHC in 2012. It was the first evidence of an elementary scalar field and, also, confirmed the existence of the electroweak phase transition. It is well-known that scalar fields might play a significant role in cosmology. For example, the most common realization of inflation is obtained with one or several scalar fields. A dynamical realization of dark energy arises in a similar process called quintessence. The presence of phase transitions in the Universe's history might drastically alter cosmology, in particular, if topological defects are produced. Cosmic strings are the main candidate among them to play a role in the Early Universe and are precisely obtained with a complex scalar field in a phase transition.

Since the presence of scalar fields is needed in cosmology, but, at the same time, they can lead to disastrous effects, it is crucial to have a clear theoretical understanding of them. In this thesis, we are particularly interested in fluctuation and dissipation dynamics. The context is the following. A scalar field is likely not an isolated object and, therefore, interacts with other degrees of freedom, for example gauge fields. The result of these interactions on the evolution of the scalar field is taken into account by an effective action. There are, in general, two competing effects appearing in the equation of motion and altering the dynamics. On one hand, the interactions lead to a transfer of energy of the scalar field into the other degrees of freedom. This process corresponds to dissipation and appears as a damping term in the equation of motion. On the other hand, the motion of the field is perturbed by fluctuations coming from the same interactions. These forces usually have a stochastic origin. In general, these two effects give rise to the theory of fluctuation-dissipation dynamics and lead to significant consequences that cannot be simply ignored. Fluctuation and dissipation are two effects of the interactions between the scalar field and other degrees of freedom. This common origin implies that the two processes must be related. This is encoded in the fluctuation-dissipation theorem and appears in different contexts in physics, from condensed matter to cosmology.

Fluctuation and dissipation dynamics originates from the Brownian motion of particles. In the nineteenth century, R. Brown, a Scottish botanist studying fertilization processes, observed microscopic particles inside a grain of pollen. He was the first to describe precisely their irregular and random motion. Brownian motion is commonly expected to appear for microscopic particles suspended in a liquid or a gas. Its origin was at first an enigma for physicists. The observation that the rapidity of the motion increases with the temperature was pointing toward a thermal origin of the molecular motion. Such ideas led to the formulation of the kinetic theory of gases by J. C. Maxwell, L. Boltzmann and R. Clausius, where the temperature of a gas is related to the kinetic energy of the particles. Shortly after the publication of the kinetic gas theory, the first main discovery on fluctuation and dissipation dynamics was made by A. Einstein in his study of the Brownian motion.

In 1905, Einstein published a quantitative analysis of the Brownian motion [3]. In this work, he reconciled thermodynamics, that takes into account a large number of particles, with Newtonian mechanics, describing the motion of a single particle. Using the kinetic theory of gases and statistical methods, Einstein derived the mean square displacement of the individual molecules. He proved that the fluctuation of the velocity of the Brownian motion is related to the mobility, defined as the inverse of the damping coefficient. This is encoded in the Einstein relation $D = \mu k_B T$, where D is the diffusion coefficient, μ the mobility, k_B the Boltzmann constant and T the temperature. The Einstein relation is one of the first examples of a relation between fluctuation and dissipation. This work of Einstein was a milestone in the history of physics. Beyond considerations on fluctuation-dissipation, this article provided a mathematical evidence to support the existence of the atoms, a way to estimate the Avogadro's number and confidence on the validity of statistical physics.

The theoretical formulation of the Brownian motion has been achieved shortly after by P. Langevin in 1909 [4]. He amended the equation of motion for the particle, given by Newton's second law, with the addition of a dissipation term and a random force, to take into account the two effects arising from the collisions with the particles in the fluid. The motion of the Brownian particle is described by the Langevin equation

$$m\ddot{q} + \eta\dot{q} + V'(q) = \xi(t) \ , \tag{1.1}$$

where $q(t)$ is the position of the particle as function of time, m the mass, η the

damping coefficient or the inverse of the mobility, $V(q)$ an external potential and $\xi(t)$ an external random force. In the simplest scenario, the random force is expected to follow Gaussian statistics, the average values given by $\langle \xi(t) \rangle = 0$ and the autocorrelation function $\langle \xi(t)\xi(t') \rangle = \Omega \delta(t - t')$, with Ω being the strength of the fluctuation. The validity of the Langevin equation is ensured if the mass m is larger than the masses of the particles in the fluid and if the timescales of interest are much longer than the typical time between two collisions. Due to the presence of stochastic forces, the Langevin equation is not deterministic and cannot be derived from a Lagrangian or a Hamiltonian. This stochastic nature drastically limits the analytical power of the equation and, in practice, it is useful to describe Brownian motion with quantities amenable to a deterministic approach.

Considering N copies of the system described by the Langevin equation introduced in the previous paragraph, the stochastic noise gives a random velocity to the particle in each of the realizations. Moreover, the Gaussian form of the noise must be imprinted on the distribution of the velocities. Instead of having N copies of the system, it is equivalent to be interested in the probability to obtain a certain velocity in a single system. This is the idea behind the Fokker-Planck description of Brownian motion. The transition probability $P(q, v, t \mid q_0, v_0, t_0)$ corresponds to the probability for a particle, initially at position q_0 with velocity v_0 and subject to random forces, to be found later at position q with velocity v. This probability is given by the Fokker-Planck equation [5, 6], which in our simple scenario[1] reads

$$\frac{\partial}{\partial t} P = - \left\{ \frac{\partial}{\partial q} v - \frac{1}{m} \frac{\partial}{\partial v} \left[\eta v + V'(q) \right] - \frac{\Omega}{2m^2} \frac{\partial^2}{\partial v^2} \right\} P \, . \tag{1.2}$$

The Fokker-Planck equation is a linear second-order differential equation and, therefore, deterministic. The solutions of the equation give the distribution functions for the quantities of interest. This formalism is also well-suited to study the approach to equilibrium. In the long time limit, the probability distribution does not depend either on the initial position and velocity or on time. Such a time-independent distribution always formally exists. A comparison with the canonical distribution gives the relation $\Omega = 2\eta k_B T$ which is another formulation of the Einstein relation in terms of the strength of the noise and the damping.

[1] This special form of the Fokker-Planck equation is sometimes referred as the Klein-Kramers, Kramers or Smoluchowski equation.

At a classical level, the Brownian motion is well-described by the Langevin and the Fokker-Planck equations. Troubles arise when considering quantum dissipative systems. The origin of the difficulties lies on the impossibility to write a Lagrangian or a Hamiltonian giving rise immediately to the Langevin equation. This deadlock forbids, a priori, a quantization with standard methods. Several solutions have been proposed, and they mainly go along two directions [7]. One possibility is the definition of a new quantization scheme. However, this approach is tedious since it requires some model-dependent hypotheses. The other direction corresponds to the system-plus-reservoir models. A dissipative system is not isolated and therefore the presence of interactions between the system that is dissipating energy and other degrees of freedom is ensured. It is hard to identify the microscopic origin of the damping, however, the statistical properties of the stochastic forces are known. The main idea behind the system-plus-reservoir models is to formulate precisely the system, the environment and the interaction between them and, then, use standard methods to perform quantization. The choice of the reservoir and the form of the interaction are constrained by the condition that Brownian motion is recovered in the classical limit.

One of the simplest system-plus-reservoir models is named after A. O. Caldeira and A. J. Leggett [8]. This system corresponds to a particle in a potential, defined as the dissipative system, linearly coupled to its environment, a fluctuating reservoir bath. The bath is parametrized as a set of non-interacting harmonic oscillators. The individual Hamiltonians of the dissipative system, the reservoir and the interaction can be written explicitly. The interaction with the environment leads to an effective potential for the dissipative system. The computation of the equation of motion gives a Langevin equation and, in particular, the Gaussian Brownian noise is recovered with a linear dissipation. This simple semi-empirical model correctly reproduces the Brownian motion in the classical limit. Moreover, the knowledge of the Hamiltonian of the system allows for a quantization using standard techniques. The Caldeira-Leggett model provides, therefore, an acceptable analytical description of a quantum dissipative system.

In general, quantum fields are not completely isolated and, therefore, interact with their environment. The analytical description of such a scenario relies on a similar reasoning as in the system-plus-reservoir models introduced for quantum dissipative systems. However, there is an extra effect, specific to a field, that must be taken into account. Beyond the interactions with other fields, self-interaction

plays a significant role. In particular, short wavelengths might influence the long ones and, in a sense, the field acts as its own thermal bath. A separation between the system and the environment is not always possible and a perturbative approach must be followed. The usual method requires to integrate out the extra degrees of freedom in order to obtain an effective action for the background field. The equation of motion that emerges is in the form of a Langevin equation, where fluctuation and dissipation effects on the scalar field are clearly identified. In general, the spectrum of the noise is colored, i.e. is a function of the field, unless there is a linear coupling between the field and the bath. A comprehensive review on the derivation of the Langevin equation for a field is performed in [9].

The formal description of the Early Universe has cosmological fields immersed in a hot medium. Fluctuation and dissipation dynamics is expected to apply and there are several situations where these effects might modify the cosmological model. The most studied example is warm inflation [10, 11]. The dissipative term leads to a continuous production of radiation during the phase of accelerated expansion. The usual picture of inflation is drastically modified. The Universe remains warm during the phase of inflation and the model allows for a smooth transition to the radiation-dominated period, avoiding a phase of (p)reheating. Fluctuation-dissipation dynamics is expected to play a major role in out-of-equilibrium situations, for example, in a phase transition, when the Universe is approaching equilibrium at the new vacuum. Beyond these two scenarios, fluctuation and dissipation effects influence the dynamics of any cosmological fields. Several situations have been identified and discussed in [12]. For these reasons, we believe that a good understanding of fluctuation-dissipation dynamics is pertinent for cosmology.

This is not the purpose of this thesis to explore the origins of the Langevin equation in quantum field theory. This topic has been extensively studied in [9] and in the references therein. The interest here is to investigate some implications of these stochastic equations in the Early Universe. We consider three situations where fluctuation-dissipation dynamics plays a role : phase transitions, warm inflation and escape problems. As a preamble, Chapter 2 is an introduction to the current model of cosmology, the Standard Big Bang Model. We review its theoretical construction based on assumptions stated in the cosmological principle and on methods of general relativity. We study the Friedmann universe, with the usual solutions corresponding to periods dominated by radiation, matter and a cosmological constant. Using the theories of particle

physics, in particular, the Standard Model, we present the thermal history of the Universe. Some considerations on observational cosmology lead us to the current parametrization of the cosmological model, the ΛCDM. The chapter is concluded with a recapitulation of the main successes and limitations of the model.

Chapter 3 is addressing phase transitions and the formation of topological defects. We are interested, in particular, in the definition of a mechanism to provide stability for embedded defects. We begin the chapter with a review of the theory leading to topological defects and present some of their applications in cosmology and in particle physics. After that, we turn our interest to the special case of embedded defects. We stress their relevance in concrete theories such as the Standard Model and state the issues related with their stability. By considering an explicit example, the pion string in the linear sigma model, we introduce the framework necessary for a study of the mechanisms needed to stabilize this kind of defect. We first study the mechanisms that are already present in the literature and consider their limitations. We then propose an extension of these mechanisms and show that, in some circumstances, interactions with a thermal and dense medium allow for the formation of pion strings. This result is the first example of a stable embedded defect in a realistic theory.

In Chapter 4, we focus on another situation where fluctuation and dissipation dynamics plays a significant role, cosmic inflation. We introduce a formalism to define classes of universality among the models of warm inflation. The general theory of inflation is introduced at the beginning of the chapter. We review the shortcomings of the Standard Big Bang Model and show how an accelerated expansion provides an elegant solution for most of the issues. We then present the simplest realization of inflation with a single scalar field. We introduce and contrast the cold and warm scenarios. Some arguments to support the identification of universal properties among the different models of inflation are presented. We also describe a method to achieve it, the β-function formalism. We then show how this formalism is extended to warm models of inflation. Beyond the definition of classes of universality, we illustrate how this approach, which is based on the Hamilton-Jacobi formalism, provides practical tools for a deeper analytical study of the dynamics of warm inflation.

We consider in Chapter 5 more formal aspects of fluctuation and dissipation dynamics, in order to formulate the Kramers problem in quantum field theory. The derivation of an escape rate is a common problem in different areas of physics, such as statistical or condensed matter systems. We begin the chapter with

a pedagogical introduction to the escape rate by considering a classical one-dimensional point particle in a potential. After a description of the problem and the introduction of the theoretical tools to study it, given by the Langevin and Fokker-Planck equations, we consider two equivalent approaches to compute the rate, the flux-over-population and the mean-first-passage-time methods. We also present an explicit proof of their equivalence. In the second part of the chapter, we turn our interest to a scalar field. We propose a definition of the escape problem in quantum field theory. The definition of an escape is not as trivial as in the classical case due to the field theory character of the problem. We propose an explicit computation of the rate of escape using a generalization of the flux-over-population method. We conclude the chapter with a discussion of situations, in cosmology and beyond, where this framework is applicable and leads to relevant effects.

We present our concluding remarks in Chapter 6. Some appendices including details on the theoretical background and on the computations performed along the different chapters are provided at the end of the thesis.

Chapter 2

The Standard Big Bang Model

The aim of cosmology is the answer of a fundamental question of mankind, understanding and describing the evolution and the large scale structure of the Universe. Along the centuries, various theories, together with more and more sophisticated instruments, have been developed to observe and explain the Cosmos. This long quest toward a satisfactory model made a significant step forward in the first half of the twentieth century. At this epoch, two scientific revolutions completely changed the paradigm of the Universe and gave birth to modern cosmology.

At the beginning of the last century, the known Universe was not larger than our galaxy, the Milky Way, and was thought to be static. The prevailing theory of gravity had been stated by I. Newton in the seventeenth century. This state-of-the-art was about to change with the publication of the theory of general relativity by A. Einstein in 1915 [13, 14]. Space and time are not eternal, absolute and independent continua anymore, but unified in a dynamical four-dimensional spacetime. The theory also predicts the geometry of the spacetime to be dependent on its energy content. The second revolution came on the observational side. The astronomer E. P. Hubble was the first to prove the existence of extra galactic objects [15]. He computed the distance to classical Cepheid variables belonging the Andromeda galaxy. With this observation the Universe suddenly became much larger than the Milky Way. This is not the only major contribution of Hubble to cosmology. By measuring the recession velocities of galaxies, he noticed that the distant ones were moving faster [16]. This observation was indicating that the Universe might be non-static but rather

expanding over time. These two revolutions of the first half of last century not only completely changed the understanding of the Universe but also provided the theoretical tools to address it. They constitute the two pillars on which modern cosmology is built.

In this chapter, we first present the theoretical construction of the Standard Big Bang Model. From the cosmological principle and using general relativity, we obtain the Friedmann-Lemaître-Robertson-Walker (FLRW) universe and discuss its energetic contributions. With the help of the Standard Model of particle physics, we introduce the thermal history of a FLRW universe. We conclude with a brief review of observational cosmology and a discussion of the current favored parametrization of the SBBM, the ΛCDM model, with its successes and limitations. For completeness, we provide a compendium on GR in Appendix A.

This brief introduction on modern cosmology is based on the books [17–19]. For the technicalities concerning GR we refer to [20, 21]. Finally, the section about observational cosmology is based on the review [22].

2.1 FLRW Cosmologies

The Standard Big Bang Model is the current theoretical model of cosmology. The construction of the SBBM relies on general relativity. Everyone with a little experience of GR knows how cumbersome it is to obtain a solution of the Einstein equations. However, on large scales[1], the energy distribution of the Universe takes a specific form that drastically simplifies the algebra. This is encoded in the cosmological principle.

2.1.1 The Cosmological Principle and the FLRW Metric

The cosmological principle states that, on large scales, the Universe is spatially homogeneous and isotropic. Today, the principle is well-motivated by independent observations, in particular, from the high degree of homogeneity observed in the cosmic microwave background and from Large Scale Structure (LSS) surveys of galaxies. Historically, however, the principle has been supported by philosophical

[1]By large scales, distances larger than $10h^{-1}$ Mpc are typically assumed. The dimensionless Hubble parameter is defined as $h \equiv H_0/\left(100 \text{ km s}^{-1}\text{Mpc}^{-1}\right)$.

arguments and can be seen as a modern formulation of the Copernican principle. To oppose the geocentric theories of his epoch, N. Copernic stated that the Earth was not occupying a specific location in the Universe. This is the same idea as homogeneity, which implies that the Universe appears the same to any observers, independently of their locations. The cosmological principle is, however, stronger than the Copernican formulation since it also imposes isotropy.

Despite its apparent simplicity, the cosmological principle is an extremely powerful tool in the construction of the metric describing the Universe. Indeed, it imposes symmetries on the spacetime and, in particular, on its spatial part. The homogeneity of space is related to the invariance of the metric over spatial translations. Isotropy means that the Universe looks the same in each direction of observation and corresponds to rotational symmetry. Translated in the language of GR the cosmological principle implies that there are six Killing vectors, three of them related to the translational invariance and the other three to the invariance over rotations. For a space of three dimensions, the maximal number of Killing vectors is six. The principle imposes that the spacetime can be foliated into maximally symmetric spatial hypersurfaces. The metric of a spacetime with a subspace that is maximally symmetric is known exactly and reads

$$\mathrm{d}s^2 = -\mathrm{d}t^2 + a^2(t)\left[\frac{\mathrm{d}r^2}{1-kr^2} + r^2(\mathrm{d}\theta^2 + \sin^2\theta\mathrm{d}\phi^2)\right] , \tag{2.1}$$

where the only two free parameters are the scale factor $a(t)$ and the scalar curvature k of space. The time t is the real time or clock time. This metric is named after A. Friedmann, G. Lemaître, H. P. Robertson and A. G. Walker and is often referred as the FLRW metric. Note that the metric is invariant under the substitutions

$$k \to k/|k| , \qquad r \to \sqrt{|k|}\cdot r , \qquad a \to a/\sqrt{|k|} , \tag{2.2}$$

which allows considering only $k/|k|$. We are left with three relevant cases for the curvature of the spacelike hypersurfaces. Those are $k = -1, 0, +1$ respectively called open, flat and closed universe.

The cosmological principle and the assumption that GR is a valid description of gravity are the only two ingredients to derive the FLRW metric. We observe that the scale factor $a(t)$ allows the Universe to expand over time. We also note the presence of a singularity when the scale factor goes to zero. However, going backward in time with the Universe contracting, a quantum theory of

gravitation is required eventually and, therefore, the current description based on a classical theory of gravity breaks down. The remaining task for cosmologists is the determination of the scalar curvature of space and the evolution of scale factor. A first step is done with GR and the Einstein equations.

2.1.2 Friedmann Equations

The dynamics of the scale factor depends on the energy content of the Universe through the Einstein equations

$$R_{\mu\nu} - \frac{1}{2} R g_{\mu\nu} = 8\pi G T_{\mu\nu} - \Lambda g_{\mu\nu} \ , \tag{2.3}$$

where $R_{\mu\nu}$ is the Ricci curvature tensor, R is the scalar curvature, $g_{\mu\nu}$ is the metric tensor, G is Newton's gravitational constant and $T_{\mu\nu}$ is the stress-energy tensor. We have also explicitly included the cosmological constant Λ.

On the right-hand side of the Einstein equations enters the matter or energy distribution. The homogeneity imposed by the cosmological principle implies the same condition on the distribution of matter. On large scales, the energy distribution must correspond to a perfect fluid, namely a fluid that is isotropic in its rest frame and is only characterized by its pressure p and energy density ρ. Moreover, the homogeneity implies that the pressure and the energy density depend on time but are constant over space. The stress-energy tensor of a perfect fluid takes the simple form of

$$T_{\mu\nu} = (p + \rho) u_\mu u_\nu + p g_{\mu\nu} \ , \tag{2.4}$$

where u_μ is a timelike unit vector, the four velocity of the fluid.

The left-hand side of the Einstein equations is fixed by the geometry of spacetime. For the FLRW metric, the Ricci tensor reads

$$R_{00} = -3\ddot{a}/a \ , \qquad\qquad R_{ij} = \left(a\ddot{a} + 2\dot{a}^2 + 2k\right) h_{ij} \ , \tag{2.5}$$

where $a^2 h_{ij}$ is the ij-component of the metric. The Ricci scalar

$$R = \frac{6}{a^2} \left(a\ddot{a} + \dot{a}^2 + k\right) \ , \tag{2.6}$$

is also directly obtained by taking the trace of the Ricci tensor.

We have all ingredients in hands to write the Einstein equations for a homogeneous and isotropic universe. These are called the Friedmann equations and read

$$H^2 \equiv \left(\frac{\dot{a}}{a}\right)^2 = \frac{8\pi G}{3}\rho + \frac{\Lambda}{3} - \frac{k}{a^2} \,, \tag{2.7}$$

$$\frac{\ddot{a}}{a} = \frac{\Lambda}{3} - \frac{4\pi G}{3}(\rho + 3p) \,, \tag{2.8}$$

where we have defined the Hubble factor H. Note that the second equation is also referred as the Raychaudhuri equation. The Friedmann equations fix the behavior of the scale factor for any given ρ, p and k. Conservation of energy is a direct consequence of the Friedmann equations

$$\dot{\rho} = -3H(\rho + p) \,, \tag{2.9}$$

and is also given by the divergence of the stress-energy tensor, as expected.

Before turning our interest to specific solutions of the Friedmann equations, let us pause to introduce some of the relevant parameters used in cosmology. We have already met the Hubble factor $H = \dot{a}/a$. The Hubble factor is the rate of expansion of the Universe at a given time. It is related to the age and spatial scale of the Universe. The value the Hubble factor today is called the Hubble constant and is denoted by H_0. In general, to indicate the current value of a parameter, the subscript $_0$ is used. The deceleration parameter $q \equiv \ddot{a}a/\dot{a}^2$ expresses the rate of change of the expansion. The critical density is defined as $\rho_{\text{crit}} \equiv 3H^2/8\pi G$. In absence of a cosmological constant, ρ_{crit} is the energy required for a spatially flat universe. The energy density parameter Ω is defined as $\Omega \equiv \rho/\rho_{\text{crit}}$. By definition, the density parameter is dimensionless and $\Omega = 1$ corresponds to a flat universe. The precise determination of the current values for these parameters is the main task of observational cosmology.

Another phenomenon that plays a significant role in cosmology is the redshift. Due to the spatial expansion, all lengths are dilated over time. This is also true for the wavelengths of the photons. In particular, a photon emitted at some time t_{emission} will be observed later with a larger wavelength and, therefore, with a shifting toward the red. This defines the redshift z as

$$z \equiv \frac{\lambda_{\text{today}}}{\lambda_{\text{emission}}} - 1 = \frac{a_0}{a(t_{\text{emission}})} - 1 \,. \tag{2.10}$$

The higher the redshift is, the earlier the photon has been emitted. The redshift is sometime used as a time coordinate. A redshift of zero corresponds to today and it diverges at the singularity. For completeness, in addition to the redshift, the mean temperature of the Universe can be used as a time coordinate. Indeed, an expanding universe is cooling down and there is a one-to-one correspondence between time, redshift and temperature.

2.1.3 Energy Contributions and Associated Solutions

The solutions of the Friedmann equations and, therefore, the evolution of the scale factor $a(t)$ are dictated by the dominant energetic contribution in the Universe. In modern cosmology, the energy budget of the Universe is usually split between three categories : matter, radiation and dark energy (DE). Before discussing them individually, let us introduce the equation of state parameter ω defined as $\omega \equiv p/\rho$. From the conservation of energy in Eq. (2.9) the energy density becomes

$$\rho \sim \exp\left\{-3\int(1+\omega)d\ln a\right\} \sim a^{-3(1+\omega)}\ , \tag{2.11}$$

assuming a constant ω in the last step. The first Friedmann equation (2.7) can be expressed as

$$\left(\frac{H(t)}{H_0}\right)^2 = \sum_i \Omega_{i,0}\left(\frac{a(t)}{a_0}\right)^{-3(1+\omega_i)} - \frac{k}{a_0^2H_0^2}\left(\frac{a(t)}{a_0}\right)^{-2}\ , \tag{2.12}$$

where the sum runs over the different energetic contributions (radiation, matter and the cosmological constant). The last term in (2.12), which depends on the curvature of space, is not a contribution to the energy density. For this reason, we have not defined a density parameter for the curvature, which is sometimes called Ω_k in the literature.

We now discuss the different contributions individually and the associated expansion when they dominate the RHS of Eq. (2.12). We will show that a FLRW universe where all energy components are present is likely to be initially dominated by radiation, then by matter and finally by DE.

Non-relativistic Matter The matter contribution includes all non-relativistic and collisionless form of matter, including cold dark matter. In this case, the

pressure is negligible with respect to the energy density and, therefore, the equation of state parameter is simply zero. Solving the Friedmann equations gives

$$\rho \sim a^{-3} \,, \qquad a(t) \sim t^{2/3} \,, \qquad H = \frac{2}{3t} \,. \tag{2.13}$$

The energy density decreases as a^{-3} since the expansion of a three-dimensional space reduces the number density by a factor of a in each direction. When this component dominates, we refer to a matter-dominated universe.

Radiation Gas of radiation and relativistic particles belong to this category. The stress-energy tensor of radiation is known and reads

$$T^{\mu\nu} = \frac{1}{4\pi}\left(F^{\mu\lambda}F^{\nu}{}_{\lambda} - \frac{1}{4}g^{\mu\nu}F^{\lambda\sigma}F_{\lambda\sigma}\right) \,, \tag{2.14}$$

with $F_{\mu\nu}$ being the electromagnetic field-strength. The trace of the electromagnetic stress-energy tensor vanishes. Comparing with the trace of Eq. (2.4) implies that radiation has an equation of state parameter $\omega = 1/3$. The solution of the Friedmann equations for a radiation-dominated universe gives

$$\rho \sim a^{-4} \,, \qquad a(t) \sim t^{1/2} \,, \qquad H = \frac{1}{2t} \,. \tag{2.15}$$

The inverse quartic dependence of the energy density on the scale factor is explained by two effects. The first is the decrease of the number density of the relativistic particles as a^{-3} due to the expansion of the Universe. This is the same effect that gives $\rho \sim a^{-3}$ in a matter-dominated universe. The second is the energy loss of individual particles which goes as the inverse of a and is due to the redshift of the frequency. Note that, going backward in time, the radiation contribution will eventually dominate over the matter due to the inverse quartic dependence. This is also expected in a very hot and dense early universe, where most of the particles are relativistic. In the SBBM, the Universe is expected to go across a radiation-dominated phase followed by a period of matter-domination.

Dark Energy The cosmological constant, also referred as dark energy, is a constant contribution to the stress-energy tensor

$$T^{\Lambda}_{\mu\nu} = -\frac{\Lambda}{8\pi G}g_{\mu\nu} \,. \tag{2.16}$$

Equating with the energy-momentum tensor of the perfect fluid Eq. (2.4), we get the following relation

$$\rho = -p = \frac{\Lambda}{8\pi G} \,, \tag{2.17}$$

which implies that $\omega = -1$. The Friedmann equation leads to a constant Hubble factor and, therefore, an exponential expansion for the scale factor. Comparing with the evolution of the energy densities for matter or radiation, we see that over time and, even if extremely small, a non-zero cosmological constant will aways dominate eventually.

The FLRW Universe is the successful application of GR to a homogeneous and isotropic universe as assumed with the cosmological principle. It realizes the desired feature of a universe expanding over time. The theoretical cosmological setup being established we can proceed in two ways. From observational cosmology, a concrete parametrization of the SBBM is obtained. This leads to the current prevailing model of cosmology, the ΛCDM model. Before discussing it in details, let us review the thermal history of the Universe. This is based on the current theories of particle physics and the main characteristics are independent on the exact parametrization of the SBBM.

2.2 Thermal History of the Hot Big Bang Model

The SBBM predicts an initially hot and dense universe that expands and, therefore, cools down over time. At sufficiently high temperatures, all particles are expected to be at thermal equilibrium. The elementary particles, as well as the interactions necessary to keep them at equilibrium, are known from the Standard Model of particle physics [23–27]. When the Universe cools down, the interaction rate Γ, that depends on the temperature, decreases. In general, when the interaction rate becomes smaller than the Hubble rate H, meaning that there is less than one interaction per Hubble time, the equilibrium cannot be maintained and the species decouples. Using the theories of particle physics, in particular, the SM, the different epochs in the history of a FLRW universe are identified and studied. This leads to the thermal history of the Hot Big Bang Model.

A precise understanding of the first two stages of the Universe's history is limited by the current status of theoretical physics. At the scale of the Planck

temperature, $T_{Pl} = 1.2 \cdot 10^{19}$ GeV, quantum gravitational interactions are relevant. Since a satisfactory quantum theory of gravity is not established yet, an exact description of this epoch is not possible. Above temperatures of order of 1 TeV, the description of the Universe is limited by the current model of particle physics. The Standard Model is robust for energies up to the electroweak transition. Above this scale, several theories have been proposed, for example Super-Symmetry (SUSY) [28–30] and Grand Unified Theories (GUT) [31, 32]. Speculations about the existence of exotic particles, possibly explaining the origin of dark matter (DM), and about the formation of topological defects, in a cascade of phase transitions from a larger symmetry group to the SM, are possible. However, a concrete and satisfactory model is still lacking.

On the cosmological side, at these energies, the Universe is assumed to undergo a phase of inflation followed by baryogenesis. Inflation is an initial accelerated expansion most likely due to a scalar field. This phase of inflation elegantly solves some problems of the SBBM and, also, provides an explanation for the formation of structures[2]. Baryogenesis is the early production of matter giving rise to the matter/anti-matter asymmetry observed in the Universe. Inflation and baryogenesis are still far from being concrete models and are among the main focuses of modern cosmology.

At a temperature of order of 100 GeV the electroweak transition is taking place. The elementary particles of the SM get their masses with the Higgs mechanism [24, 25] and the SM begins to prevail. The Universe is filled with a soup of free quarks, leptons and photons at thermal equilibrium. When the temperature drops below 300 MeV, the QCD transition happens. The quarks are not free particles anymore but get confined into hadrons. The Universe is a hot plasma made of pions, nucleons, leptons and photons. Note that, at this stage, the Universe is still opaque to light. The photons do not propagate freely but keep interacting with all the other particles.

With the temperature that keeps decreasing, the weak interaction rate becomes too small to maintain at thermal equilibrium the particles that interact only weakly. These species are the first ones to decouple. This process might happen for certain postulated form of DM species and most certainly for neutrinos. The neutrinos decouple from thermal equilibrium at a temperature of 1 MeV and their number density freezes out. When T becomes smaller than the electron mass,

[2]The basics of inflation are discussed in greater details in Chapter 4.

electrons and positions cannot be produced anymore via pair-production. They annihilate each other via the reverse process and their energy is transferred to the photons. The neutrinos being already decoupled, they are not affected and their temperature decreases simply as a^{-1} due the redshift. Therefore the SBBM predicts a different temperature for the photons and the relic neutrinos[3].

The synthesis of matter, called nucleosynthesis, starts at a temperature of about 100 keV. The energy is not high enough anymore to break the bonds between the nucleons. Neutrons and protons combine to form nuclei. The mechanism is very similar to a construction game. A proton interacts with a neutron to form a deuterium nucleus, emitting a photon. The deuterium nucleus interacts with a proton to produce helium-3 and a photon. Helium-3 and deuterium form helium-4 nuclei and protons. The process could potentially continue, however, there are no stable nuclei with exactly eight nucleons. This constitutes a bottleneck and implies that most of the production channels finish with helium-4. There are some less probable processes leading to the production of lithium-7 and also some left-over of helium-3 and deuterium. Other elements such as carbon or oxygen, with more massive nuclei, are produced later, presumably by nucleosyntheses in the interior of stars. The density being larger, it is possible to go beyond the bottleneck with an interaction of three helium-4 nuclei. The produced amount of helium-4 depends on the expansion rate and is therefore precisely predicted by the SBBM. There is a good agreement between the observed abundance of helium-4 and the value predicted by the model [33]. This is another strong support for the SBBM and the existence of an initial radiation-dominated phase. The model, however, fails to predict the observed amount of lithium-7 [34–37]. This is called the cosmological lithium problem [38] and is one of the open questions of cosmology.

At a temperature of 0.75 eV the energy densities of matter and radiation are equal. This is referred as the matter-radiation equality and the Universe enters the matter-dominated epoch. When T is of order of 0.3 eV the phase of recombination starts. The electrons combine with nuclei to form hydrogen atoms. The large number of photons compared to the abundance of baryons explains why recombination did not happen already at a temperature corresponding to the binding energy of hydrogen. During recombination the number density of free electrons drops significantly and the mean-free path of photons increases. At the end of this process, the photons propagate freely and the Universe becomes

[3]A calculation involving the conservation of entropy leads to $T_\gamma = (11/4)^{1/3} T_\nu$.

transparent to light. The photons have decoupled from all other species and form the cosmic microwave background. Before the Universe became transparent, all wavelengths of electromagnetic radiation were instantaneously absorbed. The Universe was, therefore, an almost perfect blackbody. The photons propagating freely after the time of last-scattering, the blackbody spectrum is expected to be imprinted in the CMB. The detection of the CMB in 1964 by A. A. Penzias and R. W. Wilson [39], its strong homogeneity and its blackbody spectrum [40] are another successes of the SBBM.

Finally, the Universe enters into the Dark Ages where the formation of galaxies slowly takes place.

2.3 Observational Cosmology and the ΛCDM Model

We have introduced and discussed general characteristics of FLRW cosmologies. In particular, the evolution of an initially dense and hot universe that is expanding and cooling down over time. The precise parametrization of the model is obtained from observational cosmology. We briefly review the experimental methods to measure the main parameters of the model. We then introduce the current parametrization of the SBBM. The thermal history of a FLRW universe is to a large extent fixed, however, its fate depends strongly on the actual parametrization of the model, in particular, on the presence of a cosmological constant.

2.3.1 Observing the Universe

The relevant parameters related to the global description of the Universe are the ones entering the Friedmann equations : the density parameters of the various energy species, the curvature of space and the Hubble constant. We review the experimental methods to extract these parameters and state their current measured values. Unless explicitly stated, experimental data is taken from [22]. The parameters related to the departure from homogeneity and structure formation are discussed in Chapter 4, dedicated to cosmic inflation.

Let us start with the total energy density parameter Ω, that is the sum of

the individual energetic contribution (matter, radiation and DE). One method to obtain the current value Ω_0 is summing over the values of the different contributions $\Omega_{m,0}$, $\Omega_{r,0}$ and $\Omega_{\Lambda,0}$. A precise discussion on the measurement of these parameters is given below. Another way to obtain Ω_0 relies on the equivalence between a measurement of the total energy density parameter and the spatial curvature of the Universe since Eq. (2.7) can be written as

$$\Omega_0 - 1 = \frac{k}{H_0^2 a_0^2} \, , \tag{2.18}$$

where a_0 is the current value of the scale factor, usually set to 1. Note that this method requires that the Hubble factor is measured independently. The spatial curvature of the Universe can be extracted from the properties of CMB. After the matter-radiation equality, large scale structures begin to form. Matter is attracted by gravity into regions of higher density. The increase of temperature in these regions leads to an increase of the radiation pressure. The pressure tends to push matter away, competing against gravity and creates acoustic oscillations. These oscillations influence the shape of the angular power spectrum of the anisotropy of the CMB. In particular, the locations of its peaks depend on the geometry of the Universe. The Boomerang experiment [41] obtained $0.88 < \Omega_0 < 1.12$ at 95% confidence level (CL) favoring a spatially flat universe. This measurement was then confirmed by several experiments such as the Planck satellite, measuring $\Omega_0 = 1.001 \pm 0.002$ at 68% CL [42].

Let us turn to the measurement of the individual contributions to the total energy. Several contributions appear in the matter density : ordinary baryonic matter, CDM and, possibly, massive neutrinos. There are different methods to obtain the total matter contribution, which sums up to a value of $\Omega_m = 0.3 \pm 0.1$ at 68% CL. One possibility is to estimate the abundance of baryonic matter and evaluate the ratio of dark versus ordinary matter. The baryon density Ω_b corresponds to the ordinary matter and includes dust, gas, stars and the planets. The spectrum of the anisotropies of the CMB is a precious source of information when deriving these parameters. For example, the relative heights of the peaks depend on the density of baryons and their overall amplitudes depend on the ratio between dark and ordinary matter. There are other methods to estimate Ω_b based on direct observation and on predictions of the abundance during Big Bang nucleosynthesis. The baryon contribution is measured as $\Omega_b = 0.048 \pm 0.001$ at 68% CL, implying that most of the matter contribution, about 85% in the Universe, comes from dark matter.

Photons and massless neutrinos are the main contributions to radiation. From the temperature of the CMB today, $T_\gamma = 2.73$ K, the energy density parameter of the photons can be computed to give

$$\Omega_\gamma = 5.38(10) \cdot 10^{-5} \, . \tag{2.19}$$

The contribution from the neutrinos is derived from Ω_γ. The difference in the temperature between the relic neutrinos and the photons in the CMB is known to differ by a factor of $(4/11)^{1/3}$. Keeping into account that neutrinos are left-handed fermions, such that there is only one spin state to consider, gives

$$\Omega_\nu = 3 \cdot (7/8) \cdot (4/11)^{4/3} \cdot \Omega_\gamma \, , \tag{2.20}$$

where three species of massless neutrinos have been assumed. The radiation density is currently a negligible contribution to the total energy budget of the Universe. However, due to its dependence on the scale factor, radiation was the dominating the energy budget in the past.

The last component to be determined is dark energy. For long, this contribution was supposed to vanish giving a closed matter-dominated universe, with cold dark matter as the main contribution in the energy budget. However, measurements from Type Ia supernova [43] indicated that the Universe was accelerating, by predicting a nonzero $\Omega_{\Lambda,0}$ from the constrain $\frac{4}{5}\Omega_{m,0} - \frac{3}{5}\Omega_{\Lambda,0} = -0.2 \pm 0.1$. This measurement led to an intense debate among cosmologists until the present acceleration was confirmed by observations coming from the CMB. The observed value of Ω_0 is in agreement with one and, therefore, $\Omega_\Lambda \simeq 1 - \Omega_m$. Note that the nature of DE is still an open question. One possibility is the presence of a cosmological constant. The vacuum energy coming from quantum field theory (QFT) is a natural candidate to explain its origin. However, the theoretical expectation for the vacuum energy of QFT exceeds the observed value of the cosmological constant by several orders of magnitude. This discrepancy would imply an extreme fine-tuning and constitutes the cosmological-constant problem [44]. A dynamical realization of DE is a possibility, for example with a scalar field. The features are similar to inflation and the process is called quintessence [45, 46]. In this case, the equation of state parameter might be slightly different from -1.

The last parameter related to global properties of the Universe to be discussed is the Hubble constant H_0 which corresponds to the current rate of expansion.

After this short review of observational cosmology, we should not be surprised that different methods exist to measure H_0. The historical one, originally used by Hubble, is based on astronomical measurements. H_0 is extracted from the recession velocities of distant galaxies. However, this estimation requires knowing precisely the distance to the receding galaxy, which is based on a cosmological ladder. The latest value for H_0 from astronomical observation [47] is

$$H_0 = 74.03 \pm 1.42 \text{ km s}^{-1}\text{Mpc}^{-1} \, . \tag{2.21}$$

Another method to extract the Hubble factor is from the anisotropic power spectrum of the CMB [42] and gives a value of

$$H_0 = 67.37 \pm 0.54 \text{ km s}^{-1}\text{Mpc}^{-1} \, . \tag{2.22}$$

These two measurements of H_0 are obtained from completely different methods. Despite the apparent tension between the two results, it is already promising that the actual values are close to each other. A measurement using gravitational waves (GW) will provide a third independent way to obtain H_0 and might discriminate between the other two observations.

2.3.2 ΛCDM Model

The current parametrization of the SBBM is called the ΛCDM model. It corresponds to a spatially flat universe dominated by dark energy and where the matter energy density is mostly in the form of dark matter. Let us discuss some properties of the model.

Cold Dark Matter In the ΛCDM model, about a quarter of the total energy content is in the form of non-baryonic matter (or dark matter). The idea that only a fraction of the total matter content in the Universe is made of ordinary matter exists in cosmology for about a century and is supported by indirect astrophysical and cosmological observations. One of the earliest and most known examples is the work of F. Zwicky aiming at explaining the observed rotation curves of galaxies [48].

Dark matter is expected to obey the following properties [22, 49]. From the analysis of structure formation, DM should be non-relativistic (cold) at the

epoch of the formation of the galaxies. In order to be dark, the interaction with electromagnetic radiation is very weak. It is also expected to be stable over the time scale of the Universe, otherwise, it would have decayed.

The physics of dark matter is an active topic and plays a crucial role in modern cosmology. The current and most favoured candidates for DM are axions [50, 51], primordial black holes [52, 53], sterile neutrinos [54] and weakly interacting massive particles (WIMPs) originally coming from supersymmetric extensions of the SM [55]. A full discussion of these models goes beyond the scope of this work. We send, therefore, the interested readers to the reviews [22, 49] and the references therein.

Age of the Universe The age of the Universe is derived from the Friedmann equations

$$t_0 = \int_0^{t_0} dt = \int_0^{a_0} \frac{da}{aH} = \frac{1}{H_0} \int_0^{\infty} \frac{dz}{(1+z)\mathcal{H}(z)} \,, \tag{2.23}$$

where $\mathcal{H}$ is defined as

$$\mathcal{H}^2(z) \equiv \frac{H^2}{H_0^2} = (1-\Omega_0)(1+z)^2 + \Omega_{\Lambda,0} + \Omega_{m,0}(1+z)^3 + \Omega_{r,0}(1+z)^4 \,, \tag{2.24}$$

to give an age of 13.8 ± 0.04 Gyr using value for the Hubble constant given by CMB measurements. Note that a first validity check imposes that the predicted age of the Universe is older than anything inside it. As we already mentioned, the description based on GR breaks down before reaching the singularity. Therefore, Eq. (2.23) is not strictly the age of the Universe but rather the time elapsed since the Universe could be described by a classical theory of gravity.

Fate of the Universe The ΛCDM parametrization fixes the fate of the Universe. Since the matter and the radiation energy densities are decreasing over time, the dark energy density will dominate eventually, its evolution being constant. This is already happening as the DE-matter equality was after 9 Gyrs. The Universe is currently dominated by the cosmological constant and is accelerating. A characteristic feature of the ΛCDM is the prediction of a universe that expands for ever and the expansion will be faster and faster. The expansion will be eventually faster than the speed of light and distant galaxies will not be in causal contact any more. The observable Universe will reduce to the local structure that

is tight to our galaxy by the attraction of gravity.

Successes and Limitations of the Model To conclude this introduction on the modern formulation of cosmology and its preferred model, let us summarize its successes and discuss some open questions. The SBBM is based on GR and describes a homogeneous and isotropic universe. It predicts a non-static universe, initially hot and dense that expands and cools down over time. Including an early phase of inflation, it also provides an explanation for the existence of small anisotropies in the CMB leading to the formation of structures. The SBBM underwent some significant experimental successes, in particular, the observed homogeneity of the CMB, its almost perfect blackbody spectrum and the abundance of light elements, such as helium-4.

The current cosmological model is, however, incomplete. The origin of the dark energy and a well-defined particle physics model that includes DM are still missing pieces. The main features of the early period of inflation are getting better understood. However, a precise model is still lacking. Both the presence or the absence of topological defects need to be justified. The theory is also not providing a satisfactory explanation for the apparent asymmetry between particles and anti-particles and the observed abundance of lithium-7. On the observational side, the tension in the measurement of the Hubble constant from the CMB and astronomical methods needs to be explained.

Chapter 3

Stabilization of Embedded Topological Defects

3.1 Introduction

From the Grand Unified Theory epoch, where the strong and the electroweak forces are expected to have been unified in a single gauge group, to the later stage of the Standard Model and going below the energy scale where hadrons are formed, the Early Universe is presumed to have undergone a series of phase transitions. During each spontaneous breaking of symmetry (SSB), it is possible that topological defects (TD) are produced [56]. Monopoles and domain walls usually lead to undesired effects for the cosmological model. Cosmic strings may, however, explain several open questions in cosmology, such as primordial density perturbations and structure formation [57, 58], generation of the primordial magnetic fields [59, 60] and baryogenesis [61, 62]. They also lead to the emission of high-energy particles, such as cosmic and gamma rays and neutrinos [63, 64], and relic gravitational waves [65]. Moreover, the non-observation of defects constrains the possible inflationary models and the gauge group of the GUT. For these reasons, the quest for topological defects has been an active field of research among particle physicists and cosmologists for the last 30 years.

Embedded defects are a special class of topological defects [66]. They are constructed by constraining a subset of fields in the given theory to vanish, while others continue to have solutions of the unconstrained system. If the vacuum

manifold of the remaining unconstrained part of the system results in having a non-trivial homotopy group, the formation of a topological defect can occur. This defect is, therefore, embedded in the larger theory. Embedded defects are of particular interest since they are constructed in realistic systems in nature. Two known examples are the chiral model with the pion string [67], which is the focus of our analysis in this chapter, and the Glashow-Weinberg-Salam model with the electroweak string [68, 69]. However, the stability of embedded defects is not guaranteed as their existence is not strictly due to the topology of the full theory. Usually, they are not stable in vacuum. An escape of the field into the constrained directions is always possible and the configuration is continuously deformed to the trivial vacuum. If the presence of these defects is desired, the model requires the inclusion of a stabilization mechanism.

One of the simplest examples of embedded defects appears as a special non-trivial solution in chiral models described by the linear sigma model (LSM) of quantum chromodynamics (QCD). The pion string corresponds to a classical solution of the LSM, where the charged pion fields are constrained to vanish. Chiral models are effective models commonly used to understand many aspects of QCD and, in particular, used in investigations related to heavy-ion collision experiments. One may wonder if pion strings might indeed be produced during the quark-gluon plasma to hadron phase transition. If it is the case, their presence would be relevant in both nuclear and Early Universe physics.

The question of the stability of the pion string is of crucial importance and has been the focus of some previous works. In [70], M. Nagasawa and R. H. Brandenberger proposed a realistic mechanism to stabilize the pion string by putting the system in a thermal bath of photons, whereby interactions of the electromagnetic field with the charged plasma lead to a lifting of the effective potential in the constrained fields direction. More recent works by J. Karouby and Brandenberger [71, 72] confirm the stabilization effect of this mechanism. Whether this effect is large enough to have a stable string in the region of parameters that is experimentally accessible has been the subject of recent discussions [73, 74].

In this chapter, we study an extension of this stabilization mechanism by placing the system not only in a thermal environment but also in a dense medium, which is accounted for by including a non-vanishing chemical potential. In addition to the charged plasma, the interactions with fermions (quarks) will also be included. Thus, the model we will work with is the linear sigma model with

quarks (LSMq). These interactions will then generate further corrections to the effective potential, making explicit the chiral phase transition that can occur in the LSMq for instance. These modifications will lead to a physically more realistic model than has been studied up to now [73, 74]. The string solution will now be altered, as it depends on the temperature and the chemical potential. The analysis of the stability to follow will show that the production of stable strings depends on the order of the chiral phase transition. The results presented in this chapter have been published in [1].

The chapter is organized as follows. In Sec. 3.2, we review the theory of topological defects, their construction, classification and the consequences for cosmology. We also introduce the embedded defects and stress the differences with the standard configuration. In Sec. 3.3, we briefly review the LSMq at finite temperature and chemical potential. In the same section, we introduce the pion string solution in vacuum and study its stability. We review the mechanisms introduced to stabilize the string and discuss their limitations. Section 3.4 is dedicated to the stability analysis of the strings in the thermal and dense medium, in the chiral limit. We also present a first examination of the physical case. We conclude the chapter in Sec. 3.5 with a discussion. Some technical details on the computations are given in Appendix B.

3.2 Review of Topological Defects in Cosmology

The theory of topological defects is based on the popular concept of spontaneous breaking of symmetry in field theory and the associated phase transition. The formation of defects in a phase transition is ensured by the Kibble mechanism and the homotopy theory provides a condition on the existence and a classification of the defects. If topological defects are produced in the Early Universe, they lead to important consequences for cosmology. In this section, we also introduce the special case of topological defects embedded in a larger theory. We stress their interesting characteristics but, also, the issues related to their stability. Topological defects have been introduced by T. W. B. Kibble in 1976 in [56]. For more recent discussions on this topic, we refer to [17, 57, 75–79].

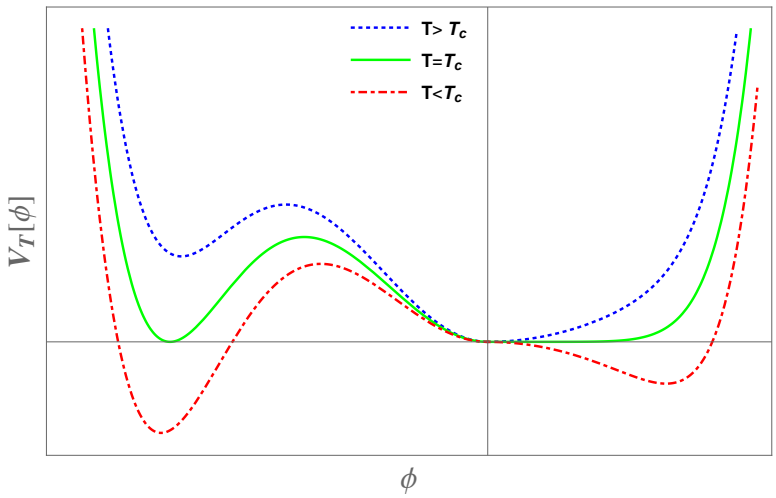

Figure 3.1 *On the left-hand side, there is an example of a first-order phase transition. Below the critical temperature T_c, the former global minimum at the origin becomes a false vacuum. On the right-hand side, an example of a second-order phase transition is shown. The minimum of the potential moves away from the origin smoothly.*

3.2.1 Spontaneous Symmetry Breaking and Phase Transitions

In the Early Universe, when the temperature is sufficiently high, electromagnetic, weak, and strong forces are possibly unified into a larger gauge symmetry group G, described in the context of Grand Unified Theory [31, 32]. The cooling down of the Universe leads to a hierarchy of spontaneous breakings of symmetry, from G into successive subgroups

$$G \to H_i \to ... \to H_1 \to H_0 \,, \tag{3.1}$$

where $H_1 = SU(3)_{\rm C} \times SU(2)_{\rm L} \times U(1)_{\rm Y}$ and $H_0 = SU(3)_{\rm C} \times U(1)_{\rm em}$. The SSB from G to H takes place when the Higgs-like field adopts a non-trivial ground state that is invariant under transformations in H but not over G. This breaks the original symmetry.

The nature of the phase transition, the critical temperature T_c and the phase diagram are obtained from the temperature dependent effective potential V_{eff} of the theory. Depending on the potential, the phase transition can be of first- or second-order. In a first-order transition, a global minimum of V_{eff} develops when $T < T_c$. In a classical description, the field would be trapped in the fake trivial ground state assuming the potential barrier between the old and new minimum

is large enough. At quantum level, tunneling effects allow the nucleation of bubbles of true vacuum. As discussed in Chapter 5, thermal fluctuations might also lead to bubble nucleation. There is a non-zero probability that a bubble of true vacuum appears at a certain point of space. Once created and if the bubble is energetically favorable[1], it expands in a sea of false vacuum. A first-order transition is mediated by quantum tunneling and thermal nucleation. The ground state $\langle\phi\rangle$ is a discontinuous function of time. A second-order transition is characterized by the smooth evolution of the ground state away from zero toward a non-vanishing value, when the temperature drops below T_c. In this case, $\langle\phi\rangle$ evolves continuously in time and the transition is homogeneous. Examples of first- and second-order phase transitions are shown on the left and right sides of Fig. 3.1 respectively.

3.2.2 Kibble Mechanism

In 1976, T. W. B. Kibble [56] demonstrated that a spontaneous breaking of symmetry might lead to the production of topological defects[2]. The mechanism, further discussed in [57, 81], is based on the formation of uncorrelated domains in which the expectation value $\langle\phi\rangle$ is coherent. In a second-order transition, the evolution of the ground state is influenced by quantum and thermal effects and there is no reason to expect $\langle\phi\rangle$ to be uniform in space. When the transition is first-order, the value the field takes in a newly created bubble is completely independent of the existing ones. In both cases, there is the formation of correlated domains, corresponding to regions of space with arbitrary orientation of the Higgs-like field. These domains correspond to different minima of the effective potential and, when they merge together, a non-trivial vacuum configuration is obtained. The value of the potential being non-minimal between the domains, some potential energy is trapped and creates a topological defect.

The Kibble mechanism ensures the existence of these domains. The argument is based on the correlation length ξ of the field responsible for the SSB. It is fair to assume that the size of a correlated domain is of order ξ. One can show that the correlation length is proportional to the inverse temperature-dependent mass of

[1] This depends in general on the energy gain from the inside of the bubble versus the energy loss in the bubble's wall.

[2] This mechanism has been later extended by W. H. Zurek in [80] and is sometimes called the Kibble-Zurek Mechanism (KZM).

the field m_ϕ

$$\xi \sim m_\phi(T)^{-1} \sim T^{-1} \, . \tag{3.2}$$

When the mass vanishes, the correlation length diverges which is in obvious contradiction with causality. Kibble pointed out that ξ should be bounded by the particle horizon d_h defined as

$$d_h(t) \equiv a(t) \int_0^t \frac{dt'}{a(t')} \, , \tag{3.3}$$

where $a(t)$ is the scale factor of the Universe. Here, d_h is the maximal proper distance a photon created at the Big Bang could have traveled until time t. It corresponds to the radius of the region of spacetime in causal contact with the field. For $a(t) \sim t^n$ and $n > 1$, we have $d_h = t/(n-1)$. The age of the Universe being finite in the Big Bang Model, the radii of the correlated domains are bounded by a finite quantity d_h. Their existence is, therefore, ensured and one defect per particle horizon is expected to be produced.

3.2.3 Existence and Classification of Topological Defects

The existence and the type of defect created in a specific model relies on algebraic topology, more specifically, on homotopy. Our aim in this subsection is to perform a brief review, based on Ref. [57], of the concepts needed to describe the different types of defects. For a complete and formal description, we suggest the reader to refer to Ref. [82].

In a spontaneous breaking of symmetry from the group G to H, the associated vacuum manifold is defined as the coset space $\mathcal{M} = G/H$. It corresponds to the set of degenerate vacuum states. The topology of the vacuum manifold determines whether the formation of a defect is possible and the type of defect that might arise. The formal description of the topology is given by the theory of homotopy.

Definition. *Let ψ_1 and ψ_2 be two maps from $\mathcal{S}^n$ to $\mathcal{M}$. ψ_1 and ψ_2 are homotopically equivalent if there exist a continuous one-parameter family of maps $\psi(t) : \mathcal{S}^n \to \mathcal{M}$ such that $\psi(0) = \psi_1$ and $\psi(1) = \psi_2$.*

The maps ψ_1 and ψ_2 are said to be homotopic, denoted by $\psi_1 \sim \psi_2$. Conceptually two maps are homotopic if they can be continuously deformed into each other.

Definition. *The n^{th}-homotopy group of $\mathcal{M}$, $\pi_n(\mathcal{M})$ is the set of all homotopy classes of maps $\mathcal{S}^n \to \mathcal{M}$: $\pi_n(\mathcal{M}) = \{\psi | \psi : \mathcal{S}^n \to \mathcal{M}\} / \sim$.*

One can show that for $n > 0$, $\pi_n(\mathcal{M})$ is a group. Despite these abstract definitions, it is not difficult to interpret the role of the homotopy group. Let us consider for example the fundamental group π_1. If this group is trivial, all loops on $\mathcal{M}$ can be deformed into a point. This is no longer true if there is a hole on the manifold, since it is not possible to shrink a loop surrounding this hole into a point. It also cannot be continuously deformed into a loop that has a different number of windings around the hole. In this case, there are infinitely many classes of loops on the manifold and $\pi_1(\mathcal{M}) = \mathbb{Z}$. Conceptually, the fundamental group simply counts the number of holes on the manifold. Similar arguments can be made for higher order homotopy groups, where instead of loops, n-spheres are considered.

The zeroth homotopy group is special and its definition need to be clarified :

Definition. *Let x and y be points in $\mathcal{M}$. We define an equivalence class on $\mathcal{M}$ by $x \cong y$ if there exist a continuous path $\gamma : [0,1] \to \mathcal{M}$, such that $\gamma(0) = x$ and $\gamma(1) = y$. The zeroth homotopy group is defined as $\pi_0(\mathcal{M}) = \{\gamma | \gamma : [0,1] \to \mathcal{M}\} / \cong$.*

Conceptually, this group corresponds to the set of path connected components of $\mathcal{M}$.

As already mentioned, the homotopy theory allows a classification of the topological defects that can be produced in a phase transition. Let us briefly present this classification :

- If $\pi_0(\mathcal{M}) \neq 1$, the vacuum manifold is disconnected. Assume that $\mathcal{M}$ has two components $\mathcal{M}_1$ and $\mathcal{M}_2$. There will be domains where $\phi \in \mathcal{M}_1$ and some others where $\phi \in \mathcal{M}_2$. At the interface of these domains, we will have $\phi \notin \mathcal{M}$. The potential is not minimized and some potential energy is trapped. This scenario corresponds to domain walls.

- If $\pi_1(\mathcal{M}) \neq \mathbb{1}$, there are non-contractible loops in the vacuum manifold. In the interior of a loop, there is a singularity of $\mathcal{M}$ where obviously $\phi \notin \mathcal{M}$. There is therefore a tube of trapped energy, known as the cosmic string. The string cannot have loose ends, since in this case the loop could be contracted to a point. This implies that the strings are either infinite or closed.

- The other two examples of topological defects usually present in the literature are the monopoles, arising when $\pi_2(\mathcal{M}) \neq \mathbb{1}$ and the textures when $\pi_3(\mathcal{M}) \neq \mathbb{1}$.

Before proceeding to the discussion of embedded defects, let us briefly review the cosmological consequences of topological defects.

3.2.4 Consequences for Cosmology

Commonly present in the theory, topological defects are of a particular interest for cosmologists and the quest for their detection has been an active field of research over the last decades. As we will learn shortly, the existence of a defect could affect the cosmological model [17, 75, 76]. They might lead to desired outcomes, such as a mechanism for the formation of structures, and undesired effects, for example overcoming the energy budget and modifying the expansion rate of the Universe. On the other hand, the non-observation of topological defects provides some further constraints on the model. This is particularly relevant for BSM theories. A candidate for the GUT gauge group or a model of inflation might predict the formation of defects. Examples of theories including inflation and defects are Supergravity [83] or Brane-Inflation [84]. Topological defects provide a top-down probe for the physics beyond the Standard Model and a non-observation might potentially rule out certain inflationary and GUT models.

We have learned that different kinds of defects are produced, depending on the homotopy group of the vacuum manifold. Among them, cosmic strings are the most promising candidates to play a decisive role in cosmology. One can show that the energy density of a non-relativistic domain-wall depends on the inverse of the scale factor. Unless the model is too highly fine-tuned to be relevant, the domain-walls will be the dominant component in the energy budget of the Universe and drastically alter the model. The production of monopoles represents also a problem in the SBBM. Computing their energy density today shows that monopoles produced at the epoch of grand unification would completely dominate the matter density, which is in obvious contradiction with their non-observation at present time. This is known as the monopole problem and is one of the original motivations for the theory of cosmic inflation[3]. For the rest of this subsection, we focus on the cosmic strings and their cosmological implications.

[3]The monopole problem and its solution is discussed with greater details in the next chapter.

Cosmic Strings In the presence of a string, the spacetime adopts a conical structure around the defect. It has been shown by A. Vilenkin in [85] that the metric outside an infinite and straight cosmic string of mass per unit length μ reads

$$ds^2 = -dt^2 + dz^2 + dr^2 + (1 - 4G\mu)^2 r^2 d\theta^2 \ , \tag{3.4}$$

with the string being in the z direction. The metric is similar to Minkoswki but with a defect angle of $\Delta\theta = 8\pi G\mu$ leading to the conical shape of the space[4]. There are three main consequences from such a geometry.

The first is gravitational lensing. An observer will see two objects located on the other side of the string and separated by an angle $\Delta\theta$ superimposed. The second effect leads to anisotropies in the CMB. A moving string leads to a Doppler shift in the frequency of a nearby light beam. The part of the beam located behind the string is blueshifted and the part ahead, redshifted. This process can explain the variations in the temperature of the CMB and predict fluctuations of order $\delta T/T \simeq 8\pi G\mu v$, where v is the velocity of the string [86, 87]. The observed anisotropies of the CMB constrain the mass per unit length to be $G\mu \leq 10^{-5}$. It is fair to point out that the string are active and incoherent, therefore they do not lead to baryonic acoustic oscillations and could only account for maximally 10% of the anisotropies in the CMB [88]. The last consequence of the conical structure of space is the formation of a wake. The mechanism is the following. In the rest frame of a string, moving with velocity v, matter moves with velocity $-v$. When passing near the string, the particles are deflected and get an inward or wake velocity of $4\pi G\mu v$. Matter converges in the region behind the string. The overdensity in this region keeps attracting matter with gravitational interaction and leads to the formation of structures [57, 58]. Cosmic strings present an alternative to inflation and provide a first principle mechanism for the formation of structures. However, it is now established that the dominant mechanism for structure formation cannot come from topological defects [41].

Another relevant cosmological consequence of cosmic strings is the production of relic gravitational waves [65]. Considering a network of cosmic strings, the interactions between them lead to the creation of closed loops. The loops interact with the strings and between themselves to create smaller and smaller loops. A small closed loop oscillates relativistically due to the tension of the string and

[4]We observe that for $dz = dt = 0$ the surface is not a plane but a cone.

emits GW. The power radiated is computed to give

$$P_{GW} \simeq \gamma_{GW} G\mu^2 \,, \tag{3.5}$$

where γ_{GW} is a constant of order 100. With cosmology entering a new era since the observation of gravitational waves, new constraints on the presence of cosmic string will emerge from their GW's signatures [89–91].

Even if cosmic strings cannot be the main mechanism to explain the formation of structures, they might still play a significant role in particle physics and cosmology. We have already mentioned that they provide constraints on BSM theories. Cosmic strings can be the origin of the primordial magnetic field [59, 60]. It has been shown in [59] that a network of superconducting strings carrying a charged current might generate a magnetic field. The string motion and the gravitational attraction in the primordial plasma generate a field by vorticity. In addition, cosmic strings have been used to explain the baryon asymmetry in the framework of the electroweak baryogenesis [61, 62] and, more recently, proposed as the origin of high-redshift supermassive black holes [92].

3.2.5 Embedded Defects

Embedded defects are a special class of topological defects. They have been originally introduced in [66] and investigated in more detail in [93–95]. The basic idea is the following. If the vacuum manifold $\mathcal{M}$ of the full theory is reduced to a lower dimensional manifold $\mathcal{M}_{\text{emb}}$, by constraining some fields to vanish, topological defects may arise from the homotopy groups of $\mathcal{M}_{\text{emb}}$ when the subgroup G_{emb} is spontaneously broken. If the theory constructed from G_{emb} allows the formation of a topological defect, i.e. there is a positive n such that $\pi_n(\mathcal{M}_{\text{emb}}) \neq \mathbb{1}$, the solution can be extended to the full theory by constraining the other fields direction. The defects are said to be embedded in a larger theory.

The main benefit of this method is to allow for the formation of defects in theories where the homotopy groups associated with the vacuum manifold are trivial. One example is the Standard Model of particle physics that does not predict any topological defect. However, the SM contains two known examples of embedded defects, the pion string [67] in the chiral model and the electroweak string [68, 69] in the Glashow-Weinberg-Salam model. One naturally expects to have similar realizations in BSM theories.

By construction, the stability of embedded defects is not guaranteed. Their existence is not strictly due to the topology of the full theory. Under infinitesimal perturbations, the unconstrained fields escape in the constrained directions and the configuration is continuously deformed to the trivial vacuum. One usually need a case-by-case analysis and an extra mechanism has to be introduced to ensure the stability. This is precisely the role of fluctuation-dissipation dynamics, in particular, the interaction with a thermal bath, as we will learn shortly, tend to stabilize the defects.

In the remainder of this chapter, we aim to study these mechanisms with an explicit example, the pion string in the linear sigma model.

3.3 The Pion String in the Linear Sigma Model

The pion string is one of the simplest examples of embedded defects. It appears in the chiral model of quantum chromodynamics (QCD) as a classical solution of the linear sigma model where the charged pions are constrained to vanish. This simple model is well-suited to perform an analysis of stability and study the mechanisms to improve it. Beside these theoretical considerations, it has some direct applications for heavy-ion collision experiments and in the quark-gluon plasma to hadron phase transition in the Early Universe.

As expected, the pion string is not stable in vacuum. It has been shown in [71] that interactions with a thermal bath tends to stabilize the string. However, the mechanism is not sufficient to have stable strings for the set of parameters that are experimentally allowed. In our analysis, we want to study the effect of the more realistic scenario of the pion string in a dense and hot medium. The theoretical framework is, therefore, the linear sigma model with quarks (LSMq).

In this section, we briefly introduce the LSMq [96–98] and the pion string solution. We discuss the instability of the strings and review the known stabilization mechanisms, in particular, the interactions with a thermal bath.

3.3.1 LSMq at Zero Temperature

It is well-known that QCD becomes non-perturbative at low energy due to color confinement. However, the approximate chiral symmetry in the QCD Lagrangian

and its spontaneous breaking allows for the definition of a low-energy effective theory with hadrons replacing the quarks and gluons as degrees of freedom. Chiral models have long been used in many applications aiming at understanding various aspects of QCD, among them, the description of disoriented chiral condensates in heavy-ion collisions or the chiral phase transition. The LMSq is, therefore, an effective model to study the chiral transition and includes the additional fermionic degrees of freedom (the quarks) that are present during the phase transition.

The aim of this chapter being the analysis of the stability of embedded defects, we only include, for simplicity, the one-loop contributions. This is already sufficient to illustrate the main characteristics of the stabilisation mechanism. Details about higher-order contributions to chiral models, in particular, the resummation of the perturbation theory (optimized perturbation theory), can be found in Refs. [99–101].

The LSMq is a concrete realization of chiral effective theory and describes interactions between nucleons, pions and sigma fields. We consider its simplest realization, containing two massless quarks in a fermionic isodoublet $\psi^{\mathrm{T}} = (u,\ d)$, a triplet of pseudoscalar pions ($\vec{\pi}$) and a scalar field sigma (σ). The Lagrangian density of the model reads

$$\mathcal{L} = \mathcal{L}_{\Phi} + \mathcal{L}_{q} \ , \tag{3.6}$$

$$\mathcal{L}_{\Phi} = \mathrm{Tr}\left[(\partial_{\mu}\Phi)^{\dagger}(\partial^{\mu}\Phi)\right] - m^{2}\mathrm{Tr}\left[\Phi^{\dagger}\Phi\right] - \lambda\left(\mathrm{Tr}\left[\Phi^{\dagger}\Phi\right]\right)^{2} + \frac{1}{2}h\mathrm{Tr}\left[\Phi^{\dagger}+\Phi\right] \ , \tag{3.7}$$

$$\mathcal{L}_{q} = \bar{\psi}(i\partial\!\!\!/ - \gamma^{0}\mu_{q} + g(\sigma + i\vec{\pi}\cdot\vec{\tau}\gamma_{5}))\psi \ , \tag{3.8}$$

where $\Phi = \sigma\cdot\frac{\mathbb{1}}{2} + i\vec{\pi}\cdot\frac{\vec{\tau}}{2}$ is the meson matrix in Dirac space, $\vec{\tau}$ are the Pauli matrices with the normalization $\mathrm{Tr}[\tau_a\tau_b] = 2\delta_{ab}$ and $\mathbb{1}$ is the identity matrix. Finally, μ_q is the quark chemical potential. The term dependent on h in Eq. (3.7) is an explicit symmetry breaking term. This term mimics the breaking of the chiral symmetry in the QCD Lagrangian due to the non-vanishing quark masses.

In the limit of vanishing h, the model has a chiral symmetry $SU(2)_L \times SU(2)_R$. The spinors $\psi_{L,R} = \frac{1}{2}(1 \pm \gamma_5)\psi$ belong to the fundamental representation of the group, transforming as

$$\psi_{L,R} \to \exp(-i\vec{\omega}_{L,R}\cdot\vec{\tau})\psi_{L,R} \ . \tag{3.9}$$

The scalar fields transform in the $(\frac{1}{2},\frac{1}{2})$ representation,

$$\Phi \to \exp(-i\vec{\omega}_L \cdot \vec{\tau})^\dagger \Phi \exp(-i\vec{\omega}_R \cdot \vec{\tau}) \ . \tag{3.10}$$

It is easy to check that under such a transformation the Lagrangian density (3.6) is invariant.

The Φ-dependent part of the Lagrangian density is often explicitly expressed in terms of the pion ($\vec{\pi} \equiv (\pi_0, \pi_1, \pi_2)$) and sigma ($\sigma$) fields,

$$\mathcal{L}_\Phi = \frac{1}{2}(\partial_\mu \sigma)^2 + \frac{1}{2}(\partial_\mu \vec{\pi})^2 - V_0(\sigma, \vec{\pi}) \ , \tag{3.11}$$

$$V_0(\sigma, \vec{\pi}) = \frac{\lambda}{4}(\sigma^2 + \vec{\pi}^2 - v_0^2)^2 - h\sigma \ , \tag{3.12}$$

where $v_0^2 = \frac{m^2}{\lambda} \equiv f_\pi^2$ corresponds to the pion decay constant in the vacuum.

The linear term in (3.7) breaks the chiral symmetry explicitly by giving a non-trivial vacuum expectation value to the σ field. To construct the classical fundamental state, the minimum of the potential is considered,

$$\frac{dV_0}{d\sigma} = \lambda(\sigma^2 + \vec{\pi}^2 - v_0^2)\sigma - h = 0 \ , \tag{3.13}$$

$$\frac{dV_0}{d\pi_i} = \lambda(\sigma^2 + \vec{\pi}^2 - v_0^2)\pi_i = 0 \ . \tag{3.14}$$

The unique solution of the system is

$$\vec{\pi}_0 = 0 \ , \qquad\qquad \lambda(\sigma_0^2 - v_0^2)\sigma_0 = h \ , \tag{3.15}$$

and the vacuum expectation value v of the σ field to first-order in h reads

$$v = f_\pi + \frac{h}{2\lambda f_\pi^2} \ . \tag{3.16}$$

Assuming that $\sigma = \sigma' + v$, where $\langle \sigma' \rangle_0 = 0$, we obtain the shifted Lagrangian density

$$\begin{aligned} \mathcal{L}_\Phi =& \frac{1}{2}(\partial_\mu \sigma')^2 + \frac{1}{2}(\partial_\mu \vec{\pi})^2 - \frac{1}{2}(-m^2 + 3\lambda v^2)\sigma'^2 - \frac{1}{2}(-m^2 + \lambda v^2)\vec{\pi}^2 \\ & - \lambda \sigma' v(\sigma'^2 + \vec{\pi}^2) - \frac{\lambda}{4}(\sigma'^2 + \vec{\pi}^2)^2 - \sigma'(-m^2 v + \lambda v^3 - h) \ , \end{aligned} \tag{3.17}$$

$$\mathcal{L}_q = \bar{\psi}\left[i\partial\!\!\!/ - \gamma^0 \mu_q + gv + g(\sigma' + i\vec{\pi} \cdot \vec{\tau}\gamma_5)\right]\psi \ . \tag{3.18}$$

Note that the term linear in σ' vanishes due to (3.15). In this shifted Lagrangian, the quarks become massive and the masses of the mesons are non-degenerate, with vacuum values,

$$m_{q,0} = gv \ , \qquad m^2_{\sigma,0} = -m^2 + 3\lambda v^2 \ , \qquad m^2_{\pi,0} = -m^2 + \lambda v^2 \ . \tag{3.19}$$

The parameters g, λ and h (note that $m^2 = \lambda f_\pi^2$) are chosen to fit the observable vacuum values, in particular, the pion mass, $m_{\pi,0} = 139$ MeV, the pion decay constant, $f_\pi = 93$ MeV, and also the constituent quark mass $m_{q,0}$ and the mass for the sigma, $m_{\sigma,0}$, whose values will be explicitly set below.

Often, the chiral limit of the model is considered. In the absence of the linear breaking term ($h = 0$), the chiral symmetry is spontaneously broken when the σ field develops a vacuum expectation value $v = v_0 \equiv f_\pi$. In the symmetry broken phase, the pions become massless and correspond to the Goldstone bosons.

3.3.2 Chiral Phase Transition at Finite Temperature and Chemical Potential

The LSMq at finite temperature and chemical potential undergoes a phase transition in the (μ_q-T) plane. Following the arguments of Ref. [102], we assume that the most important contributions to the free energy come from the interactions with the quarks[5]. The quantum and thermal fluctuations of the meson fields are neglected (note that this is also a valid assumption in the large-N approximation for the model [103]). The (renormalized) free energy or effective potential at one-loop [97, 98, 102] reads

$$V_{\text{eff}}(T, \mu_q) = V_0 + \Delta V_0 + \Delta V_{T,\mu_q} \ , \tag{3.20}$$

where

$$V_0 = -\frac{1}{2}m^2 v^2 + \frac{\lambda}{4}v^4 - hv \ , \tag{3.21}$$

$$\Delta V_0 = \frac{N_c N_f}{(4\pi)^2} m_q^4 \left(\frac{3}{2} + \ln \frac{M^2}{m_q^2} \right) \ , \tag{3.22}$$

[5]The σ and $\vec{\pi}$ fields are replaced by their expectation values. At high T and μ_q, constituent quarks are light but mesonic excitations heavy, only the quarks and antiquarks are, therefore, retained as quantum fields. Note that this approximation neglects the effects of the hadronization process at lower T and μ_q.

$$\Delta V_{T,\mu_q} = -2N_c N_f T \int \frac{d^3k}{(2\pi)^3} \left[\ln\left(1 + e^{-\frac{\omega_k}{T} - \frac{\mu_q}{T}}\right) + \ln\left(1 + e^{-\frac{\omega_k}{T} + \frac{\mu_q}{T}}\right) \right] , \quad (3.23)$$

where $\omega_k = \sqrt{k^2 + m_q^2}$, $N_c = 3$ is the number of colors, $N_f = 2$ is the number of flavors and M is the regularization scale used in dimensional regularization in the $\overline{\text{MS}}$ scheme. An explicit derivation of the effective potential is presented in Appendix B.

The expectation value of the field σ in the medium $\langle\sigma\rangle = v(T, \mu_q)$ corresponds to the minimum of the effective potential and is determined by

$$\left.\frac{dV_{\text{eff}}}{dv}\right|_{v=v(T,\mu_q)} = 0 . \quad (3.24)$$

This leads to the gap equation,

$$\begin{aligned} -m^2 + \lambda v^2 + \frac{N_c N_f}{4\pi^2} g^4 v^2 \left[1 + \ln\frac{M^2}{g^2 v^2}\right] \\ + \frac{N_c N_f}{\pi^2} g^2 \int_0^\infty dk \frac{k^2}{\omega_k} \left[n_F^+(\omega_k) + n_F^-(\omega_k)\right] = \frac{h}{v} , \end{aligned} \quad (3.25)$$

where

$$n_F^\pm = \frac{1}{e^{\frac{\omega_k}{T} \mp \frac{\mu_q}{T}} + 1} , \quad (3.26)$$

is the Fermi-Dirac distribution for particles and antiparticles.

Let us analyze the chiral limit $h = 0$ and the physical case $h \neq 0$ separately.

Chiral Limit

For large T and μ_q, the chiral symmetry is restored. Equation (3.24) is trivially satisfied with $v(T, \mu_q) = 0$, and the masses of the mesons are degenerate. The fermions are massless. The chiral symmetry is spontaneously broken when the effective potential develops a non-trivial minimum $v(T, \mu_q) \neq 0$.

The masses of the mesons σ and π are given by their tree-level contributions plus the respective self-energies, which in our approximation are given by the one-loop corrections due to the Yukawa interaction,

$$m_\sigma^2 = -m^2 + 3\lambda v^2 + \Pi_\sigma^{(\text{ren})} , \quad (3.27)$$

$$m_\pi^2 = -m^2 + \lambda v^2 + \Pi_\pi^{(\mathrm{ren})} \,, \tag{3.28}$$

where $\Pi_\sigma^{(\mathrm{ren})}$ and $\Pi_\pi^{(\mathrm{ren})}$ are the renormalized one-loop self-energies for the sigma and the pions, respectively, and given by (see, e.g., Ref. [97])

$$\begin{aligned}\Pi_\sigma^{(\mathrm{ren})} = \frac{N_c N_f}{4\pi^2}\Bigg\{ & g^4 v^2 \left(1 + 3\ln\frac{M^2}{g^2 v^2}\right) \\ & + 4g^2 \int_0^\infty dk\, \frac{k^2}{\omega_k}\left[n_F^+(\omega_k) + n_F^-(\omega_k)\right]\left(1 - \frac{g^2 v^2}{\omega_k^2}\right) \\ & - 4\frac{g^4 v^2}{T}\int_0^\infty dk\, \frac{k^2}{\omega_k^2}\left[n_F^+(\omega_k)(1 - n_F^+(\omega_k)) + n_F^-(\omega_k)(1 - n_F^-(\omega_k))\right]\Bigg\} \,,\end{aligned} \tag{3.29}$$

and

$$\Pi_\pi^{(\mathrm{ren})} = \frac{N_c N_f}{4\pi^2}\left\{ g^4 v^2 \left(1 + \ln\frac{M^2}{g^2 v^2}\right) + 4g^2 \int_0^\infty dk \frac{k^2}{\omega_k}\left[n_F^+(\omega_k) + n_F^-(\omega_k)\right]\right\} \,. \tag{3.30}$$

The explicit computation of $\Pi_\sigma^{(\mathrm{ren})}$ and $\Pi_\pi^{(\mathrm{ren})}$ is given in Appendix B.

Using Eq. (3.30) in the gap equation (3.25) gives, for $h = 0$,

$$-m^2 + \lambda v^2(T, \mu_q) + \Pi_\pi^{(\mathrm{ren})} = 0 \,, \tag{3.31}$$

which is simply the condition that the pions become massless in the broken phase, in agreement with the Goldstone theorem.

We obtain the phase diagram of the model in the (T, μ_q) plane numerically. The parameters are fixed by the following conditions. The vacuum expectation value of the field is $v_0 = f_\pi = 93$ MeV

$$\left.\frac{dV_0}{dv}\right|_{v=v_0} = 0 \,, \tag{3.32}$$

and we require that this minimum is preserved when quantum corrections are included,

$$\left.\frac{d}{dv} V_{\mathrm{eff}}(T = 0, \mu_q = 0)\right|_{v=v_0} = 0 \,. \tag{3.33}$$

This equation requires the one-loop self energy of the pion at zero temperature and zero external momentum to vanish [98], which in turn fixes the renormalization

scale $M^2 = m_q^2/e$. The mass of the sigma field in vacuum is in the broad resonance interval, $400\,\mathrm{MeV} \leq m_\sigma \leq 800\,\mathrm{MeV}$. For our analysis, we set it as

$$m_\sigma^2 = \frac{d^2}{dv^2} V_{\mathrm{eff}}(T=0,\mu_q=0)\Big|_{v=v_0} = (600\ \mathrm{MeV})^2, \tag{3.34}$$

and, for the constituent quark mass, we choose

$$m_q = gv|_{v=v_0} = 300\ \mathrm{MeV}\ . \tag{3.35}$$

Although there is some freedom in the choice of m_σ within the broad resonance interval, this barely influences the stability of the string. Thus, we find the following set of parameters,

$$\begin{aligned} m^2 = \lambda v_0^2 \simeq (567.7\ \mathrm{MeV})^2\ , \qquad & g \simeq 3.2\ , \\ \lambda = \frac{1}{2}\left(8\frac{N_c N_f}{(4\pi)^2} g^4 + \frac{m_\sigma^2}{v_0^2}\right) \simeq 37.3\ , \qquad & M^2 = \frac{m_q^2}{e} \simeq (182.0\ \mathrm{MeV})^2\ . \end{aligned} \tag{3.36}$$

An analysis of the effective potential (3.20) shows that the order of the phase transition depends on T and μ_q (which are related along the phase transition curve). For low temperatures and large chemical potential, the shape of the effective potential V_{eff} is typical of a first-order phase transition, as can be seen in Fig. 3.2. In this case, at $T = T_c$, there are degenerate minima with the origin and the expectation value jumps discontinuously at the transition point. Then, there is a critical point, which is around $T = 50$ MeV and $\mu_q = 306$ MeV, above which (as the temperature increases and the chemical potential decreases) the phase transition becomes second-order. From Fig. 3.3, we observe that the minimum of the potential moves smoothly away from zero. The phase diagram in the $(\mu_q - T)$ plane is shown in Fig. 3.4.

Physical Case

When $h \neq 0$, the symmetry is never completely restored, with $v(T,\mu_q)$ approaching zero for large values of T and μ_q. This behavior corresponds to a crossover transition. The gap equation gives

$$-m^2 + \lambda v^2(T,\mu_q) = -\Pi_\pi^{(\mathrm{ren})} + \frac{h}{v(T,\mu_q)}\ . \tag{3.37}$$

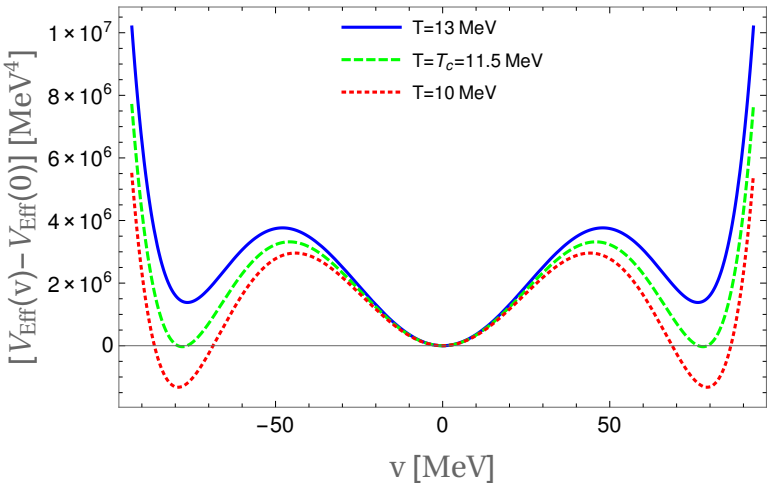

Figure 3.2 *The effective potential, in the chiral limit, for a fixed value of chemical potential $\mu_q = 322$ MeV and for values of temperature above, at and below the critical temperature T_c. Here, $T_c = 11.5$ MeV.*

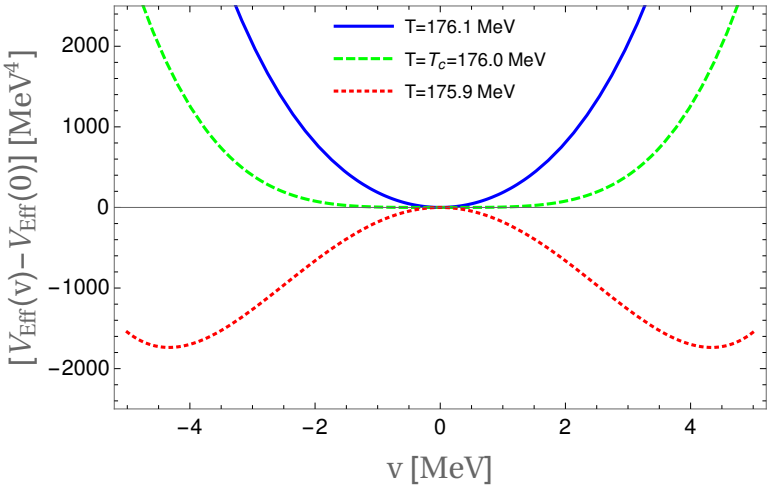

Figure 3.3 *The effective potential, in the chiral limit, for $\mu_q = 0$ MeV and for values of temperature above, at and below the critical temperature T_c. Here, $T_c = 176.0$ MeV.*

The pions are pseudo-Nambu-Goldstone bosons with mass squared $m_\pi^2 = \frac{h}{v(T,\mu_q)}$. The parameters are fixed by the same requirements as in the chiral limit and the extra condition on the pion masses in vacuum being set to their physical value $m_{\pi,0} = 139$ MeV. For this case, we find the following set of parameters,

$$\begin{aligned} m^2 &= \lambda v_0^2 - \frac{h}{v_0} \simeq (541.6 \text{ MeV})^2 , & g &\simeq 3.2 , \\ \lambda &= \frac{1}{2}\left(8\frac{N_c N_f}{(4\pi)^2}g^4 + \frac{m_\sigma^2}{v_0^2} - \frac{h}{v_0^3}\right) \simeq 36.2 , & M^2 &= \frac{m_q^2}{e} \simeq (182.0 \text{ MeV})^2 , \\ h &\simeq 1.8 \cdot 10^6 (\text{MeV})^3. \end{aligned} \tag{3.38}$$

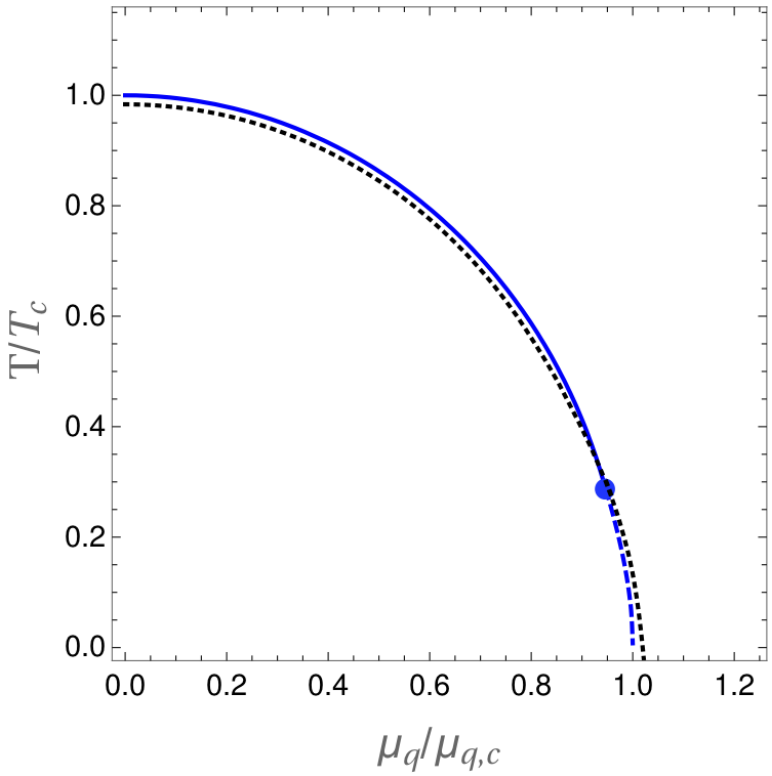

Figure 3.4 *The phase diagram in the (μ_q-T) plane. The solid and dashed curves are for the chiral limit ($h = 0$) and correspond to the second-order and first-order transition lines, respectively, with the critical point shown by a blue dot. The dotted curve is for the physical case ($h \neq 0$) and represents a crossover transition. Temperature and chemical potential are normalized by the critical values in the chiral limit: $T_c = 176\ MeV$ and $\mu_{q,c} = 323\ MeV$. For the crossover, we have the pseudocritical values $T_{pc} = 172\ MeV$ and $\mu_{q,pc} = 329\ MeV$.*

In the physical case, the effective potential exhibits a crossover transition, as shown in Fig. 3.5. Observe that the minimum of the potential moves smoothly toward zero as the temperature increases. The derivation of the crossover transition line on the $(\mu_q - T)$ plane is performed numerically, with the result depicted in Fig. 3.4 together with the case for the chiral limit for comparison. In our computation, where we have considered both vacuum and thermal fluctuations for the fermions in the effective potential, we find only a crossover line. There are though other approximations where the crossover line can end and merge with a first-order phase transition line in a critical end point (see, e.g., Refs. [98, 102]).

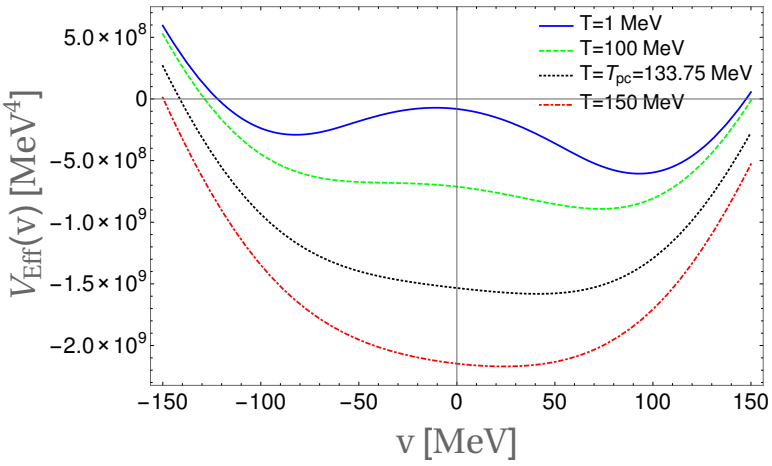

Figure 3.5 *The effective potential in the physical case for a fixed value of chemical potential $\mu_q = 220$ MeV. It shows a crossover phase transition as the temperature is changed. There is a pseudocritical temperature at $T_{pc} = 133.75$ MeV determined by the position of the inflection point of the σ field expectation value.*

3.3.3 Pion String Solution and its Stability in Vacuum

We show that the chiral limit of the LSM has an embedded defect, the pion string, and review the mechanisms already present in the literature to improve the stability.

Pion String Solution

In Ref. [67], X. Zhang, T. Huang and R. Brandenberger derived a stringlike classical solution in the LSM, in the chiral limit and in the vacuum. Defining the new fields ϕ and $\pi^{\pm}$ as

$$\phi \equiv \frac{\sigma + i\pi^0}{\sqrt{2}} , \qquad \pi^{\pm} \equiv \frac{\pi^1 \pm i\pi^2}{\sqrt{2}} , \tag{3.39}$$

the Φ-dependent part of the Lagrangian density is rewritten as

$$\mathcal{L}_{\Phi} = (\partial_\mu \phi)^*(\partial^\mu \phi) + (\partial_\mu \pi^+)(\partial^\mu \pi^-) - \lambda \left(\phi^* \phi + \pi^+ \pi^- - \frac{v_0^2}{2} \right)^2 . \tag{3.40}$$

Considering a static configuration, the energy functional, in the vacuum, reads

$$E_0 = \int d^3x \left[\vec{\nabla}\phi^* \cdot \vec{\nabla}\phi + \vec{\nabla}\pi^+ \cdot \vec{\nabla}\pi^- + \lambda \left(\phi^* \phi + \pi^+ \pi^- - \frac{v_0^2}{2} \right)^2 \right] , \tag{3.41}$$

and the time-independent equations of motion are

$$\nabla^2\phi = 2\lambda\left(\phi^*\phi + \pi^+\pi^- - \frac{v_0^2}{2}\right)\phi\ , \tag{3.42}$$

$$\nabla^2\pi^\pm = 2\lambda\left(\phi^*\phi + \pi^+\pi^- - \frac{v_0^2}{2}\right)\pi^\pm\ . \tag{3.43}$$

Since the vacuum manifold of this model is simply $\mathcal{M} = S^3$, the homotopy group is trivial and does not predict any formation of topological defects [76]. However, if one of the directions of the fields is constrained, in particular, those for the charged fields $\pi^\pm$, there is an overall $U(1)$ symmetry in the (σ, π^0) directions. When the chiral symmetry is broken, an embedded topological pion string can form. These equations admit the following pion string solution

$$\phi = \frac{v_0}{\sqrt{2}}\rho(r)e^{in\theta}\ , \qquad\qquad \pi^\pm = 0\ , \tag{3.44}$$

where r and θ are the polar coordinates in the (x, y) plane and the integer n is the winding number. The string has a linear extension in the z direction. The pion string obviously minimizes the energy of the system and satisfies the equations of motion.

The radial function $\rho(r)$ is found by substituting Eq. (3.44) into the equation of motion and using the boundary conditions,

$$\rho(r) = \begin{cases} 0\ , & r \to 0\ , \\ 1\ , & r \to \infty\ . \end{cases} \tag{3.45}$$

An exact solution is obtained with numerical methods. However, it has been shown in Ref. [67] that a variational approach can be adapted in this situation. Adopting the ansatz $\rho(r) \simeq (1-e^{-\mu r})$ obviously satisfies the boundary conditions. The variational parameter μ is the inverse width of the string and is chosen to minimize the energy. One finds that the energy per unit length E_z is

$$E_z = \frac{\pi}{4}v_0^2 + \pi v_0^2 I(\mu, R) + \frac{\lambda\pi v_0^4}{\mu^2}\frac{89}{288}\ , \tag{3.46}$$

where

$$I(\mu, R) = \int_0^R dr\ \frac{\rho^2(r)}{r}\ , \tag{3.47}$$

and R is a cut-off parameter since the energy density of a string solution is

logarithmically divergent for a global symmetry. As described in Ref. [73], the size of the horizon or the typical separation length between the strings are generally taken for R and is of order of 1 fm. The R dependence vanishes when computing the derivative of E_z with respect to μ. A straightforward computation gives $\mu^2 = \frac{89}{144}\lambda v_0^2$ and, therefore, the energy per unit length becomes

$$E_z \simeq \pi v_0^2 \left[\frac{3}{4} + \log[\mu R]\right] , \tag{3.48}$$

where we have approximated the integral $I(\mu, R)$ as $\log[\mu R]$.

Stabilization Mechanism by Thermal Effects

The string solution (3.44) is non-topological. As it stands, once formed it will decay away. The non-trivial field configuration can be continuously deformed to a trivial vacuum by escaping in the constrained directions. In other words, under an infinitesimal excitation of the fields $\pi^{\pm}$, the induced variation of the energy is negative, the string configuration unwinds and decays.

It is, however, possible to stabilize the string. If one of the directions of the fields is lifted, in this case the $\pi^{\pm}$, then we are left with the overall $U(1)$ symmetry. This is the scenario studied by Nagasawa and Brandenberger in [70], where the authors propose a mechanism to stabilize the pion string by putting the system in a finite-temperature plasma. The interactions between charged pions and photons increase the effective potential in the $\pi^{\pm}$ directions.

In the minimal coupling prescription, the Lagrangian of the model becomes

$$\begin{aligned}\mathcal{L} = (\partial_\mu \phi)^*(\partial^\mu \phi) + (D^+_\mu \pi^+)(D^{-\mu}\pi^-) - \lambda\left(\phi^*\phi + \pi^+\pi^- - \frac{v_0^2}{2}\right)^2 \\ - \frac{1}{4}F_{\mu\nu}F^{\mu\nu} ,\end{aligned} \tag{3.49}$$

where $D^+_\mu = \partial_\mu + ieA_\mu$ and $D^-_\mu = \partial_\mu - ieA_\mu$. The effective potential for the $\pi^{\pm}$ fields acquires a thermal mass due to the coupling with the photons. It has been shown in [104] that the thermal mass is $e^2T^2\pi^+\pi^-/2$ and the effective potential reads

$$V_{eff} = \lambda\left(\phi^*\phi + \pi^+\pi^- - \frac{v_0^2}{2}\right)^2 + \frac{e^2T^2}{4}\pi^+\pi^- . \tag{3.50}$$

The variation of energy, neglecting the $(\pi^+\pi^-)^2$ term, reads

$$\delta E = \int d^3x \left[\vec{\nabla}\pi^+ \vec{\nabla}\pi^- + \left(\frac{e^2T^2}{4} + 2\lambda(\phi^*\phi - \frac{v_0^2}{2}) \right) \pi^+\pi^- \right] + \mathcal{O}((\pi^+\pi^-)^2) \ . \tag{3.51}$$

Using the string solution and expanding $\pi^\pm$ in Fourier modes

$$\pi^\pm = v_0 \chi_m(r) e^{\pm im\theta} \ , \tag{3.52}$$

we find δE in cylindrical coordinates

$$\delta E = 2\pi v_0^2 \int dz \int r \ dr \left[\chi_m'^2(r) + \frac{m^2}{r^2}\chi_m^2(r) + \left(\frac{e^2T^2}{4} + \lambda(\rho^2(r) - 1) \right) \chi_m^2(r) \right] \ . \tag{3.53}$$

We set $m = 0$ to consider the minimal contribution to the energy. Since $\rho^2(r) - 1 = e^{-\mu r}(e^{-\mu r} - 2)$, variation of the mass per unit length compared to the embedded string, where $\chi = 0$, is

$$\delta E_z - \delta E_z|_{\chi=0} = 2\pi v_0^2 \int_0^R dr \ r\chi^2(r) \left[\frac{e^2T^2}{4} - 2\lambda v_0^2 e^{-\mu r}(1 - \frac{1}{2}e^{-\mu r}) \right] \ . \tag{3.54}$$

The sign of equation (3.54) gives us a sufficient condition for the stability of the string. In the integrand, $r\chi^2(r)$ is always positive and will not influence the overall sign. A positive variation of energy corresponds to

$$\frac{e^2T^2}{4} - 2\lambda v_0^2 e^{-\mu r}(1 - \frac{1}{2}e^{-\mu r}) > 0 \ . \tag{3.55}$$

The function $e^{-\mu r}(1 - \frac{1}{2}e^{-\mu r})$ has its maximal value $\frac{1}{2}$ at $r = 0$. We obtain the following condition for stability

$$\frac{e^2T^2}{4} - \lambda v_0^2 > 0 \ . \tag{3.56}$$

Using the values given in Eq. (3.36) and that $e^2 = 4\pi/137$, we find that a lower bound for the temperature of the thermal bath associated with the stability of the pion string core is

$$T_{\text{stab}} > \frac{2v_0\sqrt{\lambda}}{e} \simeq 2.8 \text{ TeV} \ . \tag{3.57}$$

This is, however, a temperature that is much above the critical temperature for chiral phase transition, $T_c \sim 176$ MeV. Thus, even if the mechanism enhances the stability of the strings, it is not sufficient enough for the production of stable strings at temperatures corresponding to the chiral phase transition. Our aim for the rest of the chapter is to try to improve the mechanism. We study the effect of the inclusion of additional thermal and dense effects from the Yukawa interaction and show that it can lead to stability, in certain situations.

3.4 Stabilization of the Pion String in a Thermal and Dense Medium

As shown previously, the interactions between the charged pions and the photons increase the effective potential in the $\pi^{\pm}$ directions and act to stabilize the string. We follow the same strategy but, in addition to the thermal bath, we also consider the effects of a dense medium due to the interactions with the fermions.

3.4.1 Pion String Solution at Finite-Temperature

Using standard techniques [105], a non-zero chemical potential μ_q is set for the fermions and the thermal bath is implemented by the electromagnetic couplings between the charged particles of the model and the photon. We assume that the fermions are in equilibrium with the thermal bath of photons, but, similar to Ref. [71], the σ and $\vec{\pi}$ fields are in a non-equilibrium state. The reason is that the masses of the scalar fields are heavy in comparison to the temperature. In the minimal coupling prescription, the Lagrangian density becomes

$$\mathcal{L} = \mathcal{L}_{\Phi} + \mathcal{L}_q - \frac{1}{4} F_{\mu\nu} F^{\mu\nu} \,, \tag{3.58}$$

$$\mathcal{L}_{\Phi} = (\partial_\mu \phi)^* (\partial^\mu \phi) + (D^+_\mu \pi^+)(D^{-\mu} \pi^-) - \lambda \left(\phi^* \phi + \pi^+ \pi^- - \frac{v_0^2}{2} \right)^2 \,, \tag{3.59}$$

$$\mathcal{L}_q = \bar{\psi} \left\{ i\gamma_\mu \left[\partial^\mu - ie \begin{pmatrix} q_u & 0 \\ 0 & q_d \end{pmatrix} A^\mu \right] - \gamma^0 \mu_q + g(\sigma + i\vec{\pi} \cdot \vec{\tau} \gamma_5) \right\} \psi \,, \tag{3.60}$$

where $D^{\pm}_\mu = \partial_\mu \pm ieA_\mu$ and $q_u = 2e/3$, $q_d = -e/3$ are the electric charges of the u quark and d quark, respectively.

As we have seen before, the interactions with the thermal bath give a thermal mass to the charged particles, modifying the effective potential in the charged field directions,

$$\Delta V_{\rm eff}|_{\rm Thermal\ Bath} = \frac{e^2 T^2}{4}\pi^+\pi^- \ . \tag{3.61}$$

Note also that the coupling to the photons gives a thermal mass [105] $m_f^2(T) = q_f^2 T^2/8$ to the quarks as well. However, this term can be safely neglected with respect to the gv term in the symmetry broken phase. In addition, at finite temperature and chemical potential, according to the gap equation (3.24), the expectation value of the σ field is no longer equal to $v_0 = f_\pi$, but depends on T and μ_q, $\langle\sigma\rangle = v \equiv v(T,\mu_q)$.

In the following, we will work in the chiral limit, $h = 0$. To discuss the pion string in the thermal and dense medium, we use a mean-field approximation, by integrating out both the fermions and the electromagnetic gauge field A_μ. The Hamiltonian field equations for σ and π_i, $i = 0,1,2$ are found to be

$$\nabla^2\sigma = \lambda\left(\sigma^2 + \vec{\pi}^2 - v_0^2\right)\sigma + g\langle\bar{\psi}\psi\rangle_{\rm (ren)} \ , \tag{3.62}$$

$$\nabla^2\pi_0 = \lambda\left(\sigma^2 + \vec{\pi}^2 - v_0^2\right)\pi_0 + g\langle\bar{\psi}i\gamma_5\tau_0\psi\rangle_{\rm (ren)} \ , \tag{3.63}$$

$$\nabla^2\pi_{1(2)} = \lambda\left(\sigma^2 + \vec{\pi}^2 - v_0^2\right)\pi_{1(2)} + g\langle\bar{\psi}i\gamma_5\tau_{1(2)}\psi\rangle_{\rm (ren)} + e^2\langle A_\mu A^\mu\rangle\pi_{1(2)} \ , \tag{3.64}$$

where we have [104]

$$\langle A_\mu\rangle = 0 \ , \qquad\qquad \langle A_\mu A^\mu\rangle = \frac{T^2}{4} \ , \tag{3.65}$$

and by taking the trace of the momentum integral of the fermion propagator, the scalar and pseudoscalar fermions densities are [102]

$$\langle\bar{\psi}\psi\rangle = -2N_c N_f g\sigma\int\frac{d^3k}{(2\pi)^3}\frac{1}{\omega_k}\left[1 - n_F^+(\omega_k) - n_F^-(\omega_k)\right] \ , \tag{3.66}$$

$$\langle\bar{\psi}i\gamma_5\vec{\tau}\psi\rangle = -2N_c N_f g\vec{\pi}\int\frac{d^3k}{(2\pi)^3}\frac{1}{\omega_k}\left[1 - n_F^+(\omega_k) - n_F^-(\omega_k)\right] \ . \tag{3.67}$$

Note that these densities depend explicitly on the σ and $\vec{\pi}$ fields [106]. After subtracting the ultraviolet divergent term in the vacuum-dependent terms of the above momentum integrals, the finite (renormalized) scalar and pseudoscalar

fermion densities are, respectively,

$$\langle\bar{\psi}\psi\rangle_{(\mathrm{ren})} = \sigma\,\Pi_\pi^{(\mathrm{ren})}/g\ , \tag{3.68}$$

$$\langle\bar{\psi}i\gamma_5\vec{\tau}\psi\rangle_{(\mathrm{ren})} = \vec{\pi}\,\Pi_\pi^{(\mathrm{ren})}/g\ , \tag{3.69}$$

where $\Pi_\pi^{(\mathrm{ren})}$ is given by Eq. (3.30).

Combining the above Eqs. (3.62)-(3.64) and expressing them in terms of $\phi = (\sigma + i\pi_0)/\sqrt{2}$, $\pi^\pm = (\pi_1 \pm i\pi_2)/\sqrt{2}$ and, also, using Eq. (3.69) together with the massless pion condition in the chiral limit, Eq. (3.31), gives

$$\nabla^2\phi = 2\lambda\left[\phi^*\phi + \pi^+\pi^- - \frac{v^2(T,\mu_q)}{2}\right]\phi\ , \tag{3.70}$$

$$\nabla^2\pi^\pm = 2\lambda\left[\phi^*\phi + \pi^+\pi^- - \frac{v^2(T,\mu_q)}{2} + \frac{e^2T^2}{8\lambda}\right]\pi^\pm\ . \tag{3.71}$$

The above equations generalize the pion string equations in the vacuum, Eqs. (3.42) and (3.43). Hence, the pion string solution Eq. (3.44) for ϕ is modified to

$$\phi = \frac{v(T,\mu_q)}{\sqrt{2}}\tilde{\rho}(r)e^{in\theta}\ , \tag{3.72}$$

where $v(T,\mu_q)$ is the solution of the gap equation (3.24), and $\tilde{\rho}$ has the same functional form as ρ except that the inverse width is now given by $v(T,\mu_q)$. The energy E_0 (3.41) is modified to

$$\begin{aligned} E_{\mathrm{eff}} = \int d^3x \Big\{ & \vec{\nabla}\phi^*\vec{\nabla}\phi + \vec{\nabla}\pi^+\vec{\nabla}\pi^- \\ & + \lambda\left[\phi^*\phi + \pi^+\pi^- - \frac{v(T,\mu_q)^2}{2}\right]^2 + \frac{e^2T^2}{4}\pi^+\pi^- \Big\}\ . \end{aligned} \tag{3.73}$$

By comparing E_{eff} with E_0 we can study the effect of the thermal and dense medium on the stability of the string.

3.4.2 Stability of the Pion String

To investigate the stability of the pion string, we first consider a variation of the energy δE of the string in the presence of infinitesimal perturbations of the

charged fields $\pi^{\pm}$,

$$\delta E = E_{\text{eff}} - E_{\pi^{\pm}=0} = \int d^3x \left\{ \vec{\nabla}\pi^+ \vec{\nabla}\pi^- + \lambda \left[\frac{e^2T^2}{4\lambda} + 2\phi^*\phi - v^2(T,\mu_q) + \pi^+\pi^- \right] \pi^+\pi^- \right\} . \quad (3.74)$$

We use the ansatz (3.72) and expand the perturbations in the direction of $\pi^{\pm}$ as

$$\pi^{\pm} = v(T,\mu_q) \sum_{m=0}^{\infty} \chi_m(r) e^{\pm im\theta} . \quad (3.75)$$

Using Eq. (3.75), the variation of the energy in cylindrical coordinates becomes

$$\delta E = 2\pi v^2(T,\mu_q) \int dz \int r\ dr \left\{ \chi_m'^2(r) + \frac{m^2}{r^2}\chi_m^2(r) + \left[\frac{e^2T^2}{4} + \lambda v^2(T,\mu_q)(\tilde{\rho}^2(r) - 1) + \chi_m^2(r) \right] \chi_m^2(r) \right\} . \quad (3.76)$$

To determine the stability of the string, it is sufficient to know the overall sign of (3.76). A negative variation of energy would imply that the string configuration is not favored under an infinitesimal perturbation and would likely decay. Considering the integrand of the above equation, the first two terms $\chi_m'^2$ and $\frac{m^2}{r^2}\chi_m^2$ are exact squares, so necessarily positive (in the next subsection we will explicitly analyze the effect of keeping these terms in the stability analysis). The only quantity that may give an instability is the last term. A sufficient condition of stability is therefore derived from the sign of

$$\left[\frac{e^2T^2}{4} + \lambda v^2(T,\mu_q)(\tilde{\rho}^2(r) - 1) + \chi_m^2(r) \right] . \quad (3.77)$$

The radial function χ_m is unknown. However, appearing as a square, it gives a positive contribution and can be neglected in a minimal condition for stability. Using $\tilde{\rho}^2(r) - 1 \simeq e^{-\tilde{\mu}r}(e^{-\tilde{\mu}r} - 2)$ [6], the variation of the mass per unit length compared to the embedded string is

$$\frac{e^2T^2}{4} - 2\lambda v^2(T,\mu_q) e^{-\tilde{\mu}r}(1 - \frac{1}{2}e^{-\tilde{\mu}r}) > 0 , \quad (3.78)$$

[6] $\tilde{\mu}$ is defined as the string width μ except that v_0 is replaced by $v(T,\mu_q)$.

or, using that $e^{-\tilde{\mu}r}(1-\frac{1}{2}e^{-\tilde{\mu}r}) \leq \frac{1}{2}$ for all r, we find

$$\frac{e^2T^2}{4} - \lambda v^2(T,\mu_q) > 0\ . \tag{3.79}$$

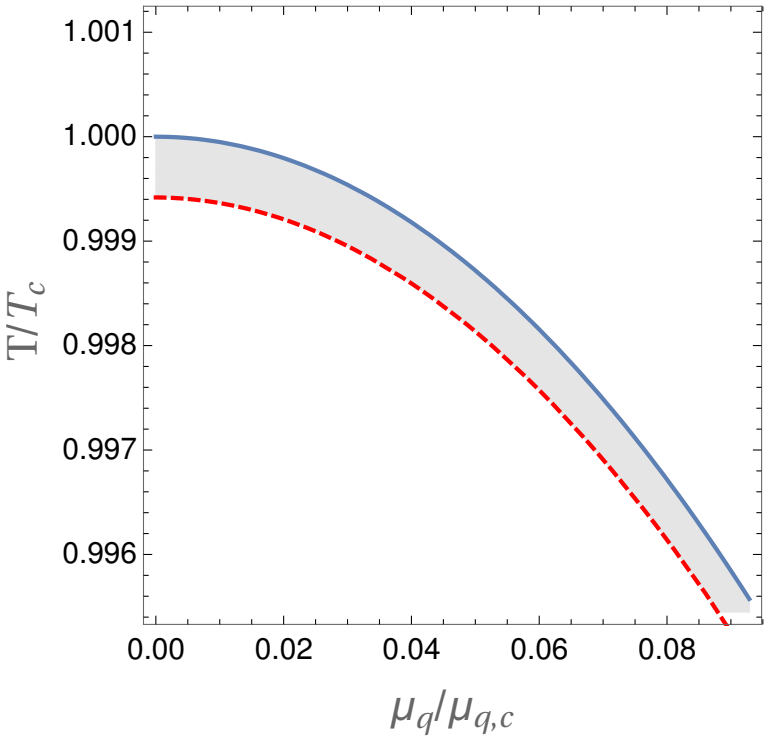

Figure 3.6 *Stability region of the pion string in a thermal and dense medium, in the chiral limit. The parameters are those given by Eq.* (3.36)*. The upper curve (blue) corresponds to the phase transition (second-order). The dashed curve (red) corresponds to the lower limit of stability of the string. The range between the lines is the region of core stability.*

We compute numerically the region of core stability using the parameters given in Eq. (3.36). Our results are shown in Fig. 3.6. The top line corresponds to the chiral phase transition, the string solution being non-trivial in the symmetry broken phase where $v(T,\mu_q)$ is non-zero. The dashed line corresponds to the limit of stability $e^2T^2/4 = \lambda v^2(T,\mu_q)$. The model predicts a tiny ribbon for values of temperature and chemical potential, in between the two lines shown Fig. 3.6, for which stable strings are allowed.

The size of the stability region is small, but the following argument makes plausible that such a region does indeed exist. We know from the results discussed for the LSMq in Sec. 3.3.2 that the phase transition is of second-order above the critical point. For a second-order phase transition, the expectation value of the

field is exactly zero on the transition line and then it moves away smoothly to finite values. There is always a region below the phase transition line where the expectation value $v(T,\mu_q)$ is small enough to satisfy the stability condition (3.79). We, therefore, expect that the stability condition is always satisfied for a second-order phase transition. This can be seen explicitly in the high-temperature approximation.

In the high-temperature region and close to the critical curve, such that $m_q/T \ll 1$, we use the approximation [105]

$$\int_0^\infty dk \frac{k^2}{\omega_k} \left[n_F^+(\omega_k) + n_F^-(\omega_k)\right] \simeq \int_0^\infty dk k \left[n_F^+(k) + n_F^-(k)\right] = \frac{\mu_q^2}{2} + \frac{\pi^2 T^2}{6} , \tag{3.80}$$

and from the gap equation (3.25), we find (in the chiral limit $h = 0$ and neglecting the vacuum contribution for simplicity)

$$\lambda v^2(T,\mu_q) \approx \lambda v_0^2 - \frac{N_c N_f}{\pi^2} g^2 \left(\frac{\mu_q^2}{2} + \frac{\pi^2 T^2}{6}\right) , \tag{3.81}$$

which using Eq. (3.79) leads to the approximate analytical stability condition,

$$\frac{e^2 T^2}{4} - \lambda v_0^2 + \frac{N_c N_f}{\pi^2} g^2 \left(\frac{\mu_q^2}{2} + \frac{\pi^2 T^2}{6}\right) > 0 . \tag{3.82}$$

Values for $T < T_c$ and $\mu_q < \mu_c$ can always be found, i.e., temperature and chemical potential below the values corresponding to those for the critical (second-order) transition line, such as to satisfy Eq. (3.82).

The situation changes drastically though when the transition is first-order. It is well-known that defects can form during a first-order phase transition as well (see, e.g. [81]). In our model however, the strings would decay immediately. The stability condition relies on the smallness of the temperature and chemical potential background value $v(T,\mu_q)$. Around the first-order transition the background value $v(T,\mu_q)$ jumps (discontinuously) from zero in the symmetry restored phase to a usually higher value in the broken phase and the condition (3.79) is never satisfied. Thus, we conclude that the existence of stable pion strings depends strongly on the order of the phase transition. The stability condition for the pion string is favored around the second-order transition line of the phase diagram, but it is disfavored around the first-order transition region.

The stability condition Eq. (3.82) should be contrasted with the case where the Yukawa interactions are absent Eq. (3.56). The inclusion of additional thermal and dense effects from the Yukawa interaction is thus fundamental for having a stable pion string.

3.4.3 Stability in the Physical Case $h \neq 0$

In the physical case, $h \neq 0$, the effective potential leads to a crossover transition, as seen in Fig. 3.5. Defect formation in a crossover region is, unfortunately, very poorly understood at the moment, either from analytical studies or from numerical (lattice) simulations. As far as we know, there is just some limited discussion in the literature of defect formation for this case, such as for example Ref. [107], where it discusses how defects can be formed by percolation of different regions with different phases.

For the present case, when accounting only for the background fields, it would appear that no string solution can be constructed for the physical case of $h \neq 0$. As shown above, e.g. in Eq. (3.72), the pion string solution is constructed in the plane of the fields (σ, π_0), which is lifted with respect to the charged pions by the thermal electromagnetic plasma effect. The potential in the plane of the fields (σ, π_0), in the chiral limit $h = 0$, is then of the form of a classical Mexican hat. The string solution interpolates between the unstable vacuum at the top of the potential to the infinitely degenerate minimum at the bottom of the potential. The solution then winds around the minima at the bottom of the potential with no cost of energy. This winding is possible due to the infinitely degenerate minimum of the potential (the pions are exactly Goldstone bosons).

In the physical case, $h \neq 0$, the chiral symmetry is explicitly broken, the pions acquire a mass and this winding freedom is no longer present (the potential now becomes a tilted Mexican hat). Under these circumstances, the string ansatz Eq. (3.72) no longer applies and for the background fields alone no string solution should be possible to construct.

The above situation, however, can change significantly when accounting for fluctuations of the fields in the thermal medium. Field fluctuations and gradient energies, which are negligible at zero temperature, can grow, particularly close to the transition and at large temperatures, where large fluctuations then start to become relevant. Under these conditions, it is then feasible that, as these

fluctuations of the fields grow around the true vacuum of the system (the global minimum of the potential), they can be sufficiently large to probe the false vacuum state (the local minimum of the potential). When this happens, we can effectively say that the winding around the potential is once again restored, at least in localized regions of space. Much of the system will consist of regions of space where the fluctuations are small and the state is that of an explicitly chiral symmetry breaking as usual. However there will some regions with larger fluctuations where the chiral symmetry effectively looks restored, and such regions become increasingly more prevalent as the temperature increases. The pion strings that we are interested in are local objects, so all we need is some suitably large regions where conditions are appropriate for them to form. Thus, in regions of large fluctuations, where the chiral symmetry is effectively restored, pion string formation can become possible once again.

This picture is similar to the mechanism discussed in Ref. [107] for the formation of defects. Typical fluctuations in the fields have the size of the correlation length, with $\xi_\sigma^{-1} \sim m_\sigma$ and $\xi_\pi^{-1} \sim m_\pi$. As the temperature grows, these fluctuations start to become more and more frequent and eventually they start coalescing. In between these regions, string formation is possible, similar to the Kibble mechanism of formation of defects we have introduced previously. Though the physics of the formation of these fluctuations in a thermal medium and their consequences goes beyond the analysis allowed within the framework of the effective potential[7], we can still provide some reasonable estimates for the importance of these fluctuations in the present problem.

Fluctuations in the fields around the true vacuum and that are large enough to probe the false vacuum of the potential should have an energy density in gradient form comparable to the difference in energy density between the false and true vacua of the potential,

$$\langle \frac{1}{2}\vec{\nabla}\sigma.\vec{\nabla}\sigma\rangle + \langle \frac{1}{2}\vec{\nabla}\pi.\vec{\nabla}\pi\rangle \approx hv \ , \tag{3.83}$$

where we have used that $\Delta V_{\text{eff}} \simeq hv$ for the energy density difference. Assuming Gaussian-like (classical) correlation sized fluctuations for the fields in the thermal

[7]We recall that the computation of the effective potential is only able to include the effects of small fluctuations and the proper treatment requires making use of the effective action instead. See, e.g., Refs. [108–110] for examples of works that try to account for the effect of fluctuations in a phase transition. Note also that in Ref. [111] a method has been proposed to study the effect of fluctuations in the chiral phase transition in the LSMq, without the assumption of the fluctuations to be small.

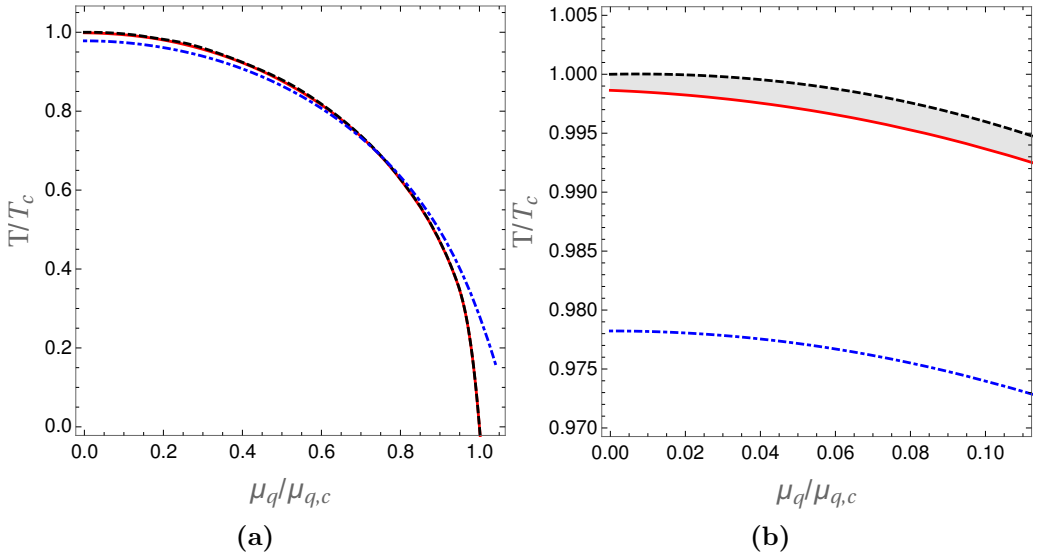

Figure 3.7 *(a) The stability condition for the pion string (red plain-line), the gradient energy condition (blue dash-dotted line) and the transition line (black dashed line), in the (μ_q, T) plane (normalized by the corresponding critical values). (b) An amplified view around the high-temperature, low chemical potential region. Strings are allowed to form in the shaded region below the transition line and above the stability condition.*

medium, we can then write [112]

$$\langle \frac{1}{2}\vec{\nabla}\sigma.\vec{\nabla}\sigma\rangle \simeq \frac{T}{4\pi^2}\int_0^{m_\sigma} dk \frac{k^4}{k^2+m_\sigma^2} = (3\pi-8)\frac{m_\sigma^3 T}{48\pi^2}\,, \tag{3.84}$$

and analogous for the gradient energy density for the pion field.

In Fig. 3.7 (a), we show the condition given by Eq. (3.83) alongside the transition line and the pion string stability line in the (T, μ_q) plane in the physical case of $h \neq 0$. In Fig. 3.7 (b), we zoom into a region similar to the one shown previously for the chiral limit in Fig. 3.6. We see from Fig. 3.7(a) that the gradient energy density is significantly closer to the transition line and remains slightly below it, down to temperatures and chemical potential around $T \simeq 0.7\, T_c$ and $\mu_q \simeq 0.8\, \mu_{q,c}$, when it then goes above the transition line. In this region of large temperatures, the variations in the fields are sufficiently large to overcome the difference in potential energy density between the local and global minima of the potential.

The stability condition, similar to what we have seen in the chiral limit $h = 0$ (see, e.g., Fig. 3.6), is also very close to the transition line and slightly below it, lying in between the gradient energy condition and the transition line. In this small

region of parameters, in between the stability condition (solid red line) and the transition line (dashed black line) and lying above the gradient energy condition (dash-dotted blue line), is where pion strings can form (we locally recover the conditions for winding of the string) and be stable at the same time. Below the line for the gradient energy condition, the fluctuations of the fields (in terms of gradient energy) are not large enough to ensure the presence of strings, as discussed above.

The above analysis is just a preliminary examination of the physical case of $h \neq 0$ and it shows that the formation of pion strings is plausible in this regime. More important, this section has laid out a conceptual framework for how to address this physical regime. An important general point that this analysis indicates is the importance that large fluctuations close to the transition may have on the formation, stability and presence of defects in general. A complete analysis would require a much more detailed treatment of the large localized fluctuations that emerge, such as through numerical simulations, which is beyond the scope of the present work. Nevertheless, our analysis, though semiquantitative, indicates the importance that gradient energy densities for the fields can have on the pion string formation and subsequent stabilization when in a thermal and dense medium. These gradient energy terms can also have important effects in the subsequent evolution and decay of these strings when formed. Our analysis here also shows that the role of fermions is an important ingredient to achieve stable pion strings even in the $h \neq 0$ case due to the effect they have on the order of the phase transition (recalling that in the absence of the fermion contributions, no stability is possible for physically motivated QCD parameters in this model). Thus, the main focus of this work on the role of fermions can be seen already to be important also for any detailed study of the $h \neq 0$ case.

3.5 Discussion and Conclusions

In this chapter, we have studied a stabilization mechanism for embedded topological defects, by considering one of the simplest realizations, the pion string. We have investigated the effect of a thermal and dense medium on the stability of the string. We have used the LSMq model to describe the chiral phase transition using realistic physical parameters. We have constructed the corresponding pion string solution for the model, which depends explicitly now on the temperature and the chemical potential. Finally, using the mechanism similar to the one

proposed in Ref. [70], we have analyzed the stability for pion strings and have derived a condition for it to be satisfied.

Our results have shown that the existence of a stable string depends crucially on the order of the phase transition. Pion strings are produced and can become stable when the phase transition is second-order. This happens because the expectation value of the field in the medium changes smoothly away from zero. In this case, the stability condition is automatically satisfied in a region close to the transition line. This argument fails when the transition is first-order since, now, the minimum of the potential can jump discontinuously to a large value, such that the stability condition no longer holds. In this respect, the presence of fermions, which is a key direction this work has explored, is crucial. The inclusion of the fermions indirectly provides stability, in the sense that fermions do not change the stability condition Eq. (3.79) but they change the order of the phase transition and, therefore, bring stability. This result is the first to find a stability region for the pion string. Although most of the analysis was done mainly in the chiral limit, in Sec. 3.4.3 we have performed a preliminary analysis also for the physical case of $h \neq 0$, where we have pointed out how fluctuations of the fields leading to large gradient energy densities, can play an important role in the formation and stability of pion strings in this regime.

A stable pion string has similar characteristics as an ordinary topological string. In particular, the string leads to a specific geometry of spacetime. The string can be seen as a string core, where the potential energy is trapped and a non-trivial winding of the scalar field around this core. The topology induced by the defect can therefore be seen far away from the actual core radius. It has been argued in [1] that this non-trivial geometry persists even after the decay of the string. The argument is the following, when the temperature drops below T_{stab} the potential energy confined in the string core is released into kinetic energy, leading to the unwinding of the field. However, at large distance from the core, the non-trivial winding of the neutral scalar field persists. This behavior is referred as a string melting.

The existence of pion strings has direct consequences for cosmology and nuclear physics. The region of the $(\mu_q - T)$ plane in Fig. 3.4 with a second-order transition and stable strings has large temperatures and a low chemical potential. This region of the plane applies for both the Early Universe and aspects of heavy-ion collision. The applications of the pion string in the Early Universe are multiple. One concrete example is the creation of primordial magnetic fields as discussed

in Ref. [60]. Pion strings in heavy-ion collisions experiments have been discussed recently in Refs. [73, 74]. The production of strings in this kind of experiments may have an influence on the distribution of baryons and one could speculate about their experimental signature.

A relevant feature of cosmic strings is the production of gravitational waves. In particular, the observation of GW in the coming years will provide greater constraints on the presence of cosmic strings in the Early Universe [91]. It would, therefore, be interesting to study the GW signature of pion strings. However, since those are expected to be produced at the epoch of the QCD transition, their energy per unit length might not be sufficiently high to produce a signal that can be detected in the near future experiments.

Another interesting area to investigate is the stabilization mechanism and its potential improvements. In order to affect the effective potential in the constrained directions, one needs to act on the charged pions only. One possibility would be to place the system in an external magnetic field. This analysis has applications beyond the LSMq of the strong interactions. Similar considerations can be used to study the stability of the Z string [68], the embedded string solution made up of the uncharged complex Higgs field with the charged complex scalar set to zero. An initial study of the thermal stabilization of the Z string was given in [113]. A similar reasoning would apply to the Z string. The embedded defect would never completely decays, but at most undergoes core melting.

Looking beyond the Standard Model of strong, weak and electromagnetic interactions, and to higher temperatures, it would be interesting to study whether there are embedded defects in BSM theories which could be stabilized not only by a photon plasma, but by a plasma of the gauge fields which are massless above the electroweak symmetry breaking scale, and above the confinement scale. BSM theories with embedded domain wall solutions stabilized by a plasma in the Early Universe could face severe cosmological problems since a single domain wall crossing our Hubble patch would overclose the Universe.

Chapter 4

Universality in Warm Inflation

4.1 Introduction

The SBBM has proven its validity as a cosmological model with several theoretical predictions confirmed by observation. Despite these great successes, the original formulation of the model faces some shortcomings. However, the simple addition of an early phase of accelerated expansion, before the epoch associated with grand unification, is sufficient to resolve most of the drawbacks of the model. Cosmic inflation is not the only way to complete the SBBM, however, and this is one of the main reasons for its success, the theory possesses a built-in mechanism to generate the formation of structures and explain the presence of the tiny anisotropies observed in the temperature of the CMB. Over the last few years, cosmic inflation has become a main ingredient of modern cosmology. The theory is currently favored by several experiments such as the Planck satellite [42, 114, 115].

The historical and most common realization of an early accelerated expansion relies on a single scalar field in the slow-roll regime. At the end of the period of inflation, the Universe is extremely cold and mostly empty, the temperature and the energy densities of matter and radiation being proportional to negative powers of the scale factor. It is then usually assumed that a reheating period [116] directly follows inflation. The energy of the scalar field responsible for inflation is transferred into particles of the Standard Model to repopulate and reheat the Universe. A slightly different scenario is proposed by the warm realization of inflation [10, 11]. The presence of dissipative effects leads to a continuous

production of radiation and, possibly, a smooth transition to the radiation-dominated era. The Universe, therefore, remains warm during the period of inflation. A first principle model of warm inflation based on a few fields has been proposed recently [117], and demonstrated that, as model building prospects, warm inflation models are on an equal footing to cold inflation.

Observational cosmology, as demonstrated by the recent Planck results, has reached an impressive level of precision that can set constraints on many cosmological models, including inflation. However, despite the level of accuracy achieved by Planck, the degeneracy problem of inflationary model building still persists. Many inflationary models can produce predictions, like for the near scale invariance and the power spectra, that are very similar and compatible with the data. In Ref. [118], the idea of universality classes was suggested as a means to classify a wide range of inflation models, and, thus, subsumes a large number of them in terms of their salient properties relevant to observation. This approach borrows ideas from the renormalization group (RG) methods of quantum field theory (QFT), such as the concept of flow away from a fixed point, here corresponding to the exact de Sitter (dS) geometry, and the use of an analog to the renormalization group equation (RGE) for the β-function.

The β-function formalism was introduced in Ref. [118] and further developed and extended in Refs. [119–124], to identify universality among the wide zoology of inflationary models. This formalism is based on the application of the Hamilton-Jacobi (HJ) approach to cosmology [125]. It relies on a formal analogy between the equation describing the evolution of a scalar field in an expanding background and a RGE of QFT. As will be explained below, this analogy is not coincidental but has underpinnings with holography. In this framework, the near scale invariance experienced by the Universe during inflation is interpreted as a departure of the corresponding RGE from a fixed point, corresponding to an exact dS spacetime. A single parametrization of the β-function, close to the dS fixed point, thus, defines a universality class of models that can be grouped together, sharing a single asymptotic behavior. As a consequence, arbitrary potentials can be classified into a small set of classes according to the behavior of their associated β-function in the neighborhood of the fixed point.

This approach has some direct advantages. First of all, by grouping different potentials into a small set of classes, it significantly reduces the number of relevant cases to consider. Furthermore, as the formalism relies on intrinsic properties of inflation, it is completely general and, in particular, it does not assume slow-

roll. For example, it has been successfully applied to constant-roll inflation [123]. Finally, as mentioned already, this formalism has deep theoretical motivations arising from the holographic description of the Early Universe (see, for example, Refs. [126–128]). Within the (A)dS-CFT correspondence of Maldacena [129], the flow away from the dS fixed point, which is realized during inflation, is dual to a deformation of the associated conformal field theory (CFT) due to relevant or marginal operators. By applying these methods to describe the Early Universe, and, in particular, inflation, it is both possible to shed a new light on some of its problematic aspects and to provide an alternative interpretation of the observational constraints [130–137].

By applying the β-function formalism to warm inflation, we show that there are two intervening characteristic functions regulating the dynamics. One of them is the function already identified in Ref. [118], which was defined in the cold inflation case, and which controls the way the inflaton drives the departure from the dS fixed point. In the warm inflation context, we show that another function controlling the level of radiation production naturally emerges. By following the evolution of these two functions, we are able not only to fully characterize the dynamics, but also to determine when the end of warm inflation smoothly connects with the radiation-dominated regime. Furthermore, these two functions allow us to classify different forms of inflationary potentials in certain universality classes. Since this description sets direct control on the dynamics, by using parameters which are different from the usual slow-roll coefficients, it offers an extremely powerful method to describe the inflationary evolution (and its end) in an independent and novel way.

In this work, we make use of the generalized framework offered by the β-function formalism to obtain an analytical understanding of warm inflation. We first show that in some toy models a full analytical description of warm inflation can be derived. We then focus on more realistic scenarios. In particular, we show that it is possible to derive a relatively accurate description of both the weak and strong dissipative regimes. Among the main results of the chapter, there is the observation that, despite a second functional dependence is introduced, a universal description of inflation, similar to the one of Ref. [118], can still be consistently formulated. This allows studying further the effect of the various forms of the dissipation terms commonly considered in warm inflation on the classes of universality and on their predictions for the scalar spectral index and the tensor-to-scalar ratio. Remarkably, we show that, within the β-function

formalism, it is easy to identify the degeneracy in the inflationary observables for some models with different dissipation coefficient forms. The results presented in this chapter have been published in [2].

This chapter is organized as follows. We start in Sec. 4.2 with a brief review of the theory behind cosmic inflation. We present and contrast the cold and warm realizations. In Sec. 4.3, we motivate the need for a universal treatment and show how this is achieved with the β-function formalism. We then present how the formalism is consistently extended to warm inflation. We provide details on the method and present explicit examples in Sec. 4.4. The results are presented and discussed in Sec. 4.5. Our concluding remarks and future perspectives are given in Sec. 4.6. Greater details on the cosmological perturbation theory of inflation are given in Appendix C.

Note that we have chosen to work in this chapter in the units of the reduced Planck mass, where $M_P/\sqrt{8\pi} = m_P = \kappa^{-1} = 1$.

4.2 Review of Cosmic Inflation

Cosmic inflation refers to an accelerated phase of expansion in the very early Universe, before the period of grand unification. It has been originally proposed to solve some of the shortcomings of the SBBM by A. H. Guth [138] and A. A. Starobinsky [139], and developed by A. D. Linde [140, 141] and A. Albrecht and P. J. Steinhardt [142].

From the Friedmann equations (2.7)-(2.8), an accelerated expansion is realized if

$$\left| -\frac{2\dot{H}}{3H^2} \right| = \left| \frac{\rho + p}{\rho} \right| < \frac{2}{3} \ . \tag{4.1}$$

This condition from the equation of state implies a nearly constant Hubble factor during the period of inflation. For illustrating purpose, let us study the case of an exactly constant Hubble factor, denoted H_I. A simple computation gives the scale factor as function of time

$$a(t) = a_{i0} \exp\left\{H_I \cdot t\right\} \ , \tag{4.2}$$

where the subscript "$_{i0}$" denotes the beginning of inflation. This solution of

the Einstein equations is referred as a de Sitter space and has been originally introduced by W. de Sitter [143, 144] and T. Levi-Civita [145]. This spacetime is realized if the Einstein tensor is constant, or, equivalently, with a constant energy-momentum tensor. However, in an exact de Sitter space, the expansion is eternal. It is therefore assumed that the phase of inflation takes place in a quasi-de Sitter space, where $|\dot{H}_I| \ll H_I^2$ but not constant, allowing for a transition to the reheating era.

The length of the period of inflation is usually characterized by the number of e-folds N associated with the growth of the scale factor. Defined as $dN \equiv -d\ln a$, one can derive $N(t)$

$$N(t) = \int_a^{a_{ie}} d\ln a' = \ln\frac{a_{ie}}{a} \simeq H_I \Delta t \ , \tag{4.3}$$

with the subscript "$_{ie}$" denoting the end of inflation. In this brief review of cosmic inflation, we first introduce the shortcomings of the SBBM and the corresponding solutions coming from a phase of inflation. We then present the simplest realization of inflation, with a scalar field, and discuss the theory of the perturbations. Finally, we introduce the warm realization of inflation and highlight the differences with respect to the cold case.

4.2.1 Shortcomings of the SBBM

The confidence on the SBBM relies on many successes, on both theoretical and experimental levels. Despite this apparent robustness, the SBBM, in its original formulation, faces a few imperfections. Fortunately, these shortcomings are resolved with the introduction of an early phase of inflation.

Horizon Problem The horizon problem is related to the observed causal connection in the Universe. FLRW cosmologies are built on the simple assumption of a large scale homogeneity and an isotropy of space. Galaxies surveys and the temperature of the CMB are strong experimental supports for the cosmological principle. However, homogeneity implies that some regions of space are sharing some properties and, therefore, must be in causal contact. The horizon problem is based on the observed homogeneity between two regions that appear as causally disconnected in the SBBM.

To be more specific, let us define the comoving particle horizon d_{ph}

$$d_{ph}(\tau) \equiv \int_{\tau_i}^{\tau} d\tau' = \int_{t_i}^{t} \frac{dt'}{a(t')} \simeq \left(\frac{t}{t_0}\right)^{\frac{1+3\omega}{3(1+\omega)}} \simeq a(t)^{\frac{1+3\omega}{2}} t_0 \ , \tag{4.4}$$

assuming a constant ω and using that $a(t) \sim (t/t_0)^{2/3(1+\omega)}$ with a_0 set to 1. The comoving particle horizon is the comoving distance[1] a photon emitted at time t_i travels until time t and is essential to study causality. The surface of the sphere of radius d_{ph}, the comoving distance, delimits the region of the space that is in causal contact at time t with the spatial position where the photon has been emitted.

A strong support for the large scale homogeneity of the Universe comes from the temperature of the CMB. The scale factor at the time of formation of the CMB is of order $a(t_{CMB}) \sim 10^{-3} a_0$. Assuming for simplicity a radiation-dominated universe until t_{CMB}, we find the comoving distance (or future horizon) at the time of last-scattering of order of $10^{-3} t_0$. On the other hand, the scale of the observed homogeneity is given by the comoving distance between t_{CMB} and today, corresponding to a past horizon. Assuming for simplicity the Universe to be dominated by matter after the time of last-scattering, one find $d_{ph} \sim t_0$. The observed area of homogeneity is 10^6 times larger than the areas in causal contact at the time of formation of the CMB. This is the horizon problem.

An early phase of inflation provides a solution. If the Universe is expanding exponentially during a time interval before t_{CMB}, the comoving radius becomes

$$d_{ph}(\tau) = \left(\int_{\tau_i}^{\tau_{i0}} + \int_{\tau_{i0}}^{\tau_{ie}} + \int_{\tau_{ie}}^{\tau} \right) d\tau' \simeq \frac{1}{a_{ie} H_I} \exp\left\{\Delta t H_I\right\} \ , \tag{4.5}$$

where the subscripts $_{i0}$ and $_{ie}$ denote the beginning and the end of inflation. The first and last integrals have been safely neglected with respect to the second. We have defined a_{ie} as the scale factor at the end of inflation and H_I as the nearly constant Hubble factor during inflation. We observe that an exponential expansion drastically enhances the comoving horizon. If the process is long enough, it will overcome the scale of homogeneity. Assuming that inflation ends

[1] Since the Universe is expanding over time, the lengths are rescaled. One has to be careful when comparing distances at different times. The comoving distance allows a definition of lengths that takes into account the expansion.

at a temperature of 10^{15} GeV[2] leads to

$$\frac{a_{ie}}{a_0} = \frac{T_0}{T_{ie}} \simeq 10^{-28} \, . \tag{4.6}$$

An estimate for H_I is found by assuming a radiation-dominated universe after inflation $H_I \sim (2t_{ie})^{-1} \sim 10^{56}(2t_0)^{-1}$. To enforce a causal connection we require

$$\exp\{\Delta t \cdot H_I\} > a_{ie} \cdot H_I \cdot t_0 \sim 10^{28} \sim e^{64} \, , \tag{4.7}$$

and, therefore, approximately 60 e-folds are necessary to solve the horizon problem.

Flatness Problem The flatness problem is related to the initial conditions at the Planck scale. In absence of constraints imposed from an underlying symmetry, naturalness implies that any dimensionless parameter is of order unity. If such a parameter takes an extremely large or small value, the model appears as excessively fine-tuned. This is exactly what happens with the energy density parameter Ω and is the origin of the flatness problem.

To be more specific, the first Friedmann equation (2.7) allows expressing the fractional deviation of Ω from unity as

$$\Omega^{-1} - 1 = -\frac{3k}{a^2\rho} \, . \tag{4.8}$$

Assuming for simplicity that before the matter-radiation equality the Universe is dominated by radiation ($\rho \sim \rho_r \sim a^{-4}$) and after by matter ($\rho \sim \rho_m \sim a^{-3}$) and using that the scale factor scales as the inverse of the temperature we find

$$\frac{\Omega_{Pl}^{-1} - 1}{\Omega_0^{-1} - 1} = \frac{\Omega_{Pl}^{-1} - 1}{\Omega_{eq}^{-1} - 1} \frac{\Omega_{eq}^{-1} - 1}{\Omega_0^{-1} - 1} = \left(\frac{T_{eq}}{T_{Pl}}\right)^2 \left(\frac{T_0}{T_{eq}}\right) \sim 10^{-60} \, , \tag{4.9}$$

using $T_{Pl} \sim 10^{32}$ K and $T_{eq} \sim 10^4$ K. The energy density parameter is 60 orders of magnitude closer to unity at the Planck epoch compared to today. Since Ω_0 is measured today as 1.001 ± 0.004 at 95% CL [42], the energy density parameter Ω_{Pl} appears as extremely fine-tuned at the Planck scale.

An early phase of accelerated expansion solves this problem by bringing an extra contribution to (4.9). Computing the deviation of the energy density parameter

[2]This is the historical choice and is related to the energy scale of GUT.

between the beginning of inflation and today, one finds

$$\frac{\Omega_{t_{i0}}^{-1}-1}{\Omega_0^{-1}-1}=\frac{\Omega_{t_{i0}}^{-1}-1}{\Omega_{t_{ie}}^{-1}-1}\frac{\Omega_{t_{ie}}^{-1}-1}{\Omega_0^{-1}-1}=\left[\frac{a(t_{ie})}{a(t_{i0})}\right]^2\left(\frac{T_{eq}}{T_{ie}}\right)^2\left(\frac{T_0}{T_{eq}}\right)\sim 1\ , \tag{4.10}$$

assuming $H_I\Delta t \geq 60$. Due to the exponential expansion, the Universe appears as spatially flat at the end of inflation even if Ω_{Pl} differs from unity. Note that both the horizon and the flatness problems are solved by approximately the same number of e-folds.

Monopole Problem The monopole problem is related to the formation of topological defects in the Early Universe. We have learned in the previous chapter that from the GUT epoch to the time when the Standard Model prevails, a cascade of phase transitions is expected to happen, potentially allowing for the creation of topological defects. We have also learned that the presence of defects drastically affects cosmology. In particular, if magnetic monopoles are created at the GUT epoch, they would dominate the energy budget today. The non-observation of magnetic monopoles and other exotic relics defines the monopole problem.

An early phase of accelerated expansion ending at the GUT epoch prevents such defects to affect the later stages of the Universe. The number density, which is proportional to a^{-3}, is suppressed by a factor of $(e^{H\Delta t})^3 \sim 10^{78}$ during inflation. More generally, since the relevant energy species and the temperature scale as negative powers of the scale factor, at the end of inflation, the Universe is extremely cold[3] and empty. Therefore, a period of reheating must follow the phase of inflation. When inflation is realized with a scalar field, the inflaton, the potential energy stored in the scalar field is transferred to the other particles via decays. However, we must stress that even if the phase of inflation empties the Universe from any undesired relics, it does not prevent the creation of defects in the later stages of the Universe's history.

We have learned that an initial phase of accelerated expansion is sufficient to solve the principal shortcomings of the SBBM. Let us now present how inflation is achieved by considering the simplest realization with a slow-rolling scalar field.

[3]Unless there is a dissipative process during the period of accelerated expansion. This is exactly the framework of warm inflation discussed in Sec. 4.2.4

4.2.2 Realization of Inflation

The simplest realization of inflation is achieved with a single scalar field, minimally coupled to gravity and with a canonical kinetic term. The dynamics is obtained from by the Einstein-Hilbert action

$$\mathcal{S} = \int dt d^3x \sqrt{|g|} \left[\frac{R}{2} - \frac{1}{2} g^{\mu\nu} \partial_\mu \phi \partial_\nu \phi - V(\phi) \right] , \tag{4.11}$$

where $g = \det(g_{\mu\nu})$, $g_{\mu\nu}$ being the FLRW metric. From the stress-energy tensor, given as

$$T_{\mu\nu} = \frac{2}{\sqrt{|g|}} \frac{\delta \mathcal{S}}{\delta g^{\mu\nu}} , \tag{4.12}$$

the pressure and energy density associated with the scalar field are derived

$$\rho_\phi = \frac{\dot{\phi}^2}{2} + \frac{a^{-2}}{2} (\nabla\phi)^2 + V(\phi) , \qquad p_\phi = \frac{\dot{\phi}^2}{2} - \frac{a^{-2}}{6} (\nabla\phi)^2 - V(\phi) . \tag{4.13}$$

The evolution of the system is given by the Friedmann equations and the equation of motion for the scalar field

$$\ddot{\phi} + 3H\dot{\phi} - \frac{\nabla^2 \phi}{a^2} + \frac{\partial V}{\partial \phi} = 0 . \tag{4.14}$$

The symmetry of the metric, which is a direct consequence of the assumed homogeneity and isotropy of space, implies that the field is homogeneous. In general, one can consider $\phi(t, \vec{x}) = \phi_c(t) + \delta\phi(t, \vec{x})$, where the field is seen as a sum of a classical homogeneous contribution and quantum fluctuations.

The condition for an accelerated expansion becomes

$$\left| -\frac{2\dot{H}}{3H^2} \right| = \left| \frac{\rho_\phi + p_\phi}{\rho_\phi} \right| = \left| \frac{\dot{\phi}^2}{\frac{\dot{\phi}^2}{2} + V(\phi)} \right| < \frac{2}{3} , \tag{4.15}$$

which is clearly satisfied in the slow-roll regime, where $|\dot{\phi}^2| < V(\phi)$. This leads to the simple picture of a scalar field slowly rolling down the potential and leading to an accelerated expansion. At the end of inflation, the field falls into a potential well and starts oscillating. The expansion stops accelerating and reheating takes place. The scalar field decays into other relativistic particles, bringing the Universe into the radiation-dominated era. This scenario is illustrated on the

left panel of Fig. 4.1, shown in Sec. 4.2.4.

A wide zoology of potentials leading to inflation is present in the literature. A comprehensive list might be found in the review [146]. For completeness, we must state that there are more sophisticated scenarios. Those are based on the relaxation of one of the simplifying assumptions we have made so far. The most popular examples involve a non-minimal coupling to gravity [139, 147], a non-canonical kinetic term [148], several scalar fields [149], couplings with gauge fields and the presence of anisotropies in the metric [150].

A part from solving the shortcomings of the SBBM, the theory of inflation provides a really important missing piece in the cosmological model, a satisfactory mechanism to explain the formation of structures.

4.2.3 Structure Formation from Inflation

Locally, the Universe is highly inhomogeneous. For example, the matter is localized in specific regions of space such as clusters, galaxies or stars. One of the main questions of cosmology is precisely the origin of the formation of structures. A simple mechanism relies on cosmological perturbations. Tiny fluctuations of the energy density grow with the constant addition of matter attracted by gravity. This process is eventually leading to the structures we observe today. However, in a universe that is homogeneous and isotropic on large scales, the origin of these instabilities has to be explained. One possibility arises from the theory of inflation[4]. The scalar field responsible for the accelerated expansion being a quantum field, the presence of quantum fluctuations might serve as seeds for the density fluctuations. The predictions from the perturbation theory of inflation can be linked with the anisotropies observed in the CMB, giving some experimental tests of the model. We briefly review the main characteristics of this mechanism. More details are given in Appendix C.

Cosmological Perturbations during Inflation The theory of perturbations has been developed by J. M. Bardeen [151], Bardeen, P. J. Steinhardt and M. S. Turner [152], V. F. Mukahnov, H. A. Feldman and R. H. Brandenberger [153] and H. Kodama and M. Sasaki [154]. In the case of inflation, the analysis relies on the inhomogeneous fluctuations around the homogeneous expressions for the

[4] Another mechanism is realized with topological defects, as discussed in the previous chapter.

scalar field and the metric

$$g_{\mu\nu}(t,\vec{x}) = g_{\mu\nu}^{FLRW}(t) + \delta g_{\mu\nu}(t,\vec{x}) \ , \qquad \phi(t,\vec{x}) = \phi_c(t) + \delta\phi(t,\vec{x}) \ , \tag{4.16}$$

where $g_{\mu\nu}^{FLRW}$ is the FLRW metric and $\phi_c(t)$ is the classical contribution of the scalar field responsible for the accelerated expansion. There are three kinds of perturbations, namely scalar, vector and tensor. However, the gauge freedom in the choice of coordinates allows for the restriction to two relevant contributions. The perturbation of the scalar curvature on comoving hypersurfaces $\mathcal{R}$ is a linear combination of the scalar perturbation of the field and the metric. The tensor perturbation u_λ comes from the tensor perturbation of the metric and is related to the propagation of GWs. λ labels the polarizations of the waves.

The physical observables are obtained from the statistical properties of the perturbations. In particular, the scalar and tensor power spectra are defined from the two-point functions

$$\langle 0|\mathcal{R}(\tau,x_1)\mathcal{R}(\tau,x_2)|0\rangle = \int d^3k e^{i\vec{k}(\vec{x}_1-\vec{x}_2)} \frac{\Delta_s^2(\vec{k},\tau)}{4\pi k^3} \ , \tag{4.17}$$

$$\langle 0|u_\lambda(\tau,x_1)u_\lambda(\tau,x_2)|0\rangle = \int d^3k e^{i\vec{k}(\vec{x}_1-\vec{x}_2)} \frac{\Delta_t^2(\vec{k},\tau)}{4\pi k^3} \ . \tag{4.18}$$

The derivation of the power spectra requires a precise analysis of evolution of the perturbations. The main characteristics are identified from the equation of motion for the perturbations called the Mukahnov-Sasaki equation. For the scalar perturbation, the equation for a mode v_k reads

$$v_k'' + \left(k^2 - \frac{z''}{z}\right) v_k = 0 \ , \tag{4.19}$$

where the prime denotes a derivative with respect to conformal time and $z \equiv a\phi'/\mathcal{H}$, with $\mathcal{H}$ being the conformal Hubble parameter $\mathcal{H} = a'/a = aH$. The Mukahnov-Sasaki variable v is related to the comoving curvature perturbation by $v = -z\mathcal{R}$.

During inflation, the comoving Hubble radius, defined as $(aH)^{-1}$, is decreasing and, therefore, two regimes are identified. On sub-horizon scales, the modes oscillate since k^2 dominates in the linear term. On super-horizon scales, the modes are constant. Since the comoving Hubble radius is decreasing during inflation, the modes are expected to oscillate until their wavelength becomes larger than the horizon when they freeze. After the phase of inflation, with the Universe evolving

in the radiation- and matter-dominated periods, the Hubble radius grows again and the modes reenter the horizon when $k = aH$. One should therefore evaluate the power spectra at horizon crossing. As highlighted in Appendix C, for the simplest realization of inflation, the scalar and tensor power spectra are given by

$$\Delta_s^2(k,\tau)\big|_{k=aH} = \frac{1}{4\pi^2}\frac{H^4}{\dot{\phi}^2} , \qquad \Delta_t^2(k,\tau)\big|_{k=aH} = 8\left(\frac{H}{2\pi}\right)^2 , \tag{4.20}$$

evaluated at horizon crossing.

One useful observable related to the power spectra is the spectral indices defined as

$$n_s - 1 = \left.\frac{d\ln\Delta_s^2(k)}{d\ln k}\right|_{k=aH} , \qquad n_t = \left.\frac{d\ln\Delta_t^2(k)}{d\ln k}\right|_{k=aH} . \tag{4.21}$$

The perturbations being created during inflation in a nearly de Sitter space, these are expected to have a nearly scale-invariant spectrum. The departure from an exact scale invariance is precisely measured from n_s and n_t. One can also consider the runnings of the spectral indices which are defined as

$$\alpha_s = \left.\frac{d\ln n_s(k)}{d\ln k}\right|_{k=aH} , \qquad \alpha_t = \left.\frac{d\ln n_t(k)}{d\ln k}\right|_{k=aH} . \tag{4.22}$$

Another observable that plays a significant role in constraining inflation is the so-called tensor-to-scalar ratio

$$r = \left.\frac{\Delta_t^2(k,\tau)}{\Delta_s^2(k,\tau)}\right|_{k=aH} , \tag{4.23}$$

corresponding to the ratio of the amplitudes of the power spectra.

The predictions for the different observables are sometimes expressed in term of the so-called Hubble flow functions (HFF) [155] defined as

$$\epsilon_1 \equiv -\dot{H}/H^2 , \qquad \epsilon_{i+1} \equiv \dot{\epsilon}_i/(H\epsilon_i) . \tag{4.24}$$

For the simplest realization of inflation with a single slow-rolling scalar field, one finds

$$n_s - 1 = -2\epsilon_1 - \epsilon_2 , \qquad \alpha_s = -2\epsilon_1\epsilon_2 - \epsilon_2\epsilon_3 , \tag{4.25}$$

$$n_t = -2\epsilon_2 , \qquad \alpha_t = -2\epsilon_1\epsilon_2 . \tag{4.26}$$

The prediction for the tensor-to-scalar ratio is proportional to n_t which gives the consistency relation $r = -8n_t$.

Constraints from the CMB The perturbations generated during the phase of inflation are expected to be the origin of the anisotropies observed in the temperature of the CMB. It is therefore possible to constrain the different parameters using the statistical properties of a map of the temperature fluctuations ΔT. The most recent experimental values are obtained from the Planck satellite [114]. The amplitude of the scalar spectrum is measured as

$$\Delta_s^2(k_*) = (2.1 \pm 0.1)10^{-9} \,, \tag{4.27}$$

where $k_* = 0.05$ Mpc^{-1} is the pivot scale. This amplitude is sometimes referred as the COBE normalization. The other two most important observables are the scalar spectral index, measured as

$$n_s(k_*) - 1 = 0.9649 \pm 0.0042 \,, \tag{4.28}$$

and the tensor-to-scalar ratio, which is constrained by an upper bound

$$r(k_*) < 0.1 \,, \tag{4.29}$$

at 95% confidence level. Note that the bound on r is measured for a pivot $k_* = 0.002$ Mpc^{-1}.

4.2.4 Warm Realization of Inflation

Warm inflation [10, 11] differs from the usual paradigm of cold inflation in the fact that dissipative processes can lead to a sustainable radiation production throughout the inflationary expansion. Warm inflation will happen for regimes of parameters such that the inflaton interactions with other field degrees of freedom are not negligible. They generate dissipation terms, allowing for a small fraction of vacuum energy density to be converted to radiation. When the magnitude of these dissipation terms is strong enough to compensate the redshift of the radiation by the expansion, a steady state can be produced, with the inflationary phase happening in a thermalized radiation bath. The mechanism is illustrated on the right panel of Fig. 4.1 and should be contrasted with the cold approach

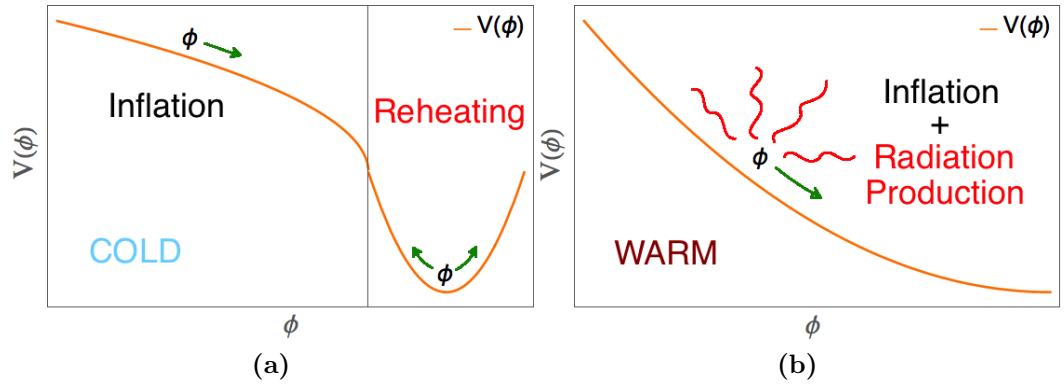

Figure 4.1 *(a) The cold realization of inflation. The scalar field rolls down the potential slowly, leading to the accelerated expansion until it falls into the potential well, where it oscillates quickly and reheats the Universe. (b) The warm realization of inflation. The scalar field is rolling down the potential with a continuous emission of radiation and evolves smoothly toward a radiation-dominated Universe.*

(left panel). Let us briefly review the construction of warm inflation.

Construction of Warm Inflation

For illustrative purposes, we restrict to the case of a single inflaton field with pressure and energy density respectively given by equation (4.13). The dynamics of warm inflation at the background level is governed by the equation of motion for the inflaton field

$$\ddot{\phi} + (3H + \Upsilon)\dot{\phi} + V_{,\phi} = 0 \,, \tag{4.30}$$

where Υ is the dissipation coefficient, which in general can be a function of both the temperature and the background inflaton field ϕ, by the equation for the evolution for the radiation energy density ρ_r

$$\dot{\rho}_r + 4H\rho_r = \Upsilon\dot{\phi}^2 \,, \tag{4.31}$$

and by the Einstein equations

$$3H^2 = \rho_\phi + \rho_r \,, \tag{4.32}$$

$$-2\dot{H} = p_\phi + \rho_\phi + p_r + \rho_r = \frac{4}{3}\rho_r + \dot{\phi}^2 \,. \tag{4.33}$$

Notice that one of these equations is redundant. Moreover, it would be equivalently possible to use the continuity equation for the inflaton energy density ρ_ϕ

$$\dot{\rho}_\phi + 3H\dot{\phi}^2 = -\Upsilon\dot{\phi}^2 \ . \tag{4.34}$$

It is common to work with the dissipation coefficient ratio Q, defined as $Q \equiv \Upsilon/3H$. Typically, the study of warm inflation assumes the radiation to be thermalized, i.e.

$$\rho_r = \frac{\pi^2 g_*}{30} T^4 = 3p_r \ , \tag{4.35}$$

where g_* is the number of relativistic degrees of freedom for the radiation bath. In general, the relevant microphysical timescales, corresponding to decay and scattering rates, should be larger than the Hubble rate to ensure thermalization. There could be other mechanisms beyond the radiation fields/inflaton interaction, which can dramatically modify this setup. For example, if the radiation fields are coupled to the Standard Model, the Schwinger process [156] should provide an extremely efficient mechanism to reach thermalization, see for example Refs. [157–159]. For the analysis performed in this chapter, we will always assume that some process ensures that radiation thermalizes and Eq. (4.35) holds. The study of these mechanisms plays a significant part in a model building perspective. This is, however, beyond the scope of this work. For a detailed quantification of the thermalization process relevant for warm inflation and done in the context of the Botzmann equation, see, e.g., Ref. [160]. Note also that the specific form for the dissipation coefficient Υ in the above equations can only be determined by the details of the microphysics during inflation. Different forms of dissipation coefficients derived from QFT have been derived explicitly e.g. in Refs. [161, 162]. It is also worth mentioning that warm inflation helps in easing the η-problem [163, 164] since in the strong dissipative regime $Q \gg 1$ the inflaton mass is larger than H.

There have been many constructions based on particle physics models demonstrating the viability of this special regime of inflation, see, for example, Refs. [165, 166] and for a review, see also Ref. [167]. Recently a first principle warm inflation model was constructed from QFT which involves just a few fields [117], thus convincingly demonstrating that warm inflation models are on an equal footing to cold inflation as model building prospects.

The dissipative effects and the presence of a non-vanishing radiation bath are able to change both the inflationary dynamics at the background and at the fluctuation levels [168–176], such that there can be distinctive differences between the two paradigms which could be testable.

Given the complexity of the warm inflation dynamics, which involves a system of coupled fluids associated with the inflaton and radiation, alongside perturbations, that could also be coupled [177, 178], an analytical treatment for the spectrum of perturbations is in general difficult. In what follows, we briefly present this analysis. For a full discussion we send the reader to the Refs. [168, 179]. The dimensionless scalar power spectrum $\Delta_s^2(k,\tau)$ at horizon crossing, meaning $k\tau = 1$ where τ is used to denote the conformal time, is a sum of thermal and vacuum contributions

$$\Delta_s^2(k,\tau) = \Delta_{s,th}^2(k,\tau) + \Delta_{s,vac}^2(k,\tau) \ , \tag{4.36}$$

where the vacuum contribution in the simplest realization of inflation is given by Eq. (4.20). In general, the thermal contribution depends on the microphysics of the model. Nevertheless, a semi-analytical expression for the full spectrum of scalar perturbations can be derived [10, 163, 180] to give the spectrum at horizon crossing as

$$\Delta_s^2(k,\tau)\big|_{\tau=k^{-1}} = \left(\frac{H^2}{2\pi\dot{\phi}}\right)^2 \left[1 + 2n_{BE}(T_{\delta\phi}) + \frac{\sqrt{12}\pi Q}{\sqrt{3+4\pi Q}}\frac{T}{H}\right] G(Q)\Bigg|_{\tau=k^{-1}} , \tag{4.37}$$

where $n_{BE} = [\exp(H/T_{\delta\phi}) - 1]^{-1}$ is the Bose-Einstein distribution. $G(Q)$ is a function of Q that accounts for the fact that the radiation fluctuations are in general coupled to the inflaton which is thus leading to a growing mode in the inflaton fluctuations [177, 178, 181]. Moreover, the temperature $T_{\delta\phi}$ inside n_{BE} corresponds to the temperature of the inflaton fluctuations and is not necessarily the same as T, corresponding to the temperature of the thermal bath. For a recent discussion based on solutions of the Boltzmann equation relevant during the warm inflation dynamics, see, e.g., Ref. [182]. In the following we assume thermal equilibrium and therefore $T_{\delta\phi} = T$. Typically, $G(Q)$ reduces to 1 for $Q = 0$ and in most of the known models it is well-approximated by a fraction

of polynomials in Q with numerically fitted coefficients [177, 178]. Notice that for $Q = 0$, which also implies $T = T_{\delta\phi} = 0$, we recover the usual cold inflation spectrum given in Eq. (4.20) as expected for consistency.

The presence of radiation induces a series of modifications in the typical CMB observables, namely n_s and r. In particular, two competing effects are expected :

1. The decay of the inflaton into radiation is effectively playing the role of an additional friction term for the inflaton beyond the usual Hubble friction. As a consequence, we expect, similarly to [183], a shift in the point of the potential probed by CMB observations. In particular, this effect is expected to produce a decrease of n_s and an increase in r.

2. The radiation will play the role of a source term for scalar field fluctuations which induces an amplification in the scalar power spectrum. Indeed, this can be noticed by Eq. (4.37). However, in general, we do not expect a similar coupling between radiation and tensor fluctuations. As a consequence this effect induces an increase in n_s and a decrease in r.

If thermal effects are already important (or at least not completely negligible) at CMB scales, the first of these two effects happens to be subdominant with respect to the second, meaning that typically n_s is increasing and r is decreasing with respect to the cold case.

For completeness, we should mention that an analysis of non-Gaussianities has been performed for warm inflation for the weak and strong dissipation regimes, see, e.g., Refs. [171, 172]. In both cases the predictions are generally in good agreement with the Planck constraints in Ref. [115].

4.3 Universality in Warm Inflation

Since the original proposals in the early eighties, many models to realize inflation have been introduced and, in some cases, theoretical predictions are so close that they are nearly indistinguishable. In order to constrain this waste zoology and possibly rule out some of these models, it is useful to introduce a systematic way to classify models of inflation. Several approaches have been introduced over the last years [184–186]. In this chapter, we work with the β-function formalism. It relies on the Hamilton-Jacobi formalism of D. S. Salopek and

J. R. Bond [125], and is based on the idea of describing inflation in terms of a renormalization group equation. In this framework, models are grouped into classes that share a minimal set of universal properties. Originally introduced for the simplest realization of inflation [118], the formalism has been extended to more sophisticated scenarios, such as non-standard kinetic terms [121], constant-roll [123] and anisotropic inflation [124]. This method is not only suitable to deal with concrete models, but it is also strongly connected to deeper theoretical aspects. In particular, this formalism has an interesting interpretation under the gauge/gravity duality of J. M. Maldacena [129]. Moreover, this approach sheds a new light on the inflationary dynamics and provides strong analytical tools to investigate the evolution of the physical quantities such as the Hubble factor and the power spectrum during inflation. The goal of our analysis in this chapter is to extend the formalism to warm models of inflation and identify universality. Let us start with a review of the β-function formalism.

4.3.1 Identifying Universality with the β-Function Formalism

In the simplest realization of inflation, the evolution of the Universe during inflation is completely specified by the equation of motion for the inflaton and one of the two Friedmann equations (2.7)-(2.8). The HJ formalism relies on the reasonable assumptions that a solution of this system exists and that the time evolution of ϕ as function of t is piecewise monotonic. It is then possible to invert to get $t(\phi)$ and use the field as a clock to describe the evolution of the system. At this point, we introduce the so-called superpotential[5]

$$W(\phi) \equiv -2H(\phi) \,, \tag{4.38}$$

and, using the Friedmann equations, we find

$$\dot{\phi} = W_{,\phi} \,, \tag{4.39}$$

implying that it is possible to express $\dot{\phi}$ (and therefore all physical quantities) as a function of ϕ only.

By following a formal analogy with the definition of the RGE describing the evolution of the renormalized coupling constant, whose role here is played by

[5]The formal analogy between the parametrization of the scalar potential in SUSY (for a review, see for example [187]) and in the formalism [118], justifies the name.

the inflaton, in terms of the renormalization scale, here the scale factor a, we introduce the cosmological β-function as

$$\beta(\phi) \equiv \frac{\mathrm{d}\phi}{\mathrm{d}\ln a} \,. \tag{4.40}$$

From this definition and with a simple algebra, we are able to show that the equation of state (4.1) becomes

$$\frac{p+\rho}{\rho} = \frac{4}{3}\frac{W_{,\phi}^2}{W^2} = \frac{\beta^2(\phi)}{3} \,, \tag{4.41}$$

and implies that a phase of accelerated expansion is realized[6] for $|\beta(\phi)| \ll 1$. In analogy with the RG approach, we identify the zeros of the β-function as fixed points, which, in the cosmological case, correspond to exact dS solutions. Depending on the sign of the β-function, inflationary periods are then represented by the flow of field away (or toward) these fixed points[7]. As a consequence, it is possible to classify the various models of inflation according to the behavior of the β-function in the neighborhood of the fixed point, rather than according to the potential. The advantage of this approach is that the specification of $\beta(\phi)$ actually defines a class of universality that encompasses many models. These might have in principle very different potentials but yield to a similar cosmological evolution (and thus to similar predictions for cosmological observables such as the scalar spectral index n_s and the tensor-to-scalar ratio r). Moreover, it allows the study of a large variety of models with a single class of function. Notice that, in order to realize a phase of accelerated expansion, we only need $|\beta(\phi)| \ll 1$ and in general this does not require $\beta \to 0$. In particular, inflation can be realized even if $\beta(\phi)$ approaches a small constant value. As discussed in [118], this is the case of power law inflation [188].

Beyond a Simple Identification of Universality In addition to the original goal of identifying universality, the formalism has several interesting outcomes. In particular, it provides strong analytical tools to study the dynamics of the period of inflation. All relevant quantities are expressed as function of $\beta(\phi)$ [118].

[6] More precisely, $\ddot{a}/a > 0$ requires $|\beta(\phi)| < \sqrt{2}$. For simplicity, in the following we assume inflation to end at $|\beta(\phi)| \sim 1$.

[7] When the flow is toward the fixed point there is no natural end to the period of accelerated expansion. Clearly, this configuration is not suitable to describe inflation.

For example, the number of e-foldings N becomes

$$N = -\ln(a/a_{\rm f}) = -\int_{\phi_{\rm f}}^{\phi} \frac{{\rm d}\phi'}{\beta(\phi')} \,, \tag{4.42}$$

where $\phi_{\rm f}$ is the value of the field at the end of inflation. Similarly, we can compute the Hubble factor which is equivalent to the superpotential

$$W(\phi) = W_{\rm f} \exp\left(-\int_{\phi_{\rm f}}^{\phi} \frac{\beta(\phi')}{2} {\rm d}\phi'\right) \,, \tag{4.43}$$

and the inflationary potential

$$V(\phi) = \frac{3}{4}W^2 - \frac{1}{2}W_{,\phi}^2 = \frac{3}{4}W^2\left(1 - \frac{\beta^2(\phi)}{6}\right) \,, \tag{4.44}$$

whose parametrization is similar to the one in the context of supersymmetric quantum mechanics (for reference, see for example [187]). It is important to stress that, so far, all the computations are exact, *i.e.* we have not performed any approximation and the analysis holds even if we are not assuming slow-roll.

Assuming now to be in a neighborhood of the fixed point, we have $|\beta(\phi)| \ll 1$ and n_s and r, at the lowest order in terms of β and its derivative, simply read

$$n_s - 1 \simeq -\left(\beta^2 + 2\beta_{,\phi}\right) \,, \qquad\qquad r = 8\beta^2 \,. \tag{4.45}$$

In order to obtain the standard expressions of n_s and r in terms of N, we first determine the value of ϕ at the end of inflation (using the condition $|\beta(\phi_{\rm f})| \sim 1$). We then proceed by computing $N(\phi)$ (using Eq. (4.42)) and invert it into $\phi(N)$ to express n_s and r in terms of the number of e-foldings.

This parametrization of inflation brings a new perspective on the theoretical side. The analogy with the QFT β-function is not only at a formal level. Indeed, it is possible to relate the cosmological β-function of Eq. (4.40) with the β-function describing the RG flow induced by some relevant operator in the dual QFT, in the context of the AdS/CFT correspondence. The departure from the exact de Sitter geometry is linked to a breaking of the dual CFT. However, in order to properly set this correspondence, we have to specify a mapping between the bulk inflaton and the coupling in the dual QFT. This typically requires the specification of some renomalization condition which in principle may require a modification of the simple expression of β in terms of W. While a detailed discussion of the

holographic interpretation is beyond the scope of this work, an accurate discussion of this procedure can be found in [189].

Finally, and for completeness, we must state that this formalism also applies to quintessence [122]. In this scenario, the flow is not away from a fixed point but toward. The full history of the Universe in the ΛCDM model with inflation can then be described by a flow between two fixed points.

Examples of Universality Classes

Let us conclude this review of the β-formalism by briefly presenting some of the classes introduced in Ref. [118], starting with the so-called monomial class, where

$$\beta(\phi) = \alpha\phi^q \ , \tag{4.46}$$

with α and q being positive constants. This class describes small field models, i.e., inflation taking place for $\phi \ll 1$, with

$$W(\phi) = W_f \exp\left[-\frac{\alpha}{2(q+1)}\left(\phi^{q+1} - \phi_f^{q+1}\right)\right] \ , \tag{4.47}$$

implying that, at the lowest order, models of this class feature a hilltop potential.

We can also consider the so-called inverse class, where

$$\beta(\phi) = -\frac{\alpha}{\phi^q} \ , \tag{4.48}$$

with α and q being positive constants. This class describes large field models, i.e., inflation taking place for $\phi \gg 1$, with

$$W(\phi) = W_f \exp\left[\frac{\alpha}{2(q-1)}\left(\frac{1}{\phi_f^{q-1}} - \frac{1}{\phi^{q-1}}\right)\right] \ , \tag{4.49}$$

implying that at the lowest order, models of this class feature an algebraically flat plateau potential. The case with $q = 1$ is special, the superpotential is of the form $W = W_f(\phi/\phi_f)^{\frac{\alpha}{2}}$ and corresponds to chaotic models of inflation.

Finally, is the so-called exponential class, where

$$\beta(\phi) = -\alpha \exp(-\gamma\phi) \ , \tag{4.50}$$

with α and γ being positive constants. This class describes large field models, with

$$W(\phi) = W_f \exp\left\{-\frac{\alpha}{2\gamma}\left[\exp\left(-\gamma\phi\right) - \exp\left(-\gamma\phi_f\right)\right]\right\} , \tag{4.51}$$

implying that at the lowest order models of this class feature an exponentially flat plateau potential.

4.3.2 β-Function Formalism for Warm Inflation

For warm inflation, a model is not only specified by the inflationary potential, but also by the dissipation coefficient ratio Q, which in general is a function of both ϕ and T. Once these two functions are specified, the evolution is completely determined by the set of equations (4.30)-(4.33). By solving these equations, we can express all the relevant quantities, i.e., $H(t)$, $\phi(t)$, $Q(t)$, and $T(t)$, as functions of time. Once again, the problem can be studied in the framework of the HJ formalism. Assuming the evolution of $\phi(t)$ to be piecewise monotonic, it is possible to compute, at least locally, $t(\phi)$ and express all the relevant quantities as functions of the field only.

Setting the Formalism

In analogy with the treatment carried out in the cold case, we introduce a superpotential $W(\phi) \equiv -2H(\phi)$. Assuming the radiation energy density to be quasi-stable[8], meaning $\dot{\rho}_r \ll 4H\rho_r$, and using the Raychauduri equation (4.33) we obtain

$$\dot{\phi} = \frac{W_{,\phi}}{1+Q} . \tag{4.52}$$

By using this equation and Eq. (4.33) we get from Eq. (4.35)

$$T^4 = \frac{45}{2\pi^2 g_*}\frac{Q}{(1+Q)^2}W_{,\phi}^2 . \tag{4.53}$$

To find the temperature as a function of ϕ only, Eq. (4.53) needs to be solved for T. Since, in general, Q depends both on T and ϕ, the solution of this equation might exist only numerically. Then, once $T(\phi)$ is known, the dissipation coefficient ratio

[8]More on this approximation is said below Eq. (4.58) where we re-express this condition in terms of the typical quantities of the formalism.

is expressed as a function of ϕ only[9] as $Q(T(\phi),\phi) \equiv \mathcal{Q}(\phi)$. A different notation, $\mathcal{Q}$, is used here to stress the difference in the functional dependence on ϕ.

We proceed our discussion by introducing the cosmological β-function as defined in Eq. (4.40), $\beta(\phi) \equiv \mathrm{d}\phi/\mathrm{d}\ln a = \dot{\phi}/H$. Note that the analogy with a RGE still holds. The equation of state reads

$$-\frac{2\dot{H}}{3H^2} = \frac{(1+Q)\dot{\phi}^2}{3H^2} = (1+Q)\frac{\beta^2(\phi)}{3} \,. \tag{4.54}$$

Interestingly, Eq. (4.54) shows that an exact dS geometry is again realized in correspondence to the zeros of $\beta(\phi)$ and the phase of accelerated expansion of the Universe stops when $(1+Q)\beta^2(\phi)$ is of order one. This is a crucial difference with respect to the cold case in Eq. (4.41). As Q is always positive, the fixed point is only attained by a vanishing β-function, but, in general, unless we have β exactly equal to zero, $\beta^2(\phi) \ll 1$ is not sufficient to ensure that the Universe is inflating. In particular, the Universe may stop to inflate because $(1+Q) \gg \beta^{-2}(\phi)$, while $\beta \ll 1$. Another original and strictly warm realization of inflation is the case in which, departing from the dS fixed point, $\beta(\phi)$ reaches a constant value smaller than one. In such a scenario, the last part of the inflationary phase is thus driven and, in particular, is concluded by the evolution of Q. As inflation can only be realized for $\beta(\phi) \ll 1$, its parametrization can still be used to fix the flow in the neighborhood of the fixed point. Once again, it is thus possible to use $\beta(\phi)$ to define a set of universality classes as in the cold inflation case.

To make the generalization from cold inflation more evident, let us define

$$\beta_{CI}(\phi) \equiv -2\frac{W_{,\phi}}{W} = (1+Q)\beta(\phi) \,, \tag{4.55}$$

which has the exact same dependence on W as the beta function of the cold inflation, Eq. (4.40). With this definition, the superpotential W can be readily expressed as

$$W(\phi) = W_f \exp\left[-\frac{1}{2}\int_{\phi_f}^{\phi} \mathrm{d}\phi' \beta_{CI}(\phi')\right] \,, \tag{4.56}$$

where the subscript $_f$ is used to denote quantities evaluated at the end of inflation. Moreover, using the definition given in Eq. (4.55), it is easy to prove that the

[9] In principle, it could also be possible to start by directly fixing a parametrization for $\mathcal{Q}(\phi)$. More on this will be commented in Sec. 4.6.

equation of state can be expressed as

$$-\frac{2\dot{H}}{3H^2} = \frac{\beta_{CI}^2(\phi)}{3(1+Q)} \ . \tag{4.57}$$

Again, the fixed point is reached when β_{CI} goes to zero and we see that inflation ends when $\beta_{CI}^2 \sim 1+Q$. According to Eq. (4.56), β_{CI} is directly associated with the superpotential and, thus, with the inflationary potential. This equation makes clear that for Q sufficiently large, the Universe is inflating for $\beta_{CI} > 1$. In this sense, the dissipation coefficient can be interpreted as a friction term that slows down the evolution of the inflaton field and this is potentially allowing for inflation in regions of the potentials that are steeper than the ones usually considered in the cold case. As already mentioned in the previous section, this could provide a mechanism to ease the η-problem. In order to generalize the universality classes defined for cold inflation in Ref. [118], we will use, in this work, the β-functions associated with these classes as choices for β_{CI}. We then observe how the different dissipation coefficient ratios will affect the predictions of any classes, this analysis is carried out in Sec. 4.4 and 4.5.

At this point, we can translate the quasi-stable assumption of the radiation energy density in the language of the β-function formalism

$$\left|\frac{\beta}{4}\frac{\mathrm{d}\ln\rho_r}{\mathrm{d}\phi}\right| = \left|\frac{\beta_{CI}}{4(1+Q)}\left[\frac{Q_{,\phi}}{Q}\left(\frac{1-Q}{1+Q}\right) + 2\frac{\beta_{CI,\phi}}{\beta_{CI}} - \beta_{CI}\right]\right| \ll 1 \ . \tag{4.58}$$

The validity of this condition has to be checked for each choice of β_{CI} and Q. However, it is possible to show that for all the cases discussed in this work, this assumption is satisfied.

Fixed-Point Interpretation

To grasp a better understanding of the competing influences of β_{CI} and Q during the phase of inflation, it is worth defining the complementary function β_T as

$$\beta_T(\phi) \equiv \frac{T}{H} = -2\frac{T}{W} \ . \tag{4.59}$$

Using Eq. (4.35) we express

$$\frac{\rho_r}{H^2} = \frac{\pi^2 g_*}{30}\frac{T^4}{H^2} = \frac{\pi^2 g_*}{30}\left[T\beta_T(\phi)\right]^2 \ , \tag{4.60}$$

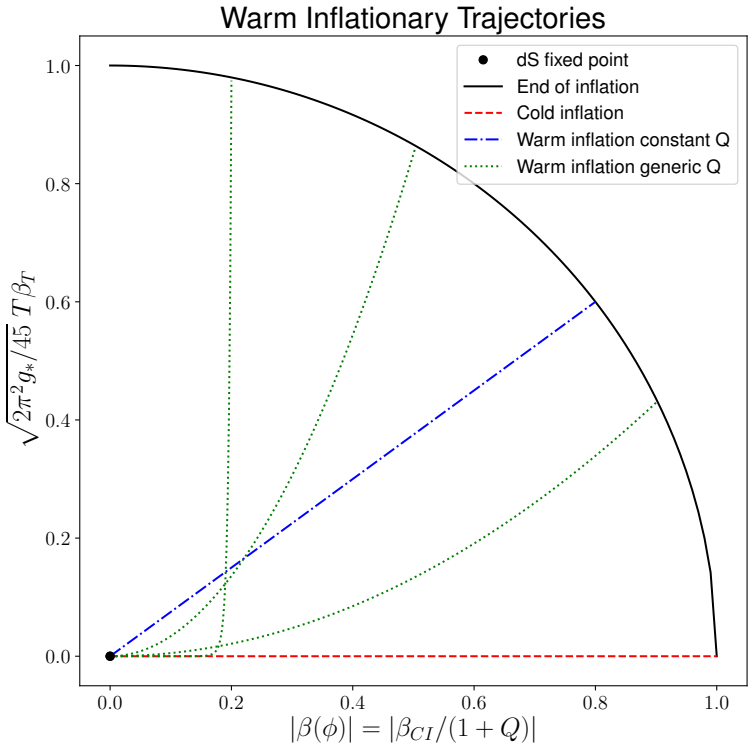

Figure 4.2 *Some possible inflationary trajectories corresponding to the flow from the dS fixed point to the solid black line and showing the departure from the usual cold inflation case (red dashed line). The curves shown in this plot are illustrative examples which are not corresponding to any concrete model.*

which makes manifest the interpretation of β_T. This function captures the amount of radiation produced during warm inflation. In particular, by considering the full equation of state,

$$\begin{aligned} -\frac{2\dot{H}}{3H^2} &= \frac{\dot{\phi}^2 + \frac{4}{3}\rho_r}{3H^2} \\ &= \frac{\beta^2(\phi)}{3} + \frac{2\pi^2 g_*}{45}\frac{[T\beta_T(\phi)]^2}{3} \\ &= \frac{1}{3}\left[\frac{\beta_{CI}(\phi)}{Q+1}\right]^2 + \frac{2\pi^2 g_*}{45}\frac{[T\beta_T(\phi)]^2}{3}\,, \end{aligned} \tag{4.61}$$

it is clear that (as $T \neq 0$) β_T parametrizes the flow from the dS fixed point induced by radiation. Interestingly, using the definitions of β_{CI} and β_T, we can represent the phase of inflation in a two-dimensional plot depicting the departure from the usual cold inflation case. In Fig. 4.2, the phase of inflation is represented as a trajectory starting from, or close to, the dS fixed point at the origin and reaching the circle of unitary radius, where $(1+Q_f)\beta_f^2 = 1$, which corresponds to the end

of inflation. From the equation of state (4.61) we note that the axes in Fig. 4.2 are proportional the square roots of the fractional kinetic and thermal energy densities. The flow along the different inflationary trajectories can be directly parametrized by the value of the inflaton field ϕ, or equivalently by the number of e-foldings N defined in Eq. (4.63). A motion in the horizontal direction is due to β_{CI}, whereas a vertical motion is an effect of production of radiation. Since we have that

$$T\beta_T(\phi) = \sqrt{\frac{45}{2\pi^2 g_*}\frac{Q}{(Q+1)^2}}|\beta_{CI}(\phi)| \,, \tag{4.62}$$

we observe that the shape of the trajectory is mostly defined by the dissipation coefficient ratio Q. In these kind of plots, any model of cold inflation is represented as a horizontal line with $T\beta_T = 0$. Conversely, warm inflation models are expected to be represented as curves departing from this line. As all the inflationary trajectories are expected to end on the solid black line, large values of β_f, i.e., for values closer to $T_f\beta_{T\,f} = 0$, imply a small radiation contribution to the equation of state at the end of inflation. Conversely, small values for $\beta(\phi_f)$ imply a non-negligible radiation contribution to the equation of state at the end of inflation.

Apart from the de Sitter fixed point at the origin, there are two other special points on Fig. 4.2. The first is (1,0), where cold inflation usually ends. When a trajectory crosses this point, the Universe stops inflating and it must then enter into the (p)reheating phase. The second point, which is not appearing on our plots, should be (0,2). This corresponds to the Universe being in the radiation-dominated era, i.e. $\rho_r/(3H^2) \simeq 1$. Notice that all trajectories describing viable cosmological models, which consistently include the evolution of the Universe after inflation, must cross this point. However, since in (0,2) we have $\dot{\rho}_r = 4H\rho_r$, for sure the assumption of quasi-stable radiation must be violated, implying that our treatment cannot be extended all the way up to this point.

A model which touches the solid black line for large (order 1) values of $\sqrt{2\pi^2 g_*/45}\,T\beta_T$, for example the vertical dotted curve in Fig. 4.2, implies that the RG flow in the last part of inflation is mainly induced by the radiation. This does not imply that the Universe is dominated by the radiation, but rather that it is rapidly approaching the moment where the transition from inflation to a radiation-dominated Universe takes place. Since in these models the radiation energy density at the end of inflation is already sizable and the inflaton kinetic energy is small, an explosive (p)reheating may not be required and the transition

from inflation to radiation may be smooth. This has to be checked model by model. Since in warm inflation it is possible to unify the treatment of inflation and (p)reheating, a self-consistant computation of N_{CMB}, the value of N at which CMB observables leave the horizon, could in principle be carried out. However, in order to perform this analysis, we need to study the trajectory until the point (0,2) is reached, which requires to violate the assumption of quasi-stable radiation. As this goes beyond the scope of this work, we will adopt $N_{CMB} = 60$ as a representative value.

Analytical Expressions

One of the main outcomes of the β-function formalism is the possibility for a deep analytical treatment of the inflationary dynamics. This is also true when applied to warm inflation. To illustrate this aspect, let us express some of the relevant quantities in terms of the β-functions.

The expression of the number of e-foldings N in this formalism reads

$$N(\phi) \equiv -\int_{a_f}^{a} \mathrm{d}\ln a' = -\int_{\phi_f}^{\phi} \frac{\mathrm{d}\phi'}{\beta(\phi')} = -\int_{\phi_f}^{\phi} \mathrm{d}\phi' \frac{1+Q(\phi')}{\beta_{CI}(\phi')} \,, \tag{4.63}$$

where ϕ_f is the field value at the end of inflation, fixed by $\beta_{CI}^2(\phi_f) = 1 + Q(\phi_f)$, and the expression of the inflationary potential which is derived using Eq. (4.32),

$$V(\phi) = \frac{3}{4} W^2(\phi) \left[1 - \frac{1}{6}\frac{(1+3Q/2)}{(Q+1)^2}\beta_{CI}^2(\phi)\right] \,. \tag{4.64}$$

As for the physically relevant cases, we expect both β_{CI} and Q to be negligible while the Universe is deep into the inflationary phase, i.e., for large values of N, the parametrization of the inflationary potential is typically mainly determined by the superpotential $W(\phi)$. It is worth mentioning that the formalism is not only valid at the background level, it can also be used to describe cosmological perturbations.

The Hubble slow-roll parameters defined in Eq. (4.24) read

$$\epsilon_1 = \frac{1}{2}\frac{\beta_{CI}^2}{1+Q} = \frac{1}{2}(1+Q)\beta^2(\phi) \,, \tag{4.65}$$

$$\epsilon_2 = \frac{2\beta_{CI,\phi}}{1+Q} - \frac{\beta_{CI} Q_{,\phi}}{(1+Q)^2} \,, \tag{4.66}$$

$$\epsilon_3 = \frac{\beta_{CI}}{1+Q}\frac{\frac{2\beta_{CI,\phi\phi}}{1+Q} - \frac{3\beta_{CI,\phi}Q_{,\phi}}{(1+Q)^2} - \frac{\beta_{CI}Q_{,\phi\phi}}{(1+Q)^2} + \frac{2\beta_{CI}Q_{,\phi}^2}{(1+Q)^3}}{\frac{2\beta_{CI,\phi}}{1+Q} - \frac{\beta_{CI}Q_{,\phi}}{(1+Q)^2}} \,, \tag{4.67}$$

$$\epsilon_{i+1} = \frac{\beta_{CI}}{1+Q}\frac{\mathrm{d}\ln\epsilon_i}{\mathrm{d}\phi} \,. \tag{4.68}$$

In order to have a better connection with the literature on warm inflation, it is also useful to define

$$\epsilon \equiv \frac{1}{2}\frac{\beta_{CI}^2}{1+Q} \,, \qquad \eta \equiv \frac{2\beta_{CI,\phi}}{1+Q} \,, \qquad \sigma \equiv -\frac{\beta_{CI}Q_{,\phi}}{(1+Q)^2} \,, \tag{4.69}$$

such that $\epsilon_1 = \epsilon$ and $\epsilon_2 = \eta + \sigma$.

Regarding cosmological perturbations, using the definitions given in Sec. 4.3, we translate the expressions of Sec. 4.2.4 in terms of the typical quantities of the β-function formalism. We start by expressing the scalar spectrum in terms of β_{CI}, β_T and $\mathcal{Q}$,

$$\Delta_s^2(k,\tau)\big|_{\tau=k^{-1}=-\frac{2}{aW}} = \left[\frac{(1+Q)W}{4\pi\beta_{CI}}\right]^2\left(1 + \frac{2}{\exp\frac{1}{\beta_T}-1} + \frac{\sqrt{12}\pi Q}{\sqrt{3+4\pi Q}}\beta_T\right)G(Q) \,. \tag{4.70}$$

This expression for the scalar spectrum is used to fix W_f, the value of the superpotential at the end of inflation, in order for the model to agree with the COBE normalization (4.27) [42, 114]. In particular, we first derive $W(\phi)$ and then we impose $W_f = W(\phi(N_{CMB}))$ with $N_{CMB} = 60$. For completeness, let us proceed by expressing the tensor power spectrum as

$$\Delta_t^2(k)\big|_{\tau=k^{-1}=-\frac{2}{aW}} = \frac{W^2}{2\pi^2} \,, \tag{4.71}$$

which has exactly the same expression as in the cold case.

Finally, we provide the predictions for n_s and r, with expressions given by

$$n_s - 1 = \frac{\beta_{CI}}{1+Q-\frac{1}{2}\beta_{CI}^2}\left[\frac{2Q_{,\phi}}{Q+1} - \beta_{CI} - \frac{2\beta_{CI,\phi}}{\beta_{CI}} + \frac{G_{,\phi}}{G} + \frac{2n^2 e^{\frac{1}{\beta_T}}\frac{\beta_{T,\phi}}{\beta_T^2} + \frac{\sqrt{12}\pi\mathcal{Q}_{,\phi}}{\sqrt{3+4\pi\mathcal{Q}}}\beta_T - \frac{\sqrt{3}\pi\mathcal{Q}}{(3+4\pi\mathcal{Q})^{3/2}}(4\pi\mathcal{Q}_{,\phi}\beta_T) + \frac{\sqrt{12}\pi\mathcal{Q}}{\sqrt{3+4\pi\mathcal{Q}}}\beta_{T,\phi}}{1+2n+\beta_T\frac{\sqrt{12}\pi Q}{\sqrt{3+4\pi\mathcal{Q}}}}\right] \,, \tag{4.72}$$

$$r = \frac{8\beta_{CI}^2(\phi)}{(1+Q)^2} \frac{1}{\left(1 + 2n + \frac{2\sqrt{3}\pi Q}{\sqrt{3+4\pi Q}}\beta_T\right) G(Q)} \,. \tag{4.73}$$

It has been a basic feature of the fluctuation-dissipation dynamics, intrinsic to warm inflation, that the tensor-to-scalar ratio in general is lower as compared to cold inflation. For the ϕ^4 model, it was predicted from warm inflation in [163, 181], well before the CMB data, that this ratio would be lower. Here, we present a compact expression for the tensor-to-scalar ratio simply written as the expression that appears for cold inflation $r_{CI} = 8\beta_{CI}^2(\phi)$ multiplied by a correction factor, the denominator of Eq. (4.73). In agreement with the literature [163, 181] and, as discussed in Section 4.2.4, this correction term lowers the prediction for r with respect to cold inflation when the dissipation coefficient ratio is of order of unity or when β_T is larger than one.

4.4 Applying the Formalism to Explicit Examples

In this section, we provide a general procedure for computing the predictions in the β-function formulation of warm inflation. In particular, we start by explaining our numerical methods for examining models, and then focus on some special cases that admit an analytical treatment. As already explained in Sec. 4.3, the model is completely specified by fixing a β-function, either $\beta(\phi)$ or $\beta_{CI}(\phi)$, and by a dissipation coefficient ratio $Q(T, \phi)$. In order to generalize the classes of universality for cold inflation [118], we choose to start by fixing a parametrization for $\beta_{CI}(\phi)$. The dissipation coefficient $\Upsilon(T, \phi)$ is derived explicitly by QFT methods, see, e.g., Refs. [161, 162]. In this work, we focus on a rather general parametrization for the dissipation ratio $Q = \Upsilon/(3H)$ that is motivated by the previous warm inflation models developed in the literature [117, 161, 162, 165, 169, 190],

$$Q = \frac{CT^m}{H\phi^n} = -\frac{2CT^m}{W\phi^n} \,, \tag{4.74}$$

where C is a constant. This example will also facilitate the illustration of the methodology. When a complete specification of the model is required, i.e. an explicit choice for $\beta_{CI}(\phi)$, we will restrict our analysis, for simplicity, to the

chaotic class

$$\beta_{CI}(\phi) = -\frac{\alpha}{\phi} \,, \tag{4.75}$$

where α is a positive constant. The generalization to other classes of models can be carried out analogously.

In general, it is unlikely to have a complete analytical description of the model and, therefore, numerical methods are required. The procedure we have used to derive numerical solutions is the following. Having $\beta_{CI}(\phi)$, $Q(T,\phi)$ and an initial guess value for the constant W_f, which fixes the normalization of the inflationary potential, as inputs, the value of the scalar field at the end of inflation ϕ_f and the corresponding temperature T_f are computed using

$$\beta^2_{CI,f} = 1 + Q_f \,, \tag{4.76}$$

$$T_f^4 = \frac{45}{8\pi^2 g_*}\frac{Q_f}{1+Q_f}W_f^2 \,, \tag{4.77}$$

where we recognize Eq. (4.53) in the second of these equations. They can be recasted as

$$T_f = \left(\frac{45C}{4\pi^2 g_*}\frac{-W_f}{\beta^2_{CI,f}\phi_f^n}\right)^{\frac{1}{4-m}} \,, \tag{4.78}$$

$$\beta^2_{CI,f} = 1 + \left(\frac{45}{8\pi^2 g_* \beta^2_{CI,f}}\right)^{\frac{m}{4-m}} \left(\frac{2C}{\phi_f^n}\right)^{\frac{4}{4-m}} (-W_f)^{\frac{2m-4}{4-m}} \,. \tag{4.79}$$

The solution of the above system of equations is obtained by first solving for ϕ_f and then computing T_f. The inflaton field then serves as a clock for the evolution of the system. We evolve the field from ϕ_f to $\phi_f \pm \Delta\phi$ with $\Delta\phi \ll \phi_f$ being an infinitesimal step. The sign of the increment is fixed by the position of the fixed point, i.e., whether the value of the field increases or decreases during inflation. At this point the relevant quantities T, Q and N are evaluated at $\phi_f \pm \Delta\phi$ using Eq. (4.53), the definition of Q and Eq. (4.63), respectively. The procedure is then repeated until the value ϕ_{CMB} is reached. The latter is defined as the value of ϕ which gives $N(\phi_{CMB}) = N_{CMB}$ where in this work we assume $N_{CMB} = 60$ as the value of N at which CMB observables leave the horizon. As a consequence, the evolution is solved for all the scales between the end of inflation and CMB scales. Finally, by comparing the amplitude of the scalar power spectrum with the COBE normalization [42, 114], it is possible to adjust the constant W_f in

order to satisfy this constraint. The predictions for the scalar spectral index and tensor-to-scalar ratio are then computed from Eqs. (4.72) and (4.73) for the values of ϕ corresponding to N_{CMB}. These quantities can finally be compared with the observational constraints [42, 114].

4.4.1 Analytical Methods

In this subsection, we focus on some cases where a complete (or partial) analytical treatment can be performed. In order to carry out this analysis, we have to

1. Compute ϕ_f and T_f, the values of the inflaton field and of the temperature at the end of inflation using Eqs. (4.76)-(4.77);
2. Derive the superpotential and its derivative using β_{CI} and Eq. (4.56);
3. Compute $T(\phi)$ by solving Eq. (4.53) with the dissipation coefficient ratio $Q(T, \phi)$ written explicitly in terms of T and ϕ. Having T as a function of the field, we can also write $Q(T(\phi), \phi)$ as a function of ϕ only;
4. Finally, we express β_T as a function of ϕ using Eq. (4.62).

Note that, in general, the third step cannot be carried out analytically for non-trivial forms of the dissipation coefficient. Typically, it is also useful to derive all the relevant quantities as functions of the number of e-folds. For this purpose, we thus compute the number of e-foldings $N(\phi)$ from Eq. (4.63) and invert it to find $\phi(N)$. Once again, we fix the constant W_f in order to be consistent with the COBE normalization (4.27). In particular, this is done by solving Eq. (4.70) for $W(N)$ at $N = N_{CMB}$. Let us now illustrate the method with some examples where a partial (or complete) analytical treatment exists.

Constant Q - Full Analytical Treatment

We first restrict to the simplest possible case, a constant dissipation coefficient ratio $Q(T, \phi) = Q$. We consider a generic β_{CI} and then study the specific example of the chaotic class specified by Eq. (4.75). For a constant Q, Eq. (4.53) admits the solution

$$T(\phi) = \left[\frac{45}{8\pi^2 g_*}\frac{Q}{(1+Q)^2}W^2(\phi)\beta_{CI}^2(\phi)\right]^{1/4}, \tag{4.80}$$

where $W(\phi)$ is directly set by Eq. (4.56). To check the consistency of the model, we can compute ρ_r, by substituting Eq. (4.80) into Eq. (4.60),

$$\rho_r = \frac{3}{16}\frac{Q}{(1+Q)}W^2(\phi)\beta_{CI}^2(\phi)\ . \tag{4.81}$$

Interestingly, this can be compared with the result

$$\rho_\phi = \frac{3}{4}W^2 - \rho_r = \frac{3}{4}W^2\left[1 - \frac{Q}{(1+Q)}\frac{\beta_{CI}^2(\phi)}{4}\right]\ , \tag{4.82}$$

to conclude that, independently on the value of Q, when we approach the dS fixed point, $\beta_{CI}(\phi) \ll 1$, we always consistently get $\rho_r \ll \rho_\phi$.

To proceed further, we need to precise a parametrization for β_{CI} and therefore, we restrict ourselves to the case of the chaotic class of Eq. (4.75). In this case, the superpotential and the temperature, respectively, read

$$W = W_f\left(\frac{\phi}{\phi_f}\right)^{\frac{\alpha}{2}}\ , \tag{4.83}$$

$$T(\phi) = \left[\frac{45}{8\pi^2 g^*}\frac{Q}{(1+Q)^2}\frac{\alpha^2 W_f^2}{\phi_f^\alpha}\phi^{\alpha-2}\right]^{1/4}\ . \tag{4.84}$$

For completeness, we also derive, using Eq. (4.64), the potential

$$V = \frac{3}{4}W_f^2\left(\frac{\phi}{\phi_f}\right)^\alpha\left[1 - \frac{\alpha^2}{12\phi^2}\frac{2+3Q}{(1+Q)^2}\right] \simeq \frac{3}{4}W_f^2\left(\frac{\phi}{\phi_f}\right)^\alpha\ , \tag{4.85}$$

where the approximation in the last step relies on $\phi \gg \alpha$, which is valid deep in the inflationary phase. The value of the field at the end of inflation is

$$\phi_f = \sqrt{\frac{\alpha^2}{1+Q}}\ , \tag{4.86}$$

and the number of e-foldings N as a function of ϕ reads

$$N = \frac{1+Q}{2\alpha}\left(\phi^2 - \frac{\alpha^2}{1+Q}\right)\ , \tag{4.87}$$

which implies

$$\phi = \sqrt{\frac{2\alpha N + \alpha^2}{1+Q}}\ . \tag{4.88}$$

At this point, we can also compute $\beta_{CI}(N)$, $T(N)$ and $\beta_T(N)$, whose expressions are given, respectively, by

$$\beta_{CI}(N) = -\sqrt{\frac{(1+Q)\alpha}{2N+\alpha}}\,, \tag{4.89}$$

$$T(N) = \left[\frac{45}{8\pi^2 g^*}\frac{Q}{1+Q}\alpha^{2-\alpha}W_f^2\left(2\alpha N+\alpha^2\right)^{\alpha/2-1}\right]^{1/4}\,, \tag{4.90}$$

$$\beta_T(N) = \left[\frac{90}{\pi^2 g_*}\frac{Q}{1+Q}\frac{\alpha^{2+\alpha}}{W_f^2}\left(2\alpha N+\alpha^2\right)^{-\alpha/2-1}\right]^{1/4}\,. \tag{4.91}$$

Notice that for $\alpha = 2$, the temperature is constant during inflation. Finally, we fix W_f using the COBE normalization, and we compute the spectral tilt n_s and the tensor-to-scalar ratio r using Eqs. (4.72) and (4.73). As Q is positive, we expect a slightly increased value of n_s and a slightly reduced value of r with respect to the cold inflation case.

Weak and Strong Dissipative Limits

For the general choice of $Q(T,\phi)$, Eq. (4.74), an analytical description does not exist in all regimes. However, similarly to the treatment of Ref. [191], an analytical description of these models can be achieved both in the strong $Q \gg 1$ and in the the weak $Q \ll 1$ dissipative limits. In particular, it is possible to derive analytical expressions for $\mathcal{Q}$ and T as function of ϕ only, which we do next.

Weak Dissipative Regime Let us consider the parametrization of $Q(T,\phi)$ given in Eq. (4.74). In the limit $Q \ll 1$ we can immediately use Eq. (4.53) to compute the temperature to obtain

$$T(\phi) = \left[\frac{45C}{4\pi^2 g_*}\frac{\beta_{CI}^2(-W)}{\phi^n}\right]^{\frac{1}{4-m}}\,, \tag{4.92}$$

and then, by substituting this expression into Eq. (4.74), we find

$$\mathcal{Q}(\phi) = 2C\left(\frac{45C}{4\pi^2 g_*}\right)^{\frac{m}{4-m}}(-W)^{\frac{2(m-2)}{4-m}}\,\phi^{\frac{-4n}{4-m}}\beta_{CI}^{\frac{2m}{4-m}}\,. \tag{4.93}$$

To completely specify the model, we need to substitute an explicit parametrization for β_{CI}. For the example of the chaotic class Eq. (4.75), we find that

$$T(\phi) \simeq \left[\frac{45C\alpha^2(-W_f\phi_f^{-\frac{\alpha}{2}})}{4\pi^2 g_*}\right]^{\frac{1}{4-m}} \phi^{\frac{\alpha-4-2n}{2(4-m)}} , \tag{4.94}$$

$$\mathcal{Q}(\phi) \simeq 2C\left(\frac{45C\alpha^2}{4\pi^2 g_*}\right)^{\frac{m}{4-m}} \left(W_f^2\phi_f^{-\alpha}\right)^{\frac{(m-2)}{4-m}} \phi^{\frac{\alpha(m-2)-2m-4n}{4-m}} . \tag{4.95}$$

It is worth noting that this regime can only be attained dynamically for a certain set of values for α, C, n and m. Recall that W_f is fixed by the COBE normalization and, thus, it should not be considered as a free parameter. In particular, as the chaotic class describes large field models, meaning that inflation takes place for large values of ϕ, this can only be attained if $\frac{\alpha(m-2)-2m-4n}{4-m} < 0$. It is interesting that since in the chaotic class both the superpotential and the β-function have the form of a power law, the temperature and $\mathcal{Q}(\phi)$ must have a power law dependence as well. This behavior can actually change for different classes[10]. The dependence of T and $\mathcal{Q}$ on ϕ for some particular choices of m and n are written in Tab. 4.1.

Table 4.1 *Power law behaviors of $\mathcal{Q}(\phi)$ and $T(\phi)$ for the chaotic class, in the weak dissipative limit.*

Dissipation Coefficient Ratio	$\mathcal{Q}(\phi) \sim \phi^{\#}$	$T(\phi) \sim \phi^{\#}$
Cubic ($m = 3$, $n = 2$)	$\alpha - 14$	$(\alpha - 8)/2$
Linear ($m = 1$, $n = 0$)	$-(\alpha + 2)/3$	$(\alpha - 4)/6$
Inverse ($m = -1$, $n = 0$)	$(-3\alpha + 2)/5$	$(\alpha - 4)/10$

A graphic representation of these behaviors for particular sets of m and n can be seen in Fig. 4.5, shown in Sec. 4.5. Assuming that the model stays in the weak dissipative regime (this assumption has to be checked model by model) for the whole period of inflation, we can proceed further with the computation of the number of e-foldings,

$$N(\phi) = \frac{1}{2\alpha}\left(\phi^2 - \alpha^2\right) . \tag{4.96}$$

[10] For both the monomial and inverse classes (see Eq. (4.46) and Eq. (4.48)) $\beta_{CI}(\phi)$ is still a power law, but $W(\phi)$ are respectively given by Eq. (4.47) and Eq. (4.49). As a consequence an approximate power law behavior can only be attained in regions where W is nearly constant, i.e., where ϕ is very close to the fixed point (meaning deep in the inflationary phase). Conversely, for the exponential class (see Eq. (4.50)) the β-function is not a power law and, thus, the power law behavior is never approached.

Using Eq. (4.77), it is now possible to compute the value of the inflaton field at the end of inflation as given by $\phi_f = \alpha$. At this point, in order to check the consistency of the approximation, we should verify that $\mathcal{Q}(\phi_f) \ll 1$ or

$$2C \left(\frac{45C}{4\pi^2 g_*} \right)^{\frac{m}{4-m}} (-W_f)^{\frac{2(m-2)}{4-m}} \alpha^{\frac{-4n}{(4-m)}} \ll 1 \, . \tag{4.97}$$

Finally, by inverting Eq. (4.96), we obtain

$$\phi(N) = \sqrt{2\alpha N + \alpha^2} \, . \tag{4.98}$$

Having derived $Q(\phi)$, $T(\phi)$ and $\phi(N)$, we can immediately compute the predictions for n_s and r using Eq. (4.72) and Eq. (4.73).

Strong Dissipative Regime Let us follow a procedure for the strong dissipative limit analogous to the one carried out above for the weak dissipative limit. As a first step, we compute the temperature and the dissipation coefficient as functions of ϕ only, such that we have

$$T(\phi) = \left[\frac{45}{16\pi^2 g_* C} \phi^n \beta_{CI}^2 (-W)^3 \right]^{\frac{1}{4+m}} \, , \tag{4.99}$$

$$\mathcal{Q}(\phi) = 2C \left(\frac{45}{16\pi^2 g_* C} \right)^{\frac{m}{4+m}} \beta_{CI}^{\frac{2m}{4+m}} W^{\frac{2(m-2)}{4+m}} \phi^{-\frac{4n}{4+m}} \, . \tag{4.100}$$

Once again, restricting to the chaotic class gives

$$T(\phi) = \left[\frac{45\alpha^2}{16\pi^2 g_* C} (-W_f)^3 \left(\phi_f^{-3\alpha/2} \right) \right]^{\frac{1}{4+m}} \phi^{\frac{3\alpha+2n-4}{2(4+m)}} \, , \tag{4.101}$$

$$\mathcal{Q}(\phi) = 2C \left(\frac{45\alpha^2}{16\pi^2 g_* C} \right)^{\frac{m}{4+m}} \left(-W_f \phi_f^{-\alpha/2} \right)^{\frac{2(m-2)}{4+m}} \phi^{\frac{\alpha(m-2)-2m-4n}{(4+m)}} \, . \tag{4.102}$$

Recall that this regime is only attained for a particular set of values for α, C, n and m and, therefore, the consistency of the condition $Q \gg 1$ has to be checked explicitly model by model. The dependence of T and Q on ϕ for different choices of m and n are presented in Tab. 4.2.

Table 4.2 *Power law behaviors of $\mathcal{Q}(\phi)$ and $T(\phi)$ for the chaotic class, in the strong dissipative limit.*

Dissipation Coefficient Ratio	$\mathcal{Q}(\phi) \sim \phi^{\#}$	$T(\phi) \sim \phi^{\#}$
Cubic ($m = 3$, $n = 2$)	$\alpha/7 - 2$	$3\alpha/14$
Linear ($m = 1$, $n = 0$)	$-(\alpha + 2)/5$	$(3\alpha - 4)/10$
Inverse ($m = -1$, $n = 0$)	$(-3\alpha + 2)/3$	$(3\alpha - 4)/6$

Once again, a graphic representation of these behaviors can be seen in Fig. 4.5 shown in Sec. 4.5. Similar to the weak dissipative case (in particular, see footnote 10), different scalings can be obtained by considering different classes of models, in particular, choosing a different parametrization of β_{CI}, which implies different expressions for $W(\phi)$. In principle, by assuming that the strong dissipative regime holds during the last 60 e-foldings, it could be possible to derive equations similar to Eq. (4.96). However, in most of the cases, this would not be physically relevant since we typically want $Q \ll 1$ at CMB scales.

4.5 Discussion of the Results

In this section, we present and discuss the results of the numerical analysis carried out by following the procedure outlined in the previous section. While all the results shown are obtained by considering β_{CI} of the chaotic class, Eq. (4.75), a similar analysis can be performed for any other class[11], such as the monomial ones, Eq. (4.46), the inverse type of potential, Eq. (4.48), or the exponential forms, Eq. (4.50). Although we restrict to a single choice for β_{CI}, we consider the four different cases introduced in Sec. 4.4, namely, the constant $Q = C$, cubic $Q = CT^3/(H\phi^2)$, linear $Q = CT/H$ and inverse $Q = C/(HT)$ forms of the dissipation coefficient ratio Q. The values of the constant C are chosen such that the value of the dissipation coefficient at the end of inflation is at most of order ten. Note also that the dimension of C varies depending on the choices of m and n.

Let us start by discussing the evolution in the plane $(\beta_{CI}, T\beta_T)$, shown in Figs. 4.3-4.4. The motivation for this kind of plots was explained in Sec. 4.3. As expected, different parametrizations of the dissipation coefficient ratio lead to different inflationary trajectories. Consistently with our expectations, all the curves start from the neighborhood of the dS fixed point $(\beta_{CI}, T\beta_T) = (0, 0)$ and end onto the solid black curve, which represents the points in the plane

[11]It is fair to stress that, according to the discussion of Sec. 4.4.1, for different classes we expect qualitatively different results for the results shown in Fig. 4.5.

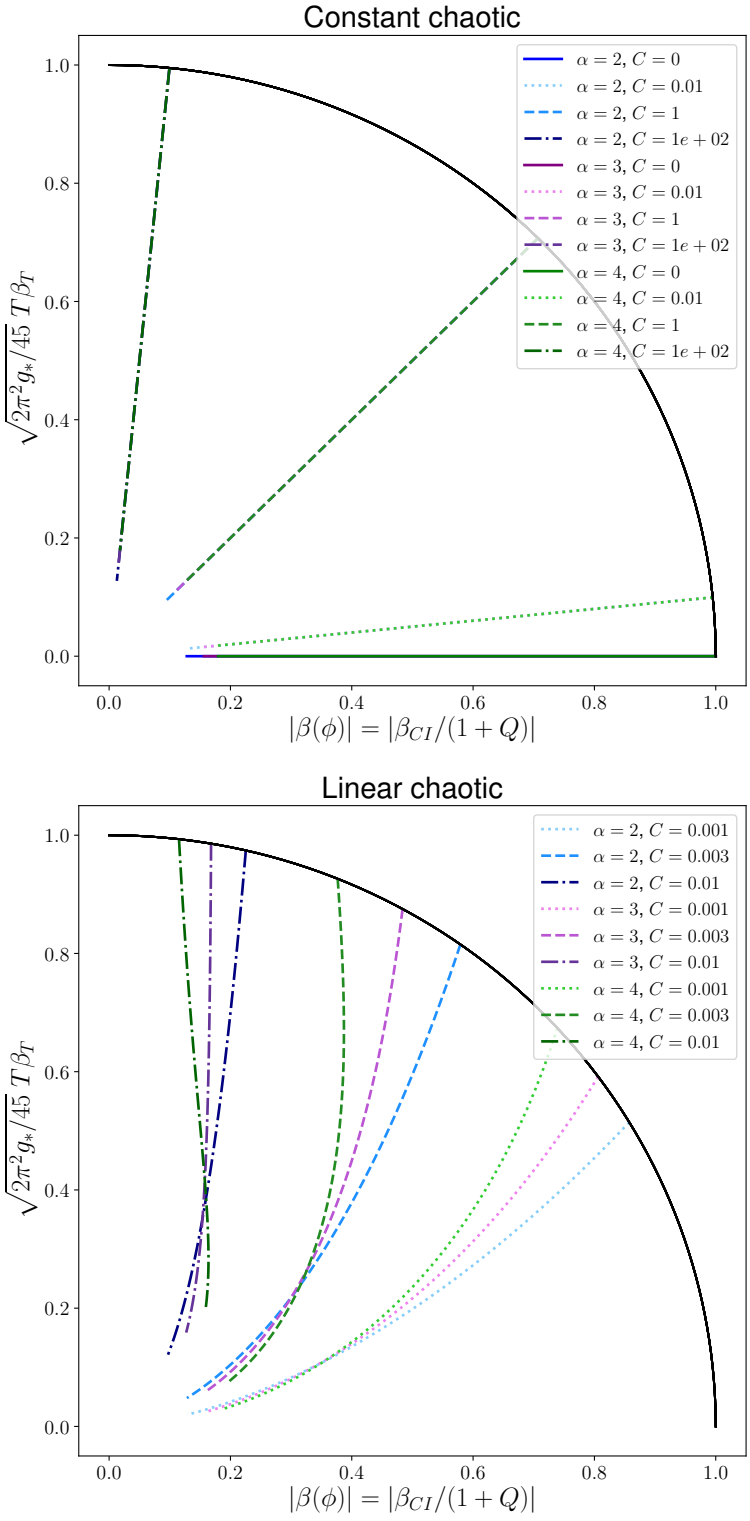

Figure 4.3 *2D plots to show the evolution of β_{CI} and $T\beta_T$ for constant and linear dissipation coefficients. The values of the constant C have been chosen to have a dissipation coefficient maximally of order ten at the end of inflation.*

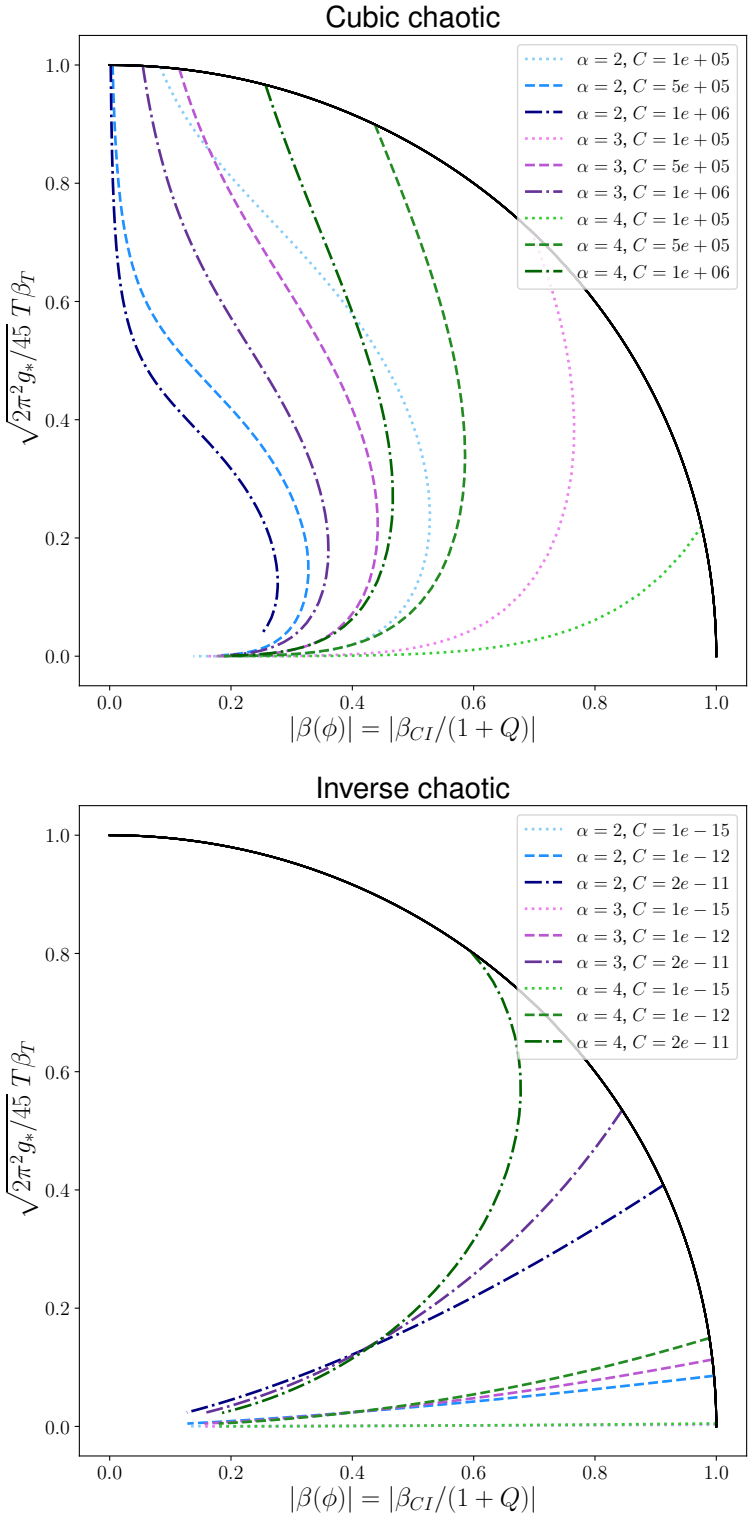

Figure 4.4 *2D plots to show the evolution of β_{CI} and $T\beta_T$ for cubic and inverse dissipation coefficients. The values of the constant C have been chosen to have a dissipation coefficient maximally of order ten at the end of inflation.*

$(\beta_{CI}, T\beta_T)$ where inflation ends. One notes that the straight trajectories of the constant case, among which we have the standard cold case with $T\beta_T = 0$, are perfectly consistent with the theoretical expectations; indeed from Eq. (4.62) we see that $(T\beta_T)^2 \propto Q\beta_{CI}^2/(1+Q)^2$. Interestingly, in many of these models inflation ends with $\sqrt{2\pi^2 g_*/45}\, T\beta_T = 4\rho_r/(9H^2) \simeq 1$. This feature implies that, in these scenarios, the amount of radiation present in the Universe at the end of inflation is already sufficiently large to quickly take over the inflaton energy density. As a consequence, already mentioned in Sec. 4.3, these models are not expected to require an explosive (p)reheating to trigger the transition from inflation to the radiation-dominated phase.

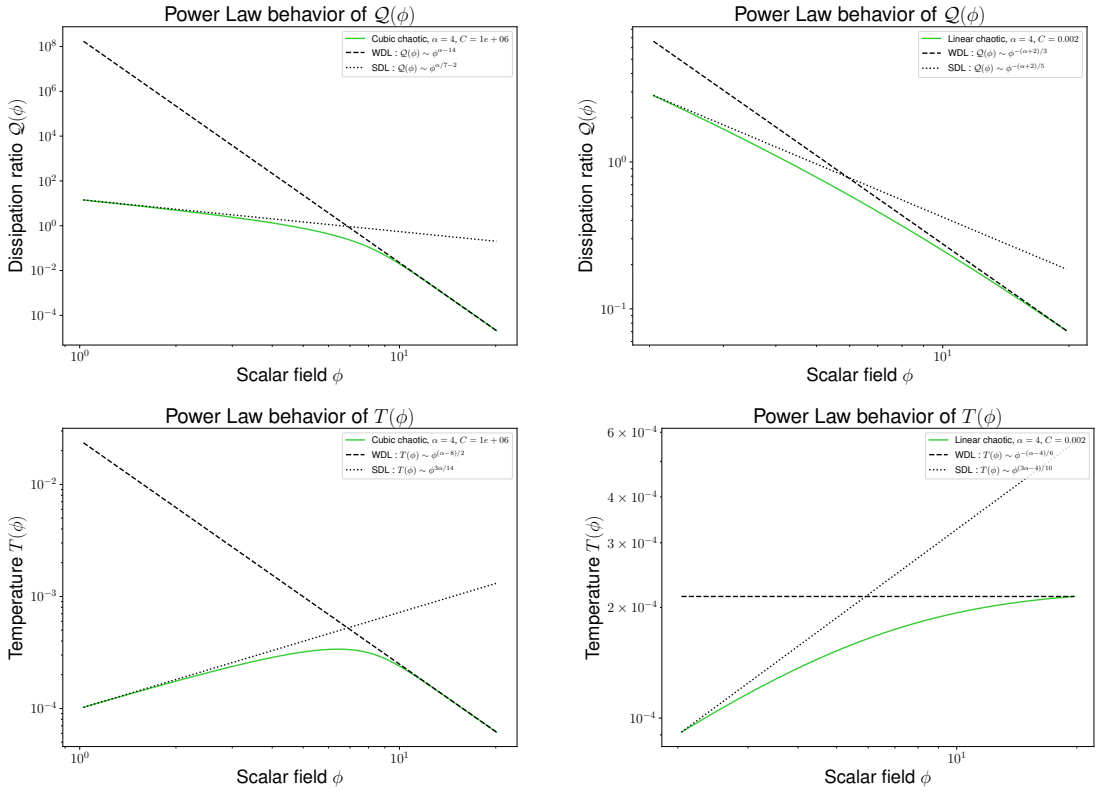

Figure 4.5 *Loglog plots of the evolution of $\mathcal{Q}(\phi) \equiv Q(\phi, T(\phi))$ (top plots) and $T(\phi)$ (bottom plots) during the last 60 e-folds of inflation for $\alpha = 4$, $C = 10^6$ (left plots) with a dissipation coefficient ratio cubic in T and $\alpha = 4$ and $C = 2 \times 10^{-3}$ (right plots) with a dissipation coefficient ratio linear in T compared with the analytical predictions of Sec. 4.4.1 in the strong (SDL) and weak (WDL) dissipative limits. In these models ϕ decreases during inflation.*

Figure 4.5 shows the evolution of $T(\phi)$ and $\mathcal{Q}(\phi) \equiv Q(\phi, T(\phi))$ for two illustrative cases, given by the values $\alpha = 2$ and $C = 10^5$, with a dissipation coefficient ratio cubic in T and $\alpha = 4$, $C = 2 \times 10^{-3}$ with a dissipation coefficient ratio linear in T. During inflation the field monotonically evolves from large to small values and

conversely the dissipation coefficient ratio (top panels of Fig. 4.5) monotonically evolves from small to large values. As a consequence, we expect the models to switch from the weak dissipative regime $Q \ll 1$ to the strong dissipative limit $Q \gg 1$ discussed in Sec. 4.4.1. We expect the dissipation coefficient $\mathcal{Q}(\phi)$ to be monotonically growing with ϕ during the phase of inflation. On the contrary, the radiation temperature $T(\phi)$ tends to approach the temperature of the thermal bath of the inflaton energy density. As the latter is expected to slightly decrease during inflation, the expected behavior of radiation temperature $T(\phi)$ is to be decreasing toward the end of inflation after a possible initial phase of growth. The top and bottom panels of Fig. 4.5 clearly reproduce these behaviors for $\mathcal{Q}(\phi)$ and $T(\phi)$.

In both the plots of $\mathcal{Q}$ and T, the curves are asymptotically approaching (both for $Q \ll 1$ and for $Q \gg 1$) the power law behaviors predicted in Sec. 4.4.1. The transition from the weak to the strong dissipative limit appears to be sharper in the cubic case. This is a direct consequence of the different dependences of $\mathcal{Q}$ on ϕ in the asymptotic behaviors. Hence, the good agreement between theory and numerical simulations confirms the robustness of the numerical methods.

For each model considered, a unique prediction for the scalar-spectral index and the tensor-to-scalar ratio is obtained. Figures 4.6-4.7 shows the evolution of the predictions for n_s and r for the chaotic class with different types of dissipation coefficient ratio. As expected, for very small values of $\mathcal{Q}$ at CMB scales, the CMB observables are, as expected, matching the predictions of the usual cold inflation case, which in the plots shown in Figs. 4.6-4.7, are represented by a red star. For larger values of $\mathcal{Q}$, the predictions are modified as typically happens in warm inflation. It is worth pointing out that the modification of the predictions, see, in particular, the linear and cubic cases with $\alpha = 4$, are qualitatively in agreement with the results of Ref. [180]. The small difference, at around the 1% level, in the predicted values of n_s is mainly due to slightly different values of T in the numerical evolution and the chosen value of N_{CMB} used in the present work. As expected, the value of n_s increases and the value of r decreases with $\mathcal{Q}$ and T and, thus, models which are in tension with (or even excluded by) the Planck constraints in the cold case can be recovered in the warm scenario. The sole exception to this behavior is the cubic case with $\alpha = 2$ of Fig. 4.6. In this case the values of $\mathcal{Q}$ and T are small at CMB scales implying that the spectrum is not modified by thermal/dissipative effects. However, as at smaller scales the production of radiation induces a friction that slows down

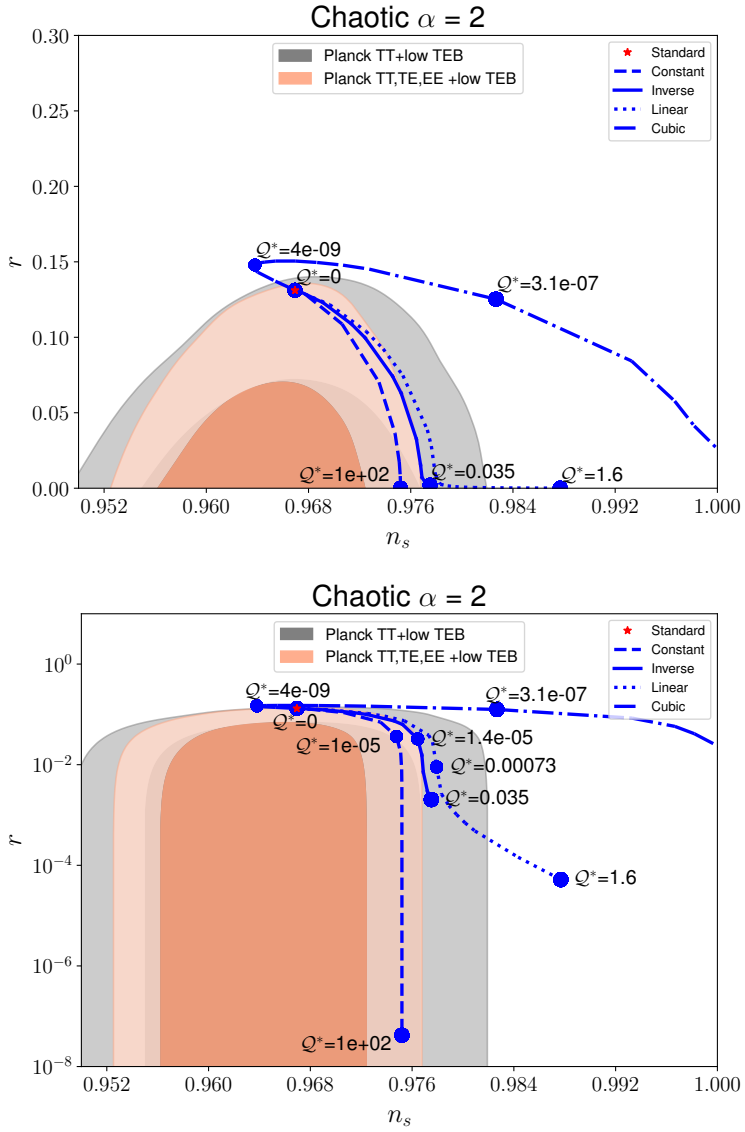

Figure 4.6 *Predictions for n_s and r in linear (top plots) and semilogarithmic (bottom plots) scale for a set of models of the chaotic class with $\alpha = 2$ and the different choices for the dissipation coefficient. For some of the models shown in this plot, we report the value of $\mathcal{Q}$ at CMB scales (denoted with $\mathcal{Q}^*$).*

the evolution of the inflaton field, we see, similarly to Ref. [183], a decrease of n_s and an increase in r due to shifting of the point of the potential probed by CMB observables. Interestingly, in the quartic case ($\alpha = 4$) the prediction for the inverse and the linear dissipation coefficient ratios are degenerate. This is explained by considering the field dependence of $\mathcal{Q}$ in the weak dissipative limit. From Tab. 4.1 we read that in this regime both $\mathcal{Q}_{\rm inverse}$ and $\mathcal{Q}_{\rm linear}$ are proportional to ϕ^{-2}, hence, the similarity in the predictions.

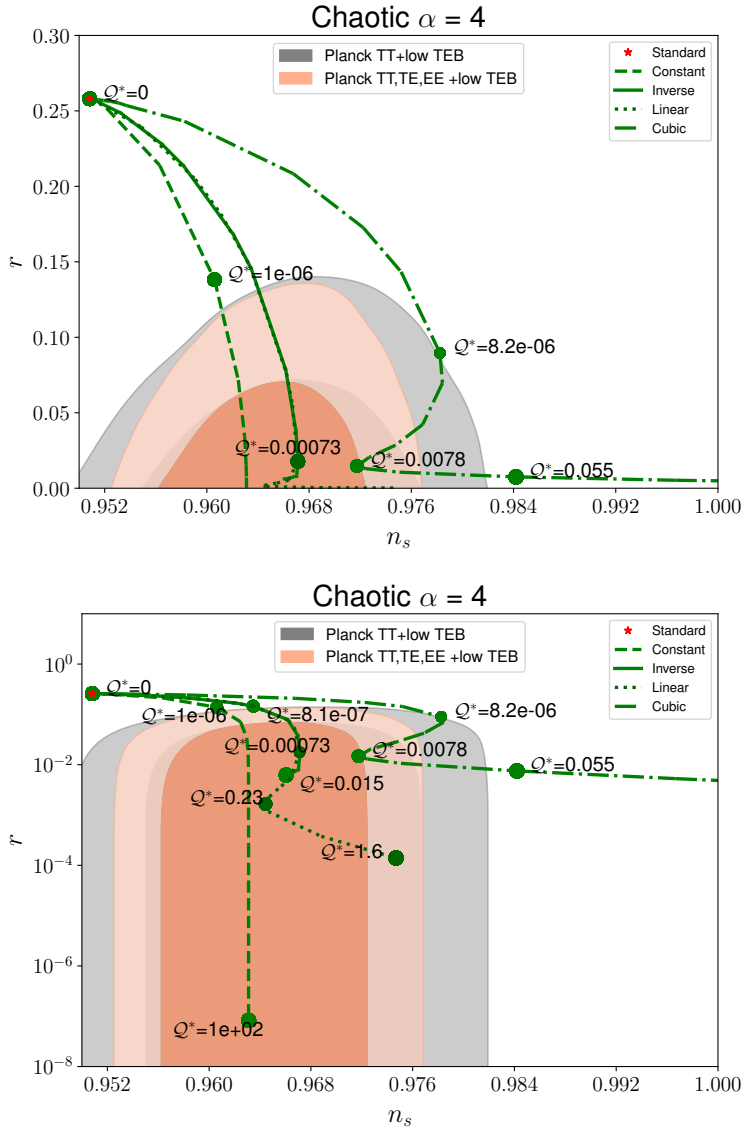

Figure 4.7 *Predictions for n_s and r in linear (top plots) and semilogarithmic (bottom plots) scale for a set of models of the chaotic class with $\alpha = 4$ and the different choices for the dissipation coefficient. For some of the models shown in this plot, we report the value of $\mathcal{Q}$ at CMB scales (denoted with $\mathcal{Q}^*$).*

We conclude this section by presenting in Fig. 4.8 a comparison between the inflationary potentials (calculated using Eq. (4.64)) for $\alpha = 4$ corresponding to some of the cases discussed in this work and some power law potentials of the form

$$V(\phi) = V_0 \phi^\alpha \, . \tag{4.103}$$

Note that the amplitudes are always fixed in order to respect the COBE normalization. For $\alpha = 2$, the ϕ dependence is the same as in the well-known

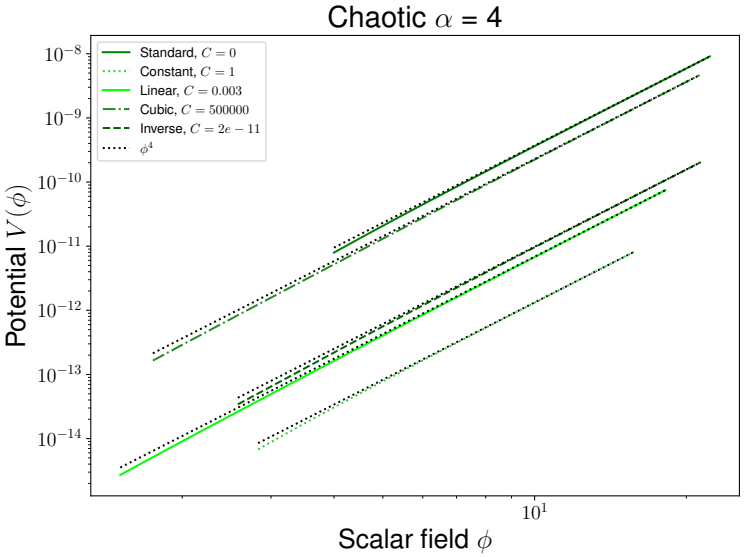

Figure 4.8 *Comparison between the inflationary potentials set by Eq.* (4.64) *(for* $\alpha = 4$*) and power law potentials* $V(\phi) = V_0\phi^4$*.*

case of chaotic inflation [141]. As expected, the two sets of curves are perfectly matching for large values of ϕ, meaning deep in the inflationary phase, where β_{CI} is much smaller than one and the potentials predicted by Eq. (4.64) are well-approximated by power laws. Conversely, for small values of ϕ, higher order corrections induce a deviation in $V(\phi)$ from the power law behavior observed at large scales. This type of analysis might be of particular use in the problem of reconstructing potentials in warm inflation [192].

4.6 Conclusions and Future Perspectives

In this chapter, we have considered a famous application of fluctuation-dissipation dynamics, warm inflation. In particular, we have discussed the application of the β-function formalism for inflation to the warm realization in order to identify universality among its models. We have shown in Sec. 4.3 that a consistent treatment of warm inflation can be carried out in the language of the β-function formalism. Interestingly, we have found that, despite the presence of an additional functional freedom with respect to the cold case, a universal description still exists. For example, we have demonstrated that models with different functional forms for the dissipation coefficient ratios can give rise to very similar cosmological observables. Moreover, we have shown that this formalism naturally offers an interesting graphical representation of the inflationary phase in

terms of bidimensional plots in a plane of the variables $(\beta_{CI}, T\beta_T)$, depicting the departure from the usual cold inflation case. A peculiar property of these results is that they provide a clear insight on the Universe energy budget in the last part of inflation, which in turns allows us to infer some of the necessary properties of (p)reheating.

We have also discussed in Sec. 4.4 the definition of both numerical and analytical techniques used to perform a systematic study of warm inflation within this framework. The results of the numerical analysis were then presented and discussed in Sec. 4.5. All the plots show an extremely good agreement between numerical results and theoretical predictions. In particular, we stress the accuracy of the predictions for the power law behaviors of the dissipation ratio Q and temperature T in both the small and large Q limits. These analytical approximations could provide an extremely useful tool for further studies on the topic. For example, by studying the consistency of the conditions $Q \ll 1$ and $Q \gg 1$ with the analytical expressions, it is possible to understand at a fully analytical level whether a given model could or could not access the cold or warm regime respectively.

While in this analysis our interest was mainly focused on the chaotic class of potential, the generalization of the analysis to different classes would be an interesting subject for future works on this topic. It should follow similar steps as the ones put forward in this work. In particular, as already explained in Sec. 4.4, different scaling solutions (for small and large Q) are expected to be obtained for different classes. These analyses would be extremely useful in expanding and strengthening our understanding of warm inflation. Moreover, the deepening of our comprehension on the effects of interactions between the inflaton and radiation could result in a definite step toward the formulation of a theory of inflation which is somehow connected with the rest of the fundamental interactions.

Finally, it is worth mentioning that, in order to keep a direct connection with previous works on this topic (and also with theory), we always proceeded by first specifying β_{CI} and $Q(\phi, T)$ and then computing $T(\phi)$ (and thus $\mathcal{Q}(\phi) \equiv Q(\phi, T(\phi))$) by numerically solving Eq. (4.53). However, it could be equivalently possible to start by fixing $\mathcal{Q}(\phi)$ and, then, identifying the parametrizations of $Q(\phi, T)$ which correspond to this choice. While formally these two possibilities are exactly equivalent, the latter presents some computational advantages and has theoretical interests, namely

- By starting with a fixed parametrization for $\mathcal{Q}(\phi)$, it could be possible to solve Eq. (4.53) analytically. This implies that a full analytical treatment of some models of warm inflation could be achieved;

- As a single parametrization of $\mathcal{Q}(\phi)$ corresponds to several parametrizations of $Q(\phi, T)$, by specifying $\mathcal{Q}(\phi)$ we are not restricting our analysis to a single model but rather to a class of models sharing the same properties. In this sense such an analysis would be more general than the one obtained by specifying $Q(\phi, T)$. Interestingly, the universality which is manifest at the background level is not expected to be broken by quantum perturbations. In particular, this can be directly seen from Eq. (4.70)-(4.71), where it is manifest that all the quantities appearing in the expressions of the spectra can be directly computed once β_{CI} and $\mathcal{Q}$ are specified.

Such an analysis would be an extremely interesting topic for future studies on warm inflation. In particular, it would be relevant to understand how, given a parametrization of β_{CI}, it could be possible to reproduce the usual parametrizations of Q given, e.g., by Eq. (4.74), using $\mathcal{Q}(\phi)$.

Chapter 5

Formulating the Kramers Problem in Field Theory

5.1 Introduction and Motivations

The problem of escaping a potential well has been an active field of research over the last century and has applications in several scientific disciplines, such as in physics and chemistry. Classically, a particle put at rest at the bottom of a potential stays there if left undisturbed. However, in any realistic physical system, we expect the presence of fluctuation and dissipation dynamics, which, for example, naturally emerge through the interactions of the system with a thermal bath. Under these conditions, an escape from the potential well might be allowed. The derivation of the escape rate is called the Kramers problem [193] and is, to a large extent, well-understood for the simplest systems such as a classical point particle. However, to our knowledge, no explicit extension of this problem to a relativistic field has been done so far. Since the physics of the Early Universe is described by cosmological fields immersed in a hot medium, there is a need to define and understand precisely the rate of escape due to thermal fluctuations only.

Computing the probability for a classical particle to diffuse has been of great interest among theoretical physicists, in particular, in the context of stochastic dynamics. Several methods have been proposed over the years. H. A. Kramers, a pioneer in the field, derived the so-called Kramers rate [193] using the flux-over-

population method based on ideas originally developed by L. Farkas in [194]. Another way to obtain the escape rate is achieved with the mean-first-passage-time (MFPT) formalism using the adjoint Fokker-Planck (FP) operator [195, 196]. However, this approach is more delicate to handle due to complex boundary conditions. A third method consists of finding the smallest positive, non-vanishing, eigenvalue of the Fokker-Planck operator. It has been shown that this eigenvalue is directly related to the escape rate [197]. A comprehensive review of these methods can be found in [198]. More recently, P. Reimann, G. J. Schmid and P. Hänggi [199] showed a universal equivalence between these approaches.

When regarding a field instead of a particle, the situation changes significantly. A lot of attention has been given to the study of quantum tunneling. The decay rate of a field has been derived by C. G. Callan and S. R. Coleman at zero-temperature [200, 201] and extended to finite-temperature by A. D. Linde [202] (also known as the nucleation problem in finite temperature quantum field theory [203]). The inclusion of gravitational effects has been studied by Coleman and F. de Luccia in [204]. Even if the formalism describing a field subject to random forces, stochastic field theory, is known [205, 206], a precise and complete discussion of the escape problem has never been performed. One of the main difficulties is the identification of the most suitable approach to be generalized to a scalar field. J. Zinn-Justin in [206] briefly states the problem and suggests deriving the smallest eigenvalue and the use of instantons. This is indeed a possibility but, unfortunately, it faces some analytical limitations when deriving the rate. The work of J. S. Langer [207, 208] in extending the flux-over-population method to a $2N$-dimensional system appears as the most promising approach to be used with a field.

The field theory aspect of the problem renders the definition of an escape more difficult and less intuitive than for a single point particle. In particular, the actual shape of the potential beyond the potential well plays a role in the computation of the rate for the field. However, as in the zero-dimensional case, the Kramers problem can be defined for both an initial true or false vacuum. Using ideas and the formalism of the flux-over-population method extended to a field, we will propose a definition of the Kramers problem and explicitly evaluate the rate. Along the way in this derivation, we will encounter some familiar situations, such as the Hawking and Moss solution [209]. We will also compare our final result for the escape rate with the known result of nucleation rate due to thermal fluctuations [202, 203]. In particular, considering the well-known result of Linde

for the quantum tunneling rate at finite temperature [202], we will show that, in the limit where the temperature is sufficiently high for the thermal fluctuations to dominate over the quantum fluctuations, the nucleation rate is proportional to the escape rate. This is remarkable since the two results are based on completely different approaches. This result shows that, when the system is initially in a false vacuum, the nucleation rate is indeed a special case of the escape rate.

Apart from the formal interest of the computation of an escape rate for a scalar field, the result has potentially many applications not only for cosmology but also beyond. The process might help in a precise understanding of out-of-equilibrium situations, for example during phase transitions. In particular, it might influence the formation of topological defects and potentially alter the stability of the embedded configurations. The formalism is not intended to be used only in cosmology. The escape rate is well-suited for situations where the field needs to probe several local minima. This scenario appears in string theory, with the string landscape, and, also, in condensed matter physics, in the context of the glass transition. Finally, the formalism is formally identical to the stochastic quantization, especially used in lattice field theory, where the origin of the stochastic forces is quantum instead of thermal. A precise knowledge of a transition rate is therefore of great interest in this context. The results of this chapter have been presented in [210].

This chapter is organized as follows. We start in Sec. 5.2 with a brief review of the Kramers problem and the methods necessary to compute the escape rate in the simplest case of a point particle. We focus on two approaches, the flux-over-population method, since it is the best candidate to be generalized to a scalar field, and the MFPT which provides a simple interpretation of the escape rate. We also present the proof of the equivalence of the two methods. In Sec. 5.3, we first state the difficulties in the formulation of an escape problem for a scalar field. We then review some basics of stochastic field theory with the Langevin and the associated Fokker-Planck equation. We then define and derive the escape rate for a scalar field using the flux-over-population method. This is the main result of this chapter. In Sec. 5.4, we discuss some potential applications for cosmology and in other domains of physics. We provide our concluding remarks in the last section. Explicit details about the computations are given in Appendix D.

5.2 Rate of Escape of a Classical Point Particle

To introduce the escape problem and the associated computations, we consider the simple example of a classical point particle in a metastable potential. We review the two formalisms, based on the Langevin and the Fokker-Planck equations. The Fokker-Planck formalism is fully equivalent to the Langevin approach and provides the tools needed for an analytical derivation of the escape rate. We investigate two methods, the flux-over-population and the mean-first-passage-time, to obtain the escape rate. Finally, the proof of the formal equivalence between the two approaches is presented and allows for a clear interpretation of the result.

5.2.1 Point Particle in a Metastable Potential

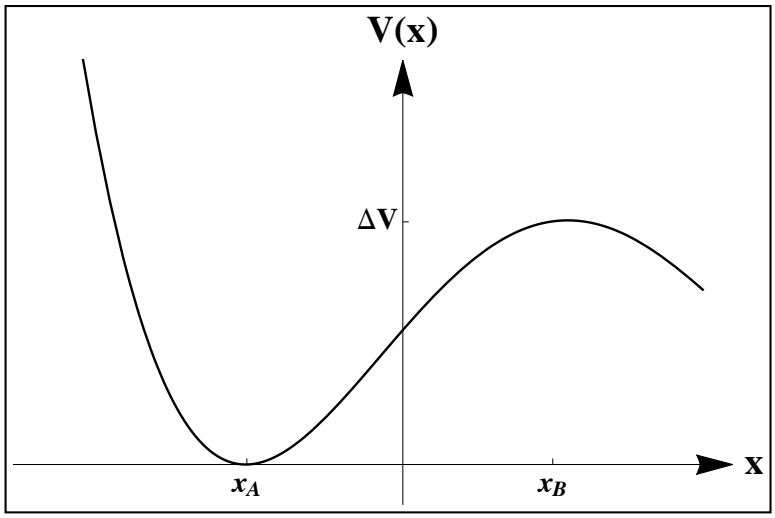

Figure 5.1 *Potential corresponding to the escape problem. The position x_A is the local minimum, where the point particle sits initially, and x_B the local maximum of the potential. The barrier height is denoted by ΔV.*

We consider a classical point particle of mass m initially located at a local minimum x_A of the potential $V(x)$. For simplicity, we assume only one direction of escape, through the closest local maximum located at x_B on the right of x_A. On the left of the local minimum, the potential diverges. The situation is depicted on Fig. 5.1. Beyond the local maximum at x_B, the potential might have another local or global minimum or be unbounded from below. The height of the barrier is denoted by ΔV.

In a classical description, the particle sitting at the local minimum stays there forever and an escape from the potential well is not allowed. The dynamics is governed by Newton's second law

$$m\frac{d^2x}{dt^2} = -V'(x) \,, \tag{5.1}$$

where the prime denotes a derivative with respect to x. The position x_A at the local minimum of the potential is stable. In other words, x_A is an attractor. Under a small perturbation, the particle comes back to the original position.

In the presence of a thermal bath or a fluid, in which the particle is placed, the situation is altered by the two competing effects intrinsic to fluctuation and dissipation dynamics. The random forces, originating from the thermal fluctuations, push the particle away from the initial position and allow for a climb of the potential barrier. In addition, the damping tends to slow-down the particle and prevents a come back once the particle is displaced from x_A. Due to the combined effect of fluctuation and dissipation, the system is not stable anymore and there is a non-zero probability for the particle to escape from the well. In particular, after a sufficiently long time, it is reasonable to expect that the particle has passed over the barrier.

We are interested in the rate at which the particle escapes from the potential well. The escape rate is closely related to the inverse of the average time needed to pass, for the first time, the local maximum of the potential. This time is known in the literature as the mean-first-passage-time [195, 196]. A naive inspection indicates that the escape rate should only depend on the damping coefficient, the strength of the noise, on the temperature and on the potential, in particular, the height of the barrier and the curvature at the minimum and the maximum. Since the escape is defined from the first-passage at the top of the barrier, the characteristics of the potential beyond the maximum should not play any role.

One clarification on terminology is worth stating here. For a classical point particle, the escape rate is different from and should not be confused with a diffusion rate to the next minimum. The diffusion rate is typically smaller than the escape rate since, once the particle has passed over the top, it must then go down the potential on the other side and, eventually, reach the minimum. If the next minimum is at lower energy, the diffusion rate is a decay rate. Let us now formulate the escape problem.

5.2.2 Langevin and Fokker-Planck Descriptions

The Langevin and the Fokker-Planck formalisms are the two equivalent approaches used to describe a particle subject to random forces. We introduce both of them and present their strengths and limitations.

Langevin The Langevin equation is obtained by the inclusion of the random force, parametrized with a stochastic noise $\xi(t)$, and the damping term to Newton's second law

$$m\frac{d^2x}{dt^2} = -\eta\frac{dx}{dt} - V'(x) + \xi(t) \,, \tag{5.2}$$

where η is the damping coefficient. For simplicity, the noise will always be assumed to be Gaussian throughout this work. The average over the noise of an operator $\mathcal{O}$ is defined as

$$\langle \mathcal{O}(x) \rangle_\xi \equiv \int d[\xi] \mathcal{O}(x) \exp\left\{ -\frac{1}{2\Omega} \int_{t_0}^{t_f} dt' \xi^2(t') \right\} \,, \tag{5.3}$$

where t_0 and t_f are the initial and final times. The measure of integration is chosen to satisfy $\langle 1 \rangle_\xi = 1$ or

$$d[\xi] = \prod_{i=1}^{M} d[\xi_i] = \prod_{i=1}^{M} d\xi_i \sqrt{\frac{\epsilon}{2\Omega\pi}} \,, \tag{5.4}$$

where time has been discretized in M steps and $\epsilon \equiv (t_f - t_0)/M$. A Gaussian noise satisfies the following relations

$$\langle \xi(t) \rangle_\xi = 0 \,, \qquad\qquad \langle \xi(t)\xi(t') \rangle_\xi = \Omega\delta(t - t') \,, \tag{5.5}$$

where Ω parametrizes the strength of the noise. The damping coefficient η is related to Ω by the Einstein relation $\Omega = 2\eta k_B T$.

The Langevin equation is a stochastic differential equation for a random variable and is therefore not deterministic. The stochastic nature of the equation drastically limits the analytical treatment. The Langevin equation is, however, useful for numerical simulations where the evolution for an infinitesimal time step

is given by

$$mv(t+dt) = mv(t) - \eta v(t)dt - V'(x)dt + \int_t^{t+dt} d\tau \xi(\tau) \ . \tag{5.6}$$

Sometimes, the overdamped limit of the equation is considered. In the case of large damping, the motion of the particle is slow and therefore the acceleration term is safely neglected with respect to the damping term. In this limit, Eq. (5.2) becomes

$$\eta \frac{dx}{dt} = -V'(x) + \xi(t) \ , \tag{5.7}$$

and is called the overdamped Langevin equation.

To proceed with an analytical treatment, we consider the deterministic formulation of the problem, described by the Fokker-Planck equation.

Fokker-Planck The idea behind the Fokker-Planck description is to consider the evolution of the probability distribution of the quantities of interest, in our case, the position and the velocity of the particle. Due to the presence of random forces, each realization is achieved with a certain probability. As we will learn next, the evolution of the probability distribution turns out to be deterministic.

We are interested in the position and the velocity of the particle as function of time. The Langevin equation gives a set of two first-order differential equations for $x(t)$ and $v(t)$

$$\frac{dx}{dt} = v \ , \tag{5.8}$$

$$m\frac{dv}{dt} = -\eta v - V'(x) + \xi(t) \ . \tag{5.9}$$

The Fokker-Planck probability distribution is defined as

$$P(x, v, t \mid x_0, v_0, t_0) \equiv \langle \delta[x(t) - x]\delta[v(t) - v] \rangle_\xi \ , \tag{5.10}$$

where the arguments $x(t)$ and $v(t)$ of the delta-functions on the right are the solutions of the Langevin equation and x and v the arguments of the probability distribution. P is the averaged probability to find the particle at position x with velocity v at time t knowing the initial position x_0 and velocity v_0 at time t_0.

The probability distribution satisfies the Fokker-Planck equation[1]

$$\frac{\partial}{\partial t}P(x,v,t \mid x_0,v_0,t_0) = -\mathcal{L}_{FP}P(x,v,t \mid x_0,v_0,t_0) \ , \tag{5.11}$$

where $\mathcal{L}_{FP}$ is the Fokker-Planck operator defined as

$$\mathcal{L}_{FP} \equiv \frac{\partial}{\partial x}v - \frac{1}{m}\frac{\partial}{\partial v}\left[\eta v + V'(x)\right] - \frac{\Omega}{2m^2}\frac{\partial^2}{\partial v^2} \ . \tag{5.12}$$

The Fokker-Planck equation is an ordinary differential equation for the probability distribution P and, therefore, analytical methods can be applied.

In the large time limit, the system is expected to reach equilibrium. The equilibrium probability distribution P_0 is a time-independent solution of the FP equation given by

$$P_0(x,v) = \frac{1}{\mathcal{Z}}\exp\left\{-\beta\left(\frac{1}{2}mv^2 + V(x)\right)\right\} = \frac{1}{\mathcal{Z}}\exp\left\{-\beta E(x,v)\right\} \ , \tag{5.13}$$

where E is the energy of the non-dissipative system and the partition function $\mathcal{Z}$ is the normalization. Note that the equilibrium distribution always formally exists as a solution of the FP equation, however, it does not necessarily imply that the system possesses an equilibrium state. The equilibrium distribution might be non-normalizable, in particular, if the potential is unbounded from below.

Finally, in the overdamped limit, the FP probability distribution is defined as

$$P(x,t \mid x_0,t_0) \equiv \langle \delta[x(t) - x] \rangle_\xi \ , \tag{5.14}$$

the FP equation reads

$$\partial_t P(x,t \mid x,t_0) = \left(\frac{1}{\eta}\frac{\partial}{\partial x}\frac{\partial V}{\partial x} + \frac{\Omega}{2\eta^2}\frac{\partial^2}{\partial x^2}\right)P(x,t \mid x_0,t_0) \ , \tag{5.15}$$

and the equilibrium distribution is simply

$$P_0(x,v) = \frac{1}{\mathcal{Z}}\exp\left\{-\beta V(x)\right\} \ , \tag{5.16}$$

which might be non-normalizable as in the general case.

[1] Explicit details on the derivation and a discussion about the properties of this equation can be found in Refs. [197, 206]. Note also that the derivation of the Fokker-Planck equation for the scalar field presented in Appendix D.1 is analogous.

5.2.3 Computation of the Escape Rate

Over the last century, several methods have been proposed to estimate the escape rate[2]. Since our final goal is to consider a cosmological scalar field, we focus on the flux-over-population method that appears as the most promising candidate for such a generalization. For a better interpretation of the escape problem, we also introduce the framework of the mean-first-passage-time and present the solution in the overdamped limit. By showing the formal equivalence between the two methods, we prove that the escape rate is indeed the inverse of the MFPT.

Flux-over-Population Method

The flux-over-population method has been introduced by L. Farkas in [194] and the explicit computation of the rate has been achieved by H. A. Kramers in [193].

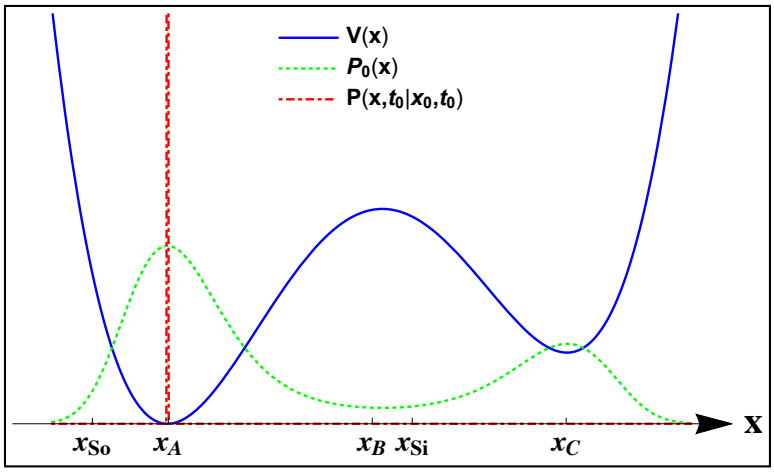

Figure 5.2 *Example of a situation studied with the flux-over-population method. The blue line is the potential $V(x)$. The red dash-dotted line is the initial and the green dotted line is the equilibrium Fokker-Planck probability distribution for the position. The position x_A is the initial location of the particle, x_B the local maximum, x_C a second local minimum, x_{So} and x_{Si} the positions of the source and the sink respectively.*

Let us consider the situation depicted in Fig. 5.2. For illustrative purposes, we have chosen an asymmetric double-well potential. Similar reasonings apply to any kind of potential as long as it possesses a local minimum in the vicinity

[2]For a comprehensive review of these methods, we invite the reader to refer to [198].

of a local maximum[3]. The particle is initially located at the minimum x_A and the Fokker-Planck probability distribution at time t_0 is a product of two delta functions

$$P(x, v, t_0 \mid x_A, 0, t_0) = \delta(x - x_A)\delta(v) \ . \tag{5.17}$$

In the large time limit, the system has reached equilibrium and the probability distribution is given by Eq. (5.13). The position-dependent parts of the initial and equilibrium probability distributions are depicted in Fig. 5.2 with the red dash-dotted line and the green dotted line respectively. During the evolution of the probability distribution, given by the Fokker-Planck equation (5.11), there is a flux of probability at the maximum of the well. The origin of this flux of probability is precisely due to the fluctuation and dissipation dynamics discussed previously.

The idea behind the flux-over-population method relies on the construction of a stationary situation. The inclusion of sources and sinks maintains a constant probability current across the well. The role of the sources, located on the left of the minimum at x_{So}, is to supply to A-well with particles and keep a constant number density inside the well. The particles thermalize and eventually leave the well before being removed by the sinks, located on the right of the maximum at x_{Si}. Since the total probability flux j is equal to the rate of escape k times the population of the A-well n_A, the flux-over-population method predicts

$$k \equiv \frac{j}{n_A} \ , \tag{5.18}$$

as a solution for the escape rate.

The population of the A-well is given by the integration over the probability density

$$n_A = \int_{A-\text{well}} dxdv \ P(x, v) \ , \tag{5.19}$$

which corresponds to the probability to be in the well, with $x \in]-\infty, x_B]$ and $v \in]-\infty, +\infty[$. The flux at the barrier is

$$j = \int_{-\infty}^{+\infty} dv \ vP(x_B, v) \ , \tag{5.20}$$

[3]The shape of the potential influences the form of the equilibrium distribution, however, the existence of a probability flux at the top of the potential is guaranteed.

which is the probability to pass over the maximum with some velocity.

The derivation of the rate requires two steps. First, we obtain the probability distribution and then compute the flux and the number-density. The probability density P is a solution of the Fokker-Planck equation (5.11) with the particular boundary conditions dictated by the specific steady-state situation in consideration. The particles are at equilibrium inside the A-well and the probability density is given by Eq. (5.13). Since the sinks remove the particles once they have passed the maximum, we impose

$$P(x > x_{Si}, v) \simeq 0 \ . \tag{5.21}$$

Finally, at the top of barrier, there are no sources nor sinks and the potential $V(x)$ is approximated as

$$V(x) \simeq V(x_B) - \frac{1}{2}|V''(x_B)|(x - x_B)^2 + \mathcal{O}[(x - x_B)^3] \ , \tag{5.22}$$

and, therefore, the FP equation (5.11) becomes

$$\left\{ -\frac{\partial}{\partial x} v + \frac{1}{m}\frac{\partial}{\partial v}\left[\eta v - |V''(x_B)|(x - x_B)\right] + \frac{\Omega}{2m^2}\frac{\partial^2}{\partial v^2} \right\} P(x, v) = 0 \ , \tag{5.23}$$

near the maximum.

The construction of $P(x, v)$ relies on the Kramers ansatz [193]

$$P(x, v) = \zeta(x, v) P_0(x, v) \ , \tag{5.24}$$

where P_0 is the equilibrium distribution and ζ is chosen to satisfy the boundary conditions

$$\lim_{x \to x_A} \zeta(x, v) = 1 \ , \qquad\qquad \zeta(x > x_{Si}, v) = 0 \ . \tag{5.25}$$

Applying the Fokker-Planck operator on the ansatz and using the equilibrium distribution Eq. (5.13), we obtain the equation for ζ

$$\left\{ -v\frac{\partial}{\partial x} - \frac{1}{m}\left[\eta v + |V''(x_B)|(x - x_B)\right]\frac{\partial}{\partial v} + \frac{\Omega}{2m^2}\frac{\partial^2}{\partial v^2} \right\} \zeta(x, y) = 0 \ , \tag{5.26}$$

where we identify the adjoint Fokker-Planck equation. In order to solve this equation, Kramers made the further assumption that ζ depends only on u, a

linear combination of x and v

$$u \equiv (x - x_B) + av \ . \tag{5.27}$$

The equation for $\zeta(u)$ becomes

$$-\left[(1+\frac{a}{m}\eta)v + \frac{a}{m}|V''(x_B)|(x-x_B)\right]\zeta' + a^2\frac{\Omega}{2m^2}\zeta'' = 0 \ , \tag{5.28}$$

where the prime denotes a u-derivative. For consistency with the assumption that ζ is a function of u only and, in order to obtain the correct behavior at the boundary, the factor in front of ζ' must be a linear function of u. Imposing

$$\lambda u \equiv -\left[(1+\frac{a}{m}\eta)v + \frac{a}{m}|V''(x_B)|(x-x_B)\right] \ , \tag{5.29}$$

the constants a and λ are found to be

$$\lambda_\pm = -\frac{\eta}{2m} \pm \sqrt{\frac{|V''(x_B)|}{m} + \left(\frac{\eta}{2m}\right)^2} \ , \qquad a = -\frac{m}{V''(x_B)}\lambda_\pm \ , \tag{5.30}$$

where the two solutions for λ have opposite signs.

Solving for $\zeta(u)$ by inserting (5.29) in the differential equation and integrating twice gives

$$\zeta(u) = \sqrt{\frac{\beta[V''(x_B)]^2}{2\pi\eta\lambda_+}}\int_u^\infty dz \ \exp\left\{-\beta\frac{[V''(x_B)]^2}{2\eta\lambda_+}z^2\right\} \ , \tag{5.31}$$

where λ_+ has been chosen to have an overall negative exponent and therefore ζ to vanish for large positive x. The factor in front of ζ has been chosen to satisfy the other condition, ζ going to unity inside the A-well.

Having all elements at disposal to compute the probability flux j, we obtain

$$\begin{aligned} j &= \int_{-\infty}^{\infty} dv \ v\zeta(x_B,v)\frac{1}{\mathcal{Z}}\exp\left\{-\beta\left[\frac{1}{2}mv^2 + V(x_B)\right]\right\} \\ &= \frac{1}{\mathcal{Z}}\left(\frac{\lambda_+}{\beta}\right)\frac{1}{\sqrt{m|V''(x_B)|}}\exp\left\{-\beta V(x_B)\right\} \ , \end{aligned} \tag{5.32}$$

where we have used integration by parts. The population n_A of the A-well is simply

$$n_A = \int_{A-\text{well}} dxdvP(x,v)$$

$$\simeq \frac{1}{\mathcal{Z}}\sqrt{\frac{2\pi}{\beta m}}\sqrt{\frac{2\pi}{\beta V''(x_A)}}\exp\left\{-\beta V(x_A)\right\} \ , \tag{5.33}$$

where the potential has been expanded around the local minimum in x_A and the limit of integration for x safely extended to infinity.

Taking the ratio of j and n_A, the escape rate is found to be

$$k = \frac{\sqrt{\frac{|V''(x_B)|}{m} + \left(\frac{\eta}{2m}\right)^2} - \frac{\eta}{2m}}{2\pi}\sqrt{\frac{V''(x_A)}{|V''(x_B)|}}\exp\left\{-\beta\left[V(x_B) - V(x_A)\right]\right\} \ , \tag{5.34}$$

which is the famous result of Kramers. As expected, the rate depends only on the parameters η (or equivalently Ω), the temperature, the curvature of the potential at the initial local minimum and the nearby maximum and the height of the barrier. The shape of the potential on the other side of the well does not influence the final result. The height of the barrier $\Delta V = V(x_B) - V(x_A)$ can be seen as the activation energy. Finally, note that in the limit of small damping, i.e. $\frac{|V''(x_B)|}{m} \gg \left(\frac{\eta}{2m}\right)^2$, the escape rate recovers the result of I. Affleck in [211].

Mean-First-Passage-Time over the Barrier

An alternative derivation of the escape rate is achieved with the method of the mean-first-passage-time. The first-passage-time (FPT) is defined as the time the particle takes to leave a domain $\mathcal{D}$. In our case, it corresponds to the time needed for the particle initially at x_A, to pass over the maximum at x_B. Since the forces acting on the particle are random and the dynamics not deterministic, the FPT is different for each realization. We can, however, define the MFPT as the average of the FPT and estimate the escape rate as its inverse.

A formal definition of the problem relies on the introduction of the survival probability $S(t \mid x_0, v_0, t_0)$. It corresponds to the probability to be still in $\mathcal{D}$ after a time $(t - t_0)$ while being initially at position x_0 with velocity v_0. In our case, the domain is the A-well where $x \in]-\infty, x_{Si}]$, where the upper limit of the domain, x_{Si}, is a point chosen to be near, but beyond, the maximum, to ensure the passing. The survival probability is defined as

$$S(t \mid x_0, v_0, t_0) = \int_{\mathcal{D}} dxdv \ P(x, v, t \mid x_0, v_0, t_0) = \text{Prob}\left[T(x_0, v_0) > (t - t_0)\right]$$

$$= \int_{(t-t_0)}^{\infty} dt \; f(t \mid x_0, v_0) \; , \tag{5.35}$$

where $T(x_0, v_0)$ is the FPT starting at x_0 with initial velocity v_0 and $f(t \mid x_0, v_0)$ is the probability distribution for $T(x_0, v_0)$. The above relation is motivated by the following reasoning, the probability to be in the domain at time t is the same as the probability of having a first-passage-time larger than $(t - t_0)$.

From equation (5.35), we deduce the following relation between $S(t \mid x_0, v_0, t_0)$ and $f(t \mid x_0, v_0)$

$$f(t \mid x_0, v_0) = -\frac{\partial S(t \mid x_0, v_0, t_0)}{\partial t} \; . \tag{5.36}$$

The moments $\langle T^n \rangle$ of the FPT are defined as

$$\begin{aligned} \langle T^n \rangle &\equiv \int_{t_0}^{\infty} dt \; (t - t_0)^n f(t \mid x_0, v_0) \\ &= n \int_{t_0}^{\infty} dt \; (t - t_0)^{n-1} S(t \mid x_0, v_0, t_0) \; , \end{aligned} \tag{5.37}$$

and, in particular, the MFPT τ reads

$$\tau \equiv \langle T \rangle = \int_{t_0}^{\infty} dt \; S(t \mid x_0, v_0, t_0) = \int_{t_0}^{\infty} dt \int_{\mathcal{D}} dx dv \; P(x, v, t \mid x_0, v_0, t_0) \; . \tag{5.38}$$

We understand this expression for τ in the following way. The averaged first-passage-time is the sum of all the probabilities to be in the domain $\mathcal{D}$ at any time t larger than t_0. If the particle is never in $\mathcal{D}$, the integrand vanishes and so does the MFPT. If, on the contrary, the particle is always in the domain, the integral over the probability distribution is normalized to one and the time integral diverges, leading to an infinite MFPT.

Using the adjoint Fokker-Planck equation, it is possible to find an explicit solution for the MFPT

$$\begin{aligned} \mathcal{L}_{FP}^{\dagger} \tau &= \int_{t_0}^{\infty} \int_{\mathcal{D}} dx dv \; \mathcal{L}_{FP}^{\dagger} P(x, v, t \mid x_0, v_0, t_0) \\ &= -\int_{\mathcal{D}} dx dv \; \left[P(x, v, \infty \mid x_0, v_0, t_0) - P(x, v, t_0 \mid x_0, v_0, t_0) \right] = 1 \; , \end{aligned} \tag{5.39}$$

where we assumed that the probability to be in the domain for t going to infinity vanishes, and used $P(x, v, t_0 \mid x_0, v_0, t_0) = \delta(x - x_0)\delta(v - v_0)$. To find the mean-first-passage-time, it is sufficient so solve $\mathcal{L}_{FP}^{\dagger} \tau = 1$ with the boundary condition

$\tau = 0$ on $\partial\mathcal{D}$. Despite the apparent simplicity of the equation describing the MFPT, the computation turns out to be rather involved in practice. However, an elegant solution exists in the overdamped limit.

Overdamped Solution In the overdamped limit, the equation for the MFPT $\mathcal{L}_{FP}^{\dagger}\tau = 1$ reads

$$-\left(-\frac{1}{\eta}\frac{\partial V}{\partial x} + \frac{\Omega}{2\eta^2}\frac{\partial}{\partial x}\right)\frac{\partial \tau}{\partial x} = 1 \; . \tag{5.40}$$

After a multiplication with the integrating factor $e^{-\beta V(x)}$, the equation for τ becomes

$$\frac{\partial}{\partial x}\left(\frac{\partial \tau}{\partial x}e^{-\beta V(x)}\right) = -\beta\eta e^{-\beta V(x)} \; . \tag{5.41}$$

The integration over the spatial coordinate from $-\infty$ to x and assuming a reflecting boundary at $x \to -\infty$, i.e. $\lim\limits_{x\to-\infty}\frac{\delta\tau}{\delta x} = 0$, we get

$$\frac{\partial \tau}{\partial x} = -\beta\eta \exp\left\{\beta V(x)\right\}\int_{-\infty}^{x} dz \exp\left\{-\beta V(z)\right\} \; . \tag{5.42}$$

Integrating again from the initial position x_0 to x_f, which is situated on the boundary of the domain $\mathcal{D}$, $x_f \in \partial\mathcal{D}$ (and so $\tau(x_f) = 0$), we obtain

$$\tau(x_0) = \eta\beta \int_{x_0}^{x_f} dy \exp\left\{\beta V(y)\right\}\int_{-\infty}^{y} dz \exp\left\{-\beta V(z)\right\} \; , \tag{5.43}$$

which is known as the Pontryagin *et al.* solution of the Kramers problem [212].

Metastable Potential The MFPT can be derived explicitly for a particle initially located at $x_0 = x_A$, the metastable minimum of the potential $V(x)$ of Fig. 5.1. The domain $\mathcal{D}$ is the range $]-\infty, x_{Si}[$. Considering the last integral in Eq. (5.43), the integrand is maximal around the minimum of the potential and therefore the following approximation is valid

$$V(z) \simeq V(x_A) + \frac{1}{2}V''(x_A)(z - x_A)^2 + \mathcal{O}[(z - x_A)^3] \; , \tag{5.44}$$

and the integral becomes

$$\int_{-\infty}^{y} dz \exp\{-\beta V(z)\} = \exp\{-\beta V(x_A)\} \int_{-\infty}^{y} dz \exp\left\{-\frac{\beta}{2} V''(x_A)(z-x_A)^2\right\}$$
$$\simeq \sqrt{\frac{2\pi}{\beta V''(x_A)}} \exp\{-\beta V(x_A)\} \ , \tag{5.45}$$

where the upper limit of integration has been safely extended to infinity in the last step. The remaining integral has its integrand maximal around the local maximum of the potential and therefore $V(y)$ is approximated as

$$V(y) \simeq V(x_B) - \frac{1}{2}|V''(x_B)|(y-x_B)^2 + \mathcal{O}[(y-x_B)^3] \ , \tag{5.46}$$

and the integral becomes

$$\int_{x_A}^{x_{Si}} dy \exp\{\beta V(y)\} = \exp\{\beta V(x_B)\} \int_{x_A}^{x_{Si}} dy \exp\left\{-\frac{\beta}{2}|V''(x_B)|(y-x_B)^2\right\} \ . \tag{5.47}$$

By the same argument as above, the limits of integration are extended to infinity allowing the computation of the integral

$$\int_{x_A}^{x_{Si}} dy \exp\{\beta V(y)\} \simeq \exp\{\beta V(x_B)\} \int_{-\infty}^{\infty} dy \exp\left\{-\frac{\beta}{2}|V''(x_B)|(y-x_B)^2\right\}$$
$$= \sqrt{\frac{2\pi}{\beta|V''(x_B)|}} \exp\{\beta V(x_B)\} \ . \tag{5.48}$$

The MFPT $\tau_{x_A \to x_{Si}}$ is then given by

$$\tau_{x_A \to x_{Si}} = \frac{2\pi\eta}{\sqrt{V''(x_A)|V''(x_B)|}} \exp\{\beta[V(x_B) - V(x_A)]\} \ . \tag{5.49}$$

We observe that the MFPT in the overdamped limit is the inverse of the rate (5.34) derived with the flux-over-population method, in the same limit. This is not a coincidence since, as we will see next, there is a formal equivalence between the two approaches.

Formal Equivalence Between the MFPT and the Flux-over-Population Method

A formal relation between the flux-over-population and the MFPT methods has been shown in Refs. [198, 199]. We have learned in the previous section that the MFPT $\tau_{\mathcal{D}}(x_0, v_0)$ is defined by the equation

$$\mathcal{L}_{FP}^{\dagger}\tau_{\mathcal{D}}(x_0, v_0) = 1 \ , \qquad (x_0, v_0) \in \mathcal{D} \ , \tag{5.50}$$

and the boundary condition $\tau_{\mathcal{D}}(x_0, v_0) = 0$ for $x_0 \in \partial\mathcal{D}$. The Green function $g(x, v_x \mid y, v_y)$ for the Fokker-Planck operator on $\mathcal{D}$ is defined as

$$\mathcal{L}_{FP}(x, v_x)g(x, v_x \mid y, v_y) = k\delta(x - y)\delta(v_x - v_y) \ , \qquad (x, v_x) \in \mathcal{D} \ , \tag{5.51}$$

$$g(x, v_x \mid y, v_y) = 0 \ , \qquad x \in \partial\mathcal{D} \ . \tag{5.52}$$

The Green function might be interpreted as a stationary probability distribution, since it is a time-independent solution of the FP equation at every point of the phase space but (y, v_y). This point might be seen as an additional point source of strength k. Moreover, the boundary $\mathcal{D}$ acts as a sink. The conservation of probability implies that the source strength is related to the probability to be absorbed per unit time or

$$\begin{aligned} k &= \int_{\mathcal{D}} dx dv_x \ \mathcal{L}_{FP}(x, v_x)g(x, v_x \mid y, v_y) \\ &= \int_{\partial\mathcal{D}} dS_i \ J_i(x, v_x \mid y, v_y) \ , \end{aligned} \tag{5.53}$$

where J_i is the probability current density defined from the Fokker-Planck equation

$$\mathcal{L}_{FP}(x, v_x)g(x, v_x \mid y, v_y) = \frac{\partial}{\partial x}J_x + \frac{\partial}{\partial v_x}J_{v_x} \ . \tag{5.54}$$

After a multiplication of the Green function with the MFPT and the integration over the domain $\mathcal{D}$, we obtain

$$\begin{aligned} &\int_{\mathcal{D}} dx dv_x \ \tau_{\mathcal{D}(x,v_x)}\mathcal{L}_{FP}(x, v_x)g(x, v_x \mid y, v_y) = k\int_{\mathcal{D}} dx dv_x \ \tau_{\mathcal{D}(x,v_x)}\delta(x - y)\delta(v_x - v_y) \ , \\ &\int_{\mathcal{D}} dx dv_x \ [\mathcal{L}_{FP}^{\dagger}(x, v_x)\tau_{\mathcal{D}}(x, v_x)]g(x, v_x \mid y, v_y) = k\tau_{\mathcal{D}(y,v_y)} \ , \end{aligned} \tag{5.55}$$

and, therefore, the MFPT becomes

$$\tau_{\mathcal{D}}(y, v_y) = \frac{\int_{\mathcal{D}} dx dv_x \; g(x, v_x \mid y, v_y)}{\int_{\partial\mathcal{D}} dS_i \; J_i(x, v_x \mid y, v_y)} \,, \tag{5.56}$$

which is precisely the inverse of the flux-over-population formula for the escape rate with a source located at y inside the well.

This result shows the equivalence between the escape rate derived with the flux-over-population method and the MFPT. The latter provides a simple interpretation of the escape problem. The escape time, given by the inverse of the escape rate, is similar to the average time needed for a particle to leave a domain. However, the MFPT faces some practical difficulties when solving for the rate, in particular, beyond the overdamped limit. The flux-over-population method is better suited to obtain an analytical solution.

5.3 Escape Rate for a Scalar Field

The main objective of this analysis is the definition of the Kramers problem in field theory. Using the knowledge gathered with the classical point particle case, we first describe the escape problem for a scalar field and show that the formulation of a meaningful definition is not straightforward. The dynamics of a field under random fluctuations is described by stochastic field theory. We introduce the two usual formulations, the first based on the Langevin equation, which has a direct interpretation but is limited in its analytical treatment, and the Fokker-Planck approach, which derivation is more involved but provides strong analytical tools. We use ideas from the flux-over-population method to define the Kramers problem, derive explicitly the escape rate for a scalar field and interpret the result.

5.3.1 Defining the Escape Problem for a Field

We consider a scalar field in a potential as depicted on Fig. 5.3. We assume, for simplicity, that the initial configuration is a homogeneous field sitting at a local minimum ϕ^A. The interactions with extra degrees of freedom, for example a thermal bath, lead to fluctuation and dissipation dynamics and potentially allow for an escape from the potential well. Our goal is to compute the rate per unit

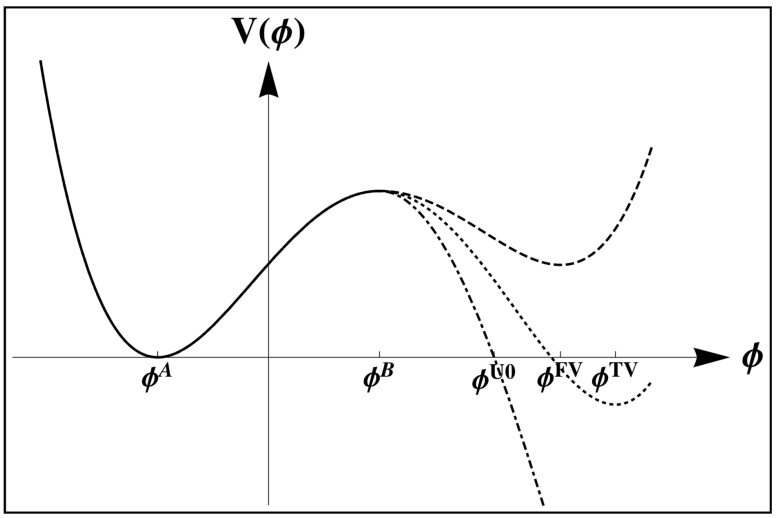

Figure 5.3 *Potentials corresponding to the escape problem. ϕ^A is the initial local minimum. ϕ^B corresponds to the local maximum of the potential. On the right-hand side of the maximum, there are several possibilities, a false vacuum at ϕ^{FV} (dashed line), a true vacuum at ϕ^{TV} (dotted line) or an unbounded potential (dash-dotted line) with $V(\phi^{U0}) = V(\phi^A)$.*

volume for the field to escape from the well, due to thermal fluctuations.

Involving a field renders the definition of an escape more difficult and less intuitive than in the one-dimensional case discussed previously. At equilibrium, the field populates both sides of the well (or have completely decayed if the potential is unbounded from below beyond the well). Comparing with the initial situation, where the field configuration is homogeneously located at ϕ^A, it is reasonable to assume the existence of a flow of the probability density across the potential well. For this reason, the flux-over-population method should apply. The naive generalization of the point particle case would be to estimate the average time needed for the field to reach the top of the potential ϕ^B for the first time at each point in space. As we will learn, this case can be related to the Hawking-Moss solution [209] in the Early Universe. However, in our situation, a Minkowski spacetime where the volume can be infinite, this solution might lead to a vanishing rate. We should therefore seek for another definition of the escape configuration.

Before going into the details of our calculations, it is important to comment on the difference between the escape problem treated in this work with two other closely related problems, the quantum tunneling and the nucleation problem. Quantum tunneling, as its name implies, is a consequence of the quantum fluctuations of the field. Such fluctuations can connect two classically disconnected values

of the field, through a forbidden region in potential energy, without giving the field any energy. This is what happens in a quantum first-order phase transition. Nucleation, on the other hand, is the mechanism that drives first-order phase transitions with small degrees of metastability (for example, small supercooling). It corresponds to the formation (or "nucleation") of bubbles of the stable phase inside the metastable phase. Such bubbles grow and complete the phase conversion. Different from tunneling, the process of nucleation is typically driven by thermal fluctuations (even though for many systems quantum fluctuations may also play a role). In this sense, it can be said that, in nucleation, the potential energy barrier is overcome with energy absorbed from the heat reservoir, in contrast to tunneling. Lastly, the problem treated in this work, the escape problem, does not necessarily require the presence of an initial false vacuum. If it is the case, the escape problem can be seen as the first stage of the nucleation problem, i.e., the generation of domains of field configurations outside the initial minimum. In general, the Kramers problem for a scalar field, defined in this work, should be understood as the derivation of the probability for the field to pass over the potential barrier in a finite region of space. Due to thermal fluctuations, a field starting at a low minimum of potential energy can gain energy from the heat reservoir and then "climb" the potential well to reach and surmount an energy barrier.

As stated in [206], it is sufficient that a finite part of space has passed the barrier. At first sight, this statement would give some freedom in the precise definition of the escape problem. In particular, once the field has reached the top at a spatial location, it can fall on the other side and attract the neighboring points without any addition of energy. This is a crucial difference with the one-dimensional case of the previous section. Considering a field, the characteristics of the potential beyond the maximum play a role in the definition of the escape problem. It is then fair to expect that the two cases, where the initial minimum is a true or a false vacuum, must be treated separately. As we will learn shortly, these features naturally emerge along the computation in a generalized flux-over-population method and this approach allows for a satisfactory definition of the escape problem. In particular, a critical volume of space that experiences hopping is precisely defined by the formalism. To perform this analysis, we should first introduce some rudiments of stochastic field theory.

5.3.2 Stochastic Field Theory

We review the basics of stochastic field theory [206] and introduce the objects needed for the derivation of the escape rate.

Langevin and Fokker-Planck Equations The usual Klein-Gordon equation describing the dynamics of the scalar field in a potential $V(\phi)$ is modified to take the thermal fluctuations into account and becomes a Langevin equation

$$(\partial_t^2 - \nabla^2)\phi(\vec{x},t) + \frac{\partial V(\phi)}{\partial \phi} + \eta\dot{\phi}(\vec{x},t) = \xi(\vec{x},t) \ , \tag{5.57}$$

where η is the dissipation coefficient and ξ is a Gaussian white noise satisfying

$$\langle \xi(\vec{x},t)\rangle = 0 \ , \qquad \langle \xi(\vec{x},t)\xi(\vec{x}',t')\rangle = \Omega\delta^3(\vec{x}-\vec{x}')\delta(t-t') \ , \tag{5.58}$$

where Ω parametrizes the strength of the noise and satisfies the Einstein relation $\Omega = 2\eta/\beta = 2\eta k_b T$. Exploring the origins of the Langevin equation in quantum field theory goes beyond the scope of this work. We invite the interested reader to refer to [9] and the references therein. For the rest of this work, we simply assume the existence of a Langevin equation of the form (5.57).

For convenience, in particular when dealing with integrals over the field-space, we discretize the space by adopting the following conventions

$$\phi(\vec{x},t) \to \phi(x_i,t) = \phi_i(t) \ , \qquad \int d^3\vec{x} \to a^3 \sum_{i=1}^{N^3} \ , \tag{5.59}$$

$$\delta(\vec{x}-\vec{y}) \to \frac{\delta_{ij}}{a^3} \ , \qquad \text{such that} \qquad \int d^3\vec{x}\ \delta(\vec{x}-\vec{y}) = 1 = a^3 \sum_{i=1}^{N^3} \frac{\delta_{ij}}{a^3} \ , \tag{5.60}$$

where the volume $\mathcal{V} = L^3 = (N\cdot a)^3$, with N being the number of discrete sites in each direction and a the spacing between two adjacent points. For simplicity, we have labelled the spatial points in the three directions with a single label $_i$ instead of $_{xyz}$. For the sake of clarity, we will denote the Laplacian as $\nabla^2_{ij}\phi_j$. The actual definition in discrete space is given by

$$\nabla^2\phi_{xyz} = \frac{1}{a^2}\left[\phi_{x+1,y,z} + \phi_{x-1,y,z} + \phi_{x,y+1,z} + \phi_{x,y-1,z} + \phi_{x,y,z+1} + \phi_{x,y,z-1} - 6\phi_{x,y,z}\right] \ , \tag{5.61}$$

where each direction of space has been explicitly labelled.

As usual when working with the Langevin equation, the analytical treatment is limited by the stochastic character of the equation. There is therefore a need to introduce the deterministic Fokker-Planck formalism for the scalar field. A full derivation of the Fokker-Planck equation in presented in Appendix D.1, and we restrict here to the most important steps. The Langevin equation gives the following set of equations for the field ϕ and the conjugate momentum π

$$\begin{aligned}
&\partial_t \phi_i(t) = \pi_i(t) \ , \\
&\partial_t \pi_i(t) = -\eta \pi_i(t) + \nabla^2_{ij}\phi_j(t) - V'(\phi_i) + \xi_i(t) \ ,
\end{aligned} \tag{5.62}$$

where the prime denotes a derivative with respect to the field. The Fokker-Planck probability density is defined as

$$P(\phi, \pi, t \mid \phi_0, \pi_0, t_0) \equiv \left\langle \prod_{i=1}^{N^3} \delta[\hat{\pi}_i(t) - \pi_i] \cdot \delta[\hat{\phi}_i(t) - \phi_i] \right\rangle_\xi \ , \tag{5.63}$$

where $\hat{\phi}_i(t)$ and $\hat{\pi}_i(t)$ are solutions of the Langevin equation (5.62) for a given noise realization ξ and ϕ_i and π_i are the arguments of the probability distribution P. The stochastic average of an operator $\mathcal{O}(\hat{\phi}, \hat{\pi})$ is defined as

$$\left\langle \mathcal{O}(\hat{\phi}, \hat{\pi}) \right\rangle_\xi \equiv \int \prod_{i=1}^{N^3} d[\xi(t)]_i \mathcal{O}(\hat{\phi}, \hat{\pi}) \exp\left\{ -\frac{a^3}{2\Omega} \sum_{j=1}^{N^3} \int dt' \xi_j^2(t') \right\} \ , \tag{5.64}$$

where the integration measure is normalized to give $\langle 1 \rangle_\xi = 1$. The probability density is a solution of the Fokker-Planck equation

$$\frac{\partial}{\partial t} P(\phi, \pi, t \mid \phi_0, \pi_0, t_0) = -\mathcal{L}_{FP} P(\phi, \pi, t \mid \phi_0, \pi_0, t_0) \ , \tag{5.65}$$

where the Fokker-Planck operator is defined as

$$\mathcal{L}_{FP} \equiv -a^3 \sum_{i=1}^{N^3} \left\{ -\pi_i \frac{\partial}{a^3 \partial \phi_i} + \frac{\partial}{a^3 \partial \pi_i} \left[\eta \pi_i - \nabla^2_{ij}\phi_j + V'(\phi_i) \right] + \frac{\Omega}{2} \frac{\partial^2}{a^6 \partial \pi_i^2} \right\} \ . \tag{5.66}$$

Probability Density Current Due to the conservation of probability, the Fokker-Planck equation can be written in terms of a probability density current J

$$\partial_t P(\phi,\pi,t) = -a^3 \sum_{i=1}^{N^3} \frac{\partial}{a^3 \partial \phi_i} J_i - a^3 \sum_{i=1}^{N^3} \frac{\partial}{a^3 \partial \pi_i} \bar{J}_i \ , \tag{5.67}$$

where the components J_i and $\bar{J}_i$ of the current are defined as

$$J_i \equiv -\left\{ -\pi_i - k_B T \frac{\partial}{a^3 \partial \pi_i} \right\} P(\phi,\pi,t \mid \phi_0,\pi_0,t) \ , \tag{5.68}$$

$$\bar{J}_i \equiv -\left\{ \left[\eta \pi_i - \nabla^2_{ij} \phi_j + V'(\phi_i) \right] + k_B T \frac{\partial}{a^3 \partial \phi_i} + \frac{\Omega}{2} \frac{\partial}{a^3 \partial \pi_i} \right\} P(\phi,\pi,t \mid \phi_0,\pi_0,t) \ , \tag{5.69}$$

for $i \in [1, N^3]$. The validity of this equation might be shown explicitly by substituting in Eq. (5.67).

Equilibrium Distribution The Fokker-Planck equation admits an equilibrium solution P_0 given by

$$P_0(\phi,\pi) = \mathcal{Z}^{-1} \exp\left\{ -\beta E[\phi,\pi] \right\} \ , \tag{5.70}$$

where $\mathcal{Z}$ is the normalization given by the partition function

$$\mathcal{Z} = \int \prod_{i=1}^{N^3} d\phi_i d\pi_i \exp\left\{ -\beta E[\phi,\pi] \right\} \ , \tag{5.71}$$

and $E[\phi,\pi]$ is given by

$$E[\phi,\pi] = a^3 \sum_{i=1}^{N^3} \left[\frac{1}{2}\pi_i^2 + \frac{1}{2}(\nabla\phi_i)^2 + V(\phi_i) \right] \ , \tag{5.72}$$

which corresponds to energy function of the system in the non-dissipative limit.

Vector-Matrix Notation Following the work of Langer [208], it is useful to introduce a vector-matrix notation. The field and its conjugate momentum are written in a $2N^3$-dimensional vector

$$\begin{pmatrix} \phi \\ \pi \end{pmatrix} = \begin{pmatrix} \phi_i(t) \\ \pi_i(t) \end{pmatrix} \ , \qquad \text{where } i \in [1, N^3] \ . \tag{5.73}$$

The deterministic limit of the Langevin equation is expressed as

$$\frac{\partial}{\partial t}\begin{pmatrix}\phi\\ \pi\end{pmatrix} = -M\cdot\begin{pmatrix}\frac{\partial}{a^3\partial\phi}\\ \frac{\partial}{a^3\partial\pi}\end{pmatrix}E[\phi,\pi]\ , \tag{5.74}$$

with $M=(M_{ij})$ being the $2N^3\times 2N^3$ block matrix defined as

$$M=\frac{1}{a^3}\begin{pmatrix}0 & -\mathbb{1}\\ \mathbb{1} & \eta\mathbb{1}\end{pmatrix}\ , \tag{5.75}$$

where $\mathbb{1}$ is the N^3-dimensional unit matrix and the multiplication $\cdot$ between two $2N^3\times 2N^3$ matrices is defined as

$$(A\cdot B)_{ij}\equiv a^3\sum_{k=1}^{2N^3}A_{ik}B_{kj}\ . \tag{5.76}$$

A similar rule applies to the scalar product. The Fokker-Planck equation is given as

$$\partial_t P(\phi,\pi,t) = -\begin{pmatrix}\frac{\partial}{a^3\partial\phi}\\ \frac{\partial}{a^3\partial\pi}\end{pmatrix}^T\cdot\begin{pmatrix}J\\ \bar{J}\end{pmatrix}\ , \tag{5.77}$$

where $(J\ \bar{J})^T$ is the $2N^3$-dimensional vector corresponding to the probability current

$$\begin{pmatrix}J\\ \bar{J}\end{pmatrix} = -M\cdot\begin{pmatrix}\frac{\partial E}{a^3\partial\phi}+k_BT\frac{\partial}{a^3\partial\phi}\\ \frac{\partial E}{a^3\partial\pi}+k_BT\frac{\partial}{a^3\partial\pi}\end{pmatrix}P(\phi,\pi,t\mid\phi_0,\pi_0,t)\ . \tag{5.78}$$

Continuum Limit We have been working in discrete space to simplify the analytical computations. However, the continuum limit can be taken at any stage of the derivation. For completeness, let us state the main quantities we have met in the continuum limit. The Fokker-Planck equation reads

$$\frac{\partial}{\partial t}P(\phi,\pi,t\mid\phi_0,\pi_0,t_0) = -\mathcal{L}_{FP}P(\phi,\pi,t\mid\phi_0,\pi_0,t_0)\ , \tag{5.79}$$

$$\mathcal{L}_{FP}\equiv-\int d^3\vec{x}\left\{-\pi(\vec{x})\frac{\delta}{\delta\phi(\vec{x})}+\frac{\delta}{\delta\pi(\vec{x})}\left[\eta\pi(\vec{x})-\nabla^2\phi(\vec{x})+V'(\phi)\right]+\frac{\Omega}{2}\frac{\delta^2}{\delta\pi(\vec{x})^2}\right\}\ , \tag{5.80}$$

and the equilibrium distribution is given by

$$P_0(\phi,\pi) = \mathcal{Z}^{-1} \exp\left\{-\beta E[\phi,\pi]\right\} \ , \quad \mathcal{Z} = \int D\phi D\pi \exp\left\{-\beta E[\phi,\pi]\right\} \ , \tag{5.81}$$

and

$$E[\phi,\pi] = \int d^3\vec{x} \left[\frac{1}{2}\pi(\vec{x})^2 + \frac{1}{2}(\nabla\phi(\vec{x}))^2 + V(\phi)\right] \ , \tag{5.82}$$

is the energy functional.

Overdamped Limit To conclude this section on stochastic field theory, let us state the equations in the overdamped limit. The Langevin equation is given by

$$\eta\dot{\phi}_i(t) = \nabla^2\phi_i(t) - V'(\phi_i) + \xi_i(t) \ . \tag{5.83}$$

The Fokker-Planck probability density is defined as

$$P(\phi, t \mid \phi_0, t_0) = \left\langle \prod_{i=1}^{N^3} \delta[\hat{\phi}_i(t) - \phi_i] \right\rangle_\xi \ , \tag{5.84}$$

and the Fokker-Planck equation reads

$$\partial_t P(\phi, t \mid \phi_0, t_0) = -\mathcal{L}_{FP} P(\phi, t \mid \phi_0, t_0) \ , \tag{5.85}$$

$$\mathcal{L}_{FP} \equiv a^3 \sum_{i=1}^{N^3} \left\{ \frac{\partial}{a^3 \partial\phi_i(t)} \frac{1}{\eta} \left[\nabla^2_{ij}\phi_j(t) - V'(\phi_i)\right] - \frac{\Omega}{2\eta^2} \frac{\partial^2}{a^6 \partial\phi_i(t)^2} \right\} \ . \tag{5.86}$$

The equilibrium distribution is given by

$$P_0 = \frac{1}{\mathcal{Z}} \exp\left\{ -\beta a^3 \sum_{i=1}^{N^3} \left(\frac{1}{2}(\nabla\phi_i)^2 + V(\phi_i) \right) \right\} \ , \tag{5.87}$$

where the partition function $\mathcal{Z}$ is the normalization.

The formalism describing a scalar field in a potential and in a presence of thermal fluctuations being established, we now turn to the computation of the escape rate.

5.3.3 Computation of the Rate

The computation of the escape rate for the scalar field is a generalization of the one-dimensional flux-over-population method to stochastic field theory. The original extension of the method to a $2N$-dimensional system has been performed by J. S. Langer in [207, 208]. We present the most important steps of the derivation, explicit details on the computation are given in Appendix D.2.

Setting-up the Problem The method relies on similar ideas as in the one-dimensional case. The initial configuration is a homogeneous field located at the local minimum of the potential,

$$\phi_i(t_0) = \phi_i^A \ , \qquad \pi_i(t_0) = 0 \ , \qquad \forall i \ . \tag{5.88}$$

On one side, the potential is diverging and, on the other, there is a local maximum located at ϕ^B, as shown on Fig. 5.3. The probability density at time t_0 is a product of delta-functions peaked at $\phi = \phi^A$ and $\pi = 0$

$$P(\phi, \pi, t_0 \mid \phi_0, \pi_0, t_0) = \prod_{i=1}^{N^3} \delta[\pi_i] \cdot \delta[\phi_i - \phi^A] \ . \tag{5.89}$$

After a sufficiently long time, the system is expected to be described by the equilibrium distribution given in Eq. (5.70). The evolution of the system implies an increasing probability to find the field on the other side of the potential and, therefore, a flux of probability at the barrier.

The probability current is expected to go along the configuration with the minimal energy on the barrier ridge. This defines the saddle-point configuration, which is found by variating the energy function

$$\begin{aligned} \delta E &= a^3 \sum_{i=1}^{N^3} \pi_i \delta\pi_i + \nabla\phi_i \delta\nabla\phi_i + V'(\phi_i)\delta\phi_i \\ &= a^3 \sum_{i=1}^{N^3} \pi_i \delta\pi_i + \left[-\nabla^2\phi_i + V'(\phi_i)\right] \delta\phi_i \ . \end{aligned} \tag{5.90}$$

We directly observe that the initial configuration is an extremum of the energy. The next configuration that extremizes the energy is given by $\pi_i^S = 0$ and ϕ_i^S

that satisfies the saddle-point equation

$$\nabla^2 \phi_i^S = V'(\phi_i^S) \ , \tag{5.91}$$

and defines the saddle-point configuration. The exact form of the solution ϕ^S is a priori not obvious.

As stated in Section 5.3.1, a simple solution is the homogeneous case where the field is at the top of the potential ϕ^B, at each point of space. This trivial solution of the saddle-point equation is relevant in a situation where the volume of space in consideration is finite. An example is the Early Universe where this solution corresponds to the Hawking-Moss instanton [209], and the volume is a sphere of Hubble Radius. In our case, where the volume of space might be unbounded, such a solution might lead to a vanishing rate. We therefore seek for another solution of the saddle-point equation.

According to [206], it is sufficient that only a finite region of space has passed the barrier. We might try to find a solution of (5.91) where the field is homogeneously sitting at the initial position ϕ^A everywhere but in some finite part where it is climbing the potential well. Using the rotational symmetry and writing the saddle-point equation in spherical coordinates, we obtain

$$\frac{\partial^2}{\partial r^2}\phi^S + \frac{2}{r}\frac{\partial}{\partial r}\phi^S = V'(\phi^S) \ , \tag{5.92}$$

where for simplicity we are working in the continuum limit. The boundary conditions are

$$\lim_{r\to\infty} \phi^S(r) = \phi^A \ , \qquad\qquad \left.\frac{\partial}{\partial r}\phi^S\right|_{r=0} = 0 \ , \tag{5.93}$$

where the second condition has been introduced to make sure the left-hand side of the saddle-point equation (5.92) is finite at the center of the coordinates. The equation can be interpreted as the equation of motion of a fictitious point particle, in an inverted potential $-V$ and with a damping term. The overshoot/undershoot technique of S. Coleman [200] shows that a solution only exists if the original minimum is a false vacuum. We should then consider separately the cases were the initial minimum is a false (dotted and dash-dotted lines on Fig. 5.3) or a true vacuum (dashed line on the same figure).

In the case of a false vacuum at ϕ^A, the saddle-point solution satisfying (5.92)

exists and is well-understood. Let us consider the two limiting cases. If the potential is unbounded from below, by continuity, there must be a field value $\phi^0 > \phi^{U0}$, where the fictitious particle starts at $r = 0$ with zero velocity and reaches ϕ^A at infinite radius. Moreover, it has been shown in [213] that ϕ^0 is of order of ϕ^{U0}. In the presence of a true vacuum at ϕ^{TV}, the existence of a solution is ensured by the overshoot/undershoot argument. If $V(\phi(r=0)) > V(\phi^A)$, the fictitious particle does not have enough potential energy to climb the inverted potential up to ϕ^A, this is an undershoot. On the other hand, if $\phi(r=0)$ is close enough to ϕ^{TV}, the fictitious particle can stay near the true minimum until the damping term becomes negligible, since it is suppressed by r, and then it will overshoot. By continuity, there is a field value to start at $r = 0$ that satisfies $V(\phi(r=0)) < V(\phi^A)$ and $\phi(r=0) < \phi^{TV}$ such that the fictitious particle ends at ϕ^A at infinite radius. By these arguments, the saddle-point configuration is uniquely defined. Moreover, it has been shown by Coleman in [214] that the Hessian matrix of the energy evaluated for this configuration has only one negative eigenvalue.

One of the main difference with nucleation is that the escape problem can be defined for an initial true vacuum at ϕ^A. However, a proper definition of the escape rate in this case requires additional care. On the one hand, by comparing the initial and the equilibrium distributions, it is fair to assume that there is a probability flow at the potential barrier and, therefore, it should be possible to define an escape. On the other hand, the undershoot argument forbids the existence of a solution of the saddle-point equation. We will come back to this issue at the end of this section and make some propositions for a well-defined escape problem. For the moment, we simply assume that the initial position ϕ^A is a false vacuum and proceed with the computation of the escape rate.

The flux-over-population method relies on the following assumptions :

- There are no sources nor sinks in the neighborhood of the saddle-point configuration. This allows writing the Fokker-Planck equation (5.65) near the saddle point as

$$a^3 \sum_{i=1}^{N^3} \left\{ -\pi_i \frac{\partial}{a^3 \partial \phi_i} + \frac{\partial}{a^3 \partial \pi_i} \left[\eta \pi_i + a^3 \sum_{k=1}^{N^3} \left[-\frac{\nabla^2_{ik}}{a^3} + \frac{V''(\phi^S_k)\delta_{ik}}{a^3} \right] (\phi_k - \phi^S_k) \right] + \frac{\Omega}{2} \frac{\partial^2}{a^6 \partial \pi_i^2} \right\} P(\phi, \pi) = 0 \,, \tag{5.94}$$

using the expansion of the energy near the saddle-point

$$E[\phi,\pi] = E[\phi^S,\pi^S] + \frac{1}{2}a^6 \sum_{i,j=1}^{N^3} (\phi_i - \phi_i^S) \left[-\frac{\nabla_{ij}^2}{a^3} + \frac{V''(\phi_i^S)\delta_{ij}}{a^3} \right] (\phi_j - \phi_j^S)$$
$$+ \frac{1}{2}a^6 \sum_{ij=1}^{N^3} (\pi_i - \pi_i^S) \frac{\delta_{ij}}{a^3} (\pi_j - \pi_j^S) + \dots \ . \tag{5.95}$$

In the spirit of the vector-matrix notation defined above, we introduce the matrix (e_{ij}^S)

$$(e_{ij}^S) = -\frac{1}{a^3} \begin{pmatrix} -\nabla_{ij}^2 + V''(\phi_k^S)\delta_{ij} & 0 \\ 0 & \mathbb{1} \end{pmatrix} , \tag{5.96}$$

which corresponds to the negative of the Hessian matrix of the energy evaluated at the saddle-point configuration[4].

- Inside the well, near the minimum where the field is located initially, the system is thermalized

$$P(\phi \simeq \phi^A, \pi \simeq \pi^A) \simeq P_0(\phi,\pi) \ , \tag{5.97}$$

where P_0 is the equilibrium distribution.

- Beyond the saddle point, the probability density is strongly suppressed due to the presence of the sinks.

Derivation of the Probability Density The computation of the flow of the probability current and the number density relies on the solution $P(\phi,\pi)$ of the Fokker-Planck equation with the boundary conditions given above. This solution is derived using the Kramers ansatz

$$P(\phi,\pi) = \zeta(\phi,\pi) P_0(\phi,\pi) \ , \tag{5.98}$$

where $\zeta(\phi,\pi)$ must be fixed to satisfy the boundary conditions

$$\zeta(\phi \simeq \phi^A, \pi \simeq \pi^A) = 1 \ , \qquad \zeta(\phi > \phi^S, \pi) \to 0 \ . \tag{5.99}$$

[4]Note that in the context of field theory, this is usually referred as a fluctuation operator.

The equation for $\zeta(\phi,\pi)$ is found by insertion in the Fokker-Planck equation. In particular, near the saddle-point, one finds

$$a^3\sum_{i=1}^{N^3}\left\{-\pi_i\frac{\partial}{a^3\partial\phi_i}+\left[-\eta\pi_i+a^3\sum_{k=1}^{N^3}\left[-\frac{\nabla^2_{ik}}{a^3}+\frac{V''(\phi_k^S)\delta_{ik}}{a^3}\right](\phi_k-\phi_k^S)\right]\frac{\partial}{a^3\partial\pi_i}\right.$$
$$\left.+\frac{\Omega}{2}\frac{\partial^2}{a^6\partial\pi_i^2}\right\}\zeta(\phi,\pi)=0\ . \tag{5.100}$$

With the same arguments as in the one-dimensional case and following the Kramers original proposal, it is assumed that $\zeta(\phi,\pi)$ depends on a linear combination u of the ϕ_i and π_i

$$\zeta(\phi,\pi)=\zeta(u)\ ,\quad \text{where}\quad u=a^3\sum_{i=1}^{N^3}\left[U_i(\phi_i-\phi_i^S)+\bar{U}_i(\pi_i-\pi_i^S)\right]\ , \tag{5.101}$$

where U_i and $\bar{U}_i$ are the coefficients associated to ϕ_i and π_i respectively. The following ansatz for $\zeta(u)$

$$\zeta(u)=\frac{1}{\sqrt{2\pi k_BT}}\int_u^\infty dz\ \exp\left\{-\frac{z^2}{2k_BT}\right\}\ , \tag{5.102}$$

satisfies the boundary conditions. To compute the coefficients U_i and $\bar{U}_i$, we substitute $\zeta(u)$ in Eq. (5.100) and obtain

$$a^3\sum_{i=1}^{N^3}\left\{\left(U_i+\eta\bar{U}_i\right)\pi_i-\bar{U}_ia^3\sum_{k=1}^{N^3}\left[-\frac{\nabla^2_{ik}}{a^3}+\frac{V''(\phi_k^S)\delta_{ik}}{a^3}\right](\phi_k-\phi_k^S)\right.$$
$$\left.+\eta\bar{U}_i^2a^3\sum_{k=1}^{N^3}U_k(\phi_k-\phi_k^S)+\eta\bar{U}_i^2a^3\sum_{k=1}^{N^3}\bar{U}_k(\pi_k-\pi_k^S)\right\}=0\ . \tag{5.103}$$

At first sight this equation seems unpromising. Fortunately, it can be written in a simple form using the vector-matrix notation. Defining the $(2N^3)$ vectors $(U\ \bar{U})^T$ and $(\phi-\phi^S\ \pi-\pi^S)^T$ such that

$$u=(U\ \bar{U})\cdot\begin{pmatrix}\phi-\phi^S\\ \pi-\pi^S\end{pmatrix}=a^3\sum_{i=1}^{N^3}\left[U_i(\phi_i-\phi_i^S)+\bar{U}_i(\pi_i-\pi_i^S)\right]\ , \tag{5.104}$$

with the scalar product being defined as in Eq. (5.76), the equation for the parameters U_i and $\bar{U}_i$ becomes

$$(U\ \bar{U}) \cdot M^T \cdot (e^S_{ij}) \cdot \begin{pmatrix} \phi - \phi^S \\ \pi - \pi^S \end{pmatrix} = \lambda (U\ \bar{U}) \cdot \begin{pmatrix} \phi - \phi^S \\ \pi - \pi^S \end{pmatrix} , \tag{5.105}$$

where the scalar λ is defined as

$$\lambda \equiv (U\ \bar{U}) \cdot M \cdot \begin{pmatrix} U \\ \bar{U} \end{pmatrix} = a^3 \sum_{i=1}^{N^3} \eta \bar{U}_i \bar{U}_i \ . \tag{5.106}$$

The matrix equation (5.105) leads to the eigenvalue equation for $(U\ \bar{U})$

$$(U\ \bar{U}) \cdot M^T \cdot (e^S_{ij}) = \lambda (U\ \bar{U}) \ , \tag{5.107}$$

in other terms $(U\ \bar{U})^T$ is a left eigenvector of the matrix $M^T \cdot (e^S_{ij})$ with eigenvalue λ. Combining the definition of λ and the eigenvalue equation, we find the normalization condition

$$1 = (U\ \bar{U}) \cdot (e^S_{ij})^{-1} \cdot \begin{pmatrix} U \\ \bar{U} \end{pmatrix} \ . \tag{5.108}$$

The eigenvalue λ is positive by definition. The positivity is in fact a direct consequence of the overall negativity of the exponent of $\zeta(u)$. This negative exponent has been chosen in order to satisfy the boundary condition imposed by the method, namely the suppression of the probability distribution beyond the saddle-point and λ is the only positive eigenvalue of the matrix $M^T \cdot (e^S_{ij})$. Recall that (e^S_{ij}) is defined as the negative of the Hessian of the energy precisely evaluated at the saddle-point.

Probability Density Current and Flux Once we have obtained the probability density $P = \zeta P_0$ we are ready to compute the associated probability density current defined in Eqs. (5.68) and (5.69). After some algebra, we find

$$J\zeta P_0 = \sqrt{\frac{k_B T}{2\pi}} M \cdot \begin{pmatrix} U \\ \bar{U} \end{pmatrix} \exp\left\{ -\frac{u^2}{2k_B T} \right\} P_0 \ , \tag{5.109}$$

and the probability flux j

$$
\begin{aligned}
j &= a^3 \sum_{i=1}^{2N^3} \int_{u=0} dS_i \; J_i(\phi,\pi) \\
&= \frac{\lambda}{2\pi\mathcal{Z}} \sqrt{\frac{k_B T}{2\pi}} \exp\left\{-\beta E[\phi^S,\pi^S]\right\} \int D\phi D\pi \int dk \exp\left\{ ik(U\ \bar{U}) \cdot \begin{pmatrix} \phi-\phi^S \\ \pi-\pi^S \end{pmatrix} \right\} \\
&\quad \cdot \exp\left\{ \frac{\beta}{2} \begin{pmatrix} \phi-\phi^S \\ \pi-\pi^S \end{pmatrix}^T \cdot (e^S_{ij}) \cdot \begin{pmatrix} \phi-\phi^S \\ \pi-\pi^S \end{pmatrix} \right\} . \qquad (5.110)
\end{aligned}
$$

Introducing the rotation $S = (S_{ij})$ in field space to diagonalize the matrix (e^S_{ij}) we obtain

$$
\begin{pmatrix} \phi-\phi^S \\ \pi-\pi^S \end{pmatrix} = S \cdot \xi \ , \quad iku = ik(U\ \bar{U}) \cdot S^\dagger \cdot S \cdot \begin{pmatrix} \phi-\phi^S \\ \pi-\pi^S \end{pmatrix} = ik\tilde{U} \cdot \xi \ , \quad (5.111)
$$

where we have defined the vector $\tilde{U}$ as $S \cdot \left(U\ \bar{U}\right)^T$ and

$$
\begin{pmatrix} \phi-\phi^S \\ \pi-\pi^S \end{pmatrix}^T \cdot (e^S_{ij}) \cdot \begin{pmatrix} \phi-\phi^S \\ \pi-\pi^S \end{pmatrix} = a^3\mu_1\xi_1^2 - a^3 \sum_{l=2}^{2N^3} \mu_l \xi_l^2 \ , \qquad (5.112)
$$

where all the scalars μ_l are defined as positive[5]. The only positive eigenvalue of (e^S_{ij}) is μ_1, all the other eigenvalues are $-\mu_l$. We finally obtain for the flux

$$
\begin{aligned}
j &= \frac{\lambda}{2\pi\mathcal{Z}} \sqrt{\frac{k_B T}{2\pi}} \exp\left\{-\beta E[\phi^S,\pi^S]\right\} \\
&\quad \cdot \int \prod_{l=1}^{2N^3} d\xi_l \int dk \exp\left\{ ika^3 \sum_{l=1}^{2N^3} \tilde{U}_l \xi_l + \frac{\beta}{2} a^3 \mu_1 \xi_1^2 - \frac{\beta}{2} a^3 \sum_{l=2}^{2N^3} \mu_l \xi_l^2 \right\} \\
&= \frac{\lambda}{2\pi\mathcal{Z}} \exp\left\{-\beta E[\phi^S,\pi^S]\right\} |\det(2\pi/\beta)^{-1} E^{(S)}|^{-\frac{1}{2}} \ , \qquad (5.113)
\end{aligned}
$$

where the matrix $E^{(S)} = -(e^S_{ij})$ is the Hessian of the energy at the saddle-point which has only one negative eigenvalue. Since this negative eigenvalue appears with a negative sign, it is the magnitude of the determinant that enters the formula. The successive integrations have been performed in the following order, first over all the modes l larger than 1, then over k and finally over ξ_1.

[5]For the moment, we ignore the possibility of vanishing eigenvalues, we shall come back to them shortly.

Zero-modes Due to the translation invariance of the saddle-point solution, there are three eigenvalues in the associated determinant that are exactly zero and, therefore, must be treated separately upon the Gaussian integration. For simplicity and in order to agree with the literature, we perform the analysis in the continuum space. First of all, let us show that $\partial_{\vec{x}}\phi^S$, $\partial_{\vec{y}}\phi^S$ and $\partial_{\vec{z}}\phi^S$ are zero-modes. Considering $\partial_{\vec{x}}\phi^S$ we have

$$\begin{aligned}[-\nabla^2 + V''(\phi^S)]\partial_{\vec{x}}\phi^S &= -\partial_{\vec{x}}\nabla^2\phi^S + V''(\phi^S)\partial_{\vec{x}}\phi^S = -\partial_{\vec{x}}V'(\phi^S) + V''(\phi^S)\partial_{\vec{x}}\phi^S \\ &= -V''(\phi^S)\partial_{\vec{x}}\phi^S + V''(\phi^S)\partial_{\vec{x}}\phi^S = 0\ . \end{aligned} \tag{5.114}$$

To remove the zero-modes, we follow the procedure described by Langer in [208] and by Callan and Coleman in [201]. First of all, the determinant has its zero-eigenvalues removed and becomes

$$|\det(2\pi/\beta)^{-1}[-\nabla^2 + V''(\phi_i^S)]| \to |\det'(2\pi/\beta)^{-1}[-\nabla^2 + V''(\phi_i^S)]|\ , \tag{5.115}$$

with the prime denoting the removal of the vanishing eigenvalues. Then, the integration over the zero-modes $\partial_{\vec{x}}\phi^S$, $\partial_{\vec{y}}\phi^S$ and $\partial_{\vec{z}}\phi^S$ becomes an integration over $d\vec{x}$, $d\vec{y}$ and $d\vec{z}$ giving an overall volume factor $\mathcal{V}$. Finally each change of variable from the zero-modes to $\partial_{\vec{x}}\phi^S$, $\partial_{\vec{y}}\phi^S$ and $\partial_{\vec{z}}\phi^S$ to $d\vec{x}$, $d\vec{y}$ and $d\vec{z}$ leads to a Jacobian. For example, for the mode $\partial_{\vec{x}}\phi^S$ we have

$$\left[\int d^3\vec{x}\ \left(\frac{\partial\phi^S}{\partial x}\right)^2\right]^{1/2}\ . \tag{5.116}$$

The Jacobian is identical for each zero-mode since

$$\int d^3\vec{x}\ \left(\frac{\partial\phi^S}{\partial x}\right)^2 = \int d^3\vec{x}\ \left(\frac{\partial\phi^S}{\partial y}\right)^2 = \int d^3\vec{x}\ \left(\frac{\partial\phi^S}{\partial z}\right)^2\ , \tag{5.117}$$

where we used the rotation-symmetry of the saddle-point solution. We then have

$$\int d^3\vec{x}\ \left(\frac{\partial\phi^S}{\partial x}\right)^2 = \frac{1}{3}\int d^3\vec{x}\ \left(\nabla\phi^S\right)^2\ . \tag{5.118}$$

So, there is an overall factor multiplying the rate

$$\left[\frac{1}{3}\int d^3\vec{x}\ \left(\nabla\phi^S\right)^2\right]^{3/2}\ , \tag{5.119}$$

coming from the Jacobian. A quick dimensional check tells us that removing the three eigenvalues from the determinant increases the dimension by 3/2. The overall volume factor has a dimension of -3 and the Jacobian 3/2, exactly compensating the removal of the zero-eigenvalues.

Population Inside the Well The last missing piece is the population inside the well. This is obtained using the condition that the system is thermalized near the minimum of the potential and by expanding the energy function around the configuration (ϕ^A, π^A)

$$E[\phi,\pi] = E[\phi^A,\pi^A] + \frac{1}{2}a^6 \sum_{i,j=1}^{N^3} (\phi_i - \phi_i^A)\left[-\frac{\nabla_{ij}^2}{a^3} + \frac{V''(\phi_i^S)\delta_{ij}}{a^3}\right](\phi_j - \phi_j^A) + \frac{1}{2}a^6 \sum_{ij=1}^{N^3} (\pi_i - \pi_i^A)\frac{\delta_{ij}}{a^3}(\pi_j - \pi_j^A) + \dots \ . \tag{5.120}$$

The population inside the well is

$$\begin{aligned} n_A &= \int D\phi D\pi P_0 \\ &= \frac{1}{\mathcal{Z}} \int D\phi D\pi \exp\left\{-\beta E[\phi^A,\pi^A] + \frac{\beta}{2}\begin{pmatrix} \phi-\phi^A \\ \pi-\pi^A \end{pmatrix}^T \cdot (e_{ij}^A) \cdot \begin{pmatrix} \phi-\phi^A \\ \pi-\pi^A \end{pmatrix}\right\} \\ &= \frac{1}{\mathcal{Z}} \exp\left\{-\beta E[\phi^A,\pi^A]\right\} [\det(2\pi/\beta)^{-1} E^{(A)}]^{-\frac{1}{2}} \ , \end{aligned} \tag{5.121}$$

where the matrix $E^{(A)}$ is the Hessian of the energy of the initial configuration at ϕ^A, all eigenvalues are positive.

Escape Rate The ratio of the flux j over the number density n_A, taking into account the zero-modes, gives the escape rate for a scalar field per unit volume

$$\frac{k}{\mathcal{V}} = \frac{\lambda}{2\pi}\left[\frac{1}{3}a^3 \sum_{i=1}^{N^3} \left(\nabla\phi_i^S\right)^2\right]^{3/2} \left[\frac{\det[(2\pi/\beta)^{-1}E^{(A)}]}{|\det'[(2\pi/\beta)^{-1}E^{(S)}]|}\right]^{1/2} \cdot \exp\left\{-\beta\left[E(\phi^S,\pi^S) - E(\phi^A,\pi^A)\right]\right\} \ . \tag{5.122}$$

Let us consider the different contributions to the rate. In the exponent, we have

$$E(\phi^S, \pi^S) - E(\phi^A, \pi^A) = a^3 \sum_{i=1}^{N^3} \frac{1}{2}(\nabla\phi_i^S)^2 + V(\phi_i^S) - V(\phi_i^A) \ , \tag{5.123}$$

which corresponds to the activation energy, the difference between the energy of saddle-point configuration with respect to the initial configuration. Since the initial configuration is homogeneous and only a difference of potential enters the rate formula, we can safely shift the potential to have $V(\phi_i^A) = 0$. The determinants can be written as

$$\det[(2\pi/\beta)^{-1}E^{(A)}] = \det[(2\pi/\beta)^{-1}(-\nabla^2 + V_A'')] \ , \tag{5.124}$$

where V_A'' is the second derivative of the potential at the initial minimum and

$$|\det'[(2\pi/\beta)^{-1}E^{(S)}]| = |\det'(2\pi/\beta)^{-1}[-\nabla^2 + V''(\phi^S)]| \ , \tag{5.125}$$

where the field configuration entering the operator is the saddle-point solution.

The escape rate per unit volume in the continuum limit is given by

$$\begin{aligned}\frac{k}{\mathcal{V}} =& \frac{\lambda}{2\pi}\left[\frac{\beta}{6\pi}\int d^3\vec{x}\ \left(\nabla\phi^S\right)^2\right]^{\frac{3}{2}}\left[\frac{\det[-\nabla^2 + V_A'']}{|\det'[-\nabla^2 + V''(\phi^S)]|}\right]^{\frac{1}{2}} \\ & \cdot \exp\left\{-\beta\int d^3\vec{x}\ \frac{1}{2}(\nabla\phi^S)^2 + V(\phi^S)\right\} \ ,\end{aligned} \tag{5.126}$$

which is the main result of this chapter. The constant λ is sometime referred as the dynamical prefactor and the ratio of determinants as the statistical prefactor [198, 203, 208, 215]. The explicit expressions of these factors depend on the saddle-point configuration ϕ^S. We choose to present here the most general form of the escape rate, and, therefore, we postpone the discussion of the methods to estimate the prefactors and the exponent to the next section.

Initial Stable Minimum The last situation left to consider is when ϕ^A is a true vacuum. As described above, the saddle-point equation (5.92) does not have any solution. However, in the presence of fluctuation and dissipation dynamics, it is fair to assume that the field starts to climb the potential and probes the other side of the well, even if it will likely come back to the original side. Moreover, as noted already, the comparison between the initial probability distribution, a delta function peaked at ϕ^A at each point of space, and the equilibrium distribution,

that probes both sides of the well, implies a flow of probability at the maximum the potential. These two arguments suggest that the escape problem for an initial true vacuum might still be defined. The rate will simply indicate how likely it is to have a region of space that passes the barrier.

Let us formulate some propositions for a meaningful definition. The first possibility is to consider a finite volume $\mathcal{V}$ of space and use the saddle-point solution $\phi^S = \phi^B$ at each point in the volume. The activation energy will be given by $E = \mathcal{V}\Delta V$. This is the simplest generalization of the one-dimensional case but is dependent on the volume in consideration. Moreover, it can lead to an underestimate of the rate since, instead of waiting at the top of the potential, the field can fall on the other side and attract the neighboring points without any addition of energy.

The method of reactive flux, described, for example, in the review [198], might be helpful in the derivation of the escape rate for an initially true minimum. At equilibrium, the ratio of particles densities in the wells is equal to the ratio of the rates between the two minima. Since the equilibrium distribution and the rate from a false to a true vacuum are known, the transition rate from an initial true vacuum can be extracted. It is reasonable to assume that, at equilibrium, the activation rate derived with the method of reactive flux will be smaller than the true escape rate. However, this method also allows studying further the approach to equilibrium by defining a relaxation rate, from an initial out-of-equilibrium distribution.

Alternatively, we can consider an approximated situation, where the false minimum on the right-hand side is replaced by a true minimum, due to a modification of the potential beyond the maximum. For example, a minimal situation could be a new true minimum, almost degenerated with $V(\phi^A)$. A saddle-point configuration is well-defined and the rate given by (5.126). Moreover, the saddle-point configuration will naturally define the typical size of the region of space that experiences hopping. As in the previous case, the escape rate might be underestimated. However, it is fair to expect that the main contribution to the escape time is given by the climbing of the potential well, which corresponds to the part of the potential that is not modified.

A last possibility is the construction of a saddle-point configuration using an analytic continuation. It was not possible to obtain a solution of Eq. (5.92), where the field is at ϕ^{FV} at $r = 0$ and respecting the boundary condition (5.93).

One can imagine giving an initial imaginary velocity to the field which would then allow for the climb. This kind of solutions have been studied in the context of tunneling [216–220]. However, this goes beyond the scope of this work, and we leave it for a future analysis.

5.3.4 Discussion of the Result

We present a comparison between the escape rate (5.126) and the related problem of quantum tunneling at a sufficiently high-temperature, where thermal effects dominate. The similarities between the two results provide some insights about the methods needed for an explicit evaluation of the escape rate, once a potential has been specified.

Comparison with Quantum Tunneling at Finite-Temperature

Quantum tunneling of a scalar field is a well-studied problem and plays a significant role in the study of first-order phase transitions and in the stability of false vacua. The problem has been solved for quantum field theory by C. G. Callan and S. Coleman at zero-temperature [200, 201] and later extended to finite-temperatures by A. D. Linde [202]. The result of Linde is particularly interesting for the current analysis since, for sufficiently high temperatures, the thermal fluctuations are dominating over the quantum fluctuations. In this regime, it is fair to expect some similarities between the tunneling and the escape rates.

The tunneling rate per unit volume, at finite-temperature and when thermal fluctuations are dominating, is given by

$$\frac{\Gamma(T)}{\mathcal{V}} = T\left(\frac{\mathcal{S}_3(\phi^S,T)}{2\pi T}\right)^{\frac{3}{2}}\left[\frac{\det[-\nabla^2+V_A'']}{|\det'[-\nabla^2+V''(\phi^S)]|}\right]^{\frac{1}{2}}\exp\left\{-\mathcal{S}_3(\phi^S,T)/T\right\}\ , \tag{5.127}$$

where the action $\mathcal{S}_3$ is defined as

$$\mathcal{S}_3(\phi,T) \equiv \int d^3\vec{x}\ \frac{1}{2}(\nabla\phi)^2 + V(\phi,T)\ , \tag{5.128}$$

and ϕ^S is a solution of

$$\frac{\partial^2}{\partial r^2}\phi^S + \frac{2}{r}\frac{\partial}{\partial r}\phi^S = V'(\phi^S, T) \ , \tag{5.129}$$

where $V(\phi, T)$ is the temperature-dependent effective potential.

Comparing with the escape problem, and assuming identical potentials[6], we immediately notice that the field configurations entering the two rates are given by the same equation, (5.92) and (5.129). This similarity implies that the ratio of determinants and the exponential term are identical in the escape (5.126) and in the tunneling (5.127) rates. Using the argument of Coleman [200, 221], that the action $\mathcal{S}_3$ is invariant under an infinitesimal scale transformation of the solution ϕ^S, we obtain

$$\mathcal{S}_3(\phi, T) = \frac{1}{3}\int d^3\vec{x}\ (\nabla\phi)^2 \ , \tag{5.130}$$

which is precisely the term given by the Jacobian in the escape rate.

The only difference between the escape and the quantum tunneling rates lies in the prefactors. In particular, the escape rate predicts a factor of $\lambda/2\pi$ replacing the temperature. We interpret this difference as follows. First of all, the escape problem, even if closely related, is not defined exactly as the transition rate due to tunneling effects. A comparable, but not identical, rate should emerge. Moreover, to derive the escape rate, we used the framework of stochastic field theory where the strength of the noise and the damping appear explicitly. One naturally expects the damping to play a role in the final result, in particular within λ. It is, however, remarkable that the two rates, computed with different methods, stochastic field theory for the escape problem and path integral formalism of QFT for tunneling, have so much in common. The escape rate takes only into account the thermal fluctuations and is valid for arbitrarily small temperatures. It is a strong support for our result that the tunneling rate, in the limit where the thermal fluctuations dominate, mostly recovers the escape rate.

[6]To be more precise, we assume that the potential of the escape rate $V(\phi)$ is equal to the effective potential $V(\phi, T)$ at a fixed value of T.

Toward an Explicit Evaluation of the Escape Rate

In general, once a potential has been specified, a complete derivation of the escape rate (5.126) requires numerical methods, for example, as in the work of G. D. Moore and K. Rummukainen [222]. However, exploiting the similarities with the quantum tunneling rate, we can use the techniques developed for the latter to provide some guidance on the explicit derivation of the escape rate. Let us consider the exponent, the dynamical and statistical prefactors separately. Recall that, in general, it is sufficient to know the order of magnitude of the prefactors, the rate being mainly dictated by the exponential.

Exponent The evaluation of the exponent requires the solution of the saddle-point equation (5.92), which, in general, is obtained numerically. However, two cases have been identified where an analytical treatment is possible [202, 213]. In the thin-wall approximation, the potential has two minima that are almost degenerated. The saddle-point configuration has the form of a bubble of true vacuum. Going along the radial direction, $\phi^S(r)$ is initially almost constant and close to ϕ^{TV}. This corresponds to the interior of the bubble. The field solution then bounces to ϕ^A, which defines the bubble's wall. The critical radius of the bubble is found by minimizing the energy. One can show that the exponent becomes

$$\int d^3\vec{x}\ \frac{1}{2}(\nabla\phi^S)^2 + V(\phi^S) = \frac{16\pi}{3\epsilon^2}\left(\int_{\phi^{TV}}^{\phi^A} d\phi\sqrt{2V(\phi)}\right)^3 , \tag{5.131}$$

where ϵ is the difference between the false and true vacuum and the integral on the right-hand side is evaluated in the limit where ϵ vanishes. The other situation where an analytical treatment applies is when the potential difference between the false and true vacuum is much larger than the barrier height. The potential can be approximated by a cubic or a quartic function leading to exact solutions.

Statistical Prefactor The exact evaluation of ratios of determinants in field theory is, in general, an involved task. Recent discussions on some analytical approaches to this problem can be found in [223–225]. For the evaluation of the escape rate and as stated in [202, 213], it is sufficient to have only a rough estimate of this prefactor. Dimensional analysis shows that the square root of the ratio of determinants has dimension m^3 corresponding to the removal of the

three eigenvalues in the denominator. Therefore, we can write

$$\left[\frac{\det[-\nabla^2 + V_A'']}{|\det'[-\nabla^2 + V''(\phi^S)]|}\right]^{\frac{1}{2}} \sim \mathcal{O}\left(\phi^3, (V'')^{3/2}, r^{-3}, T^3\right) \ , \tag{5.132}$$

where the quantities on the right-hand side (the temperature apart) should be understood as mean values. In general, ϕ^3, $(V'')^{3/2}$, and r^{-3} are of the same order of magnitude and should be compared with the temperature to find the dominant contribution. This is a difference with quantum tunneling at finite temperature, where the temperature is expected to dominate in the statistical prefactor.

Dynamical Prefactor The dynamical prefactor λ has been defined in Eq. (5.107) as the unique positive eigenvalue of the matrix $M^T \cdot (e_{ij}^S)$. The eigenvalue equation for λ can be written as

$$\left[\frac{\partial^2}{\partial r^2} + \frac{2}{r}\frac{\partial}{\partial r} - V''(\phi^S)\right] v(r) = \lambda(\lambda + \eta) v(r) \ . \tag{5.133}$$

We observe that λ has a dependence on the dissipation coefficient η. As usual, an analytical solution of the eigenvalue equation is not possible, in particular, since it requires the knowledge of the saddle-point configuration. There exists, however, certain situations where an approximated result might be obtained, for example in the thin-wall approximation discussed above. Useful discussions on this problem can be found in the references [203, 215].

5.4 Applications for Cosmology and Beyond

We identify situations, in cosmology and other areas of physics, where the escape problem defined in this chapter plays a relevant role. We are particularly interested in scenarios where the escape rate provides an alternative mechanism to quantum tunneling. Since the aim of the current analysis is a formal definition and a solution of the Kramers problem, we restrict to a general description of these applications. A deeper analysis is left for future works.

Phase Transitions and Topological Defects A concrete situation where the escape rate becomes significant is in the study of out-of-equilibrium systems, in particular, during a first-order phase transition. Our analysis is well-suited

to investigate the approach to equilibrium. We can imagine, for example, the situation of an initially quadratic effective potential that is developing another local minimum. The second minimum is, at first, a false vacuum before becoming the true vacuum of the potential. The escape rate provides the necessary tools to study the evolution of the Fokker-Planck probability distribution between the old and the new equilibrium distributions.

As already discussed in Chapter 3, phase transitions are often associated with the formation of topological defects. Fluctuation and dissipation dynamics might influence their creation, in particular, in a second-order phase transition, where the height of the potential barrier is suppressed at the beginning of the transition. These effects might also play an important role in cross-over transitions. In the special case of embedded defects, the possibility for the field to escape would have some consequences on the stability of the object. The escape rate should therefore be related to the destruction probability of such a defect.

We have mentioned in Chapter 3 that gravitational waves might be emitted during phase transitions [89–91]. The escape mechanism, since it generalizes nucleation, could play an interesting role in this context and it would be worth studying the signature associated with this process.

Landscape of Metastable Minima One of the most interesting features of the escape problem is the hopping of the field over the potential barrier. Naively, considering a potential with two minima that are almost degenerate, the escape rate between the false and the true vacua should not be sensibly different from the rate between the true and the false vacua. For these reasons, the escape rate could be relevant in theories that contain several non-degenerate minima, in particular, in order to compute the probability for a finite part of space to evolve from one minimum to the next. One can imagine, for example, a situation with two possible directions to diffuse. In one of them, there is a large potential barrier but a minimum at a lower energy beyond the well. In the other direction, the potential barrier is smaller but the next minimum is at a higher energy. Quantum tunnelling could only be applied to the first case but the escape mechanism is applicable in both cases.

Such a situation arises in string theories, which contain many metastable vacua [226]. This framework is called the string landscape [227]. The question of how a vacuum is selected is of particular interest. Our mechanism precisely

allows for the hopping from one vacuum to the next one. Moreover, the Hagedorn temperature [228, 229], sometimes associated with string theories, could be the origin of the fluctuation and dissipation dynamics. Such an analysis might require a generalization of our work to take into account gravitational effects.

An active field of research in condensed matter physics concerns the glass transition [230], corresponding to a phase transition between a liquid and a glassy state. The phenomenology of glassy systems can be described by a N-body system in a potential with several metastable minima, called the potential energy landscape [231, 232]. The escape rate provides a mechanism to probe the different minima. A generalization to a non-relativistic field might be needed in this case.

Stochastic Inflation The stochastic formulation of inflation was introduced by Starobinsky [233, 234] as a framework to study the dynamics of a quantum scalar field during inflation. The field is split into two parts, the long-wavelength part (coarse grained) and short-wavelength quantum fluctuations. The back-reaction of the quantum fluctuations on the coarse grained part is parametrized as stochastic noise. The equation of motion of the inflaton becomes a Langevin equation. The framework is particularly relevant in the computation of correlation functions of the inflaton field [235].

In general, the noise is assumed to be homogeneous and the problem reduces to the one-dimensional situation decribed in Section 5.2. This approach considers only the fluctuations that can lift an entire Hubble sphere. If, on the contrary, we imagine that the back-reaction coming from the quantum fluctuations is inhomogeneous, the formalism developed for the escape rate is particularly useful. One can also think about different regions of space that evolve along different directions in the inflationary potential.

Stochastic Quantization The stochastic approach of quantum mechanics has been first proposed by E. Nelson in [236] and then extended to fields by G. Parisi and Y. Wu in [237]. The main idea relies on the fact that the generating functional of Euclidean field theories is related to the equilibrium limit of a statistical system coupled to a heat reservoir. The temperature of the heat bath is chosen to match the Planck constant. The evolution of the system plus reservoir is in a fictitious time and the equilibrium is reached when this extra time direction goes

to infinity. This method for modelling quantum field theory is particularly useful for numerical simulations, such as in lattice field theory [238].

The stochastic field theory introduced for the derivation of the escape rate is formally equivalent to the formalism describing the stochastic quantization. The only difference is the dimension of space. The formalism described in Sec. 5.3.2 can be seen as a three-dimensional Euclidean field theory coupled to a heat bath, whereas the stochastic quantization considers a four-dimensional Euclidean field theory and an extra time dimension. In the language of stochastic quantization, in particular, using the identification $\hbar = k_B T$, we can directly write the escape rate as

$$\frac{k}{\mathcal{V}} = \frac{\lambda}{2\pi}\left[\frac{\mathcal{S}_4}{2\pi\hbar}\right]^2 \left[\frac{\det[-\Box + V_A'']}{|\det'[-\Box + V''(\phi^S)]|}\right]^{\frac{1}{2}} \exp\left\{-\mathcal{S}_4(\phi^S)/\hbar\right\} \ , \tag{5.134}$$

where

$$\mathcal{S}_4(\phi) \equiv \int d^4\vec{x}\ \frac{1}{2}(\nabla\phi)^2 + V(\phi) \ , \tag{5.135}$$

and ϕ^S is the saddle-point configuration. A similar discussion as in Sec. 5.3.4 should be performed to compare this result with the quantum tunneling rate at zero-temperature, computed in [200, 201].

5.5 Conclusion

In this chapter, we have proposed a definition and a solution of the Kramer problem in quantum field theory. Using the framework of stochastic field theory, we have studied the probability for a scalar field to escape a potential well due to thermal fluctuations. The field theory character of the problem complicated the definition of the escape configuration. Unlike the one-dimensional case, we have learned that the shape of the potential, beyond the local maximum, influences the rate. We have identified two situations that need to be treated separately, when the initial minimum corresponds to a true or a false vacuum. Using a generalization of the flux-over-population method to a field, we have derived a full solution of the escape problem from a metastable vacuum and stated some directions to address the case of an initial true vacuum.

The main result of our analysis is the expression of the escape rate (5.126). A

comparison with the quantum tunneling rate, in the limit where the thermal fluctuations dominate, shows that the two rates have much in common. These similarities provide a strong support for our result, in particular, since both rates are computed with different approaches. The rates are, however, not identical. This is not surprising since the two problems, even if related, are not exactly the same. In particular, the escape rate takes explicitly into account damping effects. Nevertheless, the well-studied framework of quantum tunneling provides some precious techniques for an explicit evaluation of the escape rate, once a potential is fixed. It is remarkable that the derivation presented in this chapter also encompasses the Hawking-Moss instanton. This solution naturally emerges along the flux-over-population method and can be studied within the framework presented here.

Beyond the formal interest of the Kramers problem in field theory, we have identified several concrete situations, in cosmology, particle physics and condensed matter physics, where the escape rate is relevant. Out-of-equilibrium scenarios, for example during a transition between two non-degenerate vacua are natural candidates. In cosmology, phase transitions and the formation of topological defects, as well as stochastic inflation are various applications. The string landscape and the glass transition present a favorable environment for an escape mechanism. On a more formal level, the analogy with the stochastic quantization might shed a new light on both the interpretation of the escape problem and on the meaning of the stochastic approach of quantum mechanics. A deeper analysis of these directions will be the subject of future works.

Chapter 6

Conclusion

In this thesis, we have studied the influence of fluctuation and dissipation dynamics on Early Universe cosmology. Fluctuation and dissipation are common effects arising when the interactions between a system and its surrounding are taken into account. Random forces tend to perturb the motion of the system and a damping leads to the dissipation of a fraction of the energy. This scenario happens for the cosmological fields used in the description of the physics of the Early Universe. Being commonly predicted by the theory, fluctuation and dissipation lead to important consequences for cosmology, which cannot be simply ignored. We have been interested in three different situations, phase transitions and formation of topological defects, warm inflation, and the Kramers problem, where these effects may play a significant role.

The theory of topological defects has been playing a major role in cosmology over the last few decades. In Chapter 3, we were particularly interested in the embedded configurations. This special kind of topological defects is interesting since it might appear in realistic theories, such as the Standard Model. However, embedded defects are not stable by construction and, without any stabilization mechanism, they would likely decay. By studying the pion string, we have shown that, in some circumstances, the interactions with a thermal and dense medium allow for the formation of stable strings in the range of parameters that are experimentally allowed. This result is the first example of a stable embedded defect in a realistic theory. It would be of great interest to verify if a similar mechanism would apply for other examples of embedded defects, for example the electroweak string. One might also wonder if a given BSM theory includes any

stable embedded defect. With cosmology entering a new era since the observation of gravitational waves, the mechanism studied in this chapter might lead to new constraints on the theories aiming at completing the SM.

In Chapter 4, we have considered another cornerstone of modern cosmology, cosmic inflation. One of the most famous cosmological applications of fluctuation and dissipation dynamics is the warm realization of inflation. In this scenario, the continuous transfer of energy from the inflaton into radiation allows the Universe to remain warm during inflation. As in the cold realization, there is a great diversity of inflationary potentials introduced in the recent years and, therefore, a need for a systematic way to classify the models. The β-function formalism is based on ideas from the renormalization group, to characterized the inflationary epoch in terms of flows away from the de Sitter regime. In this approach, different models of inflation naturally fall into classes of universality. We have shown that the universality classes defined for cold inflation can be consistently extended to the warm realization. The description of warm inflation has a second functional dependence due to dissipation, which helps in the characterization of the possible smooth transition between the era of inflation and the radiation-dominated regime. Beyond the identification of universality, we have illustrated how this approach is well-suited for an analytical treatment of warm inflation. A further analysis of the analytical potential of the formalism might lead to interesting features. For example, a study of warm inflation using a well-motivated ansatz for the dissipation coefficient, as function of the field only, would present some computational and theoretical interests, in particular, to evaluate the cosmological perturbations.

The Kramers problem is intrinsically related to fluctuation and dissipation dynamics and has applications in several domains of physics, such as statistical or condensed matter systems. The presence of these effects in the Early Universe was the main motivation to investigate and define the Kramers problem in this context. In Chapter 5, we proposed a formulation and a derivation of the escape rate for a scalar field. We showed that, unlike the one-dimensional case, the shape of the potential, beyond the barrier, influences the rate. Remarkably, along the derivation, based on stochastic field theory, we came across some known situations, such as the Hawking-Moss instanton and the quantum tunneling rate at finite temperature. The similarities between the latter, when thermal fluctuations dominate, and the escape rate offered some precious techniques for an explicit derivation of the rate, once a potential is given. Even if the chapter was

mainly dedicated to formal aspects of the Kramers problem, we have stated some situations where the escape rate would play a significant role. In cosmology, the framework is well-suited for a study of out-of-equilibrium situations, for example during a phase transition. The possibility for the field to escape might influence the formation of topological defects and alter the stability of the embedded configurations. Beyond cosmology, the framework is relevant in situations where a potential with many metastable minima is predicted, for example in the string landscape and in the glass transition. Finally, the analogy between the formalism used in this chapter with the stochastic quantization presents some theoretical interests, especially for the interpretation of the stochastic approach of quantum mechanics.

Appendix A

Review of General Relativity

General relativity is the prevailing theory describing gravitational interactions. The theory has been formulated by A. Einstein and published in 1915 [13, 14]. The main feature of GR is the relationship between the geometry of the spacetime and its energy content. This is encoded in the Einstein equations. In this appendix, we present a short review of GR and introduce the essential quantities needed to perform calculations. Since in general GR leads to a curved spacetime, the mathematical framework of differential geometry is required. For a review of this topic, we invite the reader to refer to [239].

A.1 Basics of General Relativity

In general relativity, the spacetime is a four-dimensional Lorentzian manifold (M, g) with a Levi-Civita connection. The symmetric and non-degenerate rank $(0, 2)$ tensor g is called the metric and captures the geometry of the spacetime. In curved spacetimes, the notion of derivative is non-trivial since it requires comparing objects at different points. The covariant derivative ∇T of a tensor T of rank (r, s) is the $(r, s+1)$ tensor which components are

$$\begin{aligned}\nabla_\lambda T^{\mu_1\dots\mu_r}{}_{\nu_1\dots\nu_s} = \partial_\lambda T^{\mu_1\dots\mu_r}{}_{\nu_1\dots\nu_s} + \Gamma^{\mu_1}_{\sigma\lambda} T^{\sigma\dots\mu_r}{}_{\nu_1\dots\nu_s} + \dots + \Gamma^{\mu_r}_{\sigma\lambda} T^{\mu_1\dots\sigma}{}_{\nu_1\dots\nu_s} \\ - \Gamma^{\sigma}_{\nu_1\lambda} T^{\mu_1\dots\mu_r}{}_{\sigma\dots\nu_s} - \dots - \Gamma^{\sigma}_{\nu_r\lambda} T^{\mu_1\dots\mu_r}{}_{\nu_1\dots\sigma} \,, \end{aligned} \tag{A.1}$$

where ∂ is the usual derivative. The Γ's are the components of the Levi-Civita connection. They can be computed from the metric

$$\Gamma^{\lambda}{}_{\mu\nu} = \frac{1}{2} g^{\lambda\sigma} \left(\partial_\mu g_{\sigma\nu} + \partial_\nu g_{\mu\sigma} - \partial_\sigma g_{\nu\mu} \right) \ , \tag{A.2}$$

and are called the Christoffel symbols.

The curvature of spacetime is encoded in a (1,3) tensor called the Riemann curvature tensor $R^{\sigma}{}_{\mu\rho\nu}$. It can be expressed in terms of the Christoffel symbols

$$R^{\sigma}{}_{\mu\rho\nu} = \partial_\rho \Gamma^{\sigma}{}_{\mu\nu} - \partial_\mu \Gamma^{\sigma}{}_{\rho\nu} + \Gamma^{\sigma}{}_{\alpha\rho} \Gamma^{\alpha}{}_{\mu\nu} - \Gamma^{\sigma}{}_{\alpha\mu} \Gamma^{\alpha}{}_{\rho\nu} \ . \tag{A.3}$$

Conceptually, the Riemann tensor expresses the change of a vector that is parallel transported around a small quadrilateral. For the Levi-Civita connection, the $(0,4)$ tensor $R_{\lambda\mu\rho\nu} \equiv g_{\lambda\sigma} R^{\sigma}{}_{\mu\rho\nu}$ can be expressed in terms of the components of the metric

$$R_{\lambda\mu\rho\nu} = \frac{1}{2} \left(\partial_\rho \partial_\mu g_{\lambda\nu} + \partial_\lambda \partial_\nu g_{\rho\mu} - \partial_\rho \partial_\lambda g_{\nu\mu} - \partial_\nu \partial_\mu g_{\rho\lambda} \right) \ . \tag{A.4}$$

The Ricci tensor is defined as the contraction of the Riemann tensor

$$R_{\mu\nu} = R^{\sigma}{}_{\mu\sigma\nu} \ . \tag{A.5}$$

For this particular connection, the Riemann tensor is symmetric. The Ricci scalar is the trace of the Ricci tensor

$$R = g^{\mu\nu} R_{\mu\nu} \ , \tag{A.6}$$

and is also called the scalar curvature. Finally, the Einstein tensor is a type $(0,2)$ tensor defined as

$$G_{\mu\nu} \equiv R_{\mu\nu} - \frac{1}{2} R g_{\mu\nu} \ , \tag{A.7}$$

and satisfies $\nabla^{\mu} G_{\mu\nu} = 0$. These are the important definitions related to the geometry of the space.

In general relativity, free particles move along null or timelike geodesics. A geodesic is a curve whose tangent vector field t^{μ} satisfies

$$t^{\sigma} \nabla_{\sigma} t^{\mu} = 0 \ , \tag{A.8}$$

which is called the geodesic equation and means that the tangent vector is parallel transported along itself.

General relativity relates the distribution of energy with the geometry of spacetime. The distribution of energy or matter is described by a symmetric $(0,2)$ tensor field $T_{\mu\nu}$ obeying $\nabla^\mu T_{\mu\nu} = 0$. $T_{\mu\nu}$ is the energy-momentum tensor and is usually defined as

$$T_{\mu\nu} = \frac{2}{\sqrt{|g|}} \frac{\delta \mathcal{S}_m}{\delta g^{\mu\nu}} \,, \tag{A.9}$$

where the action $\mathcal{S}_m$ describing matter and $g \equiv \det g_{\mu\nu}$. The Einstein equations relate the curvature of spacetime to the energy-momentum tensor of the matter and are given by

$$G_{\mu\nu} = R_{\mu\nu} - \frac{1}{2} R g_{\mu\nu} = 8\pi G T_{\mu\nu} - \Lambda g_{\mu\nu} \,, \tag{A.10}$$

where G is Newton's gravitational constant.

Finally, note that Einstein's equations can be obtained from a variational principle with the following action

$$\mathcal{S} = \frac{1}{16\pi G} \int d^4x \sqrt{|g|} \, (R - 2\Lambda) + \int d^4x \sqrt{|g|} \mathcal{L}_m \,, \tag{A.11}$$

where the first integral is the Einstein-Hilbert action with a cosmological constant and the second is the action $\mathcal{S}_m$ written in terms of the matter Lagrangian $\mathcal{L}_m$.

Appendix B

Details on the Computations of Chapter 3

In this appendix, we provide some explicit computations of the renormalized effective potential (3.20) and self-energies of the pions (3.30) and sigma fields (3.29) due to fermionic interactions at finite temperature and density.

B.1 Effective Potential

We derive the (renormalized) effective potential (3.20) at one-loop due to the interactions with the quarks at finite temperature and density. The effective potential is given by

$$V_{eff}(T,\mu_q) = -\frac{1}{\beta V}\ln \mathcal{Z}[\beta,\mu_q]\,, \tag{B.1}$$

where $\mathcal{Z}$ is the partition function. In this case, we are only interested in the contribution coming from the interactions with the fermions. Since the interaction between the quarks and the hadrons will give a higher order contribution, we are free to consider the non-interacting part of the partition function. We have

$$\begin{aligned}\mathcal{Z}_{q,0}[\beta,\mu_q] = &\int_{\psi(\beta)=-\psi(0)} \mathcal{D}\bar{\psi}\mathcal{D}\psi \\ &\exp\left\{-\int_0^\beta d\tau \int d^3x\ \bar{\psi}\left(\gamma^0\partial_\tau - i\gamma^i\partial_i - \gamma^0\mu_q + gv\right)\psi\right\}\,. \end{aligned}\tag{B.2}$$

Performing the fermionic Gaussian integral and using the $\ln\det = \mathrm{Tr}\ln$ identity gives

$$\begin{aligned}\mathcal{Z}_{q,0}[\beta,\mu_q] &= \mathcal{N}\det\left[\gamma^0\partial_\tau - i\gamma^i\partial_i - \gamma^0\mu_q + gv\right] \\ &= \mathcal{N}\exp\left\{V\sum_{n=-\infty}^{+\infty}\int\frac{d^3k}{(2\pi)^3}\mathrm{tr}\ln\left[i\gamma^0(\omega_n + i\mu_q) - \gamma^i k_i + gv\right]\right\}\ , \quad \text{(B.3)}\end{aligned}$$

where $\omega_n = (2n+1)\pi/\beta$ are the fermionic Matsubara frequencies and the remaining trace in the exponential is in Dirac space. Dirac Algebra tells us that

$$\begin{aligned}\mathrm{tr}\ln\left[\not{a} + b\right] &= \frac{1}{2}\mathrm{tr}\left[\ln\left(\not{a} + b\right) + \ln\left(-\not{a} + b\right)\right] = \frac{1}{2}\mathrm{tr}\left[\ln\left(\not{a} + b\right)\left(-\not{a} + b\right)\right] \\ &= \frac{1}{2}\ln\left(a^2 + b^2\right)\mathrm{tr}\ \mathbb{1}_{4\times4} = 2\ln\left(a^2 + b^2\right)\ . \quad \text{(B.4)}\end{aligned}$$

And, therefore, we obtain

$$V_{eff}(T,\mu_q) = -\frac{2}{\beta}\sum_{n=-\infty}^{+\infty}\int\frac{d^3k}{(2\pi)^3}\ln\left[\left(\omega_n + i\mu_q\right)^2 + \omega^2\right]\ , \quad \text{(B.5)}$$

where $\omega^2 = \vec{k}^2 + (gv)^2$. Note that

$$\begin{aligned}&\sum_{n=-\infty}^{+\infty}\ln\left[\left(\omega_n + i\mu_q\right)^2 + \omega^2\right] = \\ &\quad= \frac{1}{2}\sum_{n=-\infty}^{+\infty}\left(\ln\left[\left(\omega_n + i\mu_q\right)^2 + \omega^2\right] + \ln\left[\left(-\omega_n + i\mu_q\right)^2 + \omega^2\right]\right) \\ &\quad= \frac{1}{2}\sum_{n=-\infty}^{+\infty}\left(\ln\left[\omega_n^2 + \left(\omega + \mu_q\right)^2\right] + \ln\left[\omega_n^2 + \left(\omega - \mu_q\right)^2\right]\right)\ , \quad \text{(B.6)}\end{aligned}$$

using that the sum runs over all frequencies in the first step. A direct calculation shows the validity of the last equality.

Matsubara Sum We want to evaluate the fermionic sum

$$\sum_{n=-\infty}^{+\infty}\frac{1}{\omega_n^2 + \tilde{\omega}^2}\ , \quad \text{(B.7)}$$

where $\tilde{\omega}$ is a constant. The method consists in finding a function with poles for each of the ω_n to convert the sum into a complex integral. The function

$\tanh(\beta z/2)$ has precisely the desired characteristic, its poles being at $z = i\omega_n$. The residues are

$$\mathrm{Res}\left[\tanh\left(\frac{\beta z}{2}\right), z_0 = i\omega_n\right] = \left.\frac{\sinh\left(\frac{\beta z}{2}\right)}{\cosh'\left(\frac{\beta z}{2}\right)}\right|_{z=z_0} = \frac{2}{\beta}\,, \tag{B.8}$$

and, therefore, the sum becomes

$$\sum_{n=-\infty}^{+\infty} \frac{1}{\omega_n^2 + \tilde{\omega}^2} = -\frac{\beta}{2\pi i}\oint_C dz \frac{1}{z^2 - \tilde{\omega}^2}\frac{1}{2}\tanh\left(\frac{\beta z}{2}\right)\,, \tag{B.9}$$

where the contour is composed of small loops inclosing all singularities of $\tanh(\beta z/2)$. The singularities at $z = \pm\tilde{\omega}$ of the fraction in the integrand lie outside the region enclosed by C. Deforming the contour gives

$$\begin{aligned}
&\frac{\beta}{2\pi i}\oint_C dz \frac{1}{z^2 - \tilde{\omega}^2}\frac{1}{2}\tanh\left(\frac{\beta z}{2}\right) = \\
&\qquad = \frac{\beta}{2\pi i}\left(\int_{-i\infty+0^+}^{i\infty+0^+} dz + \int_{i\infty-0^+}^{-i\infty-0^+} dz\right)\frac{1}{z^2 - \tilde{\omega}^2}\frac{1}{2}\tanh\left(\frac{\beta z}{2}\right) \\
&\qquad = \frac{\beta}{2\pi i}\int_{-i\infty+0^+}^{i\infty+0^+} dz \frac{1}{z^2 - \tilde{\omega}^2}\tanh\left(\frac{\beta z}{2}\right) \\
&\qquad = -\frac{\beta}{2\tilde{\omega}}\tanh\left(\frac{\beta\tilde{\omega}}{2}\right)\,,
\end{aligned} \tag{B.10}$$

where we made the change of variable z into $-z$ between the first and second line. We used Cauchy's residue theorem in the last step, closing the contour in the positive half plane. We find for the sum

$$\sum_{n=-\infty}^{+\infty} \frac{1}{\omega_n^2 + \tilde{\omega}^2} = \frac{\beta}{2\tilde{\omega}}\tanh\left(\frac{\beta\tilde{\omega}}{2}\right) = \frac{\beta}{2\tilde{\omega}}\left[1 - 2n_F(\tilde{\omega})\right]\,. \tag{B.11}$$

Using this result, we compute the sums in (B.6). Note that

$$\frac{\partial}{\partial\tilde{\omega}}\sum_{n=-\infty}^{+\infty}\ln\left[\omega_n^2 + \tilde{\omega}^2\right] = 2\tilde{\omega}\sum_{n=-\infty}^{\infty}\frac{1}{\omega_n^2 + \tilde{\omega}^2} = \beta\left[1 - 2n_F(\tilde{\omega})\right]\,, \tag{B.12}$$

and, therefore,

$$\sum_{n=-\infty}^{+\infty}\ln\left(\omega_n^2 + \tilde{\omega}^2\right) = \beta\left[\tilde{\omega} + \frac{2}{\beta}\ln\left(1 + e^{-\beta\tilde{\omega}}\right)\right]\,. \tag{B.13}$$

Putting everything together, the effective potential reads

$$V_{eff}(T,\mu_q) = -2\int \frac{d^3k}{(2\pi)^3}\left[\omega + \frac{1}{\beta}\ln\left(1+e^{-\beta\omega-\beta\mu_q}\right) + \frac{1}{\beta}\ln\left(1+e^{-\beta\tilde{\omega}+\beta\mu_q}\right)\right] , \tag{B.14}$$

where $\omega = \vec{k}^2+(gv)^2$. The zero-temperature contribution of the effective potential is divergent and requires a renormalization.

Renormalization of the Effective Potential First of all, we show that the temperature-independent part of the effective potential can be written as

$$V_{eff}(T=0,\mu_q) = -2\int \frac{d^3k}{(2\pi)^3}\omega = -2\int \frac{d^4k_E}{(2\pi)^4}\ln\left[k_E^2+(gv)^2\right] , \tag{B.15}$$

where $k_E^2 = k_{E,0}^2 + \vec{k}^2$. It directly follows from the identity coming from Cauchy's residue theorem

$$\frac{1}{2} = \int \frac{dk_0}{2\pi i}\frac{\omega}{-k_0^2+\omega^2} . \tag{B.16}$$

Integrating the last equation over ω and performing the Euclidean rotation $k_0 = ik_{E,0}$ gives precisely (B.15). We now evaluate the $T=0$ contribution of the effective potential using dimensional regularization in the $\overline{\text{MS}}$-scheme. Going into arbitrary d-dimension, we have

$$\int \frac{d^4k_E}{(2\pi)^4}\ln\left[k_E^2+(gv)^2\right] \quad \rightarrow \quad \left(\mu^2\right)^{2-\frac{d}{2}}\int \frac{d^dk_E}{(2\pi)^d}\ln\left[k_E^2+(gv)^2\right] , \tag{B.17}$$

where μ is an arbitrary scale with dimension of mass that balances the change of dimension of the integral. To evaluate the integral, we first take the derivative with respect to $m_q^2 = (gv)^2$ and get

$$\left(\mu^2\right)^{2-\frac{d}{2}}\int \frac{d^dk_E}{(2\pi)^d}\frac{1}{k_E^2+(gv)^2} = \left(\mu^2\right)^{2-\frac{d}{2}}\frac{\pi^{d/2}}{(2\pi)^d}[(gv)^2]^{\frac{d}{2}-1}\Gamma\left(1-\frac{d}{2}\right) , \tag{B.18}$$

using known results for Euclidean integrals in d-dimensions [240]. The zero-temperature part of the effective potential becomes

$$V_{eff}(T=0,\mu_q) = -2\left(\mu^2\right)^{2-\frac{d}{2}}\frac{\pi^{d/2}}{(2\pi)^d}\frac{[(gv)^2]^{\frac{d}{2}}}{\frac{d}{2}}\Gamma\left(1-\frac{d}{2}\right)$$

$$= -2\frac{(gv)^4}{(4\pi)^2}\left(\frac{(gv)^2}{4\pi\mu^2}\right)^{\frac{d}{2}-2}\frac{\Gamma\left(2-\frac{d}{2}\right)}{\frac{d}{2}\left(1-\frac{d}{2}\right)}\,. \tag{B.19}$$

Setting $\epsilon = 2 - \frac{d}{2}$ and taking the limit ϵ going to zero gives

$$\begin{aligned} V_{eff}(T=0,\mu_q) =& -2\frac{(gv)^4}{(4\pi)^2}\left(\frac{(gv)^2}{4\pi\mu^2}\right)^{-\epsilon}\frac{\Gamma(\epsilon)}{(2-\epsilon)(\epsilon-1)} \\ =& \,2\frac{(gv)^4}{(4\pi)^2}\left(1-\epsilon\frac{(gv)^2}{4\pi\mu^2}+\mathcal{O}(\epsilon^2)\right)\left(\frac{1}{\epsilon}-\gamma_E+\mathcal{O}(\epsilon^2)\right) \\ & \left(1+\epsilon+\mathcal{O}(\epsilon^2)\right)\frac{1}{2}\left(1+\frac{\epsilon}{2}+\mathcal{O}(\epsilon^2)\right) \\ =& \,\frac{(gv)^4}{16\pi^2}\left[\frac{1}{\epsilon}+\gamma_E+\ln 4\pi-\ln\frac{(gv)^2}{\mu^2}+\frac{3}{2}+\mathcal{O}(\epsilon)\right]\,, \end{aligned} \tag{B.20}$$

where γ_E is the Euler-Mascheroni constant. In the $\overline{\text{MS}}$-scheme, the first three terms in the square bracket are absorbed by counterterms of the Lagrangian and the renormalized zero-temperature part of the effective potential is

$$V_{eff}^{(ren)}(T=0,\mu_q) = \frac{(gv)^4}{16\pi^2}\left[\ln\frac{\mu^2}{(gv)^2}+\frac{3}{2}\right]\,. \tag{B.21}$$

We finally write the one-loop renormalized effective potential due to fermionic interactions

$$\begin{aligned} V_{eff}^{(ren)}(T,\mu_q) =& \frac{m_q^4}{16\pi^2}N_cN_f\left[\ln\frac{\mu^2}{m_q^2}+\frac{3}{2}\right] \\ & -2\frac{N_cN_f}{\beta}\int\frac{d^3k}{(2\pi)^3}\left[\ln\left(1+e^{-\beta\omega-\beta\mu_q}\right)+\ln\left(1+e^{-\beta\tilde{\omega}+\beta\mu_q}\right)\right]\,, \end{aligned} \tag{B.22}$$

where N_c and N_f are the number of colors and flavors respectively.

B.2 Renormalized One-loop Self-Energies

We derive the renormalized one-loop self-energies of the σ and π fields at finite temperature and density. As usual, we only consider the interactions with the fermions fields. Those are given by

$$g\bar{\psi}\sigma\psi\,, \qquad\qquad ig\bar{\psi}\gamma_5\pi_i\psi\,, \tag{B.23}$$

the Yukawa interactions of the LSMq.

B.2.1 Self-Energy of the Sigma Field

The self-energy of the sigma field at one-loop is given by the following diagram

$$\Sigma_\sigma = \quad p \quad \underset{k-p}{\overset{k}{\bigcirc}} \quad p \quad = \Sigma_\sigma^{T=0} + \Sigma_\sigma^{T\neq 0} \, . \tag{B.24}$$

The Feynman rules for the Yukawa vertex allow writing the self-energy as

$$\Sigma_\sigma \left(i\omega, \vec{p}\right) = g^2 T \sum_{n=-\infty}^{+\infty} \int \frac{d^3k}{(2\pi)^3} \mathrm{tr} \left[S_\psi \left(i\omega_n + \mu_q, \vec{k} \right) S_\psi \left(i\omega_n - i\omega + \mu_q, \vec{k} - \vec{p} \right) \right] \, , \tag{B.25}$$

where the fermion-anti-fermion propagator in Euclidean space is

$$S_\psi \left(i\omega_n + \mu_q, \vec{k} \right) = \frac{m_q - \not{k}}{(\omega_n - i\mu_q)^2 + E_k^2} \, , \tag{B.26}$$

with $E_k = (\vec{k}^2 + m_q^2)^{1/2}$, $\not{k} = -\gamma_4 \omega_n + \vec{\gamma}.\vec{k}$ and $\omega_n = (2n+1)\pi/\beta$ are the fermionic Matsubara frequencies. The Feynman propagator can be expressed as

$$S_\psi \left(i\omega_n + \mu_q, \vec{k} \right) = - \int_{-\infty}^{+\infty} \frac{dk_0}{2\pi} \frac{\rho_F(k_0, \vec{k})}{i\omega_n + \mu_q - k_0} \, , \tag{B.27}$$

where ρ_F is the fermionic spectral function defined as

$$\rho_F(k_0, \vec{k}) = 2\pi \frac{(\not{p} + m_q)}{2\omega_k} \left[\delta(k_0 - \omega_k) - \delta(k_0 + \omega_k) \right] \, . \tag{B.28}$$

The self-energy reads

$$\begin{aligned} \Sigma_\sigma \left(i\omega, \vec{p}\right) = g^2 T \sum_{n=-\infty}^{+\infty} \int \frac{d^3k}{(2\pi)^3} \int_{-\infty}^{+\infty} \frac{dp_0}{2\pi} \int_{-\infty}^{+\infty} \frac{dk_0}{2\pi} \\ \cdot \frac{\mathrm{tr} \left[\rho_F(k_0, \vec{k}) \rho_F(p_0, \vec{k} - \vec{p}) \right]}{(i\omega_n + \mu_q - k_0)(i(\omega - \omega_n) - \mu_q - p_0)} \, . \end{aligned} \tag{B.29}$$

Let us compute the zero and finite-temperature contributions separately.

Zero-temperature Contribution For the $T = 0$ contribution of the self-energy $\Sigma_\sigma^{T=0}$, we use standard quantum field theories in Euclidean space in $d = 4 - 2\epsilon$ dimensions to extract the divergence. We have

$$\begin{aligned}\Sigma_\sigma^{T=0} &= g^2 \int \frac{d^d k_E}{(2\pi)^d} \mathrm{tr}\left[\frac{m_q - \not{k}}{k^2 + m_q^2} \frac{m_q - (\not{k} - \not{p})}{(k-p)^2 + m_q^2}\right] \\ &= 4g^2 \int \frac{d^d k_E}{(2\pi)^d} \frac{m_q^2 - k(k-p)}{[k^2 + m_q^2][(k-p)^2 + m_q^2]} \ , \end{aligned} \tag{B.30}$$

with the trace computed using Dirac algebra

$$\not{k}(\not{k} - \not{p}) = \gamma^\mu k_\mu \gamma^\nu (k-p)_\nu = \frac{1}{2}\{\gamma^\mu, \gamma^\nu\} k_\mu (k-p)_\nu = -k(p-k) \ , \tag{B.31}$$

$$\mathrm{tr}[(m_q - \not{k})(m_q - (\not{k} - \not{p}))] = 4(m_q^2 - k(k-p)) \ . \tag{B.32}$$

Using the known result for Euclidean integral in d-dimension space [240] and after some algebra, we find for the real-part

$$\begin{aligned}\mathrm{Re}\left[\Sigma_\sigma^{T=0}\right] = \frac{3g^2}{4\pi^2}\left[m_q^2 - \frac{1}{6}p^2\right]\frac{1}{\epsilon} + \frac{g^2}{4\pi^2}\left[5m_q^2 - p^2 - 3(m_q^2 - \frac{1}{6}p^2)\ln\frac{m_q^2}{M^2}\right] \\ + \frac{g^2}{4\pi^2}\begin{cases} \frac{1}{2}p^2 C^3 \log\left(\frac{1+C}{1-C}\right) & \text{for } p^2 > 4m_q^2 \text{ and } p^2 < 0 \\ -p^2 C^3 \arctan\frac{1}{C} & \text{for } 0 < p^2 < 4m_q^2 \end{cases} \ , \end{aligned} \tag{B.33}$$

where $C = \sqrt{\left|1 - 4m_q^2/p^2\right|}$ and M is the regularization scale. In the limit $p_0 \to 0$ and the rest frame of the particle $\vec{p} \to 0$ we find

$$\mathrm{Re}\left[\Sigma_\sigma^{T=0}\right] = \frac{N_c N_f}{4\pi^2} g^4 v^2 \left(1 + 3\ln\frac{M^2}{g^2 v^2}\right) \ , \tag{B.34}$$

for the renormalized contribution.

Finite-temperature Contribution To derive the real-part of the finite-temperature contribution, we need to evaluate the Matsubara sum. We use the known result [105]

$$T\sum_{n=-\infty}^{+\infty} \frac{1}{i\omega_n + \mu_q - k_0} \frac{1}{i(\omega - \omega_n) - \mu_q - p_0} = -\frac{1 - n_F^+(k_0) - n_F^-(p_0)}{i\omega - k_0 - p_0} \ , \tag{B.35}$$

where $n_F^\pm(\omega_k) = \frac{1}{e^{\beta(\omega_k \mp \mu_q)}+1}$. Performing the integrals over k_0 and p_0 using the different combinations of δ-functions allows extracting the real-part of the finite-

temperature contribution of the self-energy

$$\begin{aligned}\mathrm{Re}\left[\Sigma_\sigma^{T\neq 0}\right] =& 4g^2\int\frac{d^3k}{(2\pi)^3}\frac{1}{4\omega_k\omega_{p-k}}\{\\ &\left[-\omega_k\omega_{p-k}+\vec{k}\cdot(\vec{p}-\vec{k})+m_q^2\right]\frac{n_F^+(\omega_k)+n_F^-(\omega_{p-k})}{p_0-\omega_k-\omega_{p-k}}\\ &+\left[\omega_k\omega_{p-k}+\vec{k}\cdot(\vec{p}-\vec{k})+m_q^2\right]\frac{-n_F^+(\omega_k)+n_F^+(\omega_{p-k})}{p_0-\omega_k+\omega_{p-k}}\\ &+\left[\omega_k\omega_{p-k}+\vec{k}\cdot(\vec{p}-\vec{k})+m_q^2\right]\frac{-n_F^-(\omega_{p-k})+n_F^-(\omega_k)}{p_0+\omega_k-\omega_{p-k}}\\ &-\left[-\omega_k\omega_{p-k}+\vec{k}\cdot(\vec{p}-\vec{k})+m_q^2\right]\frac{n_F^-(\omega_k)+n_F^+(\omega_{p-k})}{p_0+\omega_k+\omega_{p-k}}\Bigg\}\ , \end{aligned}\tag{B.36}$$

where we have used the Cauchy principal value to extract the real-part of the function. We are interested in the self-energy in the rest frame of the particle and in the limit $p_0\to 0$. Due to the non-analyticity of the self-energy, the order in which we take the limits matter. According to the Ref. [241], the correct prescription is to take the limit $p_0\to 0$ first, which leads to

$$\begin{aligned}\mathrm{Re}\left[\Sigma_\sigma^{T\neq 0}\right] =& \frac{g^2}{\pi^2}\int_0^\infty dk\ \frac{k^2}{\omega_k}\left[n_F^+(\omega_k)+n_F^-(\omega_k)\right]\left(1-\frac{g^2v^2}{\omega_k^2}\right)\\ &-\frac{g^4v^2}{\pi^2T}\int_0^\infty dk\ \frac{k^2}{\omega_k^2}\left\{n_F^+(\omega_k)\left[1-n_F^+(\omega_k)\right]+n_F^-(\omega_k)\left[1-n_F^-(\omega_k)\right]\right\}\ .\end{aligned}\tag{B.37}$$

The presence of the last term in the previous equation depends on the order of the two limits. However, it turns out that this term does not affect our result on the stability.

B.2.2 Self-Energy of the Pion Fields

We compute the self-energy of the pion fields

$\Sigma_\pi =$ 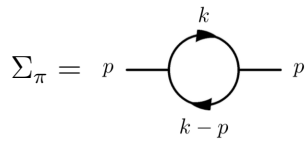

$= \Sigma_\pi^{T=0} + \Sigma_\pi^{T\neq 0}$

$$= g^2 T \sum_{n=-\infty}^{+\infty} \int \frac{d^3k}{(2\pi)^3} \mathrm{tr}\left[\gamma^5 S_\psi\left(i\omega_n + \mu_q, \vec{k}\right)\gamma^5 S_\psi\left(i\omega_n - i\omega + \mu_q, \vec{k} - \vec{p}\right)\right] . \tag{B.38}$$

The zero-temperature part $\Sigma_\pi^{T=0}$ reads

$$\begin{aligned}
\Sigma_\pi^{T=0} &= -g^2 \int \frac{d^d k_E}{(2\pi)^d} \mathrm{Tr}\left[\gamma^5 \frac{m_q - \not{k}}{k^2 + m_q^2}\gamma^5 \frac{m_q - (\not{k} - \not{p})}{(k-p)^2 + m_q^2}\right] \\
&= -4g^2 \int \frac{d^d k_E}{(2\pi)^d} \frac{m_q^2 + k(k-p)}{[k^2 + m_q^2][(k-p)^2 + m_q^2]} \\
&= \Sigma_\sigma^{T=0} - 8g^2 m_q^2 \int \frac{d^d k_E}{(2\pi)^d} \frac{1}{[k^2 + m_q^2][(k-p)^2 + m_q^2]} = \Sigma_\sigma^{T=0} - \Sigma_\pi'^{T=0} .
\end{aligned} \tag{B.39}$$

We can use the above result of $\Sigma_\sigma^{T=0}$. The only contribution left to compute is $\Sigma_\pi'^{T=0}$. We find

$$\begin{aligned}
\mathrm{Re}\left[\Sigma_\pi'^{T=0}\right] &= \frac{g^2}{2\pi^2}\left[m_q^2 \frac{1}{\epsilon} - m_q^2 \log\frac{m_q^2}{M^2} + 2m_q^2\right] \\
&\quad + \frac{g^2}{2\pi^2}\begin{cases} 2m_q^2 C \log\left(\frac{1+C}{1-C}\right) & \text{for } p^2 > 4m_q^2 \text{ and } p^2 < 0 \\ -2m_q^2 C \arctan\frac{1}{C} & \text{for } 0 < p^2 < 4m_q^2 \end{cases} .
\end{aligned} \tag{B.40}$$

Therefore, the real-part of self-energy of the pion at zero temperature reads

$$\begin{aligned}
\mathrm{Re}\left[\Sigma_\pi^{T=0}\right] &= \mathrm{Re}\left[\Sigma_\sigma^{T=0}\right] - \mathrm{Re}\left[\Sigma_\pi'^{T=0}\right] \\
&= \frac{g^2}{4\pi^2}\left[\left(m_q^2 - \frac{1}{2}p^2\right)\frac{1}{\epsilon} + m_q^2 - p^2 - (m_q^2 - \frac{1}{2}p^2)\log\frac{m_q^2}{M^2}\right] \\
&\quad + \frac{g^2}{4\pi^2}\begin{cases} (\frac{1}{2}p^2 - 6m^2) C \log\left(\frac{1+C}{1-C}\right) & \text{for } p^2 > 4m_q^2 \text{ and } p^2 < 0 \\ p^2 C \arctan\frac{1}{C} & \text{for } 0 < p^2 < 4m_q^2 \end{cases} .
\end{aligned} \tag{B.41}$$

The real-part of the finite-temperature contribution reads

$$\begin{aligned}
\mathrm{Re}\left[\Sigma_\pi^{T\neq 0}\right] = -4g^2 \int \frac{d^3k}{(2\pi)^3} \frac{1}{4\omega_k \omega_{p-k}} \{ \\
\left[\omega_k\omega_{p-k} - \vec{k}\cdot(\vec{p} - \vec{k}) + m_q^2\right] \frac{n_F^+(\omega_k) + n_F^-(\omega_{p-k})}{p_0 - \omega_k - \omega_{p-k}} \\
+ \left[-\omega_k\omega_{p-k} - \vec{k}\cdot(\vec{p} - \vec{k}) + m_q^2\right] \frac{-n_F^+(\omega_k) + n_F^+(\omega_{p-k})}{p_0 - \omega_k + \omega_{p-k}}
\end{aligned}$$

$$
\begin{aligned}
&+\left[-\omega_k\omega_{p-k}-\vec{k}\cdot(\vec{p}-\vec{k})+m_q^2\right]\frac{-n_F^-(\omega_k)+n_F^-(\omega_{p-k})}{p_0+\omega_k-\omega_{p-k}}\\
&-\left[\omega_k\omega_{p-k}-\vec{k}\cdot(\vec{p}-\vec{k})+m_q^2\right]\frac{n_F^-(\omega_k)+n_F^+(\omega_{p-k})}{p_0+\omega_k+\omega_{p-k}}\Bigg\}\\
&=\mathrm{Re}\left[\Sigma_\sigma^{T\neq0}\right]-8g^2m_q^2\int\frac{d^3k}{(2\pi)^3}\frac{1}{4\omega_k\omega_{p-k}}\{\\
&\quad\frac{n_F^+(\omega_k)+n_F^-(\omega_{p-k})}{p_0-\omega_k-\omega_{p-k}}+\frac{-n_F^+(\omega_k)+n_F^+(\omega_{p-k})}{p_0-\omega_k+\omega_{p-k}}\\
&\quad+\frac{-n_F^-(\omega_{p-k})+n_F^-(\omega_k)}{p_0+\omega_k-\omega_{p-k}}-\frac{n_F^-(\omega_k)+n_F^+(\omega_{p-k})}{p_0+\omega_k+\omega_{p-k}}\Bigg\}\\
&=\mathrm{Re}\left[\Sigma_\sigma^{T\neq0}\right]-8g^2m_q^2\int\frac{d^3k}{(2\pi)^3}\frac{1}{4\omega_k\omega_{p-k}}\left\{\frac{n_F^+(\omega_k)+n_F^-(\omega_k)}{p_0-\omega_k-\omega_{p-k}}\right.\\
&\quad\left.-\frac{n_F^+(\omega_k)+n_F^-(\omega_k)}{p_0-\omega_k+\omega_{p-k}}+\frac{n_F^-(\omega_k)+n_F^-(\omega_k)}{p_0+\omega_k-\omega_{p-k}}-\frac{n_F^+(\omega_k)+n_F^-(\omega_k)}{p_0+\omega_k+\omega_{p-k}}\right\}.
\end{aligned}
\tag{B.42}
$$

Putting everything together, the renormalized self-energy of the pion field in the limit $p_0\to0$ and the rest frame of the particle $\vec{p}\to0$ is

$$
\Pi_\pi^{(\mathrm{ren})}=\frac{N_cN_f}{4\pi^2}\left\{g^4v^2\left(1+\ln\frac{M^2}{g^2v^2}\right)+4g^2\int_0^\infty dk\frac{k^2}{\omega_k}\left[n_F^+(\omega_k)+n_F^-(\omega_k)\right]\right\},
\tag{B.43}
$$

where the limit over p_0 was taken first.

Appendix C

Perturbation Theory from Inflation

In this appendix, we provide more details on the theory of perturbations in the simplest realization of inflation. Our aim is to illustrate the most important steps leading to the derivation of the scalar and tensor power spectra. For a complete treatment, we invite the reader to consider the references [151–154, 242]. We are working in conformal time where the conformal Hubble parameter is defined as $\mathcal{H} \equiv \frac{a'}{a} = aH$ and, in a de Sitter geometry, the scale factor becomes $a(\tau) = -\frac{1}{H\tau}$.

The first step is the expansion of the metric and the scalar field around the background solutions. The perturbation in the scalar field is defined from

$$\phi(\tau, \vec{x}) = \phi_c(\tau) + \delta\phi(\tau, \vec{x}) \ , \tag{C.1}$$

where ϕ_c is the classical and homogeneous contribution responsible for the accelerated expansion during inflation. The expansion of the metric around the FLRW solution can be written in the most general form as

$$\begin{aligned} ds^2 = a^2(\tau) \big\{ &- [1 + 2A(\tau, \vec{x})]\, d\tau^2 + \\ &2\left[\partial_i B(\tau, \vec{x}) + B_i(\tau, \vec{x})\right] d\tau dx^i + \left[\delta_{ij} + h_{ij}(\tau, \vec{x})\right] dx^i dx^j \big\} \ , \end{aligned} \tag{C.2}$$

where B_i is a transverse vector. The perturbation of the spatial part of the metric can be decomposed as

$$h_{ij}(\tau, \vec{x}) = -2C(\tau, \vec{x})\delta_{ij} + 2\partial_i\partial_j E(\tau, \vec{x}) + 2\partial_{(i}E_{j)}(\tau, \vec{x}) + E_{ij}(\tau, \vec{x}) \ , \tag{C.3}$$

where E_i is a transverse vector and E_{ij} is a transverse and traceless tensor.

The perturbation of the scalar curvature on comoving hypersurfaces reads

$$\mathcal{R} = -C + \frac{\mathcal{H}}{\phi'}\delta\phi \,, \tag{C.4}$$

where the derivative with respect to the conformal time is denoted with a prime.

Scalar Perturbations Using the gauge freedom in the choice of the coordinates and the equation of motion for the scalar field, it has been shown in [153] that a single variable is sufficient to describe the scalar perturbation

$$v = a\left(\delta\phi - \frac{\phi'}{\mathcal{H}}C\right) \,. \tag{C.5}$$

This variable v is usually referred as the Mukhanov-Sasaki variable and is a linear combination of the scalar perturbations of the scalar field and the metric.

In order to study the evolution of the scalar perturbation, we need the equation of motion of v. Starting with the action during the period of inflation

$$\mathcal{S}_\phi = \int \mathrm{d}^4x\sqrt{|g|}\left(\frac{m_P^2}{2}R - \frac{1}{2}g^{\mu\nu}\partial_\mu\phi\partial_\mu\phi - V(\phi)\right) \,, \tag{C.6}$$

and with the two ansätze for the scalar field and the metric, we obtain the action for the Mukhanov-Sasaki variable

$$\mathcal{S}_v = \frac{1}{2}\int d\tau d^3\vec{x}\left[v'^2 - (\partial_i v)^2 + \frac{z''}{z}v^2\right] \,, \tag{C.7}$$

where $z \equiv a\frac{\phi'}{\mathcal{H}}$. We observe that v has an action corresponding to a scalar field with a time-dependent mass in a spacetime with a Minkowski metric. Using the definitions of z and v, one can show that

$$v = -z\mathcal{R} \,, \tag{C.8}$$

which implies that the comoving curvature perturbation is simply proportional to the Mukhanov-Sasaki variable.

We are considering quantum perturbations and therefore, before solving the equation of motion, we need to quantize the scalar field v

$$\hat{v}(\tau,\vec{x}) = \frac{1}{(2\pi)^{3/2}}\int d^3\vec{k}\left[\hat{a}_{\vec{k}}v_k(\tau)e^{i\vec{k}\cdot\vec{x}} + \hat{a}^\dagger_{\vec{k}}v_k^*(\tau)e^{-i\vec{k}\cdot\vec{x}}\right] \,, \tag{C.9}$$

where $\hat{v}$ denotes that v is now a quantum field. The annihilation and creation operators $\hat{a}_{\vec{k}}$ and $\hat{a}^{\dagger}_{\vec{k}}$ are defined by their commutation relations

$$\left[\hat{a}_{\vec{k}}, \hat{a}_{\vec{k'}}\right] = \left[\hat{a}^{\dagger}_{\vec{k}}, \hat{a}^{\dagger}_{\vec{k'}}\right] = 0 \ , \qquad \left[\hat{a}_{\vec{k}}, \hat{a}^{\dagger}_{\vec{k'}}\right] = \delta^{(3)}(\vec{k} - \vec{k'}) \ . \tag{C.10}$$

Working with the canonical quantization, the following commutation relations are valid

$$[\hat{v}(\tau, \vec{x}), \hat{v}(\tau, \vec{x'})] = [\hat{\pi}_v(\tau, \vec{x}), \hat{\pi}_v(\tau, \vec{x'})] = 0 \ , \tag{C.11}$$

$$[\hat{v}(\tau, \vec{x}), \hat{\pi}_v(\tau, \vec{x'})] = i\delta^{(3)}(\vec{x} - \vec{x'}) \ , \tag{C.12}$$

where π_v is defined as $\pi_v \equiv \frac{\delta S}{\delta v'}$, the conjugate momentum of v. In our case π_v is simply equal to v'. Inserting equation (C.9) in the commutation relation (C.12) gives

$$v_k v_k'^{*} - v_k^{*} v_k' = i \ , \tag{C.13}$$

which corresponds to the Wronskian normalization condition for the solutions v_k.

After a Fourier transformation, we find the classical equation of motion for the amplitude of the modes $v_k(\tau)$

$$v_k'' + \left(k^2 - \frac{z''}{z}\right) v_k = 0 \ . \tag{C.14}$$

Recall that the field is expected to be in the slow-roll regime. The evolution of H and ϕ' can safely be neglected with respect to the evolution of the scale factor and the ratio $\frac{z''}{z}$ becomes $\frac{a''}{a}$. With this simplification, we write a solution for the modes

$$v_k(\tau) = \frac{1}{\sqrt{2k}} e^{-ik\tau} \left(1 - \frac{i}{k\tau}\right) + \frac{1}{\sqrt{2k}} e^{ik\tau} \left(1 + \frac{i}{k\tau}\right) \ , \tag{C.15}$$

where the Wronskian normalization and the relation $\frac{a''}{a} = \frac{2}{\tau^2}$ have been used.

Going sufficiently early in time, any mode k would have its wavelength deep inside the Hubble radius, and, therefore, much smaller than the horizon

$$\frac{k}{aH} \sim |k\tau| \gg 1 \ . \tag{C.16}$$

The equation of motion for the modes (C.14) can be approximated in this limit

as

$$v_k'' + k^2 v_k = 0 \ , \tag{C.17}$$

where the modes behave as in a Minkoswki spacetime since the effect of the curvature can be safely neglected. In order to pick a physical solution, we assume that it reproduces the Minkowski vacuum $v_k \sim e^{ik\tau}$ in the limit $k|\tau| \gg 1$ and, therefore,

$$v_k(\tau) = \frac{1}{\sqrt{2k}} e^{ik\tau} \left(1 - \frac{i}{k\tau}\right) \ . \tag{C.18}$$

In quantum field theories in curved spacetime, this is usually referred as the Bunch-Davies vacuum.

The statistical properties of the fluctuations are encoded in the n-point correlation functions of the modes. In particular, from the two-point function, one defines the power spectrum

$$\langle 0|\hat{v}(\tau, x_1)\hat{v}(\tau, x_2)|0\rangle = \int d^3k e^{i\vec{k}(\vec{x}_1 - \vec{x}_2)} \frac{\Delta_v^2(\tau, k)}{4\pi k^3} \ . \tag{C.19}$$

Using the equation (C.9), we find for the spectrum

$$\Delta_v^2(\tau, k) = \frac{k^3}{2\pi^2} |v_k(\tau)|^2 \ . \tag{C.20}$$

Using that $v = -z\mathcal{R}$, we obtain the power spectrum Δ_s^2 corresponding to the comoving curvature perturbation

$$\Delta_s^2(\tau, k) = \frac{k^3}{2\pi^2} \frac{|v_k(\tau)|^2}{z^2} \ . \tag{C.21}$$

Recall that we evaluate the spectrum at the horizon crossing. In the super-horizon limit, $k \ll (aH)$, we can solve the equation of motion for the mode to find

$$v_k(\tau) \simeq -\frac{1}{\sqrt{2k}} \frac{i}{k\tau} \simeq \frac{iaH}{\sqrt{2k^3}} \ . \tag{C.22}$$

This allows writing

$$\Delta_s^2(\tau, k) = \frac{1}{4\pi^2} \frac{H^4}{\dot{\phi}^2} \ , \tag{C.23}$$

which is the spectrum of scalar cosmological perturbations generated from

vacuum fluctuations in the slow-roll realization of inflation.

Tensor Perturbations The method to obtain the tensor perturbation goes along similar lines. We start with the action for tensor linear perturbations

$$\mathcal{S} = \frac{m_P^2}{8} \int d\tau d^3\vec{x}\; a^2(\tau) \left[(E_{ij}^2 - (\partial_l E_{ij})^2 \right] \;, \tag{C.24}$$

where the reduced Planck mass has been written explicitly. Then, we use the fact that the tensor perturbation corresponds to GW and can be decomposed in their different polarizations

$$E_{ij} = \int \frac{d^3\vec{k}}{(2\pi)^{3/2}} \sum_{\lambda=1}^{2} \psi_{\vec{k},\lambda}(\tau) e_{ij}(\vec{k},\lambda) e^{i\vec{k}\cdot\vec{x}} \;, \tag{C.25}$$

with $e_{ij}(\vec{k},\lambda)$ being the polarization tensors. Inserting in the action gives

$$\mathcal{S} = \frac{m_p^2}{8} \sum_{\lambda=1}^{2} \int d\tau d^3\vec{k} a^2(\tau) \left[|\psi'_{\vec{k},\lambda}|^2 - \left(k^2 - \frac{a''}{a} \right) |\psi_{\vec{k},\lambda}|^2 \right] \tag{C.26}$$

$$= \frac{m_p^2}{2} \sum_{\lambda=1}^{2} \int d\tau d^3\vec{k} \left[|u'_{\vec{k},\lambda}|^2 - \left(k^2 - \frac{a''}{a} \right) |u_{\vec{k},\lambda}|^2 \right] \;, \tag{C.27}$$

where $u_{\vec{k},\lambda}$ has been defined as $\frac{m_P}{2} a(\tau) \psi_{\vec{k},\lambda}$. Following similar steps as the scalar case, the power spectrum for $u_{\vec{k},\lambda}$ is found to be

$$\Delta^2_{u_{\vec{k},\lambda}}(\tau,k) = \frac{k^3}{2\pi^2} |u_{\vec{k},\lambda}(\tau)|^2 \;, \tag{C.28}$$

solving for the modes in the super-horizon limit, $k \ll (aH)$, we find $u_{\vec{k},\lambda} \simeq \frac{iaH}{\sqrt{2k^3}}$ and, therefore,

$$\Delta^2_{u_{\vec{k},\lambda}}(\tau,k) = \left(\frac{H}{2\pi} \right)^2 \;. \tag{C.29}$$

Summing over the polarizations and using the relation $u_\lambda(\tau) = \frac{m_P}{2} E_\lambda(\tau)$, we obtain

$$\Delta^2_t(\tau,k) = \frac{8}{m_P^2} \left(\frac{H}{2\pi} \right)^2 \;, \tag{C.30}$$

which is the spectrum of tensor cosmological perturbations generated from vacuum fluctuations in the slow-roll realization of inflation.

Appendix D

Details on the Computations of Chapter 5

In this appendix, we provide greater details on the computations performed in the derivation of the escape rate. We start with the explicit derivation of the Fokker-Planck equation for the scalar field.

D.1 Derivation of the Fokker-Planck Equation

We generalize the method presented in [206] to derive the Fokker-Planck equation for a field. We consider a scalar field $\phi_i(t)$ in a potential $V(\phi)$. The Langevin equation for the field and its conjugate momentum $\pi_i(t)$ read

$$\begin{aligned} \partial_t \phi_i(t) &= \pi_i(t) \ , \\ \partial_t \pi_i(t) &= -\eta \pi_i(t) + \nabla^2_{ij} \phi_j(t) - V'(\phi_i) + \xi_i(t) \ , \end{aligned} \tag{D.1}$$

where we wrote the Laplacian as ∇^2_{ij} to indicate that it is a non-diagonal matrix actually given by

$$\nabla^2 \phi_{xyz} = \frac{1}{a^2} \left[\phi_{x+1,y,z} + \phi_{x-1,y,z} + \phi_{x,y+1,z} + \phi_{x,y-1,z} + \phi_{x,y,z+1} + \phi_{x,y,z-1} - 6\phi_{x,y,z} \right] \ , \tag{D.2}$$

where each direction of space has been explicitly labelled.

The white noise, being Gaussian distributed, leads to a probability distribution $P(\phi, \pi, t \mid \phi_0, \pi_0, t_0)$ corresponding to the probability to find the field configurations ϕ and π at time t knowing the initial configurations at t_0. Formally, P is defined as

$$P(\phi, \pi, t \mid \phi_0, \pi_0, t_0) = \left\langle \prod_{i=1}^{N^3} \delta[\hat{\pi}_i(t) - \pi_i] \cdot \delta[\hat{\phi}_i(t) - \phi_i] \right\rangle_\xi , \tag{D.3}$$

where $\hat{\phi}_i(t)$ and $\hat{\pi}_i(t)$ are solutions of the Langevin equation (D.1) and ϕ_i and π_i are the arguments of the probability distribution P. The stochastic average of an operator $\mathcal{O}(\hat{\phi}, \hat{\pi})$ is defined as

$$\left\langle \mathcal{O}(\hat{\phi}, \hat{\pi}) \right\rangle_\xi = \int \prod_{i=1}^{N^3} d[\xi(t)]_i \mathcal{O}(\hat{\phi}, \hat{\pi}) \exp\left\{ -\frac{a^3}{2\Omega} \sum_{j=1}^{N^3} \int dt' \xi_j^2(t') \right\} . \tag{D.4}$$

The integration measure is normalized to give $\langle 1 \rangle_\xi = 1$

$$\begin{aligned} \langle 1 \rangle_\xi &= \int \prod_{i=1}^{N^3} d[\xi(t)]_i \exp\left\{ -\frac{a^3}{2\Omega} \sum_{j=1}^{N^3} \int dt' \xi_j^2(t') \right\} \\ &= \prod_{i=1}^{N^3} \prod_{k=1}^{M} \int d[\xi]_{i,k} \exp\left\{ -\frac{a^3 \epsilon}{2\Omega} \xi_{i,k}^2 \right\} = \prod_{i=1}^{N^3} \prod_{k=1}^{M} N_{i,k} \sqrt{\frac{2\pi\Omega}{a^3\epsilon}} = 1 , \end{aligned} \tag{D.5}$$

where we have discretized time $t_f - t_0 = \epsilon M$. We find for the measure of integration

$$\prod_{i=1}^{N^3} d[\xi(t)]_i = \prod_{i=1}^{N^3} \prod_{k=1}^{M} \sqrt{\frac{a^3\epsilon}{2\pi\Omega}} d[\xi]_{i,k} . \tag{D.6}$$

In discrete space, the Gaussian white noise satisfies

$$\langle \xi_i(t) \rangle = 0 , \qquad \langle \xi_i(t) \xi_j(t') \rangle = \Omega \frac{\delta_{ij}}{a^3} \delta(t - t') , \tag{D.7}$$

which is easy to show using (D.4).

Using a bracket notation, we have

$$\langle \phi, \pi \mid \phi_0, \pi_0 \rangle = \prod_{i=1}^{N^3} \delta(\phi_i - \phi_{i,0}) \delta(\pi_i - \pi_{i,0}) , \tag{D.8}$$

and, therefore,

$$P(\phi,\pi,t \mid \phi_0,\pi_0,t_0) = \langle \phi,\pi \mid \hat{P}(t,t_0) \mid \phi_0,\pi_0\rangle$$
$$= \langle \phi,\pi \mid e^{-(t-t_0)\hat{\mathcal{L}}_{FP}} \mid \phi_0,\pi_0\rangle \ , \tag{D.9}$$

where $\hat{\mathcal{L}}_{FP}$ is the Fokker-Planck operator. Note that we used the Markov property and invariance under time translation. The Fokker-Planck equation follows immediately

$$\partial_t \hat{P} = -\hat{\mathcal{L}}_{FP}\hat{P} \ , \tag{D.10}$$

and we are left with the computation of the Fokker-Planck operator. This is achieved by taking the Fourier transform of P with respect to ϕ and π at fixed time t

$$\begin{aligned}\tilde{P}(\tilde{\phi},\tilde{\pi},t \mid \phi_0,\pi_0,t_0) &\equiv \int \prod_{i=1}^{N^3} d\phi_i d\pi_i e^{-ia^3\sum_{i=1}^{N^3}\left(\tilde{\pi}_i\pi_i+\tilde{\phi}_i\phi_i\right)} P(\phi,\pi,t \mid \phi_0,\pi_0,t_0) \\ &= \int \prod_{i=1}^{N^3} d\phi_i d\pi_i e^{-ia^3\sum_{i=1}^{N^3}\left(\tilde{\pi}_i\pi_i+\tilde{\phi}_i\phi_i\right)} \\ &\quad \cdot \left\langle \prod_{i=1}^{N^3} \delta[\hat{\pi}_i(t)-\pi_i]\cdot\delta[\hat{\phi}_i(t)-\phi_i] \right\rangle_\xi \\ &= \left\langle \exp\left\{ -ia^3 \sum_{i=1}^{N^3} \left[\tilde{\pi}_i\hat{\pi}_i(t)+\tilde{\phi}_i\hat{\phi}_i(t)\right]\right\}\right\rangle_\xi \ . \end{aligned} \tag{D.11}$$

Recall that $\hat{\phi}(t)$ and $\hat{\pi}(t)$ are solutions of the Langevin equation. For an infinitesimal time interval $\epsilon = t - t_0$, we have

$$\hat{\phi}_i(t+\epsilon) = \phi_{i,0}(t) + \epsilon\pi_{i,0}(t) \ , \tag{D.12}$$

$$\hat{\pi}_i(t+\epsilon) = \pi_{i,0}(t) + \epsilon\left[-\eta\pi_{i,0}(t) + \nabla^2_{ij}\phi_{j,0}(t) - V'(\phi_{i,0})\right] + \int_t^{t+\epsilon} d\tau\ \xi_i(\tau) \ . \tag{D.13}$$

Inserting in (D.11) gives

$$\tilde{P}(\tilde{\phi},\tilde{\pi},t+\epsilon \mid \phi_0,\pi_0,t) =$$
$$\exp\left\{ -ia^3 \sum_{i=1}^{N^3} \left[\tilde{\pi}_i\left(\pi_{i,0}+\epsilon(-\eta\pi_{i,0}+\nabla^2_{ij}\phi_{j,0}-V'(\phi_{i,0}))\right) + \tilde{\phi}_i\left(\phi_{i,0}+\epsilon\pi_{i,0}\right)\right]\right\}$$

$$\cdot \left\langle \exp\left\{ -ia^3 \sum_{i=1}^{N^3} \tilde{\pi}_i \int_t^{t+\epsilon} d\tau \; \xi_i(\tau) \right\} \right\rangle_\xi \; , \tag{D.14}$$

where we have factorized out the terms that do not depend on ξ. We then compute the stochastic average

$$\begin{aligned}
&\left\langle \exp\left\{ -ia^3 \sum_{i=1}^{N^3} \tilde{\pi}_i \int_t^{t+\epsilon} d\tau \; \xi_i(\tau) \right\} \right\rangle_\xi \\
&= \int d[\xi] \exp\left\{ a^3 \sum_{i=1}^{N^3} \left[-\frac{1}{2\Omega} \int_{-\infty}^{+\infty} dt' \xi_i^2(t') - i\tilde{\pi}_i \int_t^{t+\epsilon} d\tau \; \xi_i(\tau) \right] \right\} \\
&= \int d[\xi] \exp\left\{ a^3 \sum_{i=1}^{N^3} \left[-\frac{1}{2\Omega} \int_{t}^{t+\epsilon} dt' \xi_i^2(t') - i\tilde{\pi}_i \int_t^{t+\epsilon} d\tau \; \xi_i(\tau) \right] \right\} \\
&= \exp\left\{ -\frac{\Omega}{2} a^3 \epsilon \sum_{i=1}^{N^3} \tilde{\pi}_i^2 \right\} \; ,
\end{aligned} \tag{D.15}$$

using that for $t' \notin]t, t+\epsilon[$, the integral is normalized to unity. So, we find for the Fourier transform $\tilde{P}$ of the probability distribution

$$\begin{aligned}
\tilde{P}(\tilde{\phi}, \tilde{\pi}, t+\epsilon \mid \phi_0, \pi_0, t) = \exp\Bigg\{ -a^3 \sum_{i=1}^{N^3} \Big[i\tilde{\pi}_i \left[\pi_{i,0} + \epsilon \left(-\eta \pi_{i,0} + \nabla_{ij}^2 \phi_{j,0} - V'(\phi_{i,0}) \right) \right] \\
+ \frac{\epsilon\Omega}{2} \tilde{\pi}_i^2 + i\tilde{\phi}_i \left(\phi_{i,0} + \epsilon \pi_{i,0} \right) \Big] \Bigg\} \; .
\end{aligned} \tag{D.16}$$

On the other hand, from (D.9), we have

$$\begin{aligned}
P(\phi, \pi, t+\epsilon \mid \phi_0, \pi_0, t_0) &= \langle \phi, \pi \mid e^{-\epsilon \hat{\mathcal{L}}_{FP}} \mid \phi_0, \pi_0 \rangle \\
&= \langle \phi, \pi \mid 1 - \epsilon \hat{\mathcal{L}}_{FP} + \mathcal{O}(\epsilon^2) \mid \phi_0, \pi_0 \rangle \\
&= \prod_{i=1}^{N^3} \delta(\phi_i - \phi_{i,0}) \delta(\pi_i - \pi_{i,0}) - \epsilon \hat{\mathcal{L}}_{FP}(\phi, \pi \mid \phi_0, \pi_0) + \mathcal{O}(\epsilon^2) \; .
\end{aligned} \tag{D.17}$$

Taking the Fourier transform, we obtain

$$\tilde{P}(\tilde{\phi}, \tilde{\pi}, t+\epsilon \mid \phi_0, \pi_0, t) = e^{-ia^3 \sum_{i=1}^{N^3} \left(\tilde{\pi}_i \pi_{i,0} + \tilde{\phi}_i \phi_{i,0} \right)} - \epsilon \tilde{\hat{\mathcal{L}}}_{FP}(\tilde{\phi}, \tilde{\pi} \mid \phi_0, \pi_0) + \mathcal{O}(\epsilon^2) \; . \tag{D.18}$$

Comparing with (D.16), we find the Fourier transform of the Fokker-Planck

operator

$$\tilde{\hat{\mathcal{L}}}_{FP}(\tilde{\phi},\tilde{\pi}\mid\phi_0,\pi_0)=$$
$$e^{-ia^3\sum_{i=1}^{N^3}\left(\tilde{\pi}_i\pi_{i,0}+\tilde{\phi}_i\phi_{i,0}\right)}a^3\sum_{i=1}^{N^3}\left\{i\tilde{\pi}_i\left[-\eta\pi_{i,0}+\nabla^2_{ij}\phi_{j,0}-V'(\phi_{i,0})\right]+\frac{\Omega}{2}\tilde{\pi}_i^2+i\tilde{\phi}_i\pi_{i,0}\right\}\ . \tag{D.19}$$

We take the inverse Fourier transform to find the Fokker-Planck operator

$$\begin{aligned}
\hat{\mathcal{L}}_{FP}(\phi,\pi\mid\phi_0,\pi_0)&=\int\prod_{i=1}^{N^3}\frac{d\phi_i}{2\pi}\frac{d\pi_i}{2\pi}e^{ia^3\sum_{i=1}^{N^3}\left(\tilde{\pi}_i\pi_i+\tilde{\phi}_i\phi_i\right)}\tilde{\hat{L}}_{FP}(\tilde{\phi},\tilde{\pi}\mid\phi_0,\pi_0)\\
&=\int\prod_{i=1}^{N^3}\frac{d\phi_i}{2\pi}\frac{d\pi_i}{2\pi}e^{ia^3\sum_{i=1}^{N^3}\left(\tilde{\pi}_i(\pi_i-\pi_{i,0})+\tilde{\phi}_i(\phi_i-\phi_{i,0})\right)}\\
&\quad\cdot a^3\sum_{i=1}^{N^3}\left\{i\tilde{\pi}_i\left[-\eta\pi_{i,0}+\nabla^2_{ij}\phi_{i,0}-V'(\phi_{i,0})\right]+\frac{\Omega}{2}\tilde{\pi}_i^2+i\tilde{\phi}_i\pi_{i,0}\right\}\\
&=a^3\sum_{i=1}^{N^3}\left\{\frac{\partial}{a^3\partial\pi_i}\left[-\eta\pi_{i,0}+\nabla^2_{ij}\phi_{i,0}-V'(\phi_{i,0})\right]-\frac{\Omega}{2}\frac{\partial^2}{a^6\partial\pi_i^2}+\frac{\partial}{a^3\partial\phi_i}\pi_{i,0}\right\}\\
&\quad\cdot\int\prod_{i=1}^{N^3}\frac{d\phi_i}{2\pi}\frac{d\pi_i}{2\pi}e^{ia^3\sum_{i=1}^{N^3}\left(\tilde{\pi}_i(\pi_i-\pi_{i,0})+\tilde{\phi}_i(\phi_i-\phi_{i,0})\right)}\\
&=a^3\sum_{i=1}^{N^3}\left\{\frac{\partial}{a^3\partial\pi_i}\left[-\eta\pi_{i,0}+\nabla^2_{ij}\phi_{i,0}-V'(\phi_{i,0})\right]-\frac{\Omega}{2}\frac{\partial^2}{a^6\partial\pi_i^2}+\frac{\partial}{a^3\partial\phi_i}\pi_{i,0}\right\}\\
&\quad\cdot\prod_{i=1}^{N^3}\delta(\phi_i-\phi_{i,0})\delta(\pi_i-\pi_{i,0})\\
&=a^3\sum_{i=1}^{N^3}\left\{\frac{\partial}{a^3\partial\pi_i}\left[-\eta\pi_{i,0}+\nabla^2_{ij}\phi_{i,0}-V'(\phi_{i,0})\right]-\frac{\Omega}{2}\frac{\partial^2}{a^6\partial\pi_i^2}+\frac{\partial}{a^3\partial\phi_i}\pi_{i,0}\right\}\\
&\quad\cdot\langle\phi,\pi\mid\phi_0,\pi_0\rangle\\
&=\langle\phi,\pi\mid a^3\sum_{i=1}^{N^3}\left\{\frac{\partial}{a^3\partial\hat{\pi}_i}\left[-\eta\hat{\pi}_i+\nabla^2_{ij}\hat{\phi}_i-V'(\hat{\phi}_i)\right]\right.\\
&\quad\left.-\frac{\Omega}{2}\frac{\partial^2}{a^6\partial\hat{\pi}_i^2}+\frac{\partial}{a^3\partial\hat{\phi}_i}\hat{\pi}_i\right\}\mid\phi_0,\pi_0\rangle\ .
\end{aligned}\tag{D.20}$$

Now, since $\hat{\mathcal{L}}_{FP}(\phi,\pi\mid\phi_0,\pi_0)$ is defined as

$$\hat{\mathcal{L}}_{FP}(\phi,\pi\mid\phi_0,\pi_0)=\langle\phi,\pi\mid\hat{\mathcal{L}}_{FP}\mid\phi_0,\pi_0\rangle\ , \tag{D.21}$$

we obtain

$$\hat{\mathcal{L}}_{FP}(\phi,\pi \mid \phi_0,\pi_0) = \\ a^3\sum_{i=1}^{N^3}\left\{\frac{\partial}{a^3\partial\pi_i}\left[-\eta\pi_i+\nabla^2_{ij}\phi_i-V'(\phi_i)\right]-\frac{\Omega}{2}\frac{\partial^2}{a^6\partial\pi_i^2}+\frac{\partial}{a^3\partial\phi_i}\pi_i\right\}\,, \quad \text{(D.22)}$$

and the Fokker-Planck equation reads

$$\frac{\partial}{\partial t}P(\phi,\pi,t \mid \phi_0,\pi_0,t_0) = -\mathcal{L}_{FP}P(\phi,\pi,t \mid \phi_0,\pi_0,t_0)\,, \quad \text{(D.23)}$$

which completes the derivation.

Probability Density Current Conservation of probability implies that the Fokker-Planck equation can be written in term of a probability density current

$$\partial_t P(\phi,\pi,t) = -a^3\sum_{i=1}^{N^3}\frac{\partial}{a^3\partial\phi_i}J_i - a^3\sum_{i=1}^{N^3}\frac{\partial}{a^3\partial\pi_i}\bar{J}_i\,, \quad \text{(D.24)}$$

where and J_i and $\bar{J}_i$ are defined as

$$J_i = -\left\{-\pi_i - k_BT\frac{\partial}{a^3\partial\pi_i}\right\}P(\phi,\pi,t \mid \phi_0,\pi_0,t)\,, \quad \text{(D.25)}$$

$$\bar{J}_i = -\left\{\left[\eta\pi_i-\nabla^2_{ij}\phi_j+V'(\phi_i)\right]+k_BT\frac{\partial}{a^3\partial\phi_i}+\frac{\Omega}{2}\frac{\partial}{a^3\partial\pi_i}\right\}P(\phi,\pi,t \mid \phi_0,\pi_0,t)\,, \quad \text{(D.26)}$$

for $i \in [1, N^3]$. Computing explicitly the RHS of (D.24), we obtain

$$-a^3\sum_{i=1}^{N^3}\frac{\partial}{a^3\partial\phi_i}J_i - a^3\sum_{i=1}^{N^3}\frac{\partial}{a^3\partial\pi_i}\bar{J}_i = a^3\sum_{i=1}^{N^3}\left\{-\pi_i\frac{\partial}{a^3\partial\phi_i}-k_BT\frac{\partial}{a^3\partial\phi_i}\frac{\partial}{a^3\partial\pi_i}+\right. \\ \left.+\frac{\partial}{a^3\partial\pi_i}\left[-\nabla^2\phi_i+V'(\phi_i)+\eta\pi_i\right]+k_BT\frac{\partial}{a^3\partial\phi_i}\frac{\partial}{a^3\partial\pi_i}+\frac{\Omega}{2}\frac{\partial^2}{a^3\partial\pi_i^2}\right\}P(\phi,\pi,t) \\ = a^3\sum_{i=1}^{N^3}\left\{-\pi_i\frac{\partial}{a^3\partial\phi_i}+\frac{\partial}{a^3\partial\pi_i}\left[\eta\pi_i-\nabla^2\phi_i+V'(\phi_i)\right]+\frac{\Omega}{2}\frac{\partial^2}{a^3\partial\pi_i^2}\right\}P(\phi,\pi,t)\,, \quad \text{(D.27)}$$

which is precisely the RHS of the Fokker-Planck equation. In the vector-matrix notation, the probability current is expressed as

$$\begin{pmatrix} J \\ \bar{J} \end{pmatrix} = -M \cdot \begin{pmatrix} \frac{\partial E}{a^3 \partial \phi} + k_B T \frac{\partial}{a^3 \partial \phi} \\ \frac{\partial E}{a^3 \partial \pi} + k_B T \frac{\partial}{a^3 \partial \pi} \end{pmatrix} P(\phi, \pi, t \mid \phi_0, \pi_0, t) \,, \tag{D.28}$$

which can be shown explicitly

$$\begin{aligned} \begin{pmatrix} J \\ \bar{J} \end{pmatrix} &= -\frac{1}{a^3} \begin{pmatrix} 0 & -\mathbb{1} \\ \mathbb{1} & \eta \mathbb{1} \end{pmatrix} \cdot \begin{pmatrix} \frac{\partial E}{a^3 \partial \phi} + k_B T \frac{\partial}{a^3 \partial \phi} \\ \frac{\partial E}{a^3 \partial \pi} + k_B T \frac{\partial}{a^3 \partial \pi} \end{pmatrix} P(\phi, \pi, t) \\ &= - \begin{pmatrix} -\pi_i - k_B T \frac{\partial}{a^3 \partial \pi_i} \\ [-\nabla^2 \phi_i + V'(\phi_i)] + k_B T \frac{\partial}{a^3 \partial \phi_i} + \eta \pi_i + \frac{\Omega}{2} \frac{\partial}{a^3 \partial \pi_i} \end{pmatrix} P(\phi, \pi, t) \,. \end{aligned} \tag{D.29}$$

D.2 Flux-over-Population Method for a Scalar Field

In this section, we provide some explicit computations to complete the derivation of the escape rate for the scalar field presented in Sec. 5.3.3.

We first derive Eq. (5.100), the equation for $\zeta(\phi, \pi)$. Inserting the ansatz $P = \zeta P_0$ in the Fokker-Planck equation, we have

$$a^3 \sum_{i=1}^{N^3} \left\{ -\pi_i \frac{\partial}{a^3 \partial \phi_i} + \frac{\partial}{a^3 \partial \pi_i} \left[\eta \pi_i + \frac{\partial E}{a^3 \partial \phi_i} \right] + \frac{\Omega}{2} \frac{\partial^2}{a^6 \partial \pi_i^2} \right\} \zeta(\phi, \pi) P_0(\phi, \pi) = 0 \,. \tag{D.30}$$

Computing each contribution explicitly gives

$$\begin{aligned} -\pi_i \frac{\partial}{a^3 \partial \phi_i} \zeta P_0 &= -\pi_i \frac{\partial \zeta}{a^3 \partial \phi_i} P_0 + \pi_i \beta \zeta \frac{\partial E}{a^3 \partial \phi_i} P_0 \,, \\ \frac{\partial}{a^3 \partial \pi_i} \left[\eta \pi_i + \frac{\partial E}{a^3 \partial \phi_i} \right] \zeta P_0 &= \eta \pi_i \frac{\partial \zeta}{a^3 \partial \pi_i} P_0 + \eta \zeta \frac{\partial (\pi_i P_0)}{a^3 \partial \pi_i} \\ &\quad + \frac{\partial E}{a^3 \partial \phi_i} \frac{\partial \zeta}{a^3 \partial \pi_i} P_0 - \beta \frac{\partial E}{a^3 \partial \phi_i} \zeta \pi_i P_0 \,, \\ \frac{\Omega}{2} \frac{\partial^2}{a^6 \partial \pi_i^2} \zeta P_0 &= \frac{\Omega}{2} \frac{\partial}{a^3 \partial \pi_i} \left[\frac{\partial \zeta}{a^3 \partial \pi_i} P_0 - \beta \zeta \pi_i P_0 \right] \\ &= \frac{\Omega}{2} \frac{\partial^2 \zeta}{a^6 \partial \pi_i^2} P_0 - \beta \frac{\Omega}{2} \frac{\partial \zeta}{a^3 \partial \pi_i} \pi_i P_0 \end{aligned}$$

$$- \beta \frac{\Omega}{2} \frac{\partial \zeta}{a^3 \partial \pi_i} \pi_i P_0 - \beta \frac{\Omega}{2} \zeta \frac{\partial (\pi P_0)}{a^3 \partial \pi_i} \ .$$

The orange and the green terms cancel each other and the blue combine to give the equation for ζ

$$a^3 \sum_{i=1}^{N^3} \left\{ -\pi_i \frac{\partial}{a^3 \partial \phi_i} + \left[-\eta \pi_i + \frac{\partial E}{a^3 \partial \phi_i} \right] \frac{\partial}{a^3 \partial \pi_i} + \frac{\Omega}{2} \frac{\partial^2}{a^6 \partial \pi_i^2} \right\} \zeta(\phi, \pi) = 0 \ , \quad \text{(D.31)}$$

where we recognize the adjoint Fokker-Planck equation. Near the saddle-point, we expand the energy to obtain Eq. (5.100)

$$a^3 \sum_{i=1}^{N^3} \left\{ -\pi_i \frac{\partial}{a^3 \partial \phi_i} + \left[-\eta \pi_i + a^3 \sum_{k=1}^{N^3} \left[-\frac{\nabla^2_{ik}}{a^3} + \frac{V''(\phi_k^S) \delta_{ik}}{a^3} \right] (\phi_k - \phi_k^S) \right] \frac{\partial}{a^3 \partial \pi_i} + \frac{\Omega}{2} \frac{\partial^2}{a^6 \partial \pi_i^2} \right\} \zeta(\phi, \pi) = 0 \ . \quad \text{(D.32)}$$

We now derive the equation (5.103) for the parameters U_i and $\bar{U}_i$. Recall that $\zeta(\phi, \pi)$ depends on a linear combination of the ϕ_i and π_i

$$\zeta(\phi, \pi) = \zeta(u) \ , \quad \text{where} \quad u = a^3 \sum_{i=1}^{N^3} \left[U_i (\phi_i - \phi_i^S) + \bar{U}_i (\pi_i - \pi_i^S) \right] \ , \quad \text{(D.33)}$$

and takes the following form

$$\zeta(u) = \frac{1}{\sqrt{2\pi k_B T}} \int_u^\infty dz \ \exp \left\{ -\frac{z^2}{2 k_B T} \right\} \ , \quad \text{(D.34)}$$

which satisfies the boundary conditions. We have

$$\frac{\partial \zeta}{a^3 \partial \phi_i} = \frac{\partial \zeta}{\partial u} \frac{\partial u}{a^3 \partial \phi_i} = -\frac{U_i}{\sqrt{2\pi k_B T}} \exp \left\{ -\frac{u^2}{2 k_B T} \right\} \ , \quad \text{(D.35)}$$

$$\frac{\partial \zeta}{a^3 \partial \pi_i} = \frac{\partial \zeta}{\partial u} \frac{\partial u}{a^3 \partial \pi_i} = -\frac{\bar{U}_i}{\sqrt{2\pi k_B T}} \exp \left\{ -\frac{u^2}{2 k_B T} \right\} \ , \quad \text{(D.36)}$$

$$\begin{aligned} \frac{\partial^2 \zeta}{a^6 \partial \pi_i^2} &= u \frac{\bar{U}_i \bar{U}_i}{k_B T \sqrt{2\pi k_B T}} \exp \left\{ -\frac{u^2}{2 k_B T} \right\} \\ &= \frac{\bar{U}_i^2}{k_B T \sqrt{2\pi k_B T}} \exp \left\{ -\frac{u^2}{2 k_B T} \right\} a^3 \sum_{k=1}^{N^3} \left[U_k (\phi_k - \phi_k^S) + \bar{U}_k (\pi_k - \pi_k^S) \right] \ , \end{aligned} \quad \text{(D.37)}$$

where the minus sign in the first two equations comes from the fundamental

theorem of calculus. Inserting in the equation (D.32) for ζ we get

$$
\begin{aligned}
& a^3 \sum_{i=1}^{N^3} \left\{ \frac{\pi_i U_i}{\sqrt{2\pi k_B T}} e^{-\frac{u^2}{2k_B T}} - \left[-\eta\pi_i + a^3 \sum_{k=1}^{N^3} \left[-\frac{\nabla^2_{ik}}{a^3} + \frac{V''(\phi^S_k)\delta_{ik}}{a^3} \right] (\phi_k - \phi^S_k) \right] \cdot \right. \\
& \qquad \left. \frac{\bar{U}_i}{\sqrt{2\pi k_B T}} e^{-\frac{u^2}{2k_B T}} + \frac{\Omega}{2} \frac{u\bar{U}_i^2}{k_B T \sqrt{2\pi k_B T}} e^{-\frac{u^2}{2k_B T}} \right\} = 0 \, , \\
& a^3 \sum_{i=1}^{N^3} \left\{ \left(U_i + \eta \bar{U}_i \right) \pi_i - \bar{U}_i a^3 \sum_{k=1}^{N^3} \left[-\frac{\nabla^2_{ik}}{a^3} + \frac{V''(\phi^S_k)\delta_{ik}}{a^3} \right] (\phi_k - \phi^S_k) + \right. \\
& \qquad \left. + \eta \bar{U}_i^2 a^3 \sum_{k=1}^{N^3} U_k (\phi_k - \phi^S_k) + \eta \bar{U}_i^2 a^3 \sum_{k=1}^{N^3} \bar{U}_k (\pi_k - \pi^S_k) \right\} = 0 \, . \qquad \text{(D.38)}
\end{aligned}
$$

This equation can be written in the more elegant matrix notation

$$
(U\ \bar{U}) \cdot M^T \cdot (e^S_{ij}) \cdot \begin{pmatrix} \phi - \phi^S \\ \pi - \pi^S \end{pmatrix} = (U\ \bar{U}) \cdot M \cdot \begin{pmatrix} \phi - \phi^S \\ \pi - \pi^S \end{pmatrix} (U\ \bar{U}) \cdot \begin{pmatrix} \phi - \phi^S \\ \pi - \pi^S \end{pmatrix} . \qquad \text{(D.39)}
$$

Let us show this equality explicitly. The LHS gives

$$
\begin{aligned}
& (U\ \bar{U}) \cdot M^T \cdot (e^S_{ij}) \cdot \begin{pmatrix} \phi - \phi^S \\ \pi - \pi^S \end{pmatrix} \\
& = -\frac{1}{a^6} (U\ \bar{U}) \cdot \begin{pmatrix} 0 & \mathbb{1} \\ -\mathbb{1} & \eta\mathbb{1} \end{pmatrix} \cdot \begin{pmatrix} (-\nabla^2_{ij}) + V''(\phi^S)\delta_{ij} & 0 \\ 0 & \mathbb{1} \end{pmatrix} \cdot \begin{pmatrix} \phi - \phi^S \\ \pi - \pi^S \end{pmatrix} \\
& = -\frac{1}{a^3} (U\ \bar{U}) \cdot \begin{pmatrix} 0 & \mathbb{1} \\ -(-\nabla^2_{ij}) - V''(\phi^S)\delta_{ij} & \eta\mathbb{1} \end{pmatrix} \cdot \begin{pmatrix} \phi - \phi^S \\ \pi - \pi^S \end{pmatrix} \\
& = \begin{pmatrix} \frac{1}{a^3}\bar{U} \cdot \left[(-\nabla^2_{ij}) + V''(\phi^S)\delta_{ij} \right] \\ -\left(U + \eta\bar{U} \right) \end{pmatrix}^T \cdot \begin{pmatrix} \phi - \phi^S \\ \pi - \pi^S \end{pmatrix} \\
& = \frac{1}{a^3} \bar{U} \cdot \left[(-\nabla^2_{ij}) + V''(\phi^S)\delta_{ij} \right] \cdot (\phi - \phi^S) - \left(U + \eta\bar{U} \right) \cdot (\pi - \pi^S) \\
& = a^3 \sum_{i=1}^{N^3} a^3 \sum_{j=1}^{N^3} \bar{U}_i \left(-\frac{(\nabla^2_{ij})}{a^3} + \frac{V''(\phi^S)}{a^3}\delta_{ij} \right) (\phi_j - \phi^S_j) \\
& \quad - a^3 \sum_{i=1}^{N^3} \left(U_i + \eta\bar{U}_i \right) (\pi_i - \pi^S_i) \, . \qquad \text{(D.40)}
\end{aligned}
$$

For the RHS, we have

$$
(U\ \bar{U}) \cdot M \cdot \begin{pmatrix} U \\ \bar{U} \end{pmatrix} = \frac{1}{a^3} (U\ \bar{U}) \cdot \begin{pmatrix} 0 & -\mathbb{1} \\ \mathbb{1} & \eta\mathbb{1} \end{pmatrix} \cdot \begin{pmatrix} U \\ \bar{U} \end{pmatrix}
$$

$$= \begin{pmatrix} \bar{U} \\ -U + \eta\bar{U} \end{pmatrix}^T \cdot \begin{pmatrix} U \\ \bar{U} \end{pmatrix}$$
$$= \bar{U} \cdot U - U \cdot \bar{U} + \eta\bar{U} \cdot \bar{U} = a^3 \sum_{i=1}^{N^3} \eta \bar{U}_i \bar{U}_i \ , \qquad \text{(D.41)}$$

and therefore

$$(U\ \bar{U}) \cdot M \cdot \begin{pmatrix} \phi - \phi^S \\ \pi - \pi^S \end{pmatrix} (U\ \bar{U}) \cdot \begin{pmatrix} \phi - \phi^S \\ \pi - \pi^S \end{pmatrix}$$
$$= a^3 \sum_{i=1}^{N^3} \eta \bar{U}_i^2 a^3 \sum_{k=1}^{N^3} \left[U_k(\phi_k - \phi_k^S) + \bar{U}_k(\pi_k - \pi_k^S) \right] \ . \qquad \text{(D.42)}$$

Which show the validity of the matrix equation. Let us also derive the normalization (5.108). Multiplying the eigenvalue equation (5.107) on the right by the inverse of (e_{ij}^S) times $(U\ \bar{U})^T$ we get

$$(U\ \bar{U}) \cdot M^T \cdot (e_{ij}^S) \cdot (e_{ij}^S)^{-1} \cdot \begin{pmatrix} U \\ \bar{U} \end{pmatrix} = \lambda (U\ \bar{U}) \cdot (e_{ij}^S)^{-1} \cdot \begin{pmatrix} U \\ \bar{U} \end{pmatrix}$$
$$(U\ \bar{U}) \cdot M^T \cdot \begin{pmatrix} U \\ \bar{U} \end{pmatrix} = \lambda (U\ \bar{U}) \cdot (e_{ij}^S)^{-1} \cdot \begin{pmatrix} U \\ \bar{U} \end{pmatrix} \ , \qquad \text{(D.43)}$$

recognizing λ on the RHS we obtain the normalization (5.108)

$$1 = (U\ \bar{U}) \cdot (e_{ij}^S)^{-1} \cdot \begin{pmatrix} U \\ \bar{U} \end{pmatrix} \ . \qquad \text{(D.44)}$$

The ansatz for $\zeta(u)$ can be justified by solving Eq. (D.32) explicitly. Using

$$\frac{\partial \zeta}{a^3 \partial \phi_i} = \frac{\partial \zeta}{\partial u} \frac{\partial u}{a^3 \partial \phi_i} = U_i \zeta'(u) \ , \quad \frac{\partial \zeta}{a^3 \partial \pi_i} = \bar{U}_i \zeta'(u) \ , \quad \frac{\partial^2 \zeta}{a^6 \partial \pi_i^2} = \bar{U}_i^2 \zeta''(u) \ , \qquad \text{(D.45)}$$

we obtain

$$a^3 \sum_{i=1}^{N^3} \left\{ -\left(U_i + \eta \bar{U}_i\right) \pi_i + \bar{U}_i a^3 \sum_{k=1}^{N^3} \left[-\frac{\nabla_{ik}^2}{a^3} + \frac{V''(\phi_k^S)\delta_{ik}}{a^3} \right] (\phi_k - \phi_k^S) \right\} \zeta'(u)$$
$$+ \frac{\Omega}{2} a^3 \sum_{i=1}^{N^3} \bar{U}_i^2 \zeta''(u) = 0 \ ,$$
$$(U\ \bar{U}) \cdot M^T \cdot (e_{ij}^S) \cdot \begin{pmatrix} \phi - \phi^S \\ \pi - \pi^S \end{pmatrix} \zeta'(u) + \frac{\Omega}{2} \frac{\lambda}{\eta} \zeta''(u) = 0 \ ,$$

$$\lambda u\zeta'(u) + \beta\lambda\zeta''(u) = 0\ .$$

Solving for ζ gives precisely the ansatz

$$\zeta(u) = \frac{1}{\sqrt{2\pi k_B T}} \int_u^\infty dz\ \exp\left\{-\frac{z^2}{2k_B T}\right\}\ , \tag{D.46}$$

which has the correct asymptotic behavior, the negative exponent being a direct consequence of the positivity of the eigenvalue.

Probability Density Current We compute the probability density current corresponding to $P = \zeta P_0$

$$\begin{aligned} J\zeta P_0 &= -\begin{pmatrix} -\pi_i - k_B T \frac{\partial}{a^3 \partial \pi_i} \\ [-\nabla^2\phi_i + V'(\phi_i)] + k_B T \frac{\partial}{a^3\partial\phi_i} + \eta\pi_i + \frac{\Omega}{2}\frac{\partial}{a^3\partial\pi_i} \end{pmatrix} \zeta P_0 \\ &= -\begin{pmatrix} -k_b T \frac{\partial\zeta}{a^3\partial\pi_i} P_0 \\ k_B T \frac{\partial\zeta}{a^3\partial\phi_i} P_0 + \frac{\Omega}{2}\frac{\partial\zeta}{a^3\partial\pi_i} P_0 \end{pmatrix} \\ &= -\frac{1}{\beta} M \cdot \begin{pmatrix} \frac{\partial\zeta}{a^3\partial\phi_i} \\ \frac{\partial\zeta}{a^3\partial\pi_i} \end{pmatrix} P_0 \\ &= \sqrt{\frac{k_B T}{2\pi}} M \cdot \begin{pmatrix} U \\ \bar{U} \end{pmatrix} \exp\left\{-\frac{u^2}{2k_B T}\right\} P_0\ . \end{aligned} \tag{D.47}$$

Once we have the probability current, we can compute the probability flux j at the saddle-point

$$\begin{aligned} j &= a^3 \sum_{i=1}^{N^3} \int_{u=0} dS_i J_i(\phi,\pi) \\ &= \int D\phi D\pi\ \delta(u)\ (U\ \bar{U}) \cdot J \\ &= \int D\phi D\pi\ \delta(u)\ (U\ \bar{U}) \cdot M \cdot \begin{pmatrix} U \\ \bar{U} \end{pmatrix} \sqrt{\frac{k_B T}{2\pi}} \exp\left\{-\frac{u^2}{2k_B T}\right\} P_0 \\ &= \lambda\sqrt{\frac{k_B T}{2\pi}} \int D\phi D\pi \int \frac{dk}{2\pi} \exp\{iku\} \frac{1}{\mathcal{Z}} \exp\{-\beta E[\phi,\pi]\} \\ &= \frac{\lambda}{2\pi\mathcal{Z}}\sqrt{\frac{k_B T}{2\pi}} \exp\left\{-\beta E[\phi^S,\pi^S]\right\} \int D\phi D\pi \int dk \\ &\quad \cdot \exp\left\{ika^3 \sum_{i=1}^{N^3} \left[U_i(\phi_i - \phi_i^S) + \bar{U}_i(\pi_i - \pi_i^S)\right]\right\} \end{aligned}$$

$$\cdot \exp\left\{ -\frac{\beta}{2} a^6 \sum_{i,j=1}^{N^3} (\phi_i - \phi_i^S) \left[-\frac{\nabla_{ij}^2}{a^3} + \frac{V''(\phi_i^S)\delta_{ij}}{a^3} \right] (\phi_j - \phi_j^S) \right.$$
$$\left. + \frac{\beta}{2} a^6 \sum_{ij=1}^{N^3} (\pi_i - \pi_i^S) \frac{\delta_{ij}}{a^3} (\pi_j - \pi_j^S) \right\}$$
$$= \frac{\lambda}{2\pi\mathcal{Z}} \sqrt{\frac{k_B T}{2\pi}} \exp\left\{ -\beta E[\phi^S, \pi^S] \right\} \int D\phi D\pi \int dk \exp\left\{ ik(U\ \bar{U}) \cdot \begin{pmatrix} \phi - \phi^S \\ \pi - \pi^S \end{pmatrix} \right\}$$
$$\cdot \exp\left\{ \frac{\beta}{2} \begin{pmatrix} \phi - \phi^S \\ \pi - \pi^S \end{pmatrix}^T \cdot (e_{ij}^S) \cdot \begin{pmatrix} \phi - \phi^S \\ \pi - \pi^S \end{pmatrix} \right\} , \tag{D.48}$$

where we have adopted the vector notation in the last step. Introducing the rotation $S = (S_{ij})$ in field space to diagonalize (e_{ij}^S) we obtain

$$\begin{pmatrix} \phi - \phi^S \\ \pi - \pi^S \end{pmatrix} = S \cdot \xi \ , \quad iku = ik(U\ \bar{U}) \cdot S^\dagger \cdot S \cdot \begin{pmatrix} \phi - \phi^S \\ \pi - \pi^S \end{pmatrix} = ik\tilde{U} \cdot \xi \ , \tag{D.49}$$

where we have defined the vector $\tilde{U}$ as $S \cdot \left(U\ \bar{U}\right)^T$. Moreover, we have

$$\begin{pmatrix} \phi - \phi^S \\ \pi - \pi^S \end{pmatrix}^T \cdot (e_{ij}^S) \cdot \begin{pmatrix} \phi - \phi^S \\ \pi - \pi^S \end{pmatrix}$$
$$= \begin{pmatrix} \phi - \phi^S \\ \pi - \pi^S \end{pmatrix}^T \cdot S^\dagger \cdot S \cdot (e_{ij}^S) \cdot S^\dagger \cdot S \cdot \begin{pmatrix} \phi - \phi^S \\ \pi - \pi^S \end{pmatrix}$$
$$= \xi \cdot \mathrm{diag}\left(\frac{\mu_1}{a^3}, -\frac{\mu_2}{a^3}, \ldots, -\frac{\mu_{2N}}{a^3} \right) \cdot \xi$$
$$= a^3 \mu_1 \xi_1^2 - a^3 \sum_{l=2}^{2N^3} \mu_l \xi_l^2 \ , \tag{D.50}$$

where all the μ_l are positive. The only positive eigenvalue of (e_{ij}^S) is μ_1, all the other eigenvalues are $-\mu_l$. Recall that (e_{ij}^S) is the negative of the Hessian matrix of the energy at the saddle-point, there is only one direction that decreases the energy at that point, hence only one negative eigenvalue in the Hessian. We have

$$j = \frac{\lambda}{2\pi\mathcal{Z}} \sqrt{\frac{k_B T}{2\pi}} \exp\left\{ -\beta E[\phi^S, \pi^S] \right\} \int \prod_{l=1}^{2N^3} d\xi_l \int dk$$
$$\cdot \exp\left\{ ika^3 \sum_{l=1}^{2N^3} \tilde{U}_l \xi_l + \frac{\beta}{2} a^3 \mu_1 \xi_1^2 - \frac{\beta}{2} a^3 \sum_{l=2}^{2N^3} \mu_l \xi_l^2 \right\}$$

Integrate over the modes $l > 1$

$$= \frac{\lambda}{2\pi\mathcal{Z}}\sqrt{\frac{k_BT}{2\pi}}\exp\left\{-\beta E[\phi^S,\pi^S]\right\}\left(\prod_{l=2}^{2N^3}\sqrt{\frac{2\pi}{\beta a^3\mu_l}}\right)\int d\xi_1\int dk$$

$$\cdot\exp\left\{-\frac{a^6\sum_{l=2}^{2N^3}\frac{\tilde{U}_l^2}{\mu_l}}{2\beta a^3}k^2+ika^3\tilde{U}_1\xi_1+\frac{\beta}{2}a^3\mu_1\xi_1^2\right\}$$

Integrate over k

$$= \frac{\lambda}{2\pi\mathcal{Z}}\sqrt{\frac{k_BT}{2\pi}}\exp\left\{-\beta E[\phi^S,\pi^S]\right\}\left(\prod_{l=2}^{2N^3}\sqrt{\frac{2\pi}{\beta a^3\mu_l}}\right)\sqrt{\frac{2\pi\beta}{a^3\sum_{l=2}^{2N^3}\frac{\tilde{U}_l^2}{\mu_l}}}\int d\xi_1$$

$$\cdot\exp\left\{-\frac{\beta}{2}a^3\left(\frac{a^3\tilde{U}_1^2}{a^3\sum_{l=2}^{2N^3}\frac{\tilde{U}_l^2}{\mu_l}}-\mu_1\right)\xi_1^2\right\}$$

Integrate over ξ_1

$$= \frac{\lambda}{2\pi\mathcal{Z}}\sqrt{\frac{k_BT}{2\pi}}\exp\left\{-\beta E[\phi^S,\pi^S]\right\}\left(\prod_{l=2}^{2N^3}\sqrt{\frac{2\pi}{\beta a^3\mu_l}}\right)$$

$$\cdot\sqrt{\frac{2\pi\beta}{a^3\sum_{l=2}^{2N^3}\frac{\tilde{U}_l^2}{\mu_l}}}\sqrt{\frac{2\pi a^3\sum_{l=2}^{2N^3}\frac{\tilde{U}_l^2}{\mu_l}}{\beta a^3\mu_1\left[\frac{\tilde{U}_1^2}{\mu_1}-\sum_{l=2}^{2N^3}\frac{\tilde{U}_l^2}{\mu_l}\right]}}$$

$$= \frac{\lambda}{2\pi\mathcal{Z}}\exp\left\{-\beta E[\phi^S,\pi^S]\right\}\left(\prod_{l=1}^{2N^3}\sqrt{\frac{2\pi}{\beta a^3\mu_l}}\right)$$

$$= \frac{\lambda}{2\pi\mathcal{Z}}\exp\left\{-\beta E[\phi^S,\pi^S]\right\}|\det(2\pi/\beta)^{-1}E^{(S)}|^{-\frac{1}{2}}\ , \tag{D.51}$$

where we have used the normalization (5.108)

$$\left[\frac{\tilde{U}_1^2}{\mu_1}-\sum_{l=2}^{2N^3}\frac{\tilde{U}_l^2}{\mu_l}\right]=(U\ \bar{U})\cdot(e_{ij}^S)^{-1}\cdot\begin{pmatrix}U\\ \bar{U}\end{pmatrix}=1\ . \tag{D.52}$$

Bibliography

[1] A. Berera, R. Brandenberger, J. Mabillard, and R. O. Ramos. Stability of the pion string in a thermal and dense medium. *Phys. Rev.*, D94(6):065043, 2016.

[2] A. Berera, J. Mabillard, M. Pieroni, and R. O. Ramos. Identifying Universality in Warm Inflation. *JCAP*, 1807(07):021, 2018.

[3] A. Einstein. Über die von der molekularkinetischen theorie der wärme geforderte bewegung von in ruhenden flüssigkeiten suspendierten teilchen. *Annalen der Physik*, 322(8):549–560, 1905.

[4] P. Langevin. Sur la théorie du mouvement brownien. *C. R. Acad. Sci. (Paris) (146)*, pages 530–533, 1908.

[5] A. D. Fokker. Die mittlere Energie rotierender elektrischer Dipole im Strahlungsfeld. *Annalen der Physik*, 348:810–820, 1914.

[6] M. Planck. Über einen satz der statistischen dynamik und seine erweiterung in der quantentheorie. *Sitzungsber. Preuss. Akad. Wiss. Berlin (Math. Phys.)*, 24:324–341, 1917.

[7] U. Weiss. *Quantum Dissipative Systems*. World Scientific, 4th edition, 2012.

[8] A. O. Caldeira and A. J. Leggett. Quantum tunnelling in a dissipative system. *Annals of Physics*, 149(2):374–456, 1983.

[9] E. A. Calzetta and B.-L. B. Hu. *Nonequilibrium Quantum Field Theory*. Cambridge University Press, Jul 2008.

[10] A. Berera and L.-Z. Fang. Thermally induced density perturbations in the inflation era. *Phys. Rev. Lett.*, 74:1912–1915, 1995.

[11] A. Berera. Warm inflation. *Phys. Rev. Lett.*, 75:3218–3221, 1995.

[12] S. Bartrum, A. Berera, and J. G. Rosa. Fluctuation-dissipation dynamics of cosmological scalar fields. *Phys. Rev.*, D91(8):083540, 2015.

[13] A. Einstein. On the General Theory of Relativity. *Sitzungsber. Preuss. Akad. Wiss. Berlin (Math. Phys.)*, 1915:778–786, 1915. [Addendum: Sitzungsber. Preuss. Akad. Wiss. Berlin (Math. Phys.)1915,799(1915)].

[14] A. Einstein. The Foundation of the General Theory of Relativity. *Annalen der Physik*, 49(7):769–822, 1916.

[15] E. P. Hubble. Extragalactic nebulae. *Astrophys. J.*, 64:321–369, 1926.

[16] E. P. Hubble. A relation between distance and radial velocity among extra-galactic nebulae. *Proceedings of the National Academy of Sciences*, 15(3):168–173, 1929.

[17] E. W. Kolb and M. S. Turner. The Early Universe. *Front. Phys.*, 69:1–547, 1990.

[18] H. Mo, F. C. van den Bosch, and S. White. *Galaxy Formation and Evolution*. Cambridge University Press, May 2010.

[19] P. Binétruy. *Gravity! The Quest for Gravitational Waves*. Oxford University Press, May 2018.

[20] S. Weinberg. *Gravitation and Cosmology*. John Wiley and Sons, New York, 1972.

[21] S. M. Carroll. *Spacetime and geometry: An introduction to general relativity*. Addison-Wesley, 2004.

[22] M. Tanabashi et al. Review of Particle Physics. *Phys. Rev.*, D98(3):030001, 2018.

[23] S. L. Glashow. Partial Symmetries of Weak Interactions. *Nucl. Phys.*, 22:579–588, 1961.

[24] P. W. Higgs. Broken Symmetries and the Masses of Gauge Bosons. *Phys. Rev. Lett.*, 13:508–509, 1964.

[25] F. Englert and R. Brout. Broken Symmetry and the Mass of Gauge Vector Mesons. *Phys. Rev. Lett.*, 13:321–323, 1964.

[26] S. Weinberg. A Model of Leptons. *Phys. Rev. Lett.*, 19:1264–1266, 1967.

[27] A. Salam. Weak and Electromagnetic Interactions. *Conf. Proc.*, C680519:367–377, 1968.

[28] J.-L. Gervais and B. Sakita. Field Theory Interpretation of Supergauges in Dual Models. *Nucl. Phys.*, B34:632–639, 1971.

[29] P. Ramond. Dual Theory for Free Fermions. *Phys. Rev.*, D3:2415–2418, 1971.

[30] J. Wess and B. Zumino. Supergauge Transformations in Four-Dimensions. *Nucl. Phys.*, B70:39–50, 1974.

[31] H. Georgi and S. L. Glashow. Unity of All Elementary Particle Forces. *Phys. Rev. Lett.*, 32:438–441, 1974.

[32] A. J. Buras, J. Ellis, M. K. Gaillard, and D. V. Nanopoulos. Aspects of the grand unification of strong, weak and electromagnetic interactions. *Nucl. Phys.*, B135(1):66–92, 1978.

[33] R. H. Cyburt, B. D. Fields, K. A. Olive, and T.-H. Yeh. Big bang nucleosynthesis: Present status. *Rev. Mod. Phys.*, 88:015004, Feb 2016.

[34] R. H. Cyburt, B. D. Fields, and K. A. Olive. Primordial nucleosynthesis in light of wmap. *Phys. Lett.*, B567(3):227–234, 2003.

[35] R. H. Cyburt. Primordial nucleosynthesis for the new cosmology: Determining uncertainties and examining concordance. *Phys. Rev.*, D70:023505, Jul 2004.

[36] A. Coc, E. Vangioni-Flam, P. Descouvemont, A. Adahchour, and C. Angulo. Updated big bang nucleosynthesis compared with Wilkinson microwave anisotropy Probe Observations and the abundance of light elements. *The Astrophysical Journal*, 600(2):544–552, Jan 2004.

[37] A. Cuoco, F. Iocco, G. Mangano, G. Miele, O. Pisanti, and P. D. Serpico. Present status of primordial nucleosynthesis after wmap: Results from a new bbn code. *Int. J. Mod. Phys.*, A19(26):4431–4453, 2004.

[38] B. D. Fields. The primordial lithium problem. *Annual Review of Nuclear and Particle Science*, 61(1):47–68, 2011.

[39] A. A. Penzias and R. W. Wilson. A Measurement of excess antenna temperature at 4080-Mc/s. *Astrophys. J.*, 142:419–421, 1965.

[40] D. J. Fixsen, E. S. Cheng, J. M. Gales, J. C. Mather, R. A. Shafer, and E. L. Wright. The Cosmic Microwave Background spectrum from the full COBE FIRAS data set. *Astrophys. J.*, 473:576, 1996.

[41] P. de Bernardis et al. A Flat universe from high resolution maps of the cosmic microwave background radiation. *Nature*, 404:955–959, 2000.

[42] N. Aghanim et al. Planck 2018 results. VI. Cosmological parameters. 2018.

[43] S. Perlmutter et al. Measurements of Omega and Lambda from 42 high redshift supernovae. *Astrophys. J.*, 517:565–586, 1999.

[44] S. Weinberg. The Cosmological Constant Problem. *Rev. Mod. Phys.*, 61:1–23, 1989.

[45] B. Ratra and P. J. E. Peebles. Cosmological Consequences of a Rolling Homogeneous Scalar Field. *Phys. Rev.*, D37:3406, 1988.

[46] R. R. Caldwell, R. Dave, and Paul J. Steinhardt. Cosmological imprint of an energy component with general equation of state. *Phys. Rev. Lett.*, 80:1582–1585, 1998.

[47] A. G. Riess et al. Large Magellanic Cloud Cepheid Standards Provide a 1% Foundation for the Determination of the Hubble Constant and Stronger Evidence for Physics Beyond LambdaCDM. *Astrophys. J.*, 876(1):85, 2019.

[48] F. Zwicky. Die Rotverschiebung von extragalaktischen Nebeln. *Helv. Phys. Acta*, 6:110–127, 1933.

[49] G. Bertone, D. Hooper, and J. Silk. Particle dark matter: Evidence, candidates and constraints. *Phys. Rept.*, 405:279–390, 2005.

[50] R. D. Peccei and H. R. Quinn. CP Conservation in the Presence of Instantons. *Phys. Rev. Lett.*, 38:1440–1443, 1977.

[51] R. D. Peccei and H. R. Quinn. Constraints Imposed by CP Conservation in the Presence of Instantons. *Phys. Rev.*, D16:1791–1797, 1977.

[52] S. Hawking. Gravitationally collapsed objects of very low mass. *Mon. Not. Roy. Astron. Soc.*, 152:75, 1971.

[53] B. Carr, F. Kuhnel, and M. Sandstad. Primordial Black Holes as Dark Matter. *Phys. Rev.*, D94(8):083504, 2016.

[54] S. Dodelson and L. M. Widrow. Sterile-neutrinos as dark matter. *Phys. Rev. Lett.*, 72:17–20, 1994.

[55] G. Jungman, M. Kamionkowski, and K. Griest. Supersymmetric dark matter. *Phys. Rept.*, 267:195–373, 1996.

[56] T. W. B. Kibble. Topology of cosmic domains and strings. *Journal of Physics A: Mathematical and General*, 9(8):1387, 1976.

[57] R. H. Brandenberger. Topological defects and structure formation. *Int. J. Mod. Phys.*, A9:2117–2190, 1994.

[58] R. Durrer, M. Kunz, and A. Melchiorri. Cosmic structure formation with topological defects. *Phys. Rept.*, 364:1–81, 2002.

[59] K. Dimopoulos. Primordial magnetic fields from superconducting cosmic strings. *Phys. Rev.*, D57:4629–4641, 1998.

[60] R. H. Brandenberger and X.-M. Zhang. Anomalous global strings and primordial magnetic fields. *Phys. Rev.*, D59:081301, 1999.

[61] M. Trodden, A.-C. Davis, and R. H. Brandenberger. Particle physics models, topological defects and electroweak baryogenesis. *Phys. Lett.*, B349:131–136, 1995.

[62] R. H. Brandenberger, A.-C. Davis, and M. Trodden. Cosmic strings and electroweak baryogenesis. *Phys. Lett.*, B335:123–130, 1994.

[63] P. Bhattacharjee, C. T. Hill, and D. N. Schramm. Grand unified theories, topological defects and ultrahigh-energy cosmic rays. *Phys. Rev. Lett.*, 69:567–570, 1992.

[64] P. Bhattacharjee and G. Sigl. Origin and propagation of extremely high-energy cosmic rays. *Phys. Rept.*, 327:109–247, 2000.

[65] T. Vachaspati and A. Vilenkin. Gravitational radiation from cosmic strings. *Phys. Rev.*, D31:3052–3058, Jun 1985.

[66] T. Vachaspati and M. Barriola. A new class of defects. *Phys. Rev. Lett.*, 69:1867–1870, Sep 1992.

[67] X. Zhang, T. Huang, and R. H. Brandenberger. Pion and eta strings. *Phys. Rev.*, D58:027702, 1998.

[68] T. Vachaspati. Vortex solutions in the weinberg-salam model. *Phys. Rev. Lett.*, 68:1977–1980, Mar 1992.

[69] T. Vachaspati. Electroweak strings. *Nucl. Phys.*, B397(3):648 – 671, 1993.

[70] M. Nagasawa and R. H. Brandenberger. Stabilization of embedded defects by plasma effects. *Phys. Lett.*, B467:205–210, 1999.

[71] J. Karouby and R. H. Brandenberger. Effects of a Thermal Bath of Photons on Embedded String Stability. *Phys. Rev.*, D85:107702, 2012.

[72] J. Karouby. String melting in a photon bath. *JCAP*, 1310:017, 2013.

[73] H. Mao, Y. Li, M. Nagasawa, X.-M. Zhang, and T. Huang. Signal of the pion string at CERN LHC Pb - Pb collisions. *Phys. Rev.*, C71:014902, 2005.

[74] F. Lu, Q. Chen, and H. Mao. Pion String evolving in a thermal bath. *Phys. Rev.*, D92(8):085036, 2015.

[75] M. B. Hindmarsh and T. W. B. Kibble. Cosmic strings. *Rept. Prog. Phys.*, 58:477–562, 1995.

[76] A. Vilenkin and E. P. S. Shellard. *Cosmic Strings and Other Topological Defects*. Cambridge University Press, 2000.

[77] A. Gangui. Topological defects in cosmology. *Lecture Notes for the First Bolivian School on Cosmology*, 2001.

[78] T. Vachaspati. *Kinks and domain walls: An introduction to classical and quantum solitons*. Cambridge University Press, 2010.

[79] E. J. Copeland and T. W. B. Kibble. Cosmic Strings and Superstrings. *Proc. Roy. Soc. Lond.*, A466:623–657, 2010.

[80] W. H. Zurek. Cosmological experiments in superfluid helium? *Nature*, 317(6037):505–508, 1985.

[81] M. Hindmarsh, A.-C. Davis, and R. H. Brandenberger. Formation of topological defects in first order phase transitions. *Phys. Rev.*, D49:1944–1950, 1994.

[82] A. Hatcher. *Algebraic Topology*. Algebraic Topology. Cambridge University Press, 2002.

[83] R. Jeannerot. A Supersymmetric SO(10) model with inflation and cosmic strings. *Phys. Rev.*, D53:5426–5436, 1996.

[84] S. Sarangi and S. H. H. Tye. Cosmic string production towards the end of brane inflation. *Phys. Lett.*, B536:185–192, 2002.

[85] A. Vilenkin. Gravitational field of vacuum domain walls and strings. *Phys. Rev.*, D23:852–857, Feb 1981.

[86] A. Stebbins. Cosmic Strings and the Microwave Sky. 1. Anisotropy from Moving Strings. *Astrophys. J.*, 327:584–614, 1988.

[87] F. R. Bouchet, D. P. Bennett, and A. Stebbins. Patterns of the cosmic microwave background from evolving string networks. *Nature*, 335:410 EP, Sep 1988.

[88] P. A. R. Ade et al. Planck 2013 results. XXV. Searches for cosmic strings and other topological defects. *Astron. Astrophys.*, 571:A25, 2014.

[89] R. Durrer. Gravitational waves from cosmological phase transitions. *J. Phys. Conf. Ser.*, 222:012021, 2010.

[90] C. Caprini et al. Science with the space-based interferometer eLISA. II: Gravitational waves from cosmological phase transitions. *JCAP*, 1604(04):001, 2016.

[91] J. J. Blanco-Pillado, K. D. Olum, and X. Siemens. New limits on cosmic strings from gravitational wave observation. *Phys. Lett.*, B778:392–396, 2018.

[92] S. F. Bramberger, R. H. Brandenberger, P. Jreidini, and J. Quintin. Cosmic String Loops as the Seeds of Super-Massive Black Holes. *JCAP*, 1506(06):007, 2015.

[93] M. Barriola, T. Vachaspati, and M. Bucher. Embedded defects. *Phys. Rev.*, D50:2819–2825, 1994.

[94] N. F. Lepora and A.-C. Davis. Embedded vortices. *Phys. Rev.*, D58:125027, 1998.

[95] N. F. Lepora and A.-C. Davis. Examples of embedded defects (in particle physics and condensed matter). *Phys. Rev.*, D58:125028, 1998.

[96] M. Gell-Mann and M. Lévy. The axial vector current in beta decay. *Il Nuovo Cimento (1955-1965)*, 16(4):705–726, May 1960.

[97] H. C. G. Caldas, A. L. Mota, and M. C. Nemes. The Chiral fermion meson model at finite temperature. *Phys. Rev.*, D63:056011, 2001.

[98] R. Khan, J. O. Andersen, L. T. Kyllingstad, and M. Khan. The chiral phase transition and the role of vacuum fluctuations. *Int. J. Mod. Phys.*, A31(7):1650025, 2016.

[99] S. Chiku and T. Hatsuda. Optimized perturbation theory at finite temperature. *Phys. Rev.*, D58:076001, 1998.

[100] S. Chiku. Optimized perturbation theory at finite temperature: Two loop analysis. *Prog. Theor. Phys.*, 104:1129–1150, 2000.

[101] E. S. Fraga, L. F. Palhares, and M. B. Pinto. Nonperturbative Yukawa theory at finite density and temperature. *Phys. Rev.*, D79:065026, 2009.

[102] O. Scavenius, A. Mocsy, I. N. Mishustin, and D. H. Rischke. Chiral phase transition within effective models with constituent quarks. *Phys. Rev.*, C64:045202, 2001.

[103] J. O. Andersen and R. Khan. Chiral transition in a magnetic field and at finite baryon density. *Phys. Rev.*, D85:065026, 2012.

[104] E. Braaten and R. D. Pisarski. Simple effective Lagrangian for hard thermal loops. *Phys. Rev.*, D45(6):R1827, 1992.

[105] M. Le Bellac. *Thermal Field Theory.* Cambridge Monographs on Mathematical Physics. Cambridge University Press, 2011.

[106] L. P. Csernai and I. N. Mishustin. Fast hadronization of supercooled quark-gluon plasma. *Phys. Rev. Lett.*, 74:5005–5008, Jun 1995.

[107] S. Wenzel, E. Bittner, W. Janke, and A. M. J. Schakel. Percolation of Vortices in the 3D Abelian Lattice Higgs Model. *Nucl. Phys.*, B793:344–361, 2008.

[108] M. Gleiser and R. O. Ramos. Thermal fluctuations and validity of the one loop effective potential. *Phys. Lett.*, B300:271–277, 1993.

[109] R. O. Ramos. Subcritical fluctuations at the electroweak phase transition. *Phys. Rev.*, D54:4770–4779, 1996.

[110] M. Gleiser, R. Howell, and R. O. Ramos. Dynamical precursor model for the onset of percolation. *Phys. Rev.*, E65:036113, 2002.

[111] A. Mocsy, I. N. Mishustin, and P. J. Ellis. Role of fluctuations in the linear sigma model with quarks. *Phys. Rev.*, C70:015204, 2004.

[112] J. Dziarmaga and M. Sadzikowski. Anti-baryon density in the central rapidity region of a heavy ion collision. *Phys. Rev. Lett.*, 82:4192–4195, 1999.

[113] M. Nagasawa and R. H. Brandenberger. Stabilization of the electroweak Z string in the early universe. *Phys. Rev.*, D67:043504, 2003.

[114] Y. Akrami et al. Planck 2018 results. X. Constraints on inflation. 2018.

[115] P. A. R. Ade et al. Planck 2015 results. XVII. Constraints on primordial non-Gaussianity. *Astron. Astrophys.*, 594:A17, 2016.

[116] L. F. Abbott, E. Farhi, and M. B. Wise. Particle Production in the New Inflationary Cosmology. *Phys. Lett.*, 117B:29, 1982.

[117] M. Bastero-Gil, A. Berera, R. O. Ramos, and J. G. Rosa. Warm Little Inflaton. *Phys. Rev. Lett.*, 117(15):151301, 2016.

[118] P. Binetruy, E. Kiritsis, J. Mabillard, M. Pieroni, and C. Rosset. Universality classes for models of inflation. *JCAP*, 1504(04):033, 2015.

[119] M. Pieroni. β-function formalism for inflationary models with a non minimal coupling with gravity. *JCAP*, 1602(02):012, 2016.

[120] M. Pieroni. *Classification of inflationary models and constraints on fundamental physics*. PhD thesis, APC, Paris, 2016.

[121] P. Binétruy, J. Mabillard, and M. Pieroni. Universality in generalized models of inflation. *JCAP*, 1703(03):060, 2017.

[122] F. Cicciarella and M. Pieroni. Universality for quintessence. *JCAP*, 1708(08):010, 2017.

[123] F. Cicciarella, J. Mabillard, and M. Pieroni. New perspectives on constant-roll inflation. *JCAP*, 1801(01):024, 2018.

[124] F. Cicciarella, J. Mabillard, M. Pieroni, and A. Ricciardone. An Hamilton-Jacobi formulation of anisotropic inflation. 2019.

[125] D. S. Salopek and J. R. Bond. Nonlinear evolution of long-wavelength metric fluctuations in inflationary models. *Phys. Rev.*, D42:3936–3962, Dec 1990.

[126] K. Skenderis and P. K. Townsend. Hidden supersymmetry of domain walls and cosmologies. *Phys. Rev. Lett.*, 96:191301, 2006.

[127] P. McFadden and K. Skenderis. Holography for Cosmology. *Phys. Rev.*, D81:021301, 2010.

[128] P. McFadden and K. Skenderis. The Holographic Universe. *J. Phys. Conf. Ser.*, 222:012007, 2010.

[129] J. M. Maldacena. The Large N limit of superconformal field theories and supergravity. *Int. J. Theor. Phys.*, 38:1113–1133, 1999. [Adv. Theor. Math. Phys.2,231(1998)].

[130] P. McFadden and K. Skenderis. Holographic Non-Gaussianity. *JCAP*, 1105:013, 2011.

[131] A. Bzowski, P. McFadden, and K. Skenderis. Holography for inflation using conformal perturbation theory. *JHEP*, 04:047, 2013.

[132] J. Garriga and Y. Urakawa. Holographic inflation and the conservation of ζ. *JHEP*, 06:086, 2014.

[133] J. Garriga, K. Skenderis, and Y. Urakawa. Multi-field inflation from holography. *JCAP*, 1501(01):028, 2015.

[134] N. Afshordi, C. Coriano, L. Delle Rose, E. Gould, and K. Skenderis. From Planck data to Planck era: Observational tests of Holographic Cosmology. *Phys. Rev. Lett.*, 118(4):041301, 2017.

[135] N. Afshordi, E. Gould, and K. Skenderis. Constraining holographic cosmology using Planck data. *Phys. Rev.*, D95(12):123505, 2017.

[136] S. W. Hawking and T. Hertog. A Smooth Exit from Eternal Inflation? *JHEP*, 04:147, 2018.

[137] G. Conti, T. Hertog, and Y. Vreys. Squashed Holography with Scalar Condensates. *JHEP*, 09:068, 2018.

[138] A. H. Guth. Inflationary universe: A possible solution to the horizon and flatness problems. *Phys. Rev.*, D23:347–356, Jan 1981.

[139] A. A. Starobinsky. A New Type of Isotropic Cosmological Models Without Singularity. *Phys. Lett.*, B91:99–102, 1980.

[140] A. D. Linde. A new inflationary universe scenario: A possible solution of the horizon, flatness, homogeneity, isotropy and primordial monopole problems. *Phys. Lett.*, B108:389–393, Feb 1982.

[141] A. D. Linde. Chaotic Inflation. *Phys. Lett.*, B129:177–181, 1983.

[142] A. Albrecht and P. J. Steinhardt. Cosmology for grand unified theories with radiatively induced symmetry breaking. *Phys. Rev. Lett.*, 48:1220–1223, Apr 1982.

[143] W. de Sitter. On the relativity of inertia. Remarks concerning Einstein's latest hypothesis. *Koninklijke Nederlandse Akademie van Wetenschappen Proceedings Series B Physical Sciences*, 19:1217–1225, Mar 1917.

[144] W. de Sitter. On the curvature of space. *Koninklijke Nederlandse Akademie van Wetenschappen Proceedings Series B Physical Sciences*, 20:229–243, Mar 1917.

[145] T. Levi-Civita. Realtà fisica di alcuni spazî normali del Bianchi. *Rendiconti, Reale Accademia Dei Lincei,*, 26:519–531, 1917.

[146] J. Martin, C. Ringeval, and V. Vennin. Encyclopædia Inflationaris. *Phys. Dark Univ.*, 5-6:75–235, 2014.

[147] F. L. Bezrukov and M. Shaposhnikov. The Standard Model Higgs boson as the inflaton. *Phys. Lett.*, B659:703–706, 2008.

[148] C. Armendariz-Picon, T. Damour, and V. F. Mukhanov. k - inflation. *Phys. Lett.*, B458:209–218, 1999.

[149] A. D. Linde. Hybrid inflation. *Phys. Rev.*, D49:748–754, 1994.

[150] M.-A. Watanabe, S. Kanno, and J. Soda. Inflationary Universe with Anisotropic Hair. *Phys. Rev. Lett.*, 102:191302, 2009.

[151] J. M. Bardeen. Gauge-invariant cosmological perturbations. *Phys. Rev.*, D22:1882–1905, Oct 1980.

[152] J. M. Bardeen, P. J. Steinhardt, and M. S. Turner. Spontaneous creation of almost scale-free density perturbations in an inflationary universe. *Phys. Rev.*, D28:679–693, Aug 1983.

[153] V. F. Mukhanov, H. A. Feldman, and R. H. Brandenberger. Theory of cosmological perturbations. Part 1. Classical perturbations. Part 2. Quantum theory of perturbations. Part 3. Extensions. *Phys. Rept.*, 215:203–333, 1992.

[154] H. Kodama and M. Sasaki. Cosmological Perturbation Theory. *Progress of Theoretical Physics Supplement*, 78:1–166, Jan 1984.

[155] D. J. Schwarz, C. A. Terrero-Escalante, and A. A. Garcia. Higher order corrections to primordial spectra from cosmological inflation. *Phys. Lett.*, B517:243–249, 2001.

[156] J. S. Schwinger. On gauge invariance and vacuum polarization. *Phys. Rev.*, 82:664–679, 1951.

[157] T. Hayashinaka, T. Fujita, and J. Yokoyama. Fermionic Schwinger effect and induced current in de Sitter space. *JCAP*, 1607(07):010, 2016.

[158] W. Tangarife, K. Tobioka, L. Ubaldi, and T. Volansky. Dynamics of Relaxed Inflation. *JHEP*, 02:084, 2018.

[159] R. Z. Ferreira and A. Notari. Thermalized Axion Inflation. *JCAP*, 1709(09):007, 2017.

[160] I. G. Moss and C. M. Graham. Particle production and reheating in the inflationary universe. *Phys. Rev.*, D78:123526, 2008.

[161] M. Bastero-Gil, A. Berera, and R. O. Ramos. Dissipation coefficients from scalar and fermion quantum field interactions. *JCAP*, 1109:033, 2011.

[162] M. Bastero-Gil, A. Berera, R. O. Ramos, and J. G. Rosa. General dissipation coefficient in low-temperature warm inflation. *JCAP*, 1301:016, 2013.

[163] A. Berera. Warm inflation at arbitrary adiabaticity: A Model, an existence proof for inflationary dynamics in quantum field theory. *Nucl. Phys.*, B585:666–714, 2000.

[164] A. Berera. Warm inflation solution to the eta problem. *AHEP2003/069*, 2004.

[165] A. Berera, M. Gleiser, and R. O. Ramos. A First principles warm inflation model that solves the cosmological horizon / flatness problems. *Phys. Rev. Lett.*, 83:264–267, 1999.

[166] A. Berera and R. O. Ramos. Construction of a robust warm inflation mechanism. *Phys. Lett.*, B567:294–304, 2003.

[167] A. Berera, I. G. Moss, and R. O. Ramos. Warm Inflation and its Microphysical Basis. *Rept. Prog. Phys.*, 72:026901, 2009.

[168] R. O. Ramos and L. A. da Silva. Power spectrum for inflation models with quantum and thermal noises. *JCAP*, 1303:032, 2013.

[169] S. Bartrum, M. Bastero-Gil, A. Berera, R. Cerezo, R. O. Ramos, and J. G. Rosa. The importance of being warm (during inflation). *Phys. Lett.*, B732:116–121, 2014.

[170] M. Bastero-Gil, A. Berera, I. G. Moss, and R. O. Ramos. Cosmological fluctuations of a random field and radiation fluid. *JCAP*, 1405:004, 2014.

[171] M. Bastero-Gil, A. Berera, I. G. Moss, and R. O. Ramos. Theory of non-Gaussianity in warm inflation. *JCAP*, 1412(12):008, 2014.

[172] I. G. Moss and C. Xiong. Non-Gaussianity in fluctuations from warm inflation. *JCAP*, 0704:007, 2007.

[173] G. S. Vicente, L. A. da Silva, and R. O. Ramos. Eternal inflation in a dissipative and radiation environment: Heated demise of eternity. *Phys. Rev.*, D93(6):063509, 2016.

[174] R. Arya, A. Dasgupta, G. Goswami, J. Prasad, and R. Rangarajan. Revisiting CMB constraints on warm inflation. *JCAP*, 1802(02):043, 2018.

[175] M. Bastero-Gil, S. Bhattacharya, K. Dutta, and M. R. Gangopadhyay. Constraining Warm Inflation with CMB data. *JCAP*, 1802(02):054, 2018.

[176] R. Rangarajan. Current Status of Warm Inflation. In *18th Lomonosov Conference on Elementary Particle Physics Moscow, Russia, August 24-30, 2017*, 2018.

[177] C. Graham and I. G. Moss. Density fluctuations from warm inflation. *JCAP*, 2009(07):013–013, Jul 2009.

[178] M. Bastero-Gil, A. Berera, and R. O. Ramos. Shear viscous effects on the primordial power spectrum from warm inflation. *JCAP*, 1107:030, 2011.

[179] A. N. Taylor and A. Berera. Perturbation spectra in the warm inflationary scenario. *Phys. Rev.*, D62:083517, 2000.

[180] M. Benetti and R. O. Ramos. Warm inflation dissipative effects: predictions and constraints from the Planck data. *Phys. Rev.*, D95(2):023517, 2017.

[181] M. Bastero-Gil and A. Berera. Warm inflation model building. *Int. J. Mod. Phys.*, A24:2207–2240, 2009.

[182] M. Bastero-Gil, A. Berera, R. O. Ramos, and J. G. Rosa. Adiabatic out-of-equilibrium solutions to the Boltzmann equation in warm inflation. *JHEP*, 02:063, 2018.

[183] V. Domcke, M. Pieroni, and P. Binétruy. Primordial gravitational waves for universality classes of pseudoscalar inflation. *JCAP*, 1606:031, 2016.

[184] V. F. Mukhanov. Quantum Cosmological Perturbations: Predictions and Observations. *Eur. Phys. J.*, C73:2486, 2013.

[185] D. Roest. Universality classes of inflation. *JCAP*, 1401:007, 2014.

[186] J. Garcia-Bellido and D. Roest. Large-N running of the spectral index of inflation. *Phys. Rev.*, D89(10):103527, 2014.

[187] P. Binetruy. *Supersymmetry: Theory, experiment and cosmology*. Oxford University Press, 2006.

[188] F. Lucchin and S. Matarrese. Power-law inflation. *Phys. Rev.*, D32:1316–1322, Sep 1985.

[189] P. McFadden. On the power spectrum of inflationary cosmologies dual to a deformed CFT. *JHEP*, 10:071, 2013.

[190] Y. Zhang. Warm Inflation With A General Form Of The Dissipative Coefficient. *JCAP*, 0903:023, 2009.

[191] K. Sayar, A. Mohammadi, L. Akhtari, and Kh. Saaidi. Hamilton-Jacobi formalism to warm inflationary scenario. *Phys. Rev.*, D95(2):023501, 2017.

[192] R. Herrera. Reconstructing warm inflation. *Eur. Phys. J.*, C78(3):245, 2018.

[193] H. A. Kramers. Brownian motion in a field of force and the diffusion model of chemical reactions. *Physica*, 7(4):284–304, 1940.

[194] L. Farkas. Keimbildungsgeschwindigkeit in übersättigten dämpfen. *Zeitschrift für Physikalische Chemie*, 125U:236, 1927.

[195] B. Matkowsky and Z. Schuss. The exit problem for randomly perturbed dynamical systems. *SIAM Journal on Applied Mathematics*, 33(2):365–382, 1977.

[196] P. Talkner. Mean first passage time and the lifetime of a metastable state. *Zeitschrift für Physik B Condensed Matter*, 68(2):201–207, Jun 1987.

[197] H. Risken and T. Frank. *The Fokker-Planck Equation: Methods of Solution and Applications*. Springer Series in Synergetics. Springer Berlin Heidelberg, 1996.

[198] P. Hänggi, P. Talkner, and M. Borkovec. Reaction-rate theory: fifty years after kramers. *Rev. Mod. Phys.*, 62:251–341, Apr 1990.

[199] P. Reimann, G. J. Schmid, and P. Hänggi. Universal equivalence of mean first-passage time and kramers rate. *Phys. Rev.*, E60:R1–R4, Jul 1999.

[200] S. R. Coleman. The Fate of the False Vacuum. 1. Semiclassical Theory. *Phys. Rev.*, D15:2929–2936, 1977. [Erratum: Phys. Rev.D16,1248(1977)].

[201] C. G. Callan, Jr. and S. R. Coleman. The Fate of the False Vacuum. 2. First Quantum Corrections. *Phys. Rev.*, D16:1762–1768, 1977.

[202] A. D. Linde. Decay of the false vacuum at finite temperature. *Nucl. Phys.*, B216(2):421–445, 1983.

[203] L. P. Csernai and J. I. Kapusta. Nucleation of relativistic first-order phase transitions. *Phys. Rev.*, D46:1379–1390, Aug 1992.

[204] S. R. Coleman and F. De Luccia. Gravitational Effects on and of Vacuum Decay. *Phys. Rev.*, D21:3305, 1980.

[205] G. Parisi. *Statistical Field Theory*. Frontiers in Physics. Addison-Wesley, 1988.

[206] J. Zinn-Justin. *Quantum Field Theory and Critical Phenomena*. International series of monographs on physics. Clarendon Press, 2002.

[207] J. S. Langer. Theory of the condensation point. *Annals of Physics*, 41(1):108–157, 1967.

[208] J. S. Langer. Statistical theory of the decay of metastable states. *Annals of Physics*, 54(2):258–275, 1969.

[209] S. W. Hawking and I. G. Moss. Supercooled phase transitions in the very early universe. *Phys. Lett.*, B110(1):35–38, 1982.

[210] A. Berera, J. Mabillard, B. W. Mintz, and R. O. Ramos. Formulating the Kramers problem in field theory. 2019.

[211] I. Affleck. Quantum Statistical Metastability. *Phys. Rev. Lett.*, 46:388, 1981.

[212] L. Pontryagin, A. Andronov, and A. Vitt. On the statistical treatment of dynamical systems. *Zh. Eksp. Teor. Fiz.*, 3:165, 1933.

[213] A. D. Linde. Particle physics and inflationary cosmology. *Contemp. Concepts Phys.*, 5:1–362, 1990.

[214] S. R. Coleman. Quantum tunneling and negative eigenvalues. *Nucl. Phys.*, B298(1):178–186, 1988.

[215] J. S. Langer and L. A. Turski. Hydrodynamic model of the condensation of a vapor near its critical point. *Phys. Rev.*, A8:3230–3243, Dec 1973.

[216] G. F. Bonini, A. G. Cohen, C. Rebbi, and V. A. Rubakov. Tunneling of bound systems at finite energies: Complex paths through potential barriers. 1999.

[217] J. Ankerhold. *Quantum Tunneling in Complex Systems*, volume 224. Springer Tracts in Modern Physics, Jan 2007.

[218] C. M. Bender and D. W. Hook. Quantum tunneling as a classical anomaly. *J. Phys.*, A44:372001, 2011.

[219] A. G. Anderson, C. M. Bender, and U. I. Morone. Periodic orbits for classical particles having complex energy. *Phys. Lett.*, A375:3399–3404, 2011.

[220] H. Harada, A. Mouchet, and A. Shudo. Riemann surfaces of complex classical trajectories and tunnelling splitting in one-dimensional systems. *J. Phys.*, A50(43):435204, Oct 2017.

[221] S. R. Coleman. *Aspects of Symmetry: Selected Erice Lectures*. Cambridge University Press, 1985.

[222] G. D. Moore and K. Rummukainen. Electroweak bubble nucleation, nonperturbatively. *Phys. Rev.*, D63:045002, 2001.

[223] M. Gleiser, G. C. Marques, and R. O. Ramos. On the evaluation of thermal corrections to false vacuum decay rates. *Phys. Rev.*, D48:1571–1584, 1993.

[224] G. V. Dunne. Functional determinants in quantum field theory. *J. Phys.*, A41:304006, 2008.

[225] A. Andreassen, W. Frost, and M. D. Schwartz. Scale Invariant Instantons and the Complete Lifetime of the Standard Model. *Phys. Rev.*, D97(5):056006, 2018.

[226] M. R. Douglas. The Statistics of string / M theory vacua. *JHEP*, 05:046, 2003.

[227] L. Susskind. The Anthropic landscape of string theory. *In "Carr, Bernard (ed.): Universe or multiverse?"*, pages 247–266, 2003.

[228] J. J. Atick and E. Witten. The Hagedorn Transition and the Number of Degrees of Freedom of String Theory. *Nucl. Phys.*, B310:291–334, 1988.

[229] M. J. Bowick and S. B. Giddings. High Temperature Strings. *Nucl. Phys.*, B325:631–646, 1989.

[230] L. Berthier, G. Biroli, J.-P. Bouchaud, L. Cipelletti, and W. Saarloos. *Dynamical Heterogeneities in Glasses, Colloids, and Granular Media*. Oxford University Press, Jan 2011.

[231] F. H. Stillinger. A topographic view of supercooled liquids and glass formation. *Science*, 267(5206):1935–1939, 1995.

[232] P. G. Debenedetti and F. H. Stillinger. Supercooled liquids and the glass transition. *Nature*, 410(6825):259–267, 2001.

[233] A. A. Starobinsky. Dynamics of phase transition in the new inflationary universe scenario and generation of perturbations. *Physics Letters B*, 117(3):175–178, 1982.

[234] A. A. Starobinsky. Stochastic de Sitter (Inflationary) Stage in the Early Universe. *Lect. Notes Phys.*, 246:107–126, 1986.

[235] V. Vennin and A. A. Starobinsky. Correlation Functions in Stochastic Inflation. *Eur. Phys. J.*, C75:413, 2015.

[236] E. Nelson. Derivation of the Schrödinger Equation from Newtonian Mechanics. *Phys. Rev.*, 150:1079–1085, Oct 1966.

[237] G. Parisi and Y.-S. Wu. Perturbation Theory Without Gauge Fixing. *Sci. Sin.*, 24:483, 1981.

[238] P. H. Damgaard and H. Hüffel. Stochastic quantization. *Physics Reports*, 152(5):227 – 398, 1987.

[239] C. J. Isham. *Modern differential geometry for physicists*. 1999.

[240] C. Itzykson and J. B. Zuber. *Quantum Field Theory*. Dover Books on Physics. Dover Publications, 2012.

[241] J. F. Nieves and P. B. Pal. Thermal selfenergies at zero momentum. *Phys. Rev.*, D51:5300–5304, 1995.

[242] E. D. Stewart and D. H. Lyth. A More accurate analytic calculation of the spectrum of cosmological perturbations produced during inflation. *Phys. Lett.*, B302:171–175, 1993.